DOCTOR OF PHILOSOPHY

# The dynamics of small-scale fronts in estuaries.

Nunes, Richard A.

*Award date:*
1982

*Awarding institution:*
Bangor University

# THE DYNAMICS OF SMALL-SCALE FRONTS IN ESTUARIES

RICHARD A. NUNES

MAY 1982

A thesis submitted to the
UNIVERSITY OF WALES
in candidature for
the degree of
Philosophiae Doctor.

University College of North Wales
Marine Science Laboratories
Menai Bridge, Anglesey.

For my parents and for Gilly

ACKNOWLEDGEMENTS

Firstly, my sincere thanks and gratitude go to John Simpson for his enthusiasm, his willingness to give time and energy at a moment's notice and, above all, his considered and expert guidance.

With cheerful and helpful technical assistance throughout the project at all times of the day and night, and his simple but effective approach to design (the current-direction indicator system for the Conwy is one example) it would be hard to beat the many talents of Dave Boon. With Alan Nield in support, the team is definitely unbeatable. My gratitude and thanks to them both, and to Gary Crawshaw for his assistance in the early stages of the project.

The cine photography, which turned out to be so useful and informative, was expertly arranged by Bill Rowntree. I would also like to thank him for the considerable effort that went into producing the photographs for this thesis, and many more besides.

During two visits to Scotland, the Scottish Marine Biological Association kindly allowed use of their facilities, also the research vessel Seol Mara, and provided willing helpers. I would particularly like to thank Dave Booth and Anton Edwards.

The other John Simpson, John E. Simpson (D.A.M.T.P. Cambridge), suspended his own programme of modelling to guide an experimental attempt to reproduce the three-dimensional aspects of the tidal-intrusion front. With sophisticated apparatus and his familiarity with density currents, I think we came as close as a non-specific model would allow.

Dr. John West of the Civil Engineering Department of Birmingham University kindly provided the synoptic cross-sectional density data for the Conwy estuary.

Pete Bowyer jointly organized the Seiont investigation during the summer of 1978, and Rick Lailey and Jose Pelegri covered much of the work in the outer Conwy during the summer of 1979. Assistance was also gratefully received from Dave Bowers (who helped on numerous occasions), Brian Holmes (who assisted with ideas for and use of the current direction indicators in the Conwy and with diving in the Seiont), Nick Collins and Chris Lumb (also for diving), Hazel Clark (for help in the field and with diagrams) and Eddy Gmitrowicz.

Both the Welsh National Water Development Authority and the Clyde River Purification Board kindly provided information on river runoff levels. The Department of the Environment (Ancient Monuments Division) gave us unlimited access to Caernarfon and Conwy castles for observations, and Caernarfon Council granted permission to use the swing bridge over the Seiont as an instrument patform.

Finally, during the period of work covered by this thesis I was supported by a N.E.R.C. research studentship.

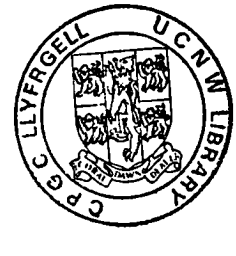

CONTENTS

LIST OF FIGURES

8.10-8.12 Synoptic cross-sectional salinity in the Tremorfa reach on 9.9.81 (data supplied by Dr. J. West, Birmingham University).

8.13 Vertical profiles of lateral secondary velocity from solution of equation 8.25.

8.14-8.17 Secondary circulations generated by the density distributions of 13.10.80, 15.10.80, 9.9.81 (at 10:33hrs) and 9.9.81 (at 18:00hrs).

8.18 Individual lateral and vertical secondary components of the circulation shown in figure 8.14.

8.19 Variation of maximum lateral and vertical secondary velocities with changing channel depth.

8.20 Variation of maximum lateral and vertical secondary velocities with changing channel width.

8.21 Decay of the maximum lateral secondary velocity as a result of secondary flow advection.

8.22-8.24 Model results for the density fields generated by secondary advection on the initial distributions of 13.10.80, 15.10.80 and 9.9.81 (at 18:00hrs)

8.25 Model equilibrium between primary input of density anomaly and secondary re-distribution.

8.26 Variation of maximum lateral secondary velocity from the initial distributions of 13.10.80 and 15.10.80 under the combined effects of longitudinal density input and secondary re-distribution.

8.27 The assembled current-direction indicator and attached vane.

8.28 Exploded view of the components of the direction-indicating instrument.

8.29 Instrument support frame in position in the Tremorfa reach of the estuary.

8.30 Results from the current-direction indicating instruments in the Conwy.

10.1 Debris collections in Loch Linnhe, Scotland.

10.2 Debris collection in the Menai Straits, North Wales.

# CHAPTER 1

# INTRODUCTION

## 1.1 ESTUARIES AND FRONTS

The estuary is the transition zone from freshwater, terrestrial conditions inland, to fully saline oceanic conditions at the coast. Many factors influence the form of this transition e.g. tidal range, river runoff, wind, topography etc. and estuarine regimes occupy a continuous spectrum between highly-stratified and cross-sectionally homogeneous types.

The degree of stratification in an estuary reflects the relative inputs of buoyancy (from runoff or heat) and tidal (or wind) energy. To create vertically-mixed conditions requires a supply of energy to raise the centre of mass of the water column. In the absence of a tidal source, a relatively small supply comes from the hydraulic (barotropic) and longitudinal density gradient (baroclinic) pressure forces. The highly-stratified estuary is the ground state or state of lowest potential energy, which tends towards a two-layer flow in which slow mixing gradually raises the salinity of the upper layer on its journey to the coast. At the other extreme, in which tidal dissipation is considerable, the increase of gravitational potential energy required to create a homogeneous cross-section is easily met and only the longitudinal

gradients remain. Between the two extremes is a continuous range of partially stratified or partially mixed states.

This is the conventional view of estuarine classification: that the different categories of estuaries may be distinguished by their mean levels of stratification. The use of mean is important. Until quite recently it was assumed that horizontal gradients in estuaries are continuous and generally small (except at the 'nose' of a salt wedge) and that a particular category could be used as a shorthand description of the anticipated horizontal circulation. The mean stratification, which does reflect the ratio of buoyancy to tidal energy inputs, does not necessarily describe the instantaneous picture of stratification. The presence of discontinuous horizontal density gradients, or fronts, in estuaries may change a conventional classification of partially stratified to one of equal proportions (in time or length) of highly-stratified and well-mixed types. It would be unwise to base an estuary model on the energy and buoyancy inputs without considering factors that might indicate the presence of fronts.

Fronts of all scales and types are conspicuous because their associated circulations include convergence which, in the surface examples, can be an effective collector of foam, debris and contaminants (posing a stress to the constraints of water quality). To see why convergence is a ubiquitous property of fronts, consider the introduction of a small lens-shaped pool of freshwater onto a large stationary, homogeneous body of saltwater. In order to produce a level of no motion (or as a result of buoyancy) the surface of the light water pool is elevated with respect to the ambient level. This leads to a (downhill) freshwater flow towards the surface boundary to supply the radial expansion of the layer. The expansion, in a reference frame fixed at a point on the front, appears as a convergent flow of saltwater towards the boundary which then sinks below the fresh layer. On the freshwater side, convergence is produced as a result of mixing losses to the ambient fluid. The losses demand a surface current towards the front greater than that required to supply the layer expansion.

The density-driven circulation and the effects of mixing thus combine to produce a two-sided convergence. In the larger

scale i.e. shelf sea and oceanic types, the convergent flows are turned by the Coriolis effect into shear currents parallel to the frontal boundary. This latter effect can be neglected in most coastal and estuarine situations.

## 1.2 COASTAL AND ESTUARINE FRONTS.

When a source of buoyant fluid (e.g. a river, estuary or industrial outfall) discharges into a denser ambient fluid, an abrupt frontal boundary will often be seen, particularly along the leading edge of the discharged plume. This type of front, the 'plume' front, is a reasonably common feature of coastal waters and is well represented in the literature (Garvine and Monk, 1974, Bowman and Iverson, 1977). Vigorous mixing is normally present at the surface and subsurface boundaries, which continuously erodes the plume identity as it moves away from its source. The estuary discharge plume, relying as it does on a substantial source of buoyant fluid, tends to be larger and more stable during the ebb phase of the tide; this is because the flood tide reduces both the total estuary discharge and the layer density contrast (by increased shear-produced mixing). Garvine (1974) has developed an integral numerical model to describe plume frontal dynamics.

Most of the literature concerned with fronts inside estuaries, disregarding the man-made plume fronts, centres on what is unfortunately termed an 'estuarine' front. (Unfortunate, because fronts in estuaries are not exclusively 'estuarine' fronts.) It is a stratified/mixed frontal boundary, analogous to the shelf sea front, produced by differential mixing over the estuarine bottom topography. The front normally lies approximately parallel to the tidal streams and shows an equal tendency to form during flood or ebb phases of the tide. Klemas and Polis (1977) decribe remote detection of 'estuarine' fronts in the Delaware and their considerable ability to collect buoyant contaminants at their surface boundaries.

A 'tide-induced' estuarine front reported by Ingram (1976) separates the colder, saltier waters of the Laurentian channel from

the warmer, fresher waters of the South channel in the St. Lawrence estuary. Ingram refers to its landward "advance" during the flood tide when the boundary was very sharp, and the subsequent "retreat" of a considerably more diffuse front on the ebb.

Fronts in fjords have been observed in Norway by McClimans (1978) and in the Port Hacking inlets in Australia (Godfrey and Parslow, 1976). The latter, in particular, occur during the flooding tide when vigorous mixing over the entrance sill contrasts with stratified conditions inside the basin. Beyond the sill, the inflowing current sinks below the inner surface layer and is outlined by a front at the confluence of the two water masses. Stratification extends over the sill on the ebb.

## 1.3 THE THESIS

This thesis describes the investigation of an estuarine front, the 'tidal-intrusion' front, which was initially found in the Seiont estuary, North Wales but has subsequently been observed at other locations. In the Seiont, the front forms after low water, moves a considerable distance into the estuary to an upstream limit, retreats from the estuary and finally weakens, all within the duration of the flooding tide. It separates mixed from stratified regimes and is characterised by its surface appearance; inside the estuary, the front is 'V'-shaped with its apex directed towards the estuary head. Associated convergent flows include collection of all surface buoyant material at the apex of the 'V'. Following a considerable field investigation of the front in the Seiont, two short periods were spent studying a similar feature in Loch Creran, Scotland.

In the process of investigating other sites to determine the range of estuarine parameters appropriate to a stable tidal-intrusion front, an alternative estuarine convergence was discovered in the Conwy estuary, North Wales. The Conwy shows similar frontal behaviour to the Seiont during the early part of the flood tidal phase, but increased flood currents subsequently break down stratification producing an estuary of the 'well-mixed' class.

Throughout the remainder of the flood tide an axial line of debris forms along a substantial proportion of the estuary length. The persistence of the line indicates a secondary circulation which includes surface convergence towards the estuary axis. However, the line disperses at high water and no similar system is apparent during the ebb.

The specific aims of the thesis may be summarised with respect to:

a) the tidal-intrusion or T.I. front;

i) to understand the parameters which govern the movements of the front.

ii) to explain and/or reproduce by modelling, the three-dimensional aspects of the 'V'-shaped frontal boundary.

b) the axial convergence or A.C.

i) to detrmine the nature of the secondary circulation in the Conwy i.e. the pattern of cross-sectional secondary velocities.

ii) to determine a mechanism which accounts for both the production of a sustained secondary circulation and its existence only during the flood phase of the tide.

and finally, we attempt to define the stable parameter ranges for both types of convergence.

## 1.4 THESIS FORMAT

Chapter 2 provides a brief theoretical background and chapter 3 describes the instrumentation and the various measuring and observational techniques.

With this background, the thesis is subsequently divided into three sections. Section I is entirely devoted to the tidal-intrusion front; chapter 4 describes the Seiont investigation, chapter 5 looks at a similar feature in Loch Creran, Scotland and Chapter 6 presents an account of the frontal interface including its three-dimensional aspects. Section II is devoted to the axial convergence found in the Conwy; chapter 7 describes the system and its place within the estuarine regime and chapter 8 attempts to isolate and confirm a cause, and includes a diagnostic numerical model. Section III (chapter 9) uses the results of the two previous sections to examine the stable ranges of occurrence of both T.I. and A.C. forms of convergence. Chapter 10 presents the discussion and summary.

## 1.5 TERMINOLOGY

To avoid a repetitive style the following terms will be used synonymously;

i) landward, upestuary and upstream.
ii) seaward, downestuary and downstream.

and thus upstream and downstream do not refer to flow directions.

# CHAPTER 2

## THEORETICAL CONSIDERATIONS

A simple Froude number criterion, derived from internal wave theory, expresses the only control upon the discharge of freshwater in the two-layered flow of an estuary. If, however, the fresh/saltwater interface outcrops at a boundary (surface or bed) knowledge of density current behaviour is required to determine the frontal movement.

A density current may loosely be defined as the buoyant (positive or negative) flow of a fluid body through an ambient fluid of differing density. Examples include the avalanche of snow down a mountainside, the desert haboob, the flow of methane along the roof of a mineshaft, land and sea breezes, and the dustcloud of a volcanic eruption. Within the definition is a subdivision separating flows in the horizontal from those down an incline.

G. Keulegan, in the 1950's (1957,1958) conducted a systematic experimental programme to determine the parameters controlling the rate of progress, $u_d$, of the density current head. Using a lock exchange arrangement in a rectangular channel, he

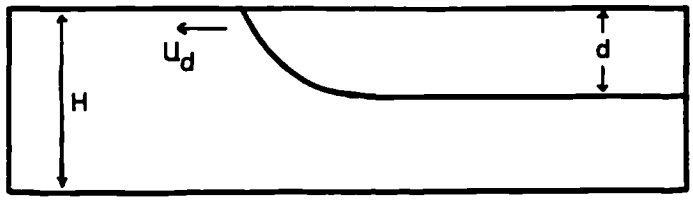


Figure 2.1 Schematic two-layer density current.

obtained the result:

$$u_d \approx 0.46(g'H)^{1/2} \qquad 2.1$$

where $g'=g\Delta\rho/\rho$ is the reduced gravity and H is the total water depth. (The form of this result remains for channels of differing shape, only the leading constant is changed.)

The flows investigated by Keulegan belong to the first two of three regimes of density current behaviour outlined by Koh (1976). The initial or slumping (Huppert and Simpson, 1980) phase immediately follows lock gate removal, as the denser fluid body collapses into the lighter fluid and begins its advance. The second, or inertial phase, covers the majority of investigated density current flows, when the head velocity remains approximately constant due to a balance between inertial and buoyancy forces. The third phase, the viscous regime, describes the final balance between buoyancy and viscous drag.

Benjamin (1968), in a theoretical study of the inertial phase, defines the physical limits upon the fractional depth (d/H in figure 2.1) of the current. Theoretically, an energy conserving flow is possible for d/H=0.5, however, this requires a supercritical flow of the ambient fluid below (or above) the current, and is not realised in practice. The fractional depth has an upper bound of $d/H < 0.35$ for all physically realisable flows, and these necessarily suffer an energy loss at a head wave behind the front.

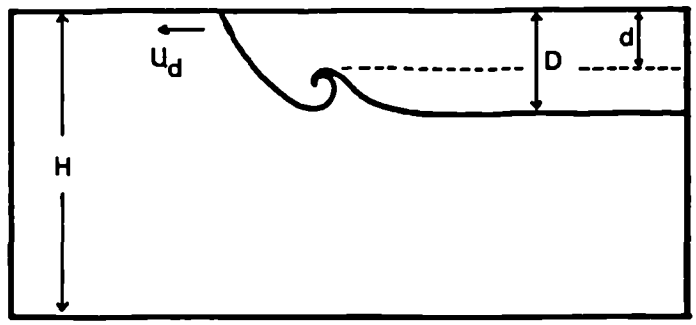


Figure 2.2 Schematic three-layer density current.

Application of the Bernoulli condition in the steady flow regions on either side of the current head leads to an equation for the rate of advance of the density current (Benjamin, 1968);

$$u_d = \{(H-d)(2H-d)/H(H+d)\}^{1/2}(g'd)^{1/2} \qquad 2.2$$

which may be rewritten as (Britter and Simpson, 1978);

$$u_d = \{(1-\phi)(2-\phi)/(1+\phi)\}^{1/2}(g'd)^{1/2} \qquad 2.3$$

where $\phi = d/H$ is the fractional depth of the current.

Laboratory modelling of density currents in the steady state is well documented by Simpson (1972), Britter and Simpson (1978) (hereafter referred to as BS) and Simpson and Britter (1979) (or SB). In the majority, these have been bottom boundary density flows, because the effects of surface tension interfere with surface currents on a small scale. In order to maintain a vertically-uniform velocity profile in the ambient fluid, a moving floor was employed in the apparatus of these authors (to be described in more detail in section 6.2) which eliminated the bottom boundary layer, (figures 6.3 and 6.4).

Modelled density currents show a three-layered structure behind the head wave (figure 2.2). The uncontaminated water that constitutes the density current advances toward the head in a relatively thin layer of near-vertically-uniform velocity. The major fraction of the depth is occupied by the ambient fluid but there is also an intermediate layer found to be the site of the maximum density and velocity gradients.

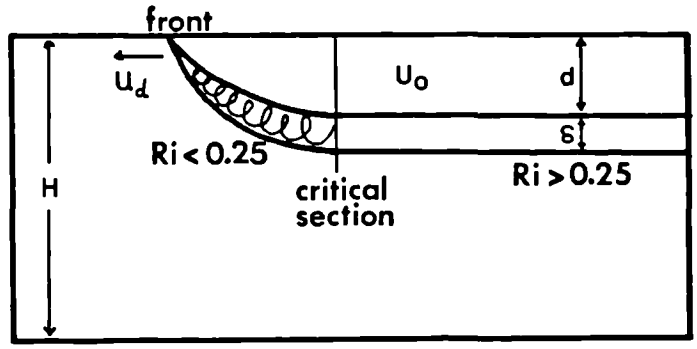


Figure 2.3 Definition sketch for Stigebrandt's analysis.

Equation 2.3 does not account for mixing between the layers, nevertheless, BS and SB have shown that it correctly expresses the frontal velocity $u_d$ if the mixed layer is excluded from the quantity d. Entrainment of fluid from the density current into the mixed layer creates a further demand on the supply of fluid to the head which increases the current velocity $u_o$ by ~16% above the frontal velocity. This results in a flow which converges on the head, where it mixes with the ambient fluid and is then laid down below (or above) the following current.

Stigebrandt (1980) treats the dynamics of density currents from a simple, first-principle standpoint. He assumes that all significant mixing takes place in a 'frontal zone' (figure 2.3) where the isopycnals rise toward the surface. The 'frontal zone' is bound by the front to one side and a 'critical section' to the other which, itself, separates stable from unstable interfaces. Stigebrandt considers the case of an infinitely deep ambient fluid and assumes linear density and velocity gradients in the pycnocline. Conservation of buoyancy within the 'frontal zone' leads to an expression which relates the frontal velocity to the density current velocity;

$$u_d = 2u_o(3+S)/3(2+S) \qquad 2.4$$

in which S is the ratio of pycnocline thickness $\delta$ to the density current depth d. Integration of the velocity field gives the net flux through the 'critical section';

$$Q_s/u_o d = -S(4+S)/6(2+S) \qquad 2.5$$

which expresses the net entrainment of ambient fluid into the pycnocline.

Stigebrandt considers S to be the fundamental quantity which is obtained from observation and from which he derives representative values of the frontal velocity, the convergence velocity ($u_o - u_d$) and the proportions of fresh and saltwater contained in the pycnocline. For S~0.2 (after correcting a numerical error) his analysis gives a density current velocity 3% larger than the frontal velocity, and a saltwater/freshwater ratio ($Q_s/Q_f$) of ~2:1 in the mixed layer. The experimental finding of BS, i.e. $u_o/u_d$~1.16 requires that S~2.0 and $Q_s/Q_f$~3:1. Certainly, a value of S~1.0 is more realistic for the laboratory density currents than the value S~0.2 that Stigebrandt borrowed from the experiments of Anati et al (1977), but whether the same conclusion applies to natural, large-scale density currents remains to be tested.

# CHAPTER 3

# INSTRUMENTATION AND METHODS.

## 3.1 OBSERVATIONS

In the early stages of both the Seiont and Conwy investigations, the most profitable return on investment of time and resources was found to be time-lapse cine photography. It proved to be an invaluable means of understanding a surface circulation from visual observation alone; always highlighting the less obvious aspects that might nevertheless offer important clues to the operative forces. Fortunately, in both of these locations, a high vantage point was available overlooking the mouth of each estuary in the form of the Caernarfon and Conwy castles. For lower perspectives the Seiont, Tal y Cafn and Dolgarrog bridges were suitable and easily accessible.

For the time-lapse sequences we used a 'super 8' Niko camera which incorporated through-the-lens metering and, necessarily, a facility for single frame exposure. When using time-lapse for an extended period (a few hours) the internal batteries were inadequate and an external (motor bicycle) battery was attached as the power source. Most of the sequences were taken at the rate of one frame every 1.5 seconds which was found to be the most suitable rate for the estuarine circulations, but intervals up to 5 seconds per frame gave useful results.

## 3.2 MEASUREMENTS

Available hardware for monitoring water properties comprised:

i) several Electronic Switchgear temperature/salinity probes which conveyed conductivity and temperature to a balancing circuit onshore (or boat) where it was converted electronically to salinity. These instruments resolved salinity from 0.5‰-38‰ on two scales (0.5-32 and 32-38) with an accuracy of ~1% f.s.d. and temperatures between -1° and 30° accurate to ~0.1°. They were considered particularly suited to estuarine work because the cylindrical shape of the probe, when aligned horizontally, presented a very small aspect to a water column in which vertical gradients could be very large. The limitations of their accuracy were not important where the full fresh to oceanic salinity range was normally encountered.

ii) several Braystoke current meters, all but one of which were direction-indicating and with 0.127m (5 inch) impellors. Rotation of the impellor by a current activated a reed switch sending pulses to the counter onshore. The total number of pulses received, depending on the timing interval, was converted by tables into a current speed, and current direction was displayed to the nearest 10°. To accomodate requirements in a highly stratified environment, a Braystoke current meter fitted with a 5cm impellor (and without the direction-finding facility) was used and, in fact, more frequently than the larger types. By excluding the directional facility the instrument gained in compactness and, although intended for use in sheltered waters, it seemed adequately robust for most estuarine purposes. The smaller instrument could accurately resolve currents down to $0.03ms^{-1}$

iii) a turbidity-indicating instrument consisting of a light source and detecting photocell separated by a fixed distance. For the purposes of monitoring estuarine fronts, water turbidity was considered to be of secondary value.

The instrument did indicate large turbidity gradients coincident with abrupt salinity gradients although the levels were too small to have contributed to density changes. It was a bulky instrument which was quite awkward to handle, and was discarded at an early stage of the work.

iv) an N.B.A. inductive conductivity/temperature probe with a liquid crystal display (acquired in the late stages of the project). The display gave temperature ($-5°$ to $45°$, $\pm 0.1°$) and conductivity (6 to 80m.mhocm$^{-1}$, ±1.5% f.s.d.) each to a single decimal place which was converted to salinity from tables. However, the combination of single place accuracy in both conductivity and temperature displays presented a limitation to the accuracy of the salinity result. The probe was nevertheless small and very robust and was quick to use because balancing was not required.

These instruments were used either from the available bridges or from boats which were either moored or mobile. A great deal of the measurements in the Seiont were taken beneath the swing bridge using instruments lowered from a hand-operated winch that was projected through the railings and over the seaward side. The winch was particularly useful for preventing unwanted vertical movements and thus allowed the water column to be sampled at well-defined 10cm vertical intervals. The winch solved most of the difficulty associated with measuring vertical salinity gradients of as much as 30% in 20cm, but in order to avoid ambiguities when linking salinity to velocity records, the T/S probe was normally attached to the shaft of the current meter as in figure 3.1.

For measurements at different stations along the estuary we used a 13 foot Dory (fibreglass flat-bottomed dinghy) fitted with an outboard engine. On station it was laterally very stable and between stations, very fast. Occasionally during fixed station work use was made of a small inflatable dinghy.

Ideally, a measurement of salinity or velocity should be representative and reproducible despite the presence of large turbulent eddy structures. This requires a minimum timing interval for the measurement of the order of 100s. In the rapidly changing

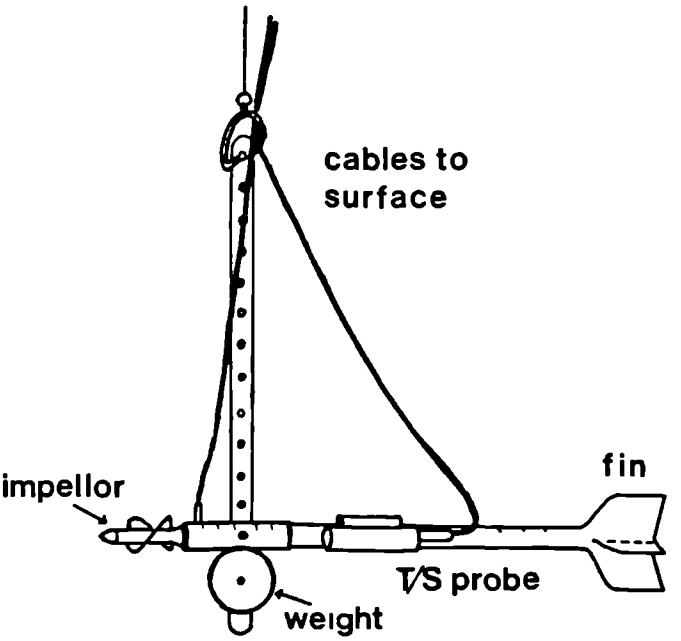


Figure 3.1 Temperature/salinity probe and current meter arrangement.

environment of an estuary, however, such a timing interval encounters problems with the time variation of properties at a point and also severely restricts the possible spatial coverage of a near-synoptic survey. A compromise was therefore necessary, and timing intervals of 10, 30 or 50 seconds were chosen depending on the local current speed.

# SECTION I - THE TIDAL-INTRUSION FRONT

# CHAPTER 4

# THE SEIONT ESTUARY, NORTH WALES.

## 4.1 THE ESTUARY

The Seiont estuary forms the western boundary of the town of Caernarfon and discharges into the Menai Straits near its western extremity (figure 4.1). Its source is the Padarn Lake, some 15km inland, in the heart of the Snowdonia National Park. Steep-sided valleys are responsible for the small catchment area (77.9km $^2$) and the relatively sparse vegetation promotes a fast response to local weather. Day to day runoff variations, gauged at Peblig Mill on the southern outskirts of Caernarfon, may be quite substantial ranging from 0.2 cumecs (cubic metres per second) to 20 cumecs, with a mean of 4.8 cumecs.

Figure 4.2 shows a plan view of the Seiont estuary from the Menai Straits to the upstream limit of salt contamination, a distance of ~1.7km. As indicated in the figure, the mouth is situated ~50m downstream of the bridge where the cross-section abruptly widens in the seaward direction. For the sake of brevity in the following description we distinguish three reaches of the estuary length. The first, the 'outer estuary', lies between the mouth and the Straits and has a length of ~300m. The second, termed the 'frontal channel', extends ~600m landward from the mouth to a

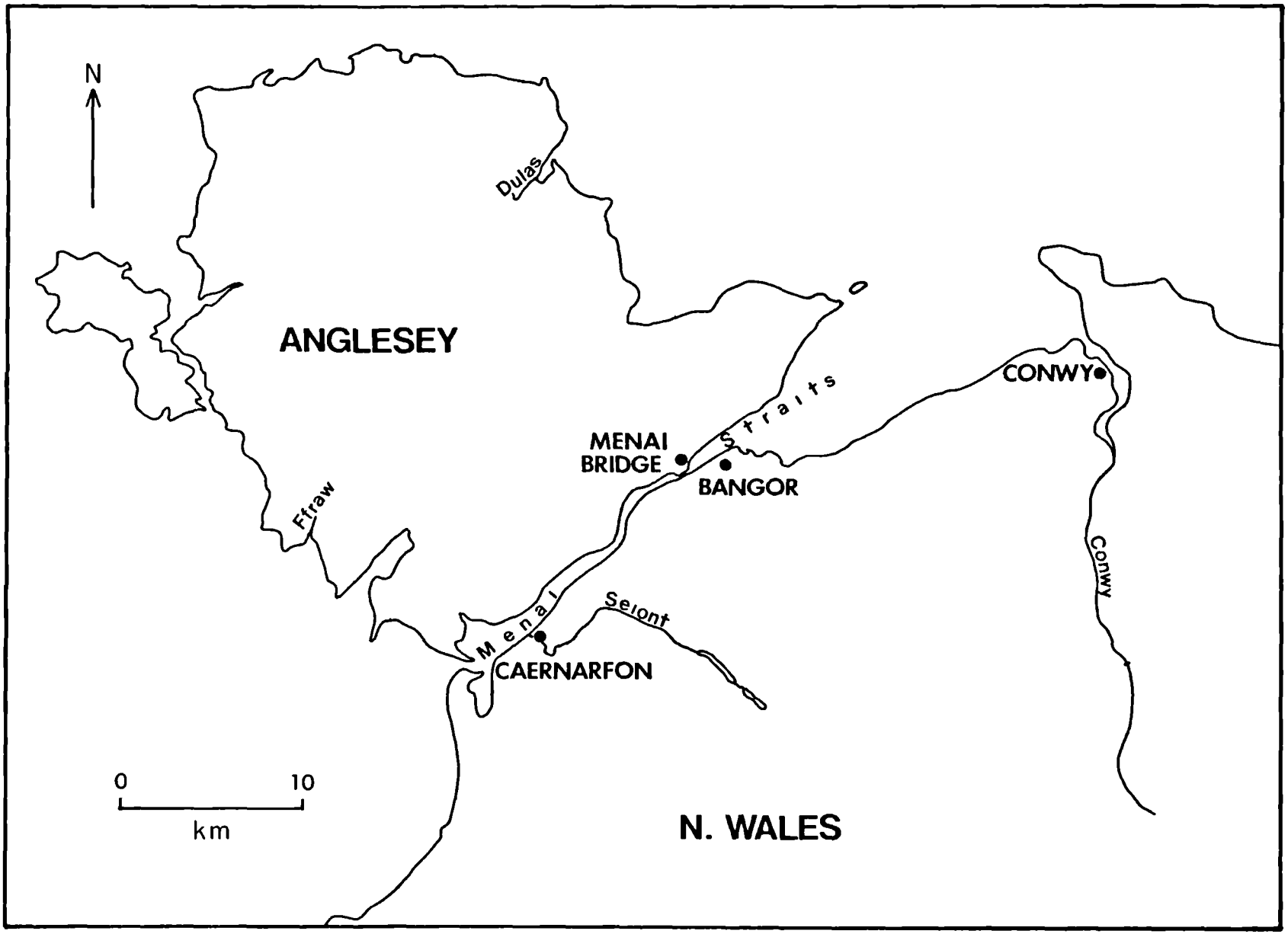


Figure 4.1 The North Wales coast, showing the locations of the Seiont, Conwy, Dulas and Ffraw estuaries.

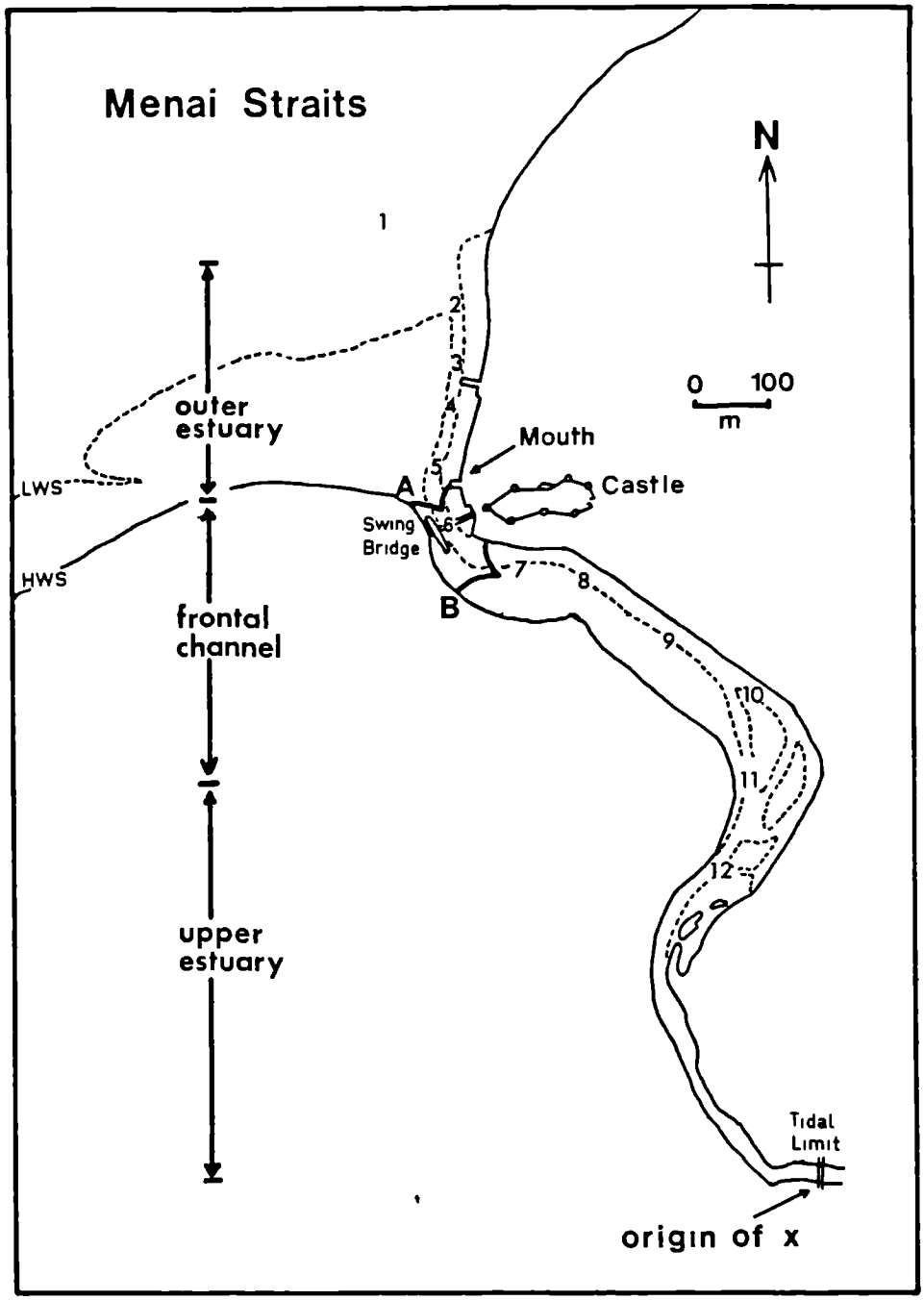


Figure 4.2 Plan view of the Seiont estuary showing topographic features and station positions for longitudinal surveys. Also indicated are typical frontal positions: A (LW+2.5 and LW+3.5) and B (LW+3), and the origin of x for use in the analysis sections (4.4 and 4.5).

sharp bend in the channel. It is in this reach of the estuary that the tidal-intrusion front may be observed and its movement may cover up to the entire length of the frontal channel. Landward of the bend is the 'upper estuary' in which the cross-section reduces from ~80m to ~20m, and which has a total length of ~800m.

Figures 4.3a and 4.3b illustrate the results of the estuarine bathymetry surveys. Depths were measured using a weighted line at up to eight transverse positions on each of eighteen cross-sections along the estuary. Measured at, or near to high water, relative corrections were small, amounting to less than 20cm. Note that the deepest part of the cross-section runs along the eastern harbour wall throughout the length of the frontal channel.

The bed datum of the estuary, being above the height of most low waters in the Menai Straits, means that complete flushing of salt from the estuary occurs each tidal cycle. Salt does remain, however, if the runoff is particularly low or during small neap tides. The discharge from the estuary is swept away by a strong tidal crossflow in the Straits which is maintained throughout most of the tidal cycle. The energetic Straits' flow ensures that there is no significant return of freshwater to the estuary during the following flood tidal phase. With turbulence levels insufficient to overcome the stability of the stratification, a distinct two-layered flow is the dominant estuarine regime for most of the tidal cycle.

The tidal curve for the Menai Straits near Caernarfon shows little harmonic distortion; the tides are semi-diurnal with mean neaps and springs ranges of 2.1m and 4.9m respectively. Within the estuary the tidal characteristics are those of a standing wave with slack water occurring in the lower layer at high water. Some distortion of the estuary tidal curve is present, however, as a result of the prolonged seaward flow of freshwater maintained at the start of the flood, until the tidal flow enters the estuary. This distortion increases at successive landward positions. The maximum tidal transport below the pedestrian bridge ranges between 10 cumecs and 30 cumecs for neaps and springs respectively, with equivalent maximum central channel velocities of 25cms$^{-1}$ to 50cms$^{-1}$

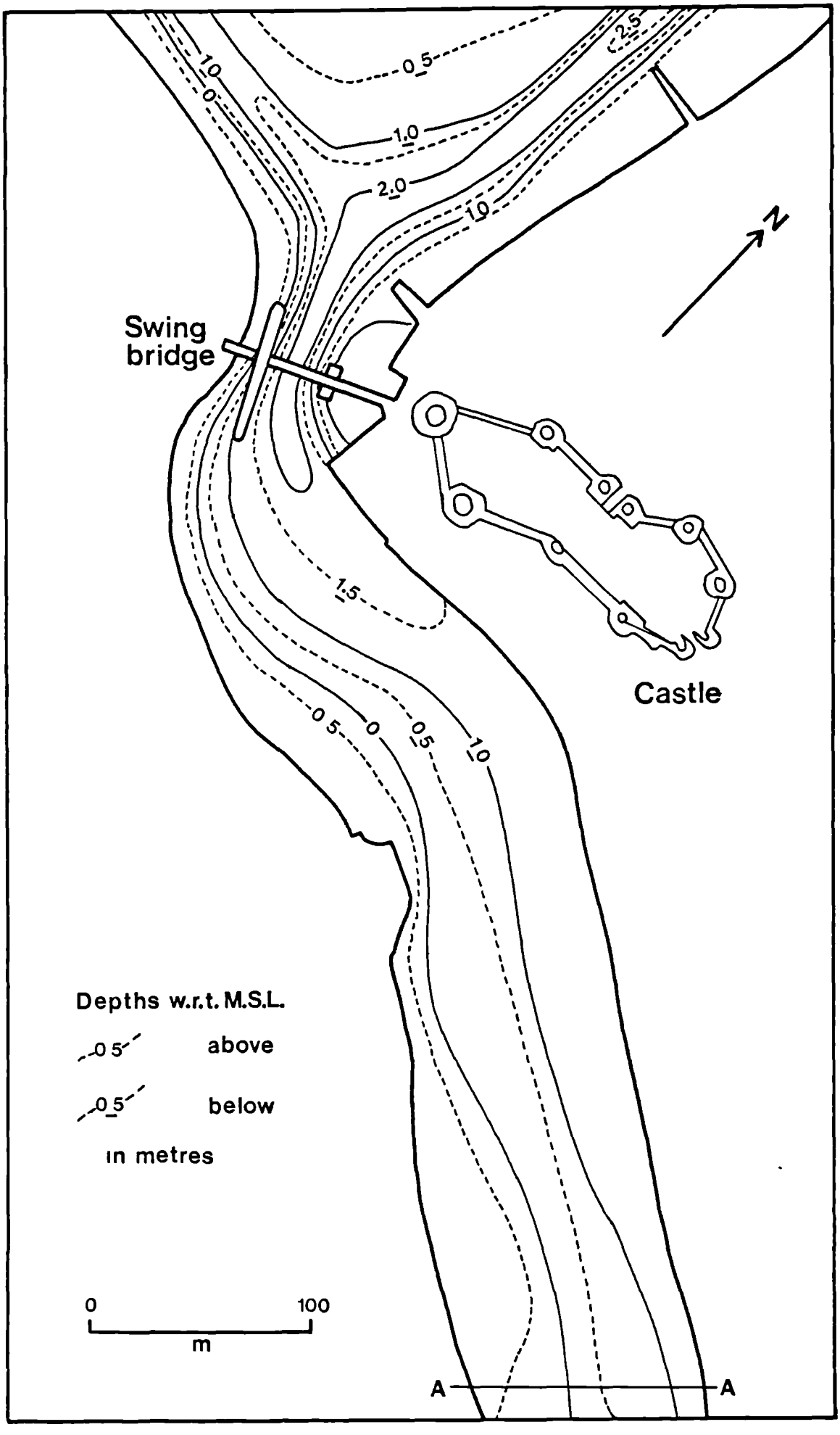


Figure 4.3a Bathymetry of the Seiont estuary.

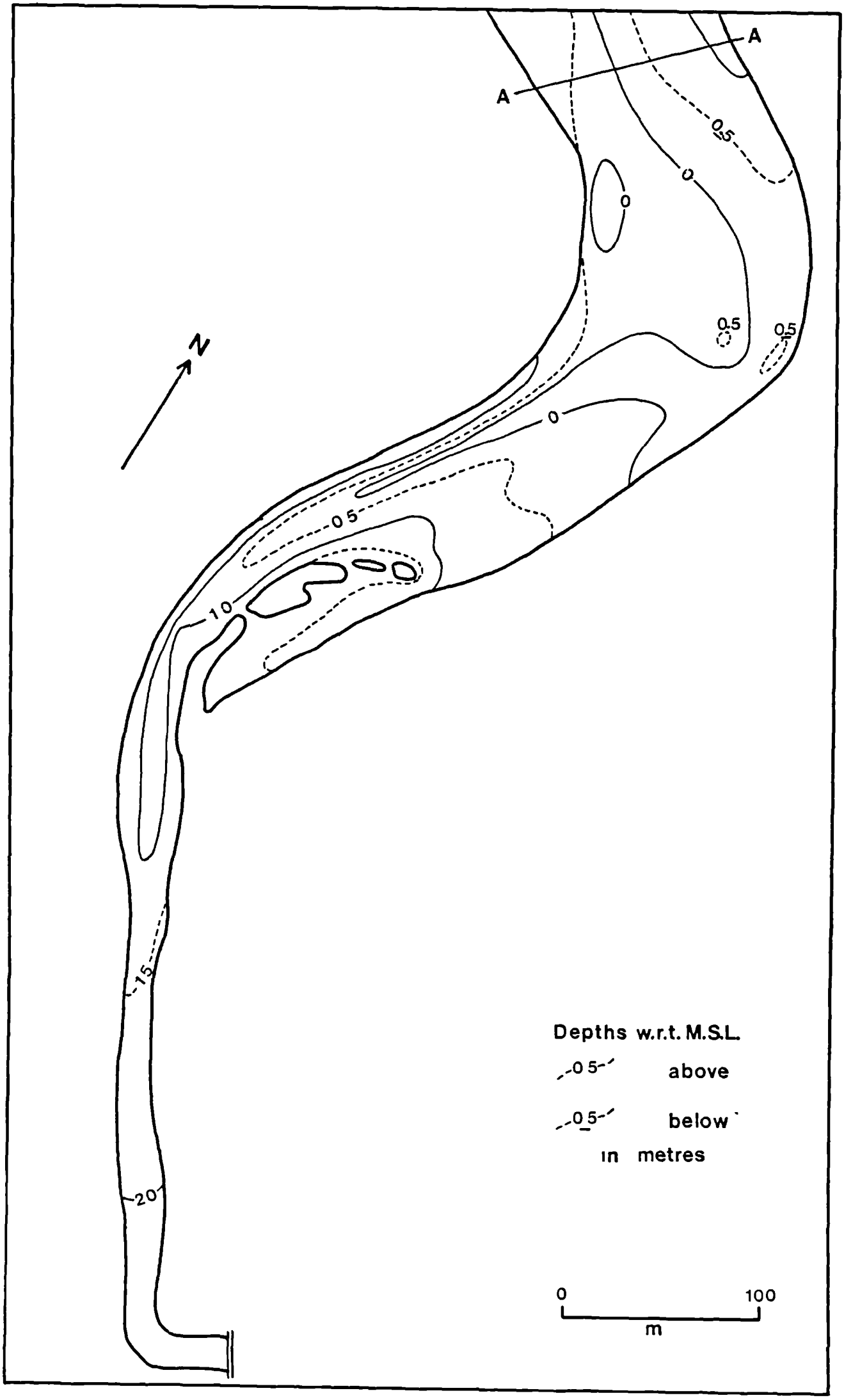
A
A
0.5
0
0
0.5
0.5
N
0
0.5
1.0
1.5
2.0
Depths w.r.t. M.S.L.
0.5 above
0.5 below
in metres
0
100
m

## 4.2 VISUAL DEVELOPMENT.

An hour either side of low water, for mean tides, the estuary channel carries a stream of freshwater to the Straits which it meets at right angles some 300m seaward of the bridge, The discharge is here swept away as a plume by the external crossflow and is outlined by a sharp, often meandering, visible surface front (figure 4.4).

As the tide turns at low water, there is a short slack period followed by quickening eastward flow in the Straits which pushes the leading edge of the plume across the end of the channel. Flow in the channel begins to deepen, inundating the large sandbank in the outer estuary. The lighter freshwater spreads over the enlarging surface area such that, when the outer estuary is totally submerged, the front lies across and virtually encloses the outer estuary. A small freshwater discharge to the Straits is maintained only by a flow of 10m-20m width flanked to one side by the eastern, outer wall of the estuary, and to the other side by the plume front which extends hundreds of metres along the Straits before becoming visibly indistinguishable. For neap tides during average runoff, and for all tides during high runoff, this situation persists throughout the flood tidal phase with some minor adjustments to the shape and position of the front. For spring tides and mean runoff the quickening pace of the flood currents forces the front into the estuary towards the bridge and, by so doing, stems all freshwater discharge from the estuary.

On reaching the mouth, at approximately 2.5hrs after low water (LW+2.5) (e.g. position A in figure 4.2), the surface front takes on a characteristic 'V' outline. The apex of the 'V' lies centrally within the channel and points upestuary, with an angular separation of 30° - 90° between the 'arms' of the 'V', both of which reach their respective shores (figure 4.5). The 'V' front, the tidal-intrusion front, continues its advance into the estuary until approximately mid-flood (LW+3) when it reaches its landward limit (e.g. position B in figure 4.2).

Surface flow associated with the T.I. front has a well-developed and distinct character, shown schematically in

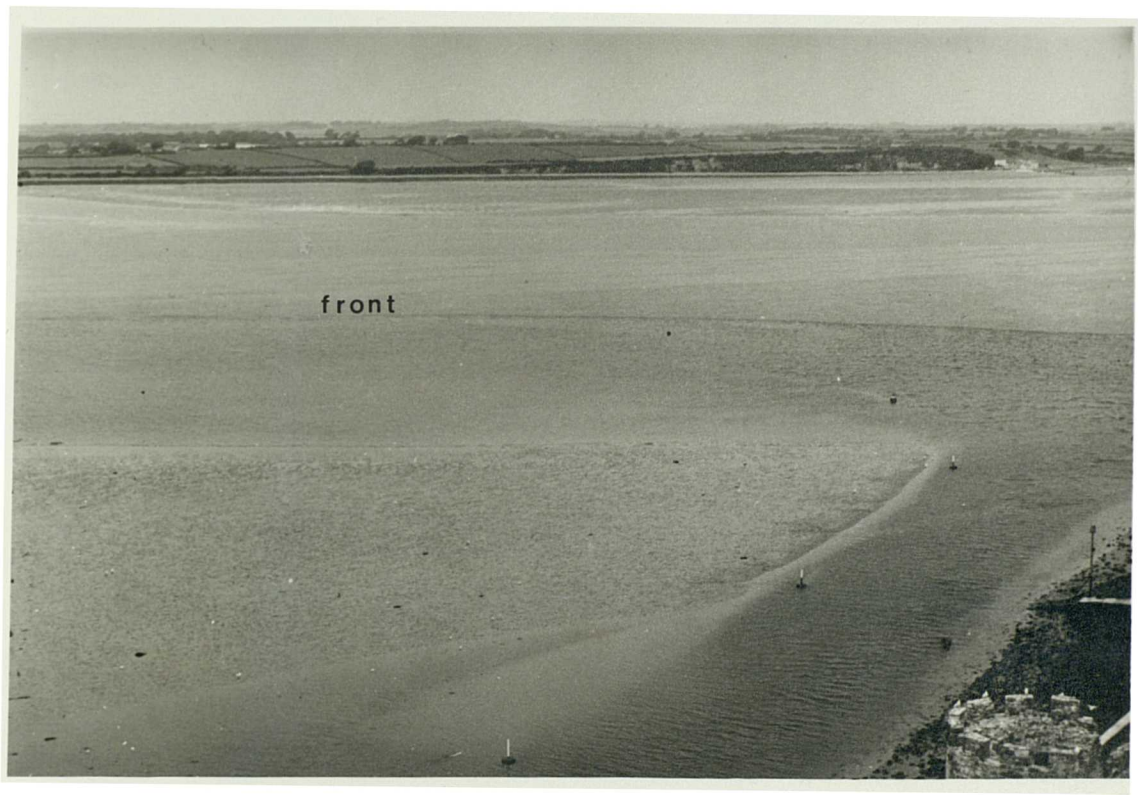


Figure 4.4 The Seiont discharge plume front in the late stages of the ebb tide.

Figure 4.5 The tidal-intrusion front in the Seiont estuary. The two-layer estuarine regime is on the left and the mixed water from the Straits flows in from the right. The person at bottom left adds a scale to the picture.

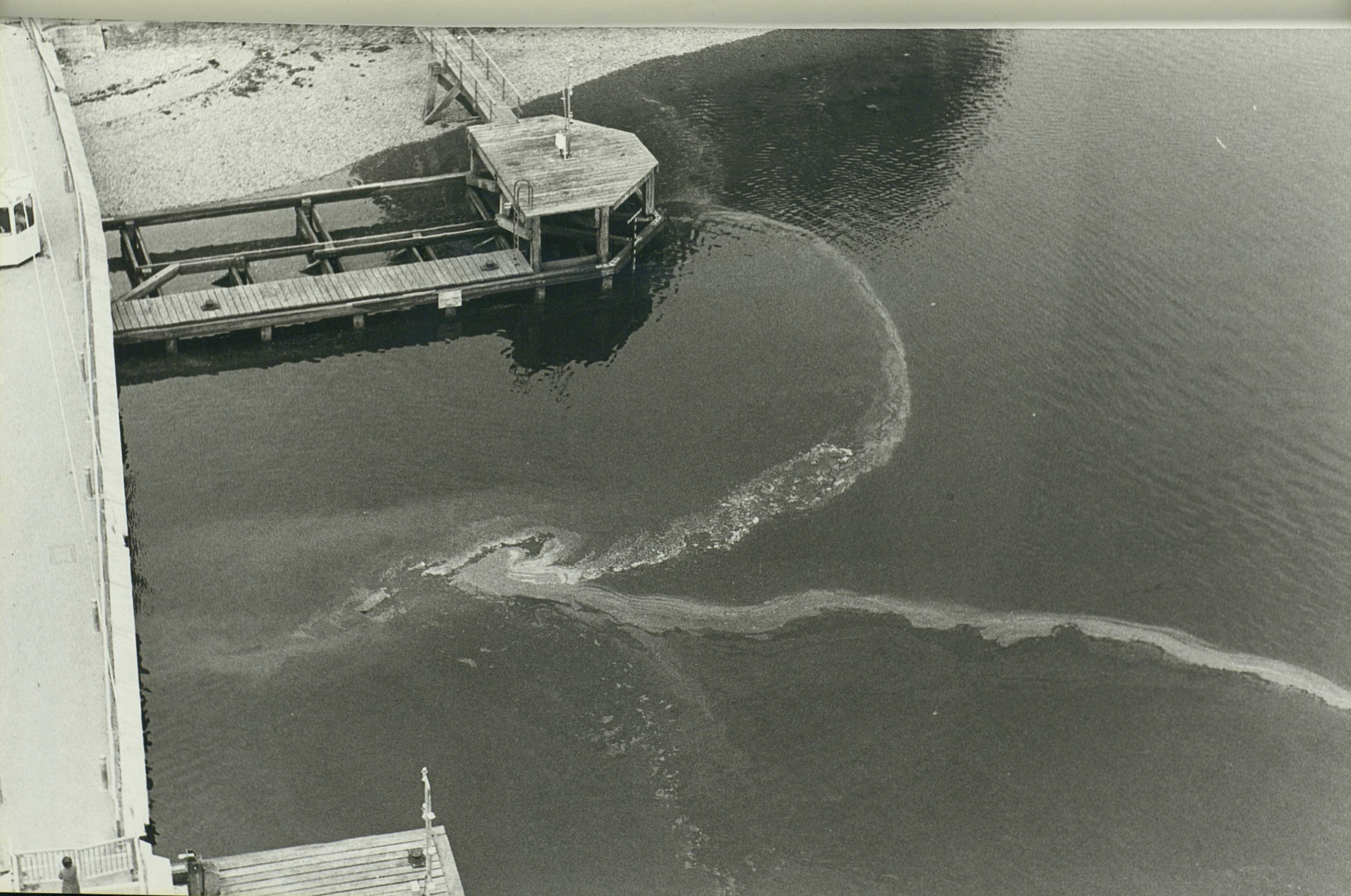

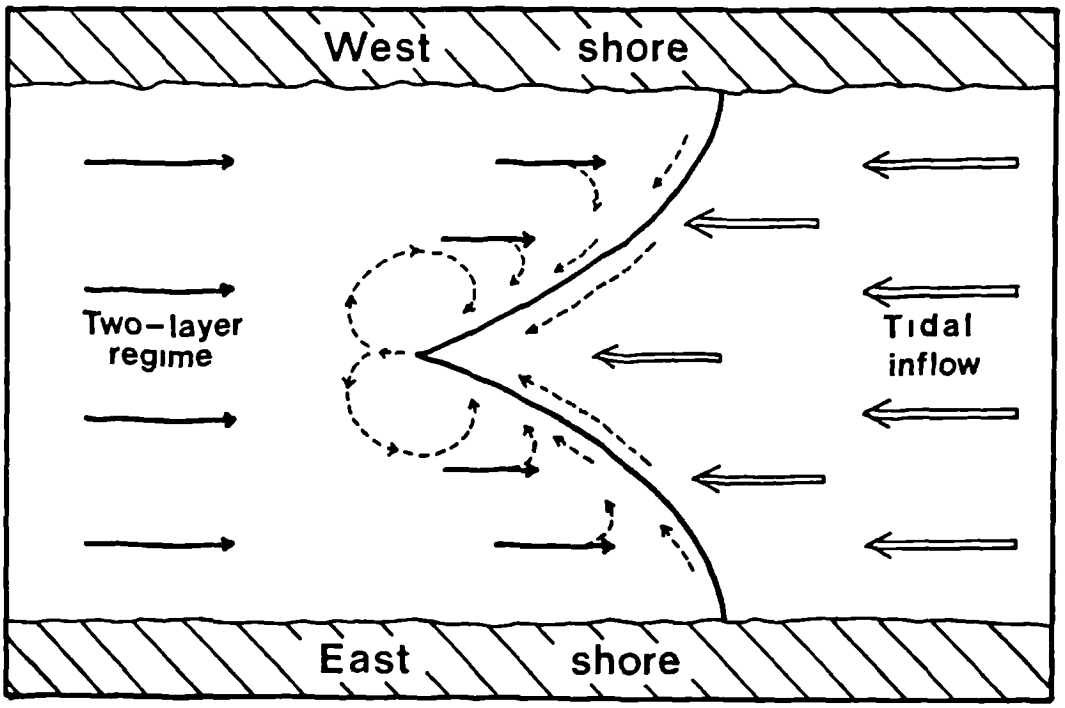


Figure 4.6 Schematic surface current structure (complete arrows) at the tidal-intrusion front, and the surface paths of buoyant debris (dotted arrows).

figure 4.6. The frontal arms are marked by large collections of surface buoyant material and foam collected by the convergence. Tidal flow on the seaward side is unperturbed upstream flow to the front itself. On the landward side, however, surface flow is seaward until reaching the front where the freshwater (marked with dye) then rapidly sinks and returns upestuary as a subsurface current.

The secondary flow displayed by buoyant debris and foam (see figure 4.6) differs from this picture in that the frontal arms arrest the movement of debris in either longitudinal direction. This collected material experiences shear from below which tends to drive it slowly into the apex of the 'V'. Debris in the fast, saline flow near the axis of the estuary may penetrate a short distance into the statified side, but is then returned to the front by a gyre, or a counter-rotating pair of gyres.

When the tidal currents start to weaken, after a short stationary period the front begins to retreat down the estuary. It reaches the mouth at about LW+3.5 where it undergoes a transformation, emerging from the mouth as a convex plume front

which slowly moves out toward the Straits. A sequence of photographs of the T.I. front retreat and transformation are shown in figure 4.7 taken at intervals of less than one minute.

The plume front in the Straits at LW+4 appears similar to the plume seen after low water. Slackening tidal currents permit the front to push further out into the Straits where it weakens considerably on the final approach to high water. Ebb flow in the Straits then re-forms the plume front which runs westwards persisting throughout the entire ebb phase. No surface fronts have been seen inside the estuary during the ebb.

The landward limit of frontal intrusion and the associated residence time within the frontal channel are both observed to vary with conditions of tidal range and river runoff. Furthermore, on three occasions a departure from the 'V' outline was observed at the intrusion limit. This took the form of a single linear, obliquely-aligned front, lying furthest upestuary on the eastern side, but which reformed to a 'V' soon after the start of its retreat.

Figure 4.7 A sequence taken after maximum flood currents showing the retreat of the front and its transformation to a plume front at the mouth of the estuary.

## 4.3 ESTUARY SURVEY RESULTS.

Fieldwork results divide into three categories:

i) time series measurements at a fixed station - the swing bridge.

ii) quasi-synoptic profiles at stations along the estuary axis.

iii) non-synoptic profiling at stations in a front-based frame of reference.

From the swing bridge vertical profiles of salinity, temperature and current velocity were made at frequent intervals using the instrument arrangement shown in figure 3.1.

For the major fraction of the tidal cycle the front lies seaward of the bridge, during which time the water column below the bridge exhibits a highly stratified, two-layered structure (figure 4.8a). A sharp, well-defined interface is invariably present, separating an upper layer of low salinity from fully saline water (~33‰) below. The interface is normally ~20cm in thickness and separates rapid landward flow in the lower layer from a slow seaward movement above. (Surface flow may become landward if the frontal velocity exceeds the downstream velocity of the freshwater.)

On occasions when the frontal movement is sufficient to allow bridge-based profiles in the water mass seaward of the front, the picture is very different. All such profiles (figure 4.8b) display a homogeneous column of fully saline water from the surface to the bed. The velocity profile then resembles a typical homogeneous, frictional channel profile.

Bridge-based measurements during the passage of the front in either direction show an abrupt change of surface salinity, by as much as 30‰, but no simultaneous change occurs near the bed. The front thus marks the boundary between the two-layer and mixed regimes.

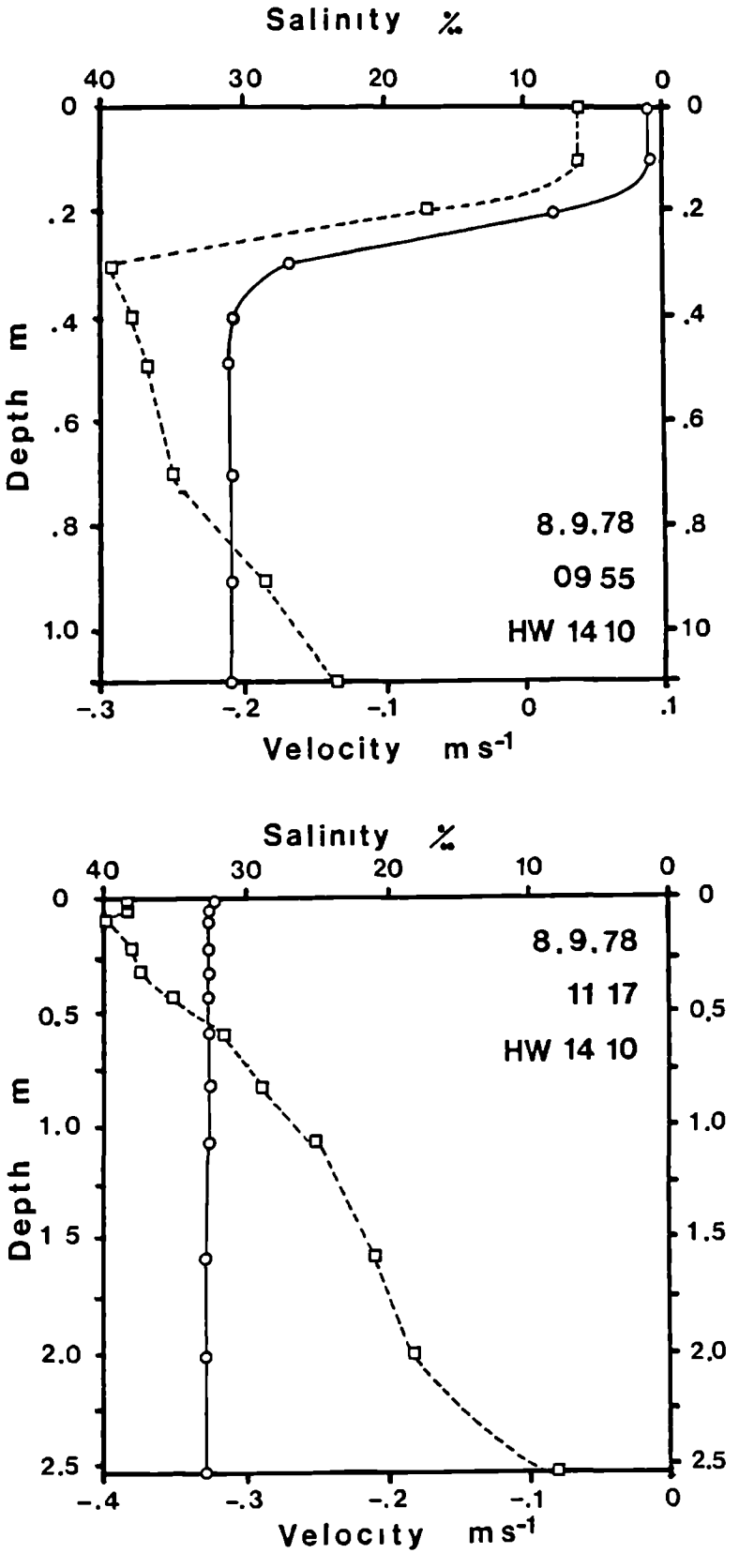


Figure 4.8 Vertical profiles of salinity and velocity below the swing bridge, landward (upper) and seaward (lower) of the tidal-intrusion front position.

Figures 4.9a and 4.9b show the results of time-series measurements of salinity and current speed from the bridge on 19.9.78. The passage of the front into the estuary can be seen at about 08:50hrs after which time, both salinity and velocity were near-vertically uniform. After 09:30hrs tidal currents weakened from a maximum of 50cms$^{-1}$ and at 10:50hrs the front passed below the bridge moving seawards. Both the interfacial depth and thickness increased after high water accompanied by a rise of the interface Richardson number Ri from marginal stability at ~11:00hrs to strong stability by 15:00hrs, as a result of the greatly reduced shear. Figures 4.10 to 4.12 (a and b) show results from other occasions under differing conditions of tidal range and river runoff.

Figures 4.10a and b were obtained on 8.9.78 which was a smaller range tide than that on 19.9.78; nevertheless, a front passed the bridge moving upstream at ~11:15hrs. Unfortunately, a broken cable precluded measuring the frontal retreat which occurred at ~12:00hrs and by ~13:00hrs, when the problem had been solved, the two-layer system was already well-established below the bridge. During the remainder of the tidal cycle the interface gradually deepened as the salt intrusion moved down the estuary and, after reaching a maximum at ~16:00hrs, the surface salinity also diminished. Surface velocities reached maximum landward at ~11:20hrs and maximum seaward at ~15:00hrs.

Figures 4.11a and b show results from the neap tide of 10.9.78 and on this occasion a front was not seen to enter the estuary. During the ebb phase, before ~13:00hrs, both surface and bottom salinities decreased although the bed salinity never fell below 30‰. At low water bottom currents reversed and began flooding while surface flow remained seaward. This increased the bottom salinity but allowed the surface salinity to continue falling which set up the maximum vertical gradients at ~14:00hrs. Subsequently increased flood currents reversed the surface flow and eroded the identity of the upper layer but this trend was halted when the surface flow again turned seaward at ~15:45hrs.

Figures on the following eight pages:

Figure 4.9a Time-series measurements of salinity below the swing bridge on 19.9.78 (after Bowyer, 1979).

Figure 4.9b Time-series measurements of velocity below the swing bridge on 19.9.78 (after Bowyer, 1979).

Figure 4.10a Time-series measurements of salinity below the swing bridge on 8.9.78.

Figure 4.10b Time-series measurements of velocity below the swing bridge on 8.9.78.

Figure 4.11a Time-series measurements of salinity below the swing bridge on 12.9.78.

Figure 4.11b Time-series measurements of velocity below the swing bridge on 12.9.78.

Figure 4.12a Time-series measurements of salinity below the swing bridge on 18.9.78.

Figure 4.12b Time-series measurements of velocity below the swing bridge on 18.9.78.

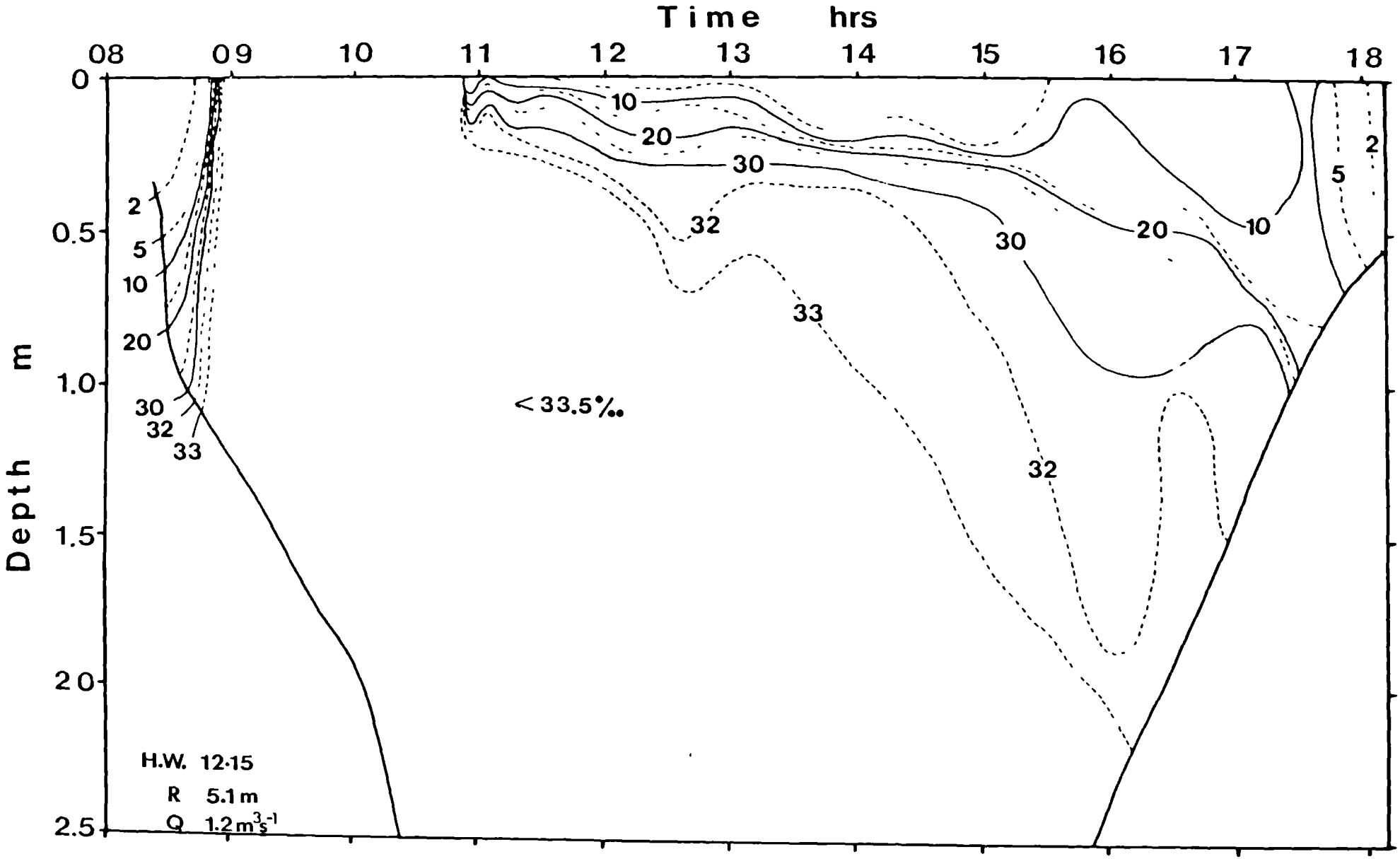
Time hrs
08
09
10
11
12
13
14
15
16
17
18
Depth m
0
0.5
1.0
1.5
2.0
2.5
10
20
30
32
33
2
5
< 33.5‰
H.W. 12·15
R 5.1 m
Q 1.2 m³s⁻¹

4.9a

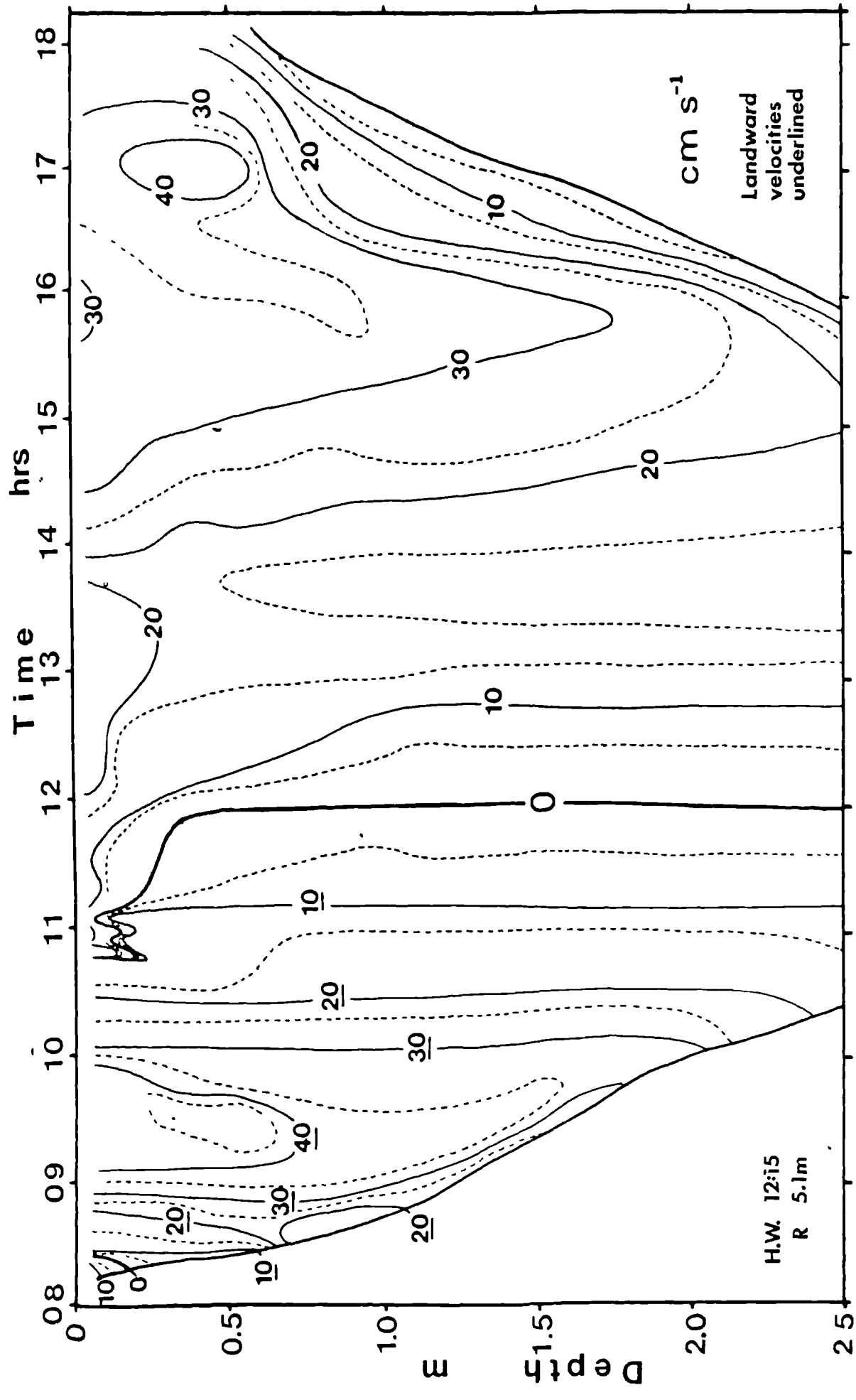
Time hrs
08
09
10
11
12
13
14
15
16
17
18
Depth m
0
0.5
1.0
1.5
2.0
2.5
cm s⁻¹
Landward velocities underlined
H.W. 12:15
R 5.1m

4 9b

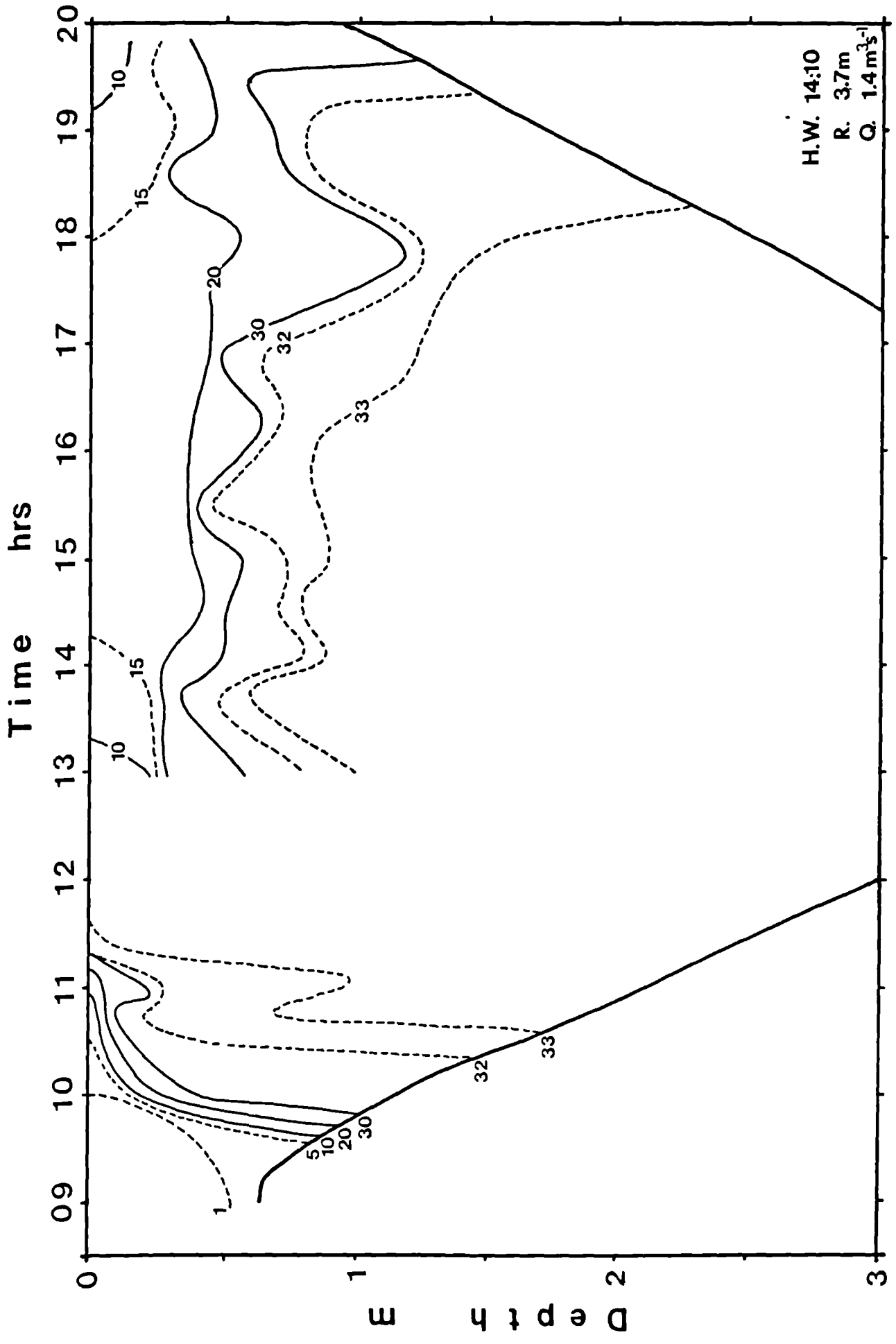
H.W. 14:10
R. 3.7m
Q. 1.4 m³s⁻¹
Time hrs
Depth m
09
10
11
12
13
14
15
16
17
18
19
20
0
1
2
3
1
5
10
15
20
30
32
33

4.10a

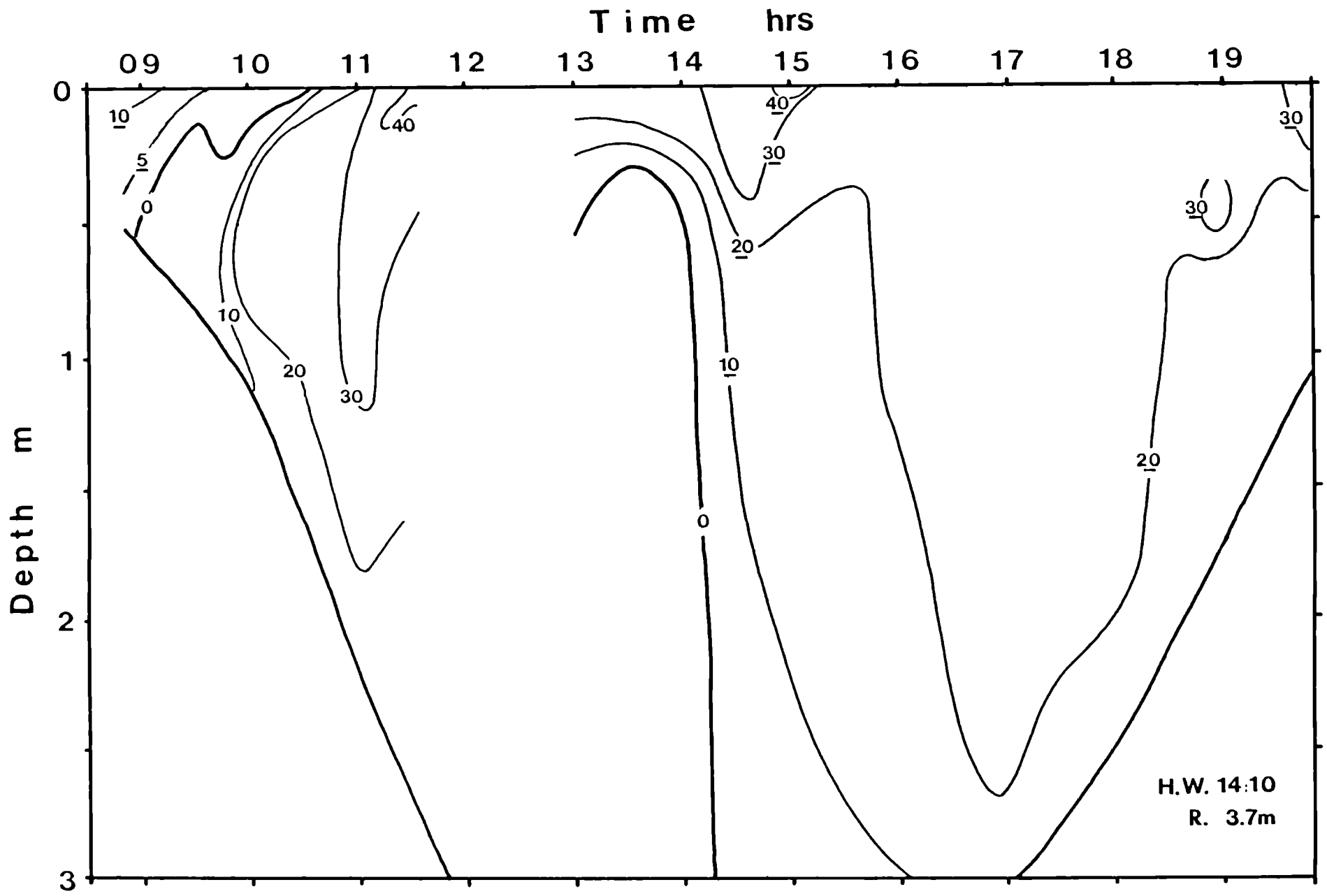
Time hrs
09
10
11
12
13
14
15
16
17
18
19
Depth m
0
1
2
3
10
5
0
40
10
20
30
40
30
20
10
0
30
30
20
H.W. 14:10
R. 3.7m

4.10b

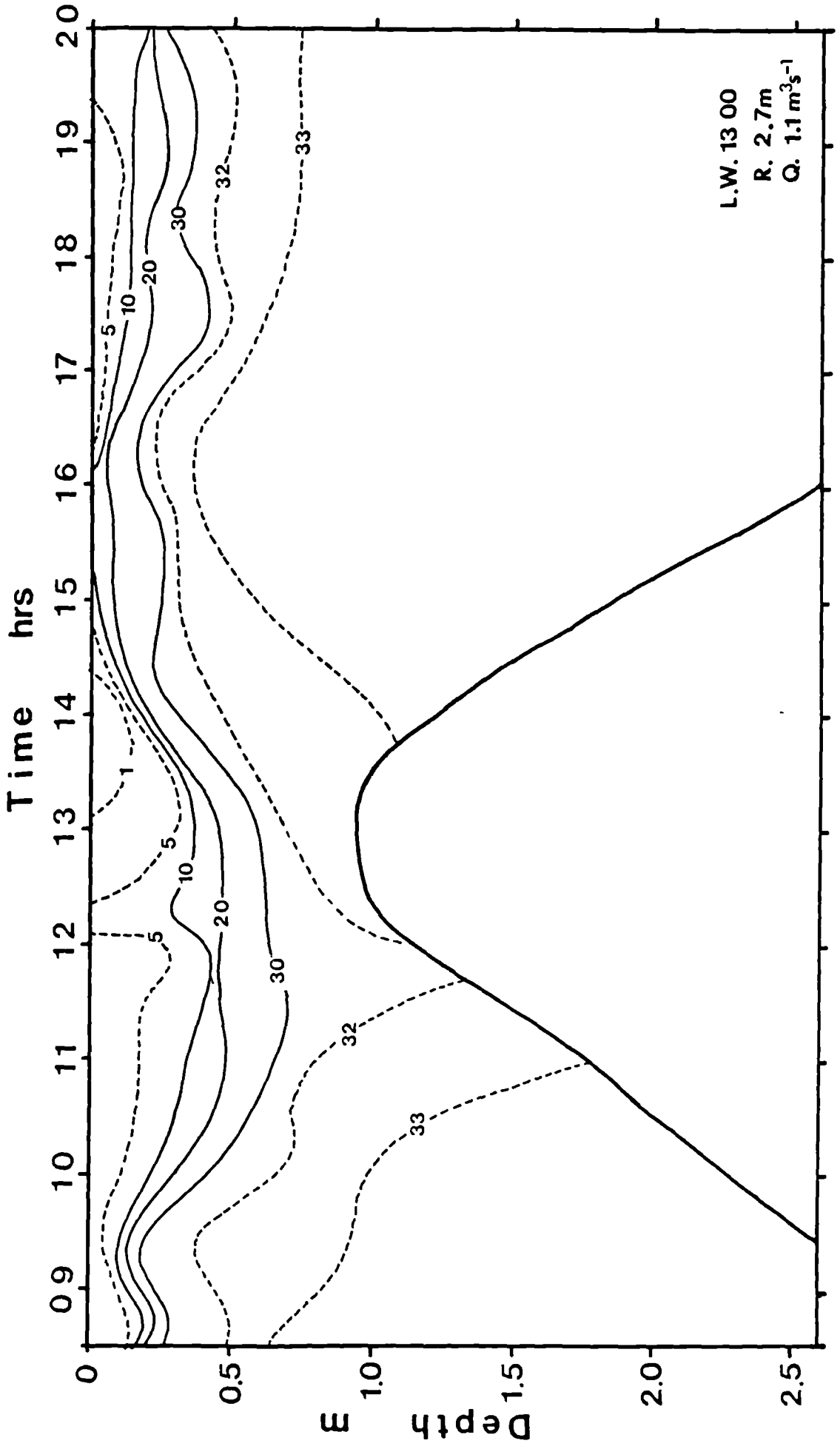
Time hrs
09
10
11
12
13
14
15
16
17
18
19
20
Depth m
0
0.5
1.0
1.5
2.0
2.5
1
5
10
20
30
32
33
L.W. 13 00
R. 2.7m
Q. 1.1 m³s⁻¹

4.11a

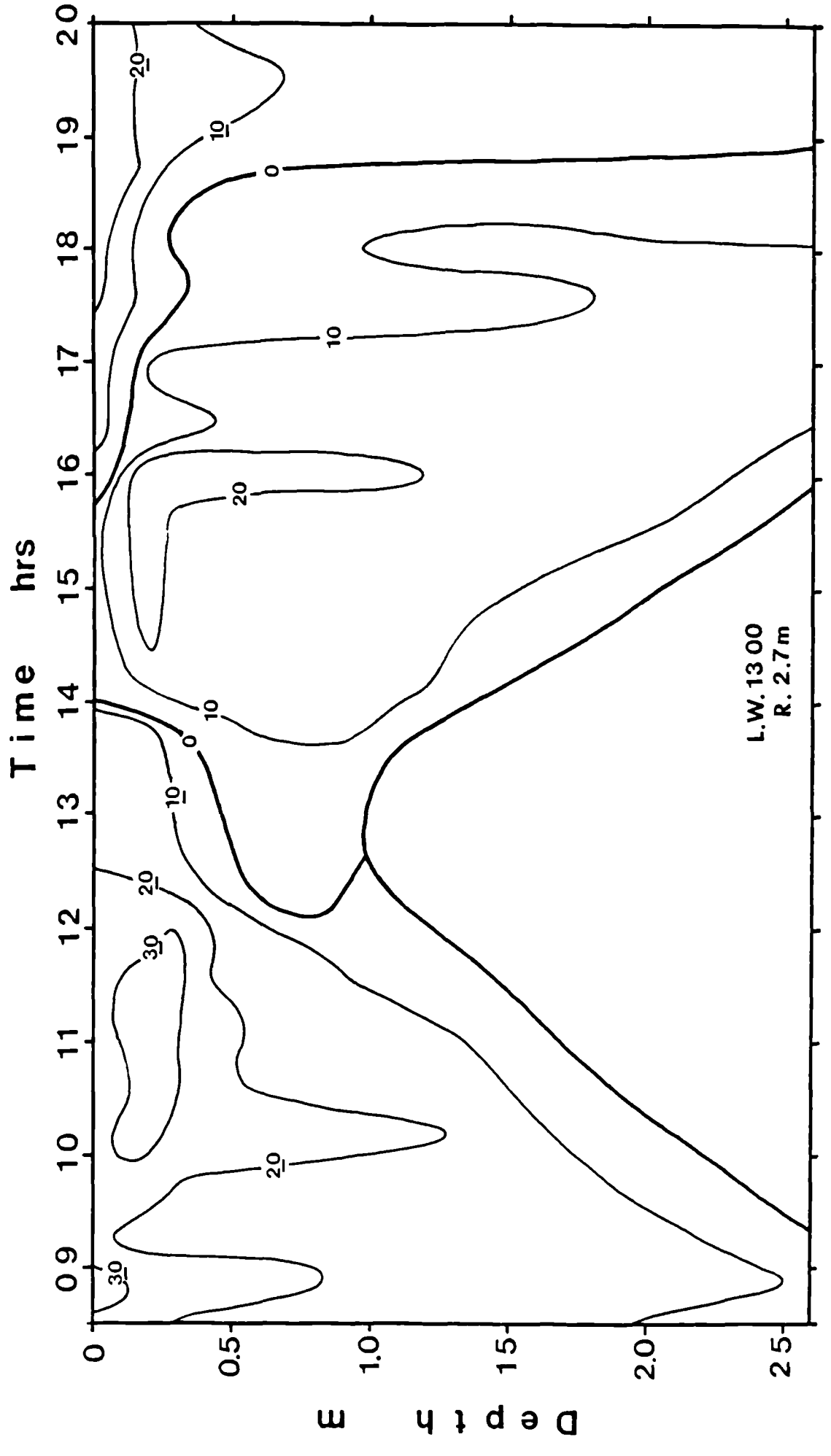
Time hrs
09
10
11
12
13
14
15
16
17
18
19
20
Depth m
0
0.5
1.0
1.5
2.0
2.5
L.W. 13 00
R. 2.7 m
0
10
20
30

4.11b

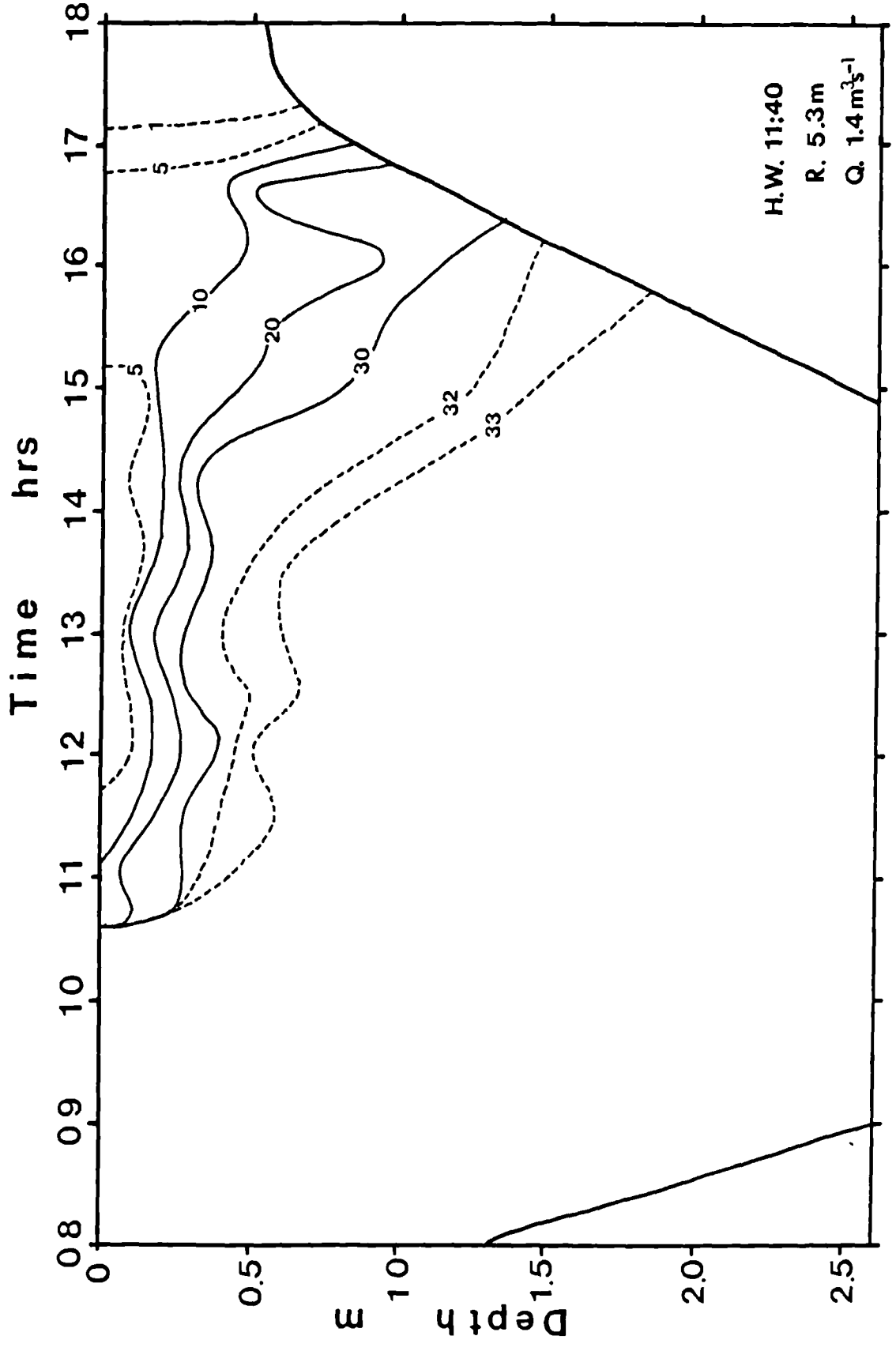
H.W. 11:40
R. 5.3m
Q. 1.4 m³s⁻¹
1
5
10
20
30
32
33
5
Time hrs
08
09
10
11
12
13
14
15
16
17
18
Depth m
0
0.5
1.0
1.5
2.0
2.5

4.12a

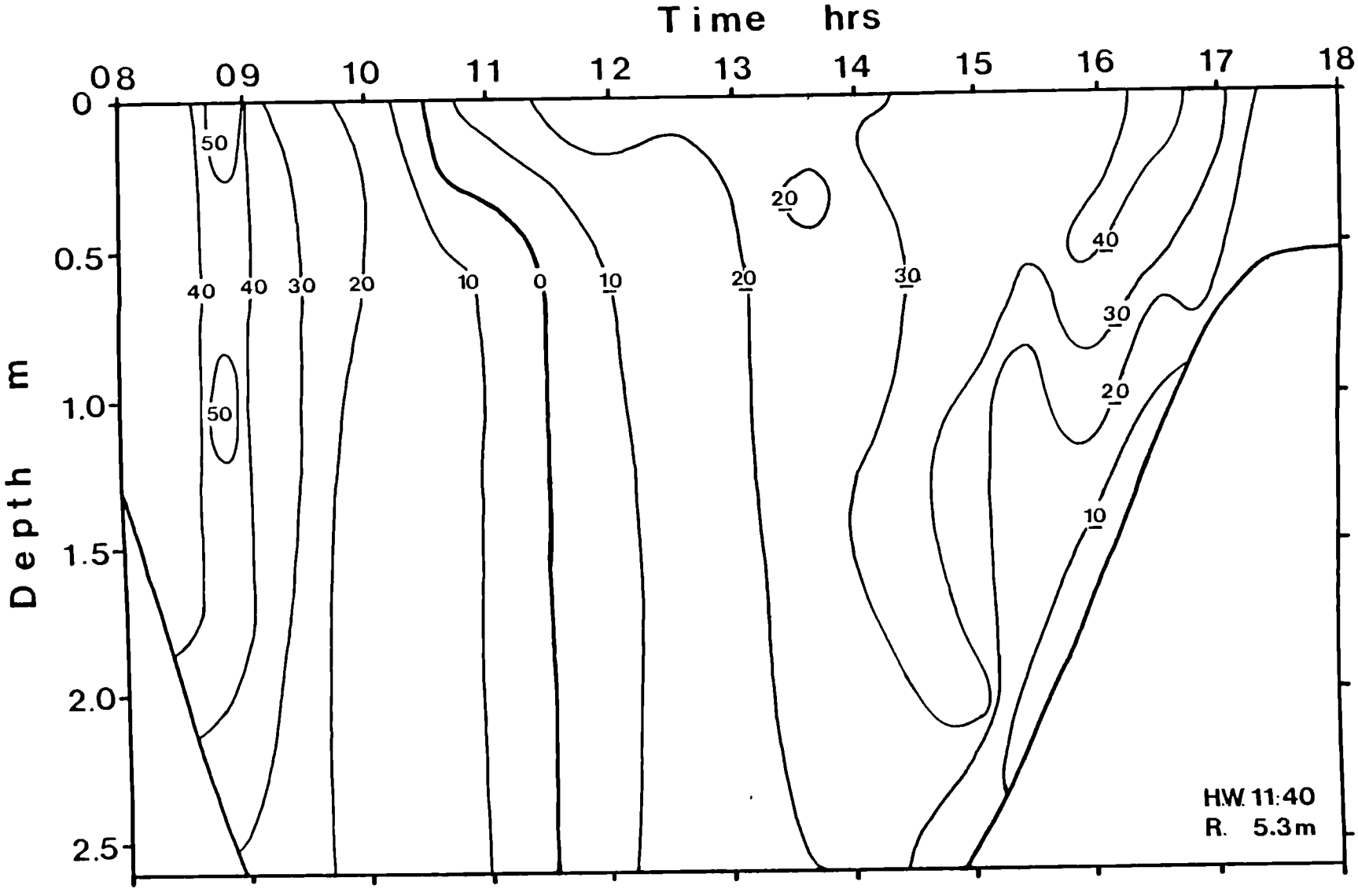
Time hrs
08
09
10
11
12
13
14
15
16
17
18
Depth m
0
0.5
1.0
1.5
2.0
2.5
50
40
40
30
20
10
0
10
20
20
30
40
30
20
10
50
H.W. 11:40
R. 5.3m

4.12b

Finally, in figures 4.12a and b, recordings started after the front had passed upstream of the bridge on this large spring tide. Conditions were near-verically uniform at this time but by ~10:40hrs the front had returned to the seaward side of the bridge. On the ebb the depth of the isohalines increased and the bottom salt intrusion left the estuary relatively smoothly between 16:00hrs and 17:00hrs.

Some important conclusions with respect to the vertical exchange processes may be drawn from the results illustrated in figures 4.9 to 4.12. An upward transfer of salt is indicated by the increasing upper layer salinity recorded at the bridge, particularly after high water. Such an observation suggests a change in the rate of vertical salt transfer. Increasing ebb tidal velocities combined with the diminishing length of the interface reduce the duration of saltwater contact felt by the upper layer in its travel from the head to the bridge. Uncontaminated freshwater meets and overruns the saltwater near the estuary head at approximately high water and takes typically about 2 hours to reach the bridge, (a time which reduces to zero as the bottom saline intrusion retreats). Increasing upper layer salinity during the ebb is thus indicative of a greater mass transfer of salt per unit time. Such a change may be produced by a change in magnitude of the exchange coefficient itself or by an increase in the area of exchange, both of which may be operating. As the bottom saline intrusion retreats, the area of its head (the region of greatest instability and mixing) increases proportionally with the estuary width. The results also indicate the considerable extent to which diffusion reduces the abruptness of the bottom saline intrusion head, thus permitting a freer exchange between the layers.

Figure 4.2 shows the station positions used for longitudinal salinity sections from the Menai Straits to the upper estuary (at intervals of ~100m). Representative profiles are shown in figures 4.13 and 4.14. These exhibit the frontal transition from a well-defined, two-layer structure to the mixed regime and also frontal movement with time. (In the second set the front was prevented from moving downstream by very strong landward winds.) Away from the frontal region, the upper layer depth is approximately constant along the estuary but a characteristic deepening of the

Figure 4.13 Successive longitudinal salinity sections before and after high water on 26.7.78, showing the structure of the frontal layer and the late stages of flood tide frontal movement. (R=3.3m, $Q=2.2m^3s^{-1}$).

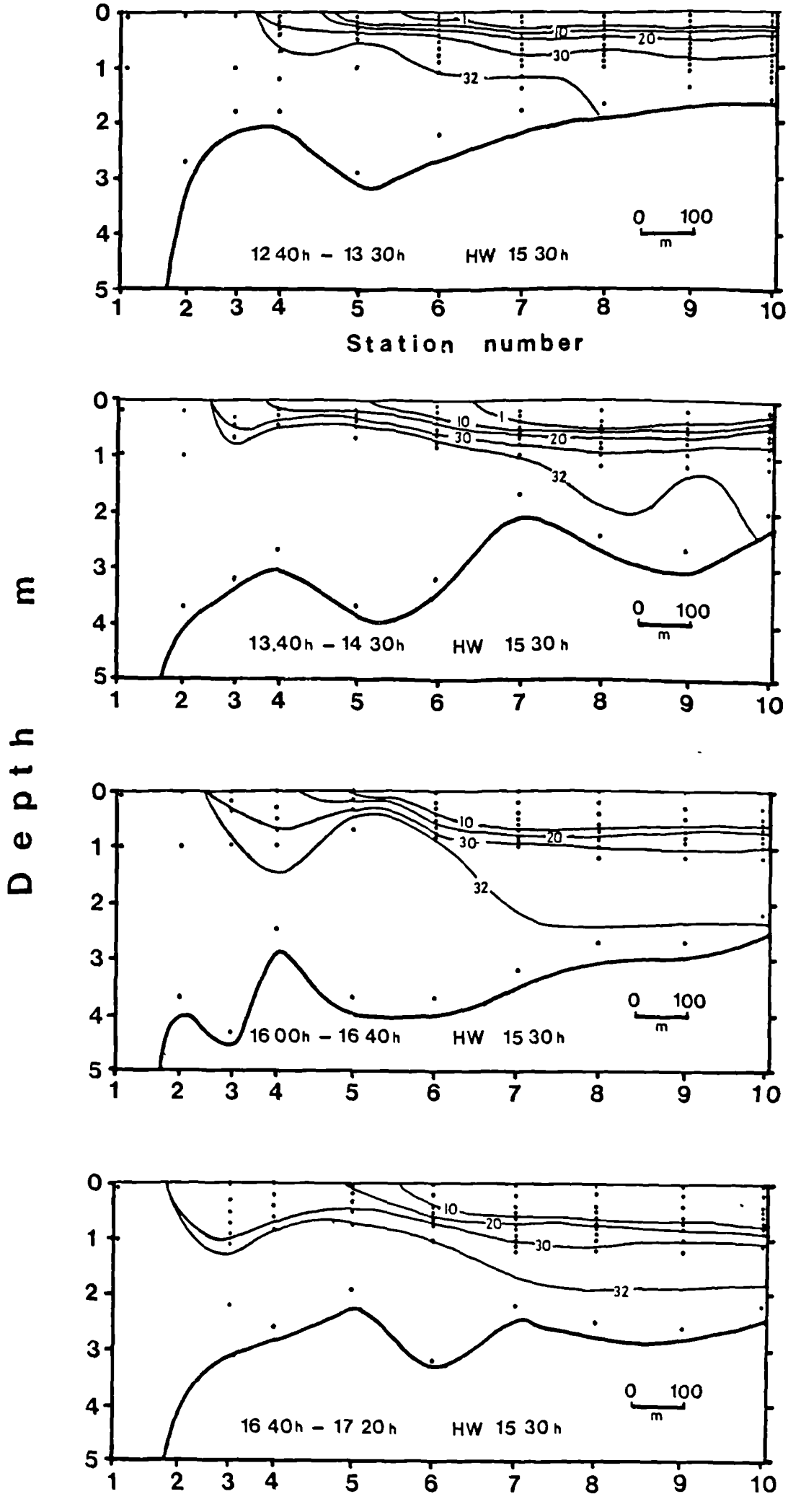
Depth m
Station number
1
10
20
30
32
0 100
m
12 40h – 13 30h HW 15 30h
13.40h – 14 30h HW 15 30h
16 00h – 16 40h HW 15 30h
16 40h – 17 20h HW 15 30h

Figure 4.14 Successive longitudinal salinity sections during the flood tide of 28.4.79 showing the tidal-intrusion front advance phase. The retreat phase, after mid-flood was absent due to the effect of very strong landward winds. (R=5.0m, Q=1.4$m^3s^{-1}$)

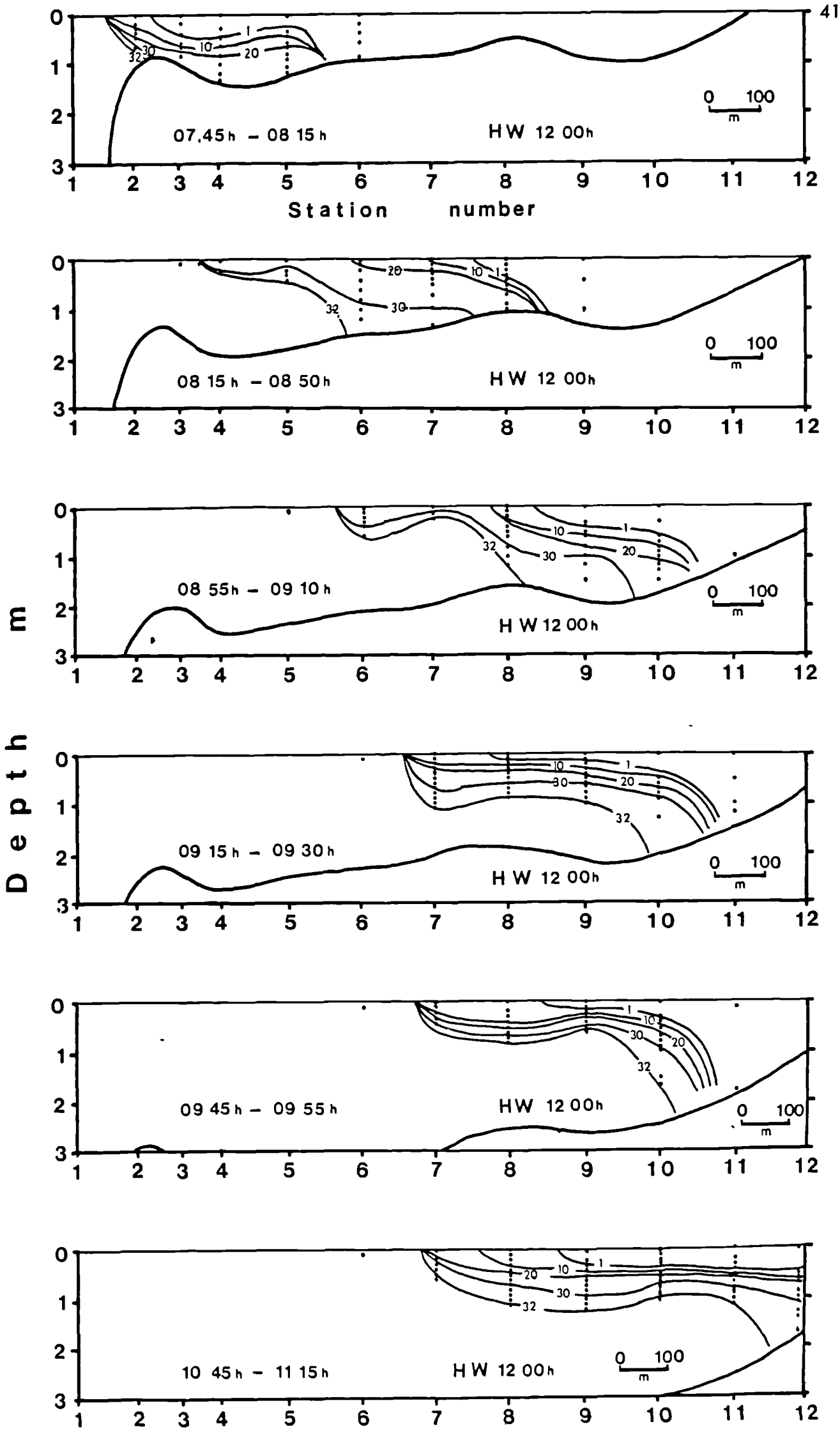
07.45h – 08 15h
HW 12 00h
08 15h – 08 50h
HW 12 00h
08 55h – 09 10h
HW 12 00h
09 15h – 09 30h
HW 12 00h
09 45h – 09 55h
HW 12 00h
10 45h – 11 15h
HW 12 00h
0 100
m
Station number
Depth
m

interface is invariably seen near the front which indicates substantial vertical exchange at the front itself. (A similar feature was observed in the modelled fronts of Kao, Park and Pao 1977.)

Many attempts were made to determine the longitudinal and transverse interfacial structure in a front-based reference frame, by profiling systematically across and around the 'V'. However, the T.I. front travels at speeds within the estuary of up to 12cms$^{-1}$, and the time required for profiles placed relative to the front frustrated most of these efforts. Nevertheless, profiles across the frontal arms did reveal similar abrupt transitions of regime to those indicated in the longitudinal profiles.

To provide a data base for testing a model formulated to explain frontal behaviour, observations of frontal position within the estuary against time were made on numerous occasions. Together with time-lapse cine, these 'tracking' results show disruptions from a smooth progress. Movement into and out of the estuary is sometimes accompanied by 'jumps' in which the front weakens considerably, shortly to be seen re-forming some distance away. The jumps appear to occur at specific regions of the estuary, notably the bend 50m upestuary of the bridge, and thus seem to be associated with the topography, but jumps do not always occur. Typical frontal tracks are shown in figure 4.15. Disruption to the stability of the frontal arms by the frequent passage of power boats is minimal (see figure 4.7) and breaks appear to 'heal' rapidly.

Following the British heat wave of April/May 1980, freshwater runoff from the Seiont was at a very low level (~0.5 cumecs). Tracks of the frontal progress in May showed a frontal intrusion amounting to half of the estuary length. Measurements from the bridge and an intermediate station (an inflatable dinghy at station 8) on one occasion (17.5.80) clearly indicated the upward passage of the front at an early stage of the flooding tide, preceded by a very thin, increasingly salt-contaminated upper layer. After a short-lived stationary period near the landward end of the frontal channel, the retreat phase began. The frontal identity was soon lost, however, and

Figure 4.15 Distance of the front from the estuary head against time during five flood tides:

| | | |
|---|---|---|
| 19.3.80 | R = 5.8m | Q = 4.1m$^3$s$^{-1}$ |
| 16.4.80 | R = 5.6m | Q = 1.4m$^3$s$^{-1}$ |
| 14.5.80 | R = 5.3m | Q = 0.4m$^3$s$^{-1}$ |
| 15.5.80 | R = 5.2m | Q = 0.4m$^3$s$^{-1}$ |
| 23.5.80 | R = 2.2m | Q = 0.5m$^3$s$^{-1}$ |

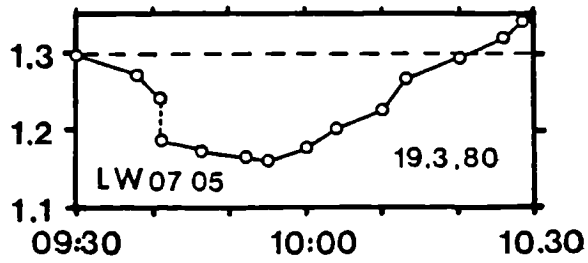
1.3
1.2
1.1
LW 07 05
19.3.80
09:30
10:00
10.30
Time hrs

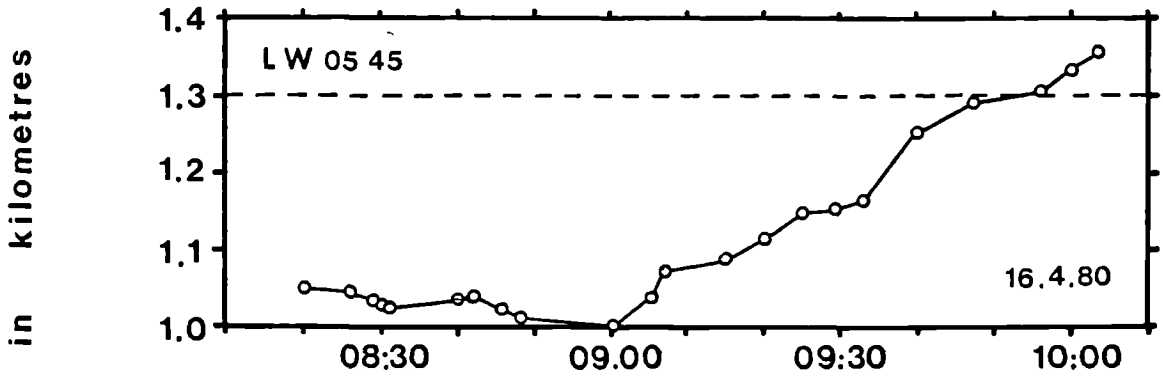
in kilometres
1.4
1.3
1.2
1.1
1.0
LW 05 45
16.4.80
08:30
09.00
09:30
10:00

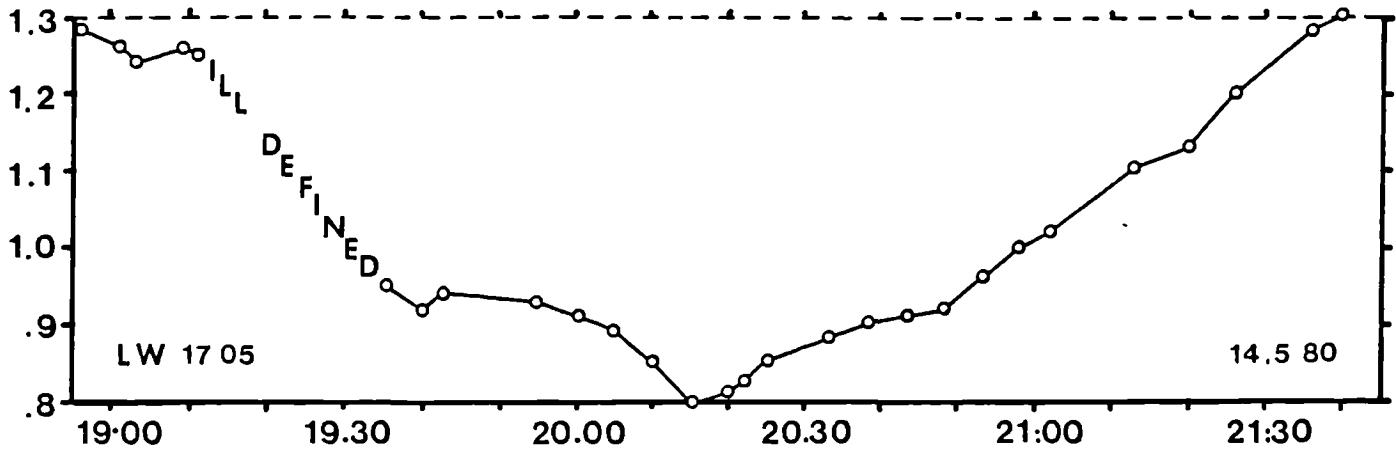
1.3
1.2
1.1
1.0
.9
.8
ILL DEFINED
LW 17 05
14.5 80
19·00
19.30
20.00
20.30
21:00
21:30

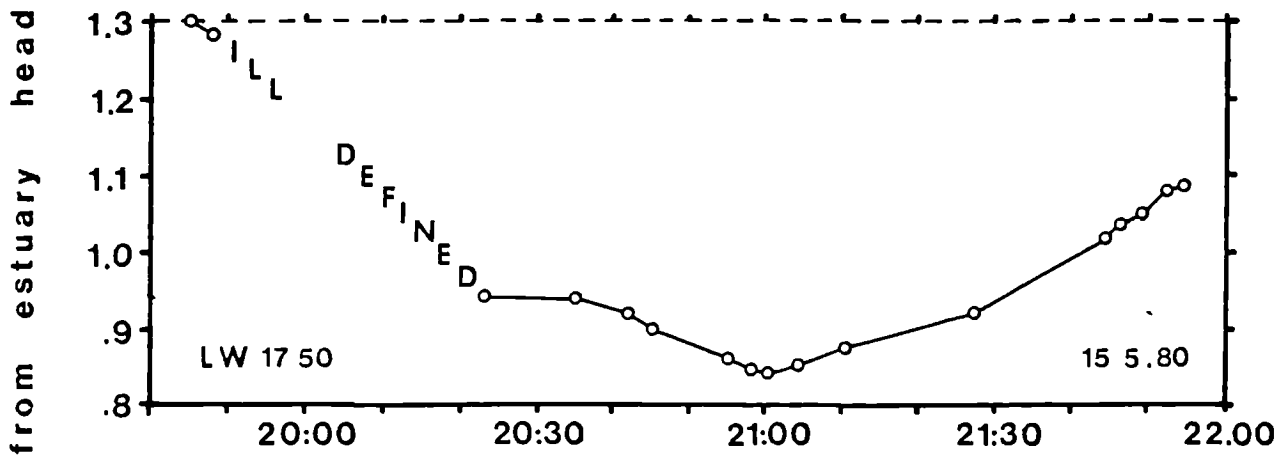
from estuary head
1.3
1.2
1.1
1.0
.9
.8
ILL DEFINED
LW 17 50
15 5.80
20:00
20:30
21:00
21:30
22.00

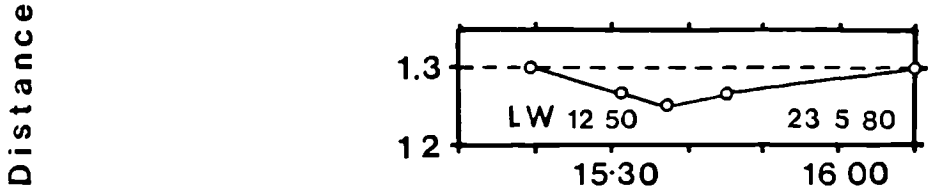
Distance
1.3
1.2
LW 12 50
23 5 80
15·30
16 00

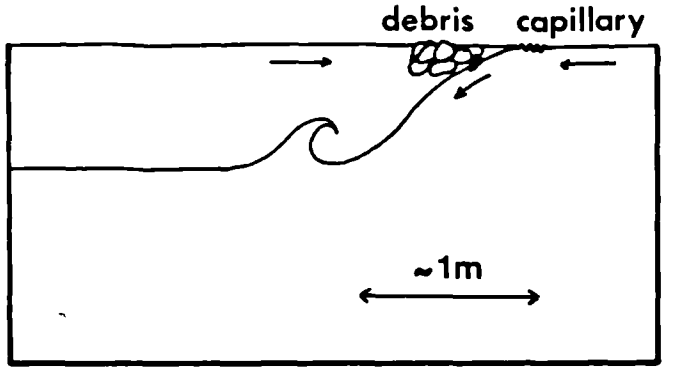


Figure 4.16 Position of capillary waves in relation to the frontal boundary and the debris line.

salinities subsequently recorded at the dinghy and bridge decreased smoothly and gradually with time.

In contrast to the weather of late spring 1980, a period in July 1978 was one of Wales' wettest summers, and runoff was consequently very inflated (~14 cumecs). During daily observations over a fortnight's cycle of tides the front did not, at any time, even approach the mouth of the estuary, although it was always clearly visible as an external plume front.

Finally, before embarking upon a more detailed analysis of these findings, another feature of the observations should be mentioned. The frontal convergence, in both T.I. and plume forms, renders itself visible by drawing buoyant debris towards its surface boundary. The debris is seen slightly toward the two-layered side of the front (figure 4.16) at a position of equilibrium determined by the vertical shear and the vertical extent of the debris. Consequently, it does not truly indicate the position of the surface convergence. On a number of occasions the convergence has been seen as a bow wave (figure 4.17), similar to the series of ripples or capillary waves set up by a fishing line on the upstream side of the flow (Lamb, 1932). Fluorescein dye reveals that the bow wave is the point at which sinking occurs and that the shear layer at the surface diminishes there to minute proportions.

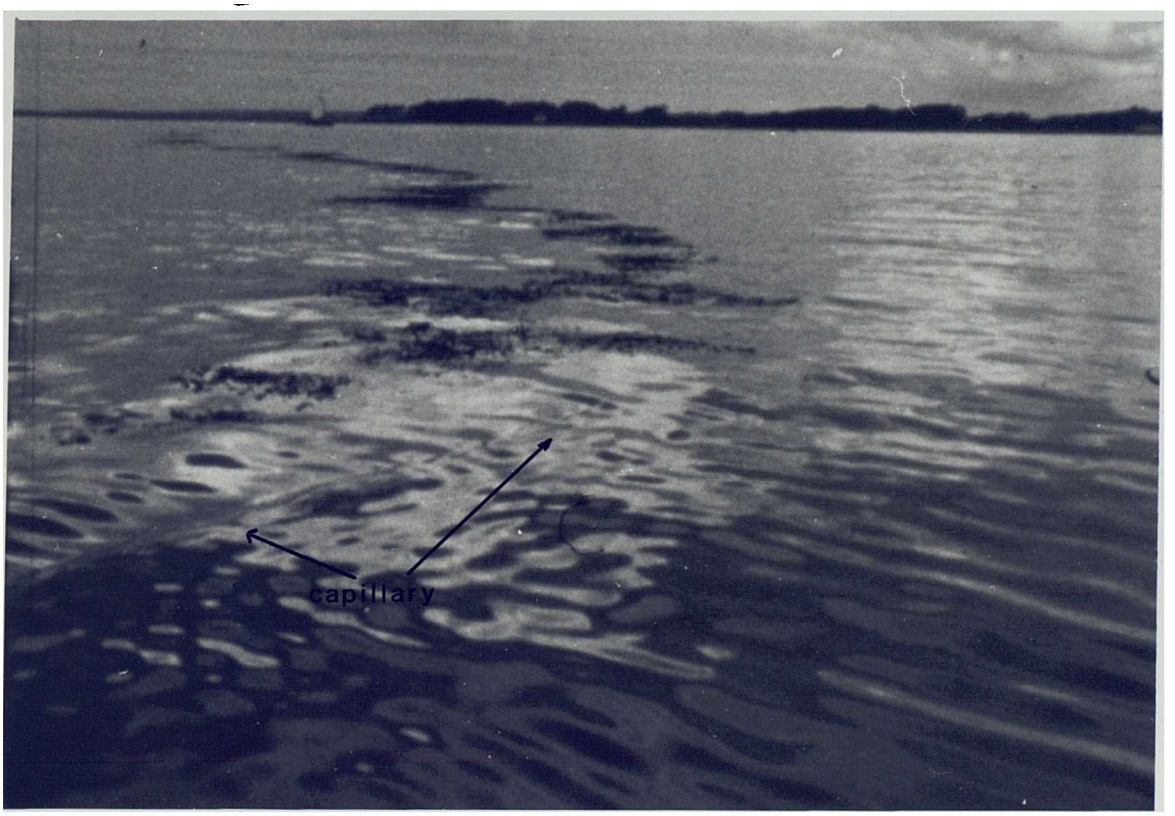


Figure 4.17 Debris line and capillary line at the plume frontal boundary (enlarged cine frame). The estuary is to the left.

## 4.4 APPLICATION OF DENSITY CURRENT THEORY.

We proceed with the assumption that the upper freshwater layer in the Seiont, being so distinctly separated from the lower salt layer, constitutes a natural example of a density current. In the stationary ambient flow of the Straits at high water, the frontal boundary propagates forward at a rate given by equation 2.3. In the event of a non-stationary ambient flow, the front moves within the estuary at the resultant of the two velocities, and may thus be forced into retrograde motion by a flood tidal current of sufficient magnitude. Two effects then come into play tending to slow and eventually arrest the landward progress of the front. The first becomes evident when considering tidal velocities in estuaries, which arise in response to surface level changes at the mouth. Bulk water motions, and tidal velocities, diminish toward the head of an estuary in proportion to the intertidal volume contained on the landward side. The front, being pushed in with the tidal flood, would thus experience slackening currents as it moved toward the head of the estuary. The second effect arises both from increasing upper layer depth as a result of longitudinal shortening, and input from runoff. An increase of density current depth produces a corresponding increase of current velocity.

Upper layer velocities, predicted on the basis of density current theory, interact with the tidal flow to advect the front within the estuary. Knowledge of the bathymetry, tidal range and river runoff proves sufficient to allow prediction of the frontal movement, as will be shown in the following section.

The tide within the estuary responds to the external tide by preserving a near-level water surface at all times. This is because the Seiont estuary reflects almost all of the ingoing tidal energy and responds virtually as a pure standing wave. Communication of upstream events (a level change) travels at $(gH)^{1/2}$, which, in the Seiont (length ~2km, mean depth ~2.5m) requires a time lag of ~10 minutes. For a mean springs tidal cycle, the maximum value of $d\zeta/dt$ ($\sim 3\times10^{-4} ms^{-1}$ would result in a level difference of ~18cm from the mouth to the estuary head. The mean level difference throughout the tidal cycle is <10cm, with the major part to be found in the shallow sections nearer the head.) Furthermore, since the channel flow does

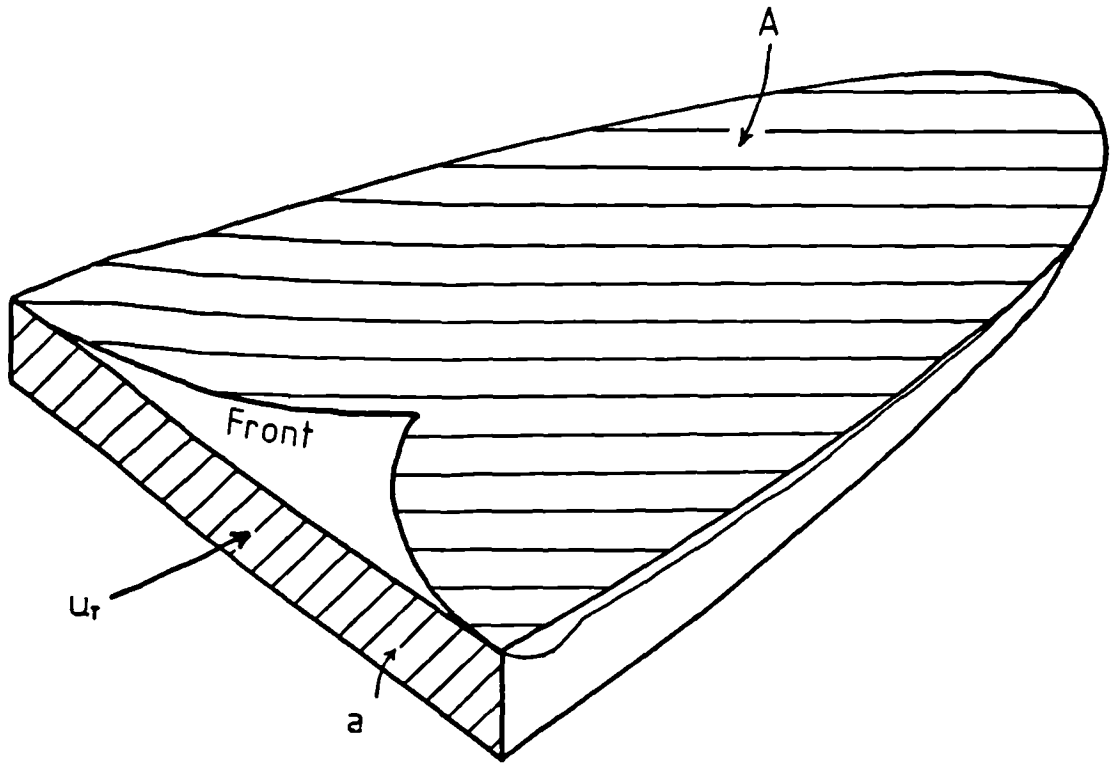


Figure 4.18 Schematic estuary for computation of tidal velocities.

not approach critical conveyance at any time during the flood, little error results from the assumption of a level water surface.

The external tide is taken to be sinusoidal;

$$\xi(t) = -(R/2)\cos\omega t \qquad 4.1$$

where $\xi$ is the external tidal elevation, giving a time rate of change of depth;

$$\frac{d\xi}{dt} = (\omega R/2)\sin\omega t \qquad 4.2$$

In the schematic estuary of figure 4.18, flow through any particular cross-section equates to the upestuary change in volume from continuity. Runoff may be ignored if it is assumed that the fresh layer depth remains approximately constant, thus;

$$\langle u_T(x,t)\rangle\, a(x,t) = A(x,t)\,\frac{d\zeta}{dt} \qquad 4.3$$

where the cross-sectional average tidal velocity $\langle u_T(x,t)\rangle$ flows through the cross sectional area $a(x,t)$ raising the level $\zeta$ over the entire landward surface area $A(x,t)$. With the assumption of a level surface then;

$$\frac{d\zeta}{dt} = \frac{d\xi}{dt} = (\omega R/2)\sin\omega t \qquad 4.4$$

Thus;

$$\langle u_T(x,t)\rangle = (\omega R/2)\sin\omega t \frac{A(x,t)}{a(x,t)} \qquad 4.5$$

From the previous discussion the fresh layer, as a density current, travels at a rate given by equation 2.3;

$$u_d(x,t) = [(1-\phi)(2-\phi)/(1+\phi)]^{1/2} (g'd)^{1/2} \qquad 2.3$$

where $\phi(x,t) = d(t)/H_f(x,t)$, $H_f(x,t)$ is the total water depth at the position of the front and d(t) is the density current or fresh layer depth. At the moment of frontal advance a certain volume of freshwater $V_o$ is present in the estuary which is enclosed by the front and thereafter supplemented by runoff Q. The fresh layer depth is assumed constant along the estuary according to;

$$d(t) = (V_o+Qt)/A_f \qquad 4.6$$

(suffix 'f' refers to quantities measured at the front.)

Observations show that the freshwater depth within the estuary at low water responds to variations in river runoff. The quantity $V_o$ contained at the moment of frontal enclosure is assumed to be linearly dependent on runoff, such that equation 4.6 may be rewritten;

$$d(t) = Q(t+t_o)/A_f \qquad 4.7$$

where $V_o = Qt_o$.

The frontal velocity is the resultant of both tidal ($u_T$) and density current ($u_d$) velocities measured at the front. After substitution from eq 4.7;

$$\frac{dx_f}{dt} = \left[\frac{(1-\phi)(2-\phi)}{(1+\phi)}\right]^{1/2} \left[\frac{g'Q(t+t_o)}{A_f}\right]^{1/2} - (\omega R/2)\sin\omega t \frac{A_f}{a_f} \qquad 4.8$$

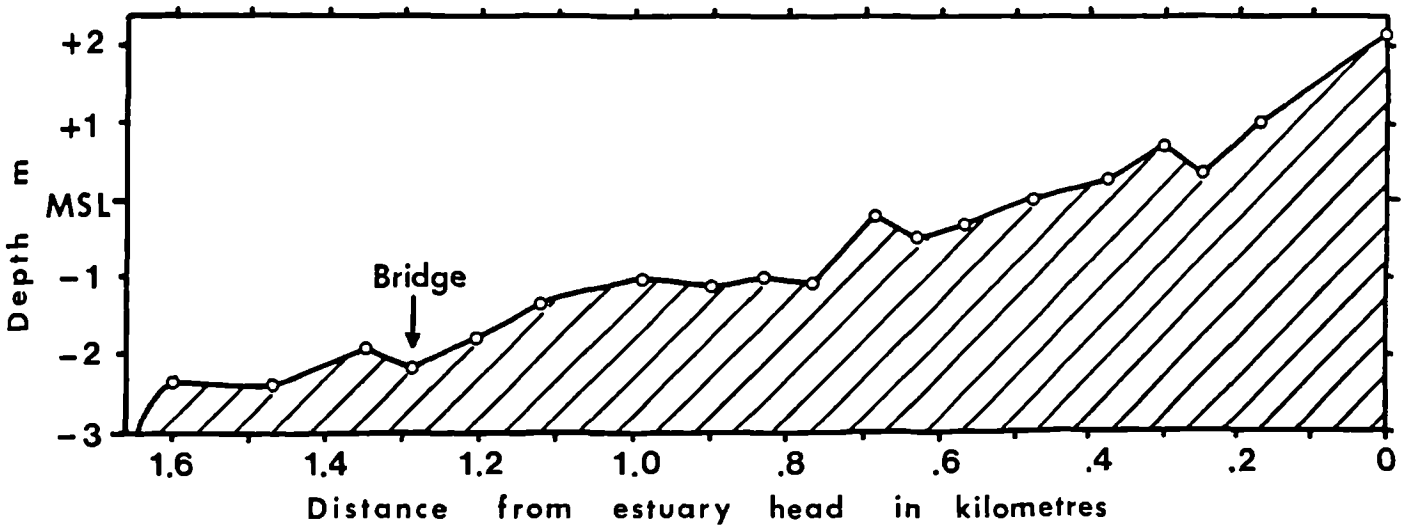


Figure 4.19 Longitudinal section along the line of maximum cross-sectional depth in the Seiont estuary.

At the time of maximum flood currents ($t_c$=T/4) when $\sin\omega t_c$=1, the frontal advance ceases and is followed shortly by a retreat phase. (On the 26 occasions when a note was made of the location and time of the frontal intrusion limit, the value of $\sin\omega t_c$ was always greater than 0.97.) Applying this condition to equation 4.8, making the further assumption that $\phi$ the fractional depth of the density current is approximately constant at the upestuary limit on all occasions, and rearranging gives;

$$A_f^3 = \frac{4g'k}{\omega^2} a_f^2 (t + T/4) \frac{Q}{R^2} \qquad 4.9$$

where k is $\sim[(1-\phi)(2-\phi)/(1+\phi)]^{1/2}$

If $x_f$ represents the frontal position, then $A_f$ may be replaced according to;

$$A_f = x_f \bar{b} \qquad 4.10$$

provided that the estuary width does not vary greatly from its mean value $\bar{b}$. The origin of x is taken to be the high water limit of salt intrusion and, as such, varies with tidal range. However, near the head the estuary is narrow and the bed slope is sufficiently large (figure 4.19) that the assumption of a fixed origin is valid. Using equation 4.10 in 4.9 gives;

$$x_c^3 = \frac{4g'k}{\omega^2} (t_o + T/4) \frac{a_f^2}{\bar{b}^3} \frac{Q}{R^2} \qquad 4.11$$

where $x_c$ represents the upestuary limit of frontal intrusion.

Equation 4.11 states that the limiting position $x_c$ is controlled by some geometric factors, tidal range and river runoff. If changes of $a_f$ and $\bar{b}$ with position in the estuary may be ignored, then a relationship of the form;

$$x_c \propto (Q/R^2)^{1/3} \qquad 4.12$$

may be tested.

That the relationship of equation 4.12 represents a useful model of frontal movement can be seen in figure 4.20, showing a plot of the observed frontal limit on differing occasions, against $(Q/R^2)^{1/3}$. Departure from the inferred behaviour of equation 4.12 occurs for the portion beyond $x_c$=1.4km. For these points the front remains in the outer part of the estuary where the assumptions of the model break down.

Figure 4.20 Observed frontal intrusion limits related to the derived parameter $(Q/R^2)^{1/3}$

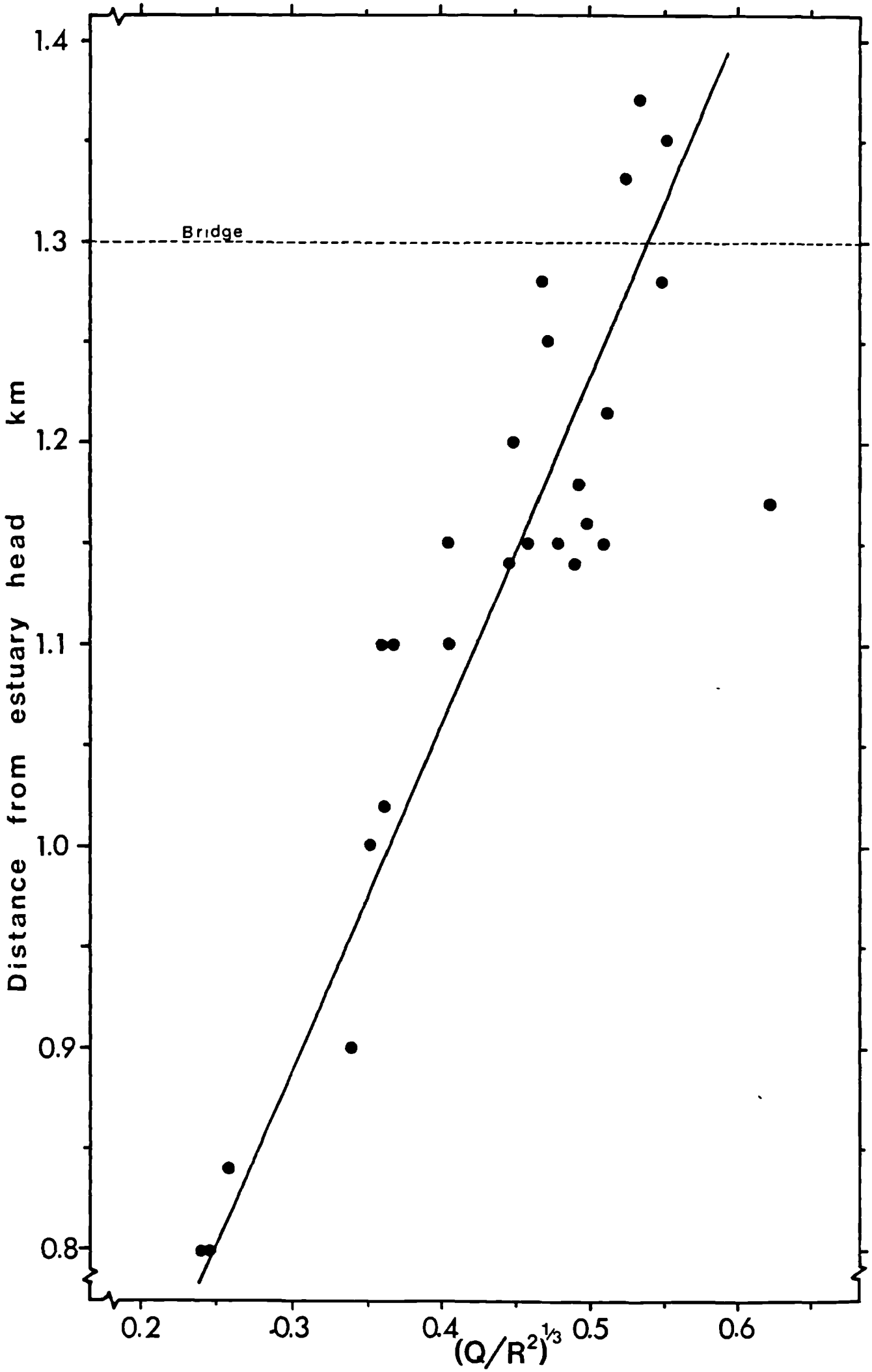
1.4
1.3
1.2
1.1
1.0
0.9
0.8
Bridge
Distance from estuary head km
0.2
0.3
0.4
0.5
0.6
$(Q/R^2)^{1/3}$

## 4.5 NUMERICAL MODEL OF FRONTAL MOVEMENT.

Making the assumption that frontal movement in the Seiont reflects an imbalance of tidal and density current velocities at the front, lays the basis for a time-dependent model of frontal behaviour. A two-dimensional model (longitudinal x and vertical z) was constructed around the bulk parameters tidal range and river runoff and, when adjusted to its optimum reproduction of observed behaviour, was used to learn of;

i) the instantaneous variation of quantities at the front throughout the tidal cycle.

ii) the effects on the intrusion limit of varying individually either river runoff or tidal range.

The numerical approach described below, in contrast to the analytical result of the previous section, takes account of;

i) the non-sinusoidal nature of tidal velocity, by computing velocities at the front from knowledge of the estuarine bathymetry.

ii) the fractional depth of the density current in determining $u_d$.

Taking the simplest view we allow no gains to, or losses from the fresh layer and also no input from runoff. At low water the upper layer contains a fixed volume of freshwater which remains constant throughout the flood tide. We thus arrive at the single free parameter employed in optimising the model to the observed behaviour; i.e. the estuary fluid volume (F) at low water. The estuary is normally salt-free at low water and observations show that the fluid volume contained at one instant reflects, in some way, the level of runoff. The relationship is assumed to be linear

and of the form;

$$F = M + NQ \qquad 4.13$$

where M and N are constants and Q is runoff. The two quantities, tidal range and runoff are therefore responsible for determining frontal movement through their effects on tidal velocities and F respectively.

A comprehensive bathymetry of the estuary was constructed by interpolation from the field survey data. Depths relative to mean sea level at ten equally spaced positions along each of sixty-four transverse sections (at 25m intervals) were found from the results shown in figure 4.3. Cross-sectional mean tidal velocities were calculated from transport requirements on the basis of maintaining a level, but sinusoidally varying surface;

$$\zeta = -(R/2)\cos\omega t \qquad 4.14$$

At a given cross-section and time, velocities were found by equating the estuary volume increment on the landward side to the flux required through the given area, and in those sections upstream of the frontal position allowance was also made for the presence of the freshwater layer. A comparison between computed and measured tidal velocities is shown in figure 4.21 for two positions in the estuary (stations 6 and 8 of figure 4.2). The graphs show similar trends but, due to the non-uniformity of flow in the prototype channel, measured values were significantly elevated during periods when the total boundary stress was large.

Density current velocities were found from;

$$u_d = [(1-\phi)(2-\phi)/(1+\phi)]^{1/2} (g'd)^{1/2} \qquad 2.3$$

where d is the depth of the freshwater layer, $g'=0.2$ corresponding to a layer contrast of 30‰ salinity and the fractional depth was evaluated at the frontal position. The theoretical result of equation 2.3 remains valid as the rate of advance of a physical density current even though mixing losses induce a faster freshwater current supplying the head (Britter and Simpson, 1978). The

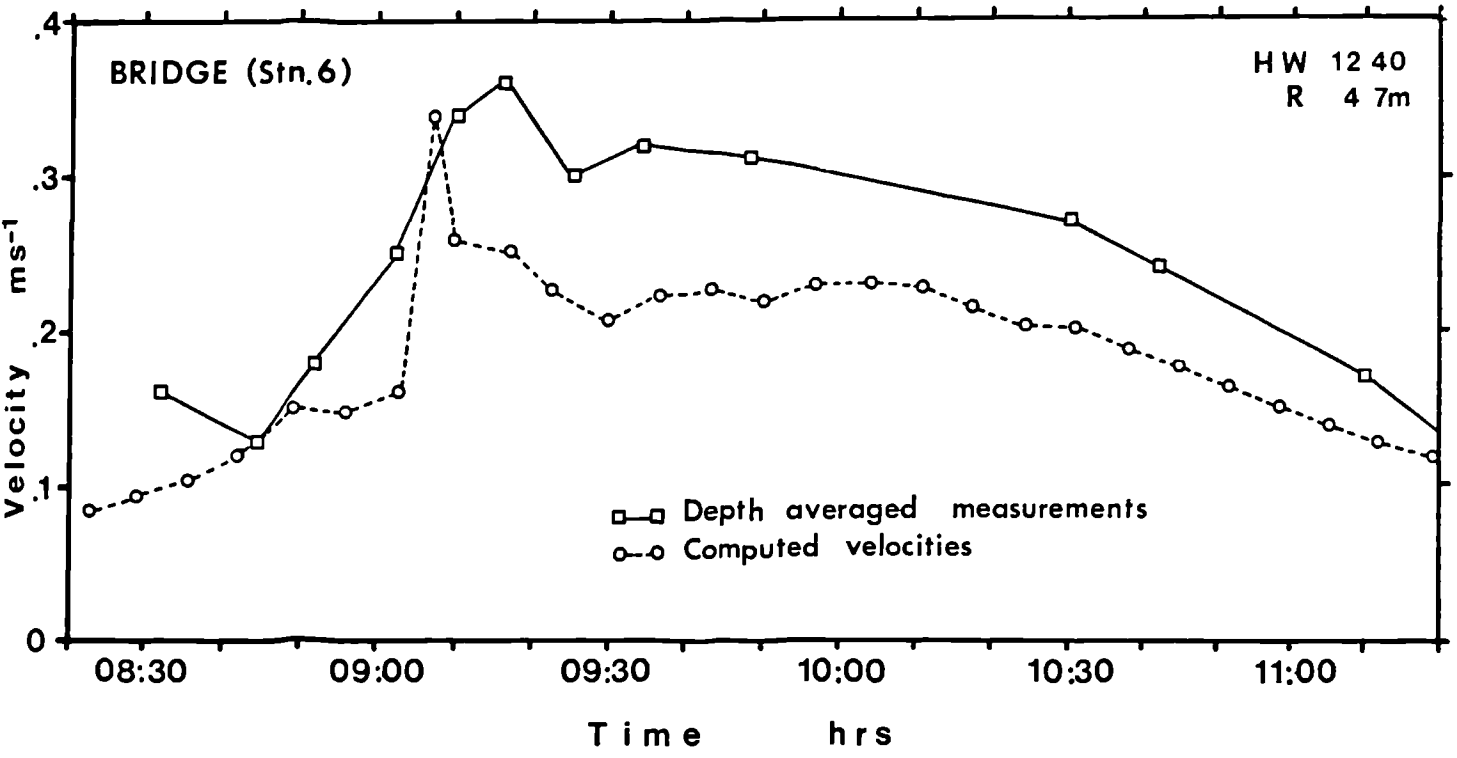


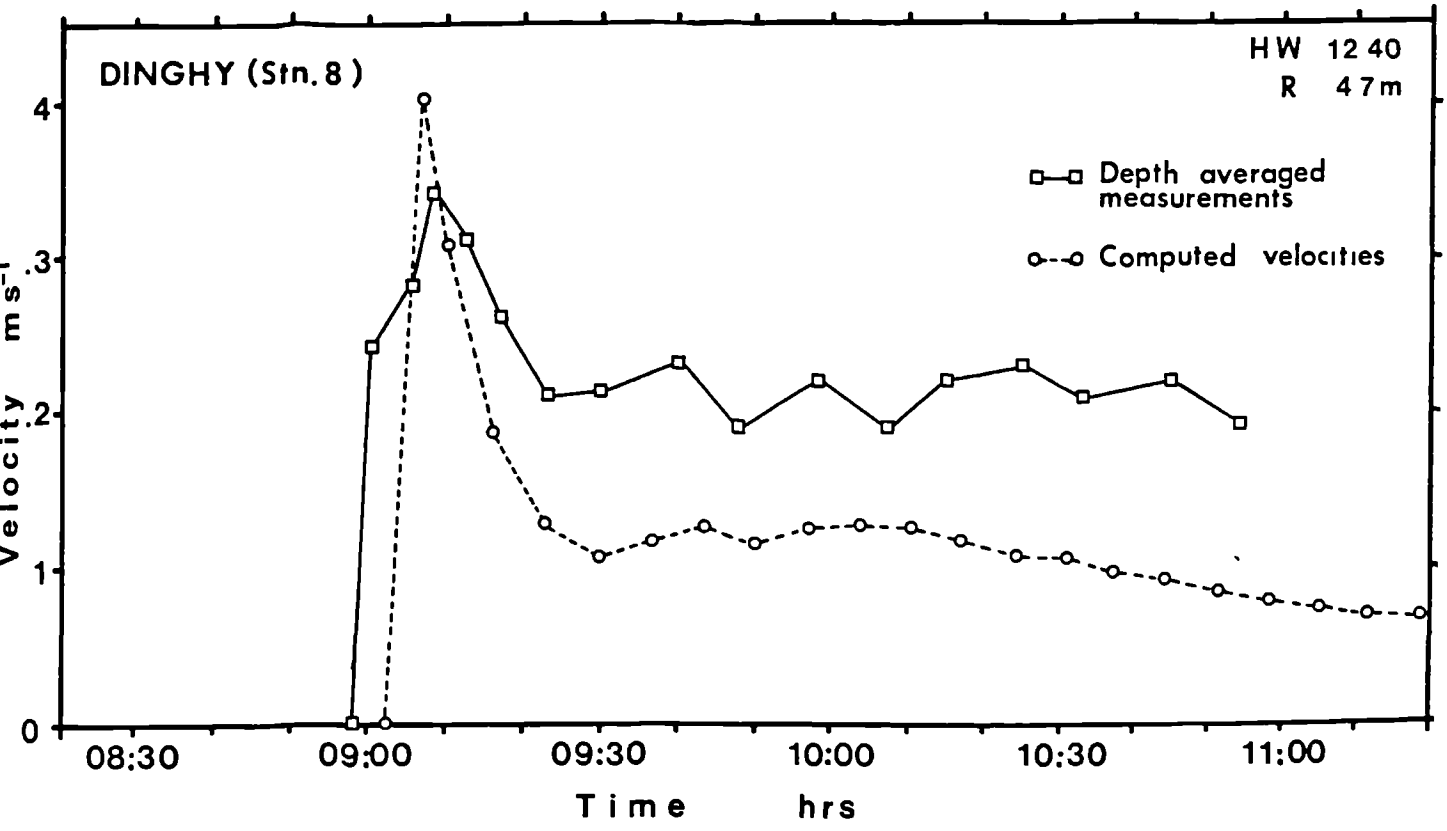


Figure 4.21 Computed and measured tidal velocities at two positions in the estuary for the conditions of 17.5.80 (R=4.7m, $Q=0.3m^3s^{-1}$). See figure 4.2 for station positions.

freshwater depth, which was assumed longitudinally constant, was determined by the initial freshwater volume F, a representative mean estuary width of 80m, and the position of the front, through its shortening and lengthening effect on the layer.

At each time step both the tidal velocity at the front and the density current velocity were evaluated, leading to the frontal velocity $u_f$;

$$u_f = u_d - u_T \qquad 4.15$$

The front was advected according to equation 4.15 throughout a time step of 150s to a new position at which all quantities were re-evaluated.

Observations provided 26 data points relating the upstream limit of tidal movement ($x_c$) to specific conditions of tidal range and river discharge. The model was considered to be optimised when the quantity $\kappa$, where;

$$\kappa = \sum_{i=1}^{26} [x_c(\text{observed}) - x_c(\text{model})]^2 \qquad 4.16$$

was reduced to a minimum which was achieved by adjustment of the low water volume F. The following procedure was used to find the optimum values of the constants M and N in equation 4.15: $\kappa$ was minimised at a particular M by varying N. A series of such operations indicated that the best fit to the observations (i.e. least $\kappa$ ) was achieved with $M=425m^3$ (see figure 4.22) and N=2125s. To illustrate the contribution of the proportionality constant N to this optimisation, figure 4.23 shows $\kappa$ vs. N with $M=425m^3$. $\kappa$ expresses one form of correlation (a least squares) between the observed and predicted intrusion limits; the least squares gradient of $x_c(\text{model})/x_c(\text{observed})$ expresses another. Included in figure 4.23 is the value of this gradient which, at the optimum choices of M and N, has a value of unity. Figure 4.24 gives the plot of $x_c(\text{model})$ against $x_c(\text{observed})$ for the optimum low water volume;

$$F = 425 + 2125Q \qquad 4.17$$

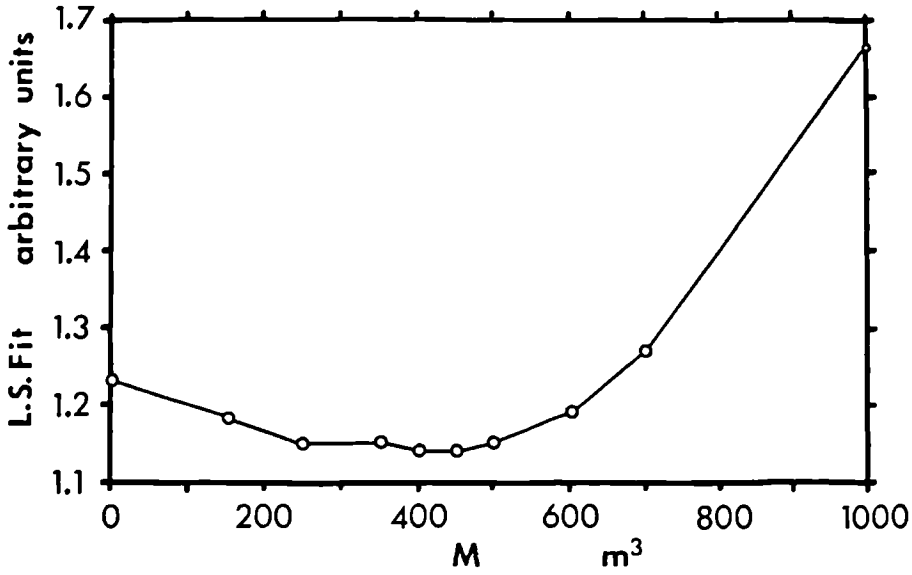


Figure 4.22 Model optimisation (i.e. minimum $\kappa$) for a particular value of M (achieved by varying N).

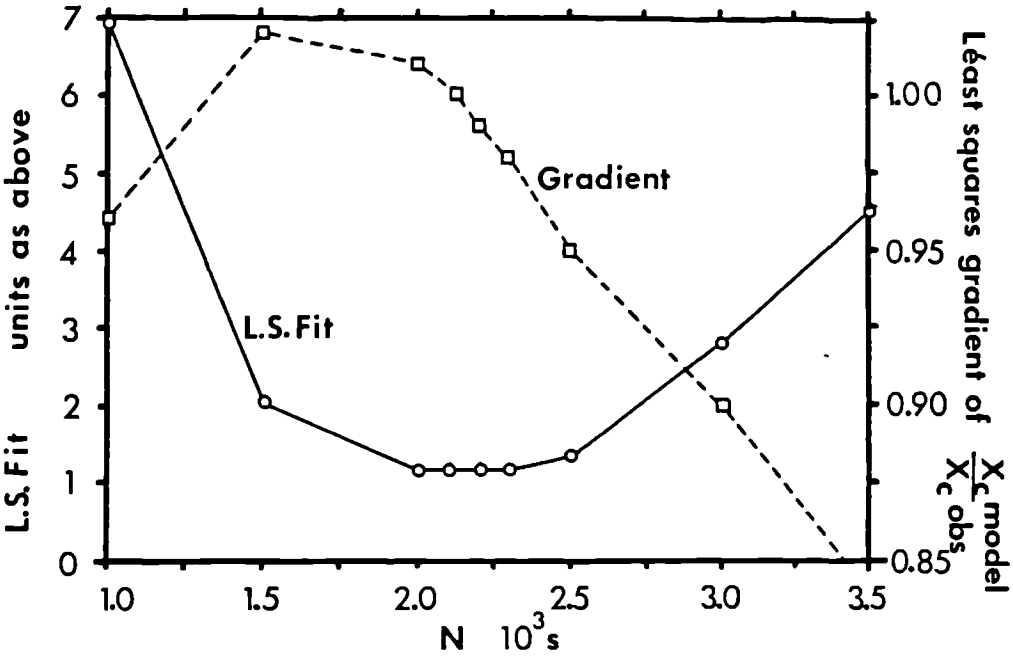


Figure 4.23 Model optimisation for a particular value of N (with M constant at 425m³). Also shown is the value of the least squares gradient of $x_c$(model)/$x_c$(observed) as a function of N.

(Uncertainties in estimating the position of the front account for a horizontal error of ±10m.) Subsequent computations were made with F specified as above.

Figures 4.25 and 4.26 give model values of tidal velocity at the front $u_T$, upper layer velocity $u_d$, predicted frontal position $x_f$ and observed frontal position for the conditions of 16.4.80 (R=5.7m, Q=1.4m³s⁻¹) and 14.5.80 (R=5.3m, q=0.4m³s⁻¹) respectively. The erratic nature of tidal velocity highlights the inadequacy of a sinusoidal assumption and is accentuated because it refers to a

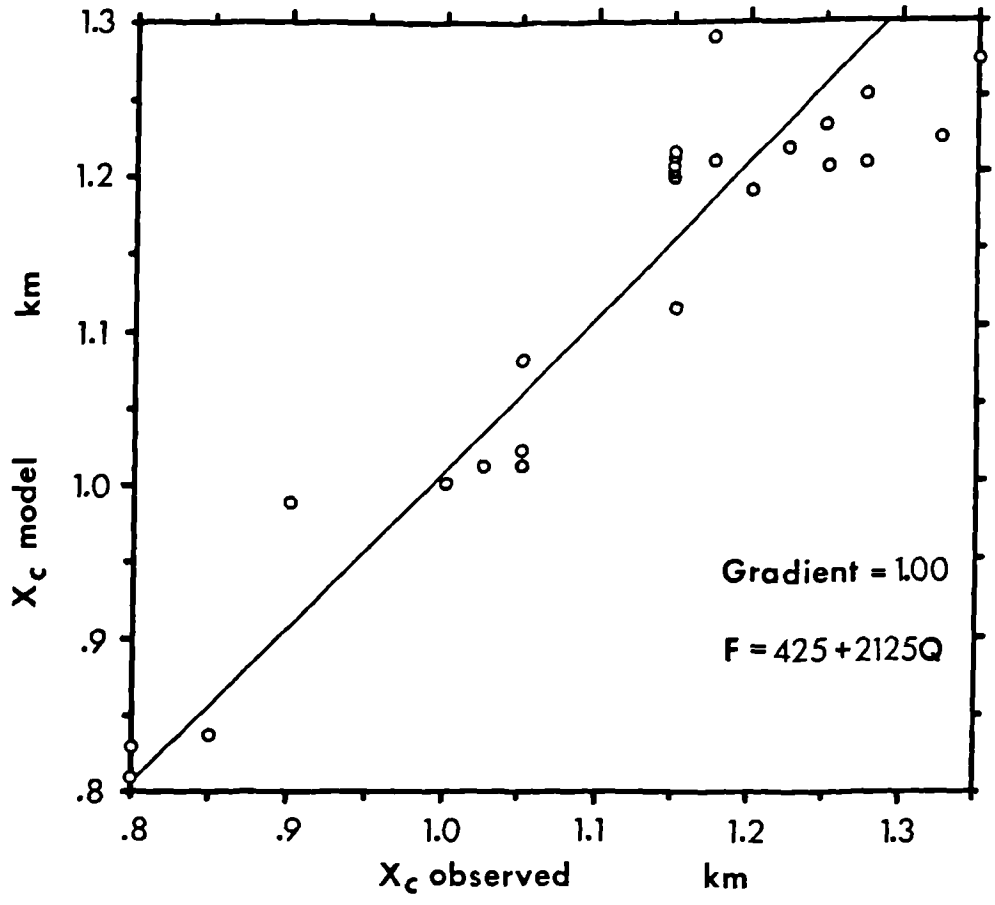


Figure 4.24 Model predictions of the frontal intrusion limit against the observed intrusion limit.

mobile position in the estuary. The large oscillations of tidal velocity, particularly in the early part of the flood tide, may be attributed to using a time step length of more than a few seconds. The sharp rise of $u_d$, also in the initial stages, reflects an an equally sharp decrease in fractional depth at the front.

When $u_d \sim u_T$ i.e. $u_f$ is large, frontal adjustments are fast, causing a substantial compression of the upper layer which may be seen as larger (though still small) gradients of $u_d$.

Comparing the observed and predicted frontal tracks, we note that the prototype front experiences considerably larger accelerations than the model front. The slow response of the model is clearly inadequate for the retreat phase. This aspect of the model will be discussed in chapter 9.

Figure 4.25 Model predictions of: tidal velocity at the frontal position $u_T$, density current velocity (in a stationary ambient fluid) $u_d$, and frontal position, together with the observed frontal position on 16.4.80.

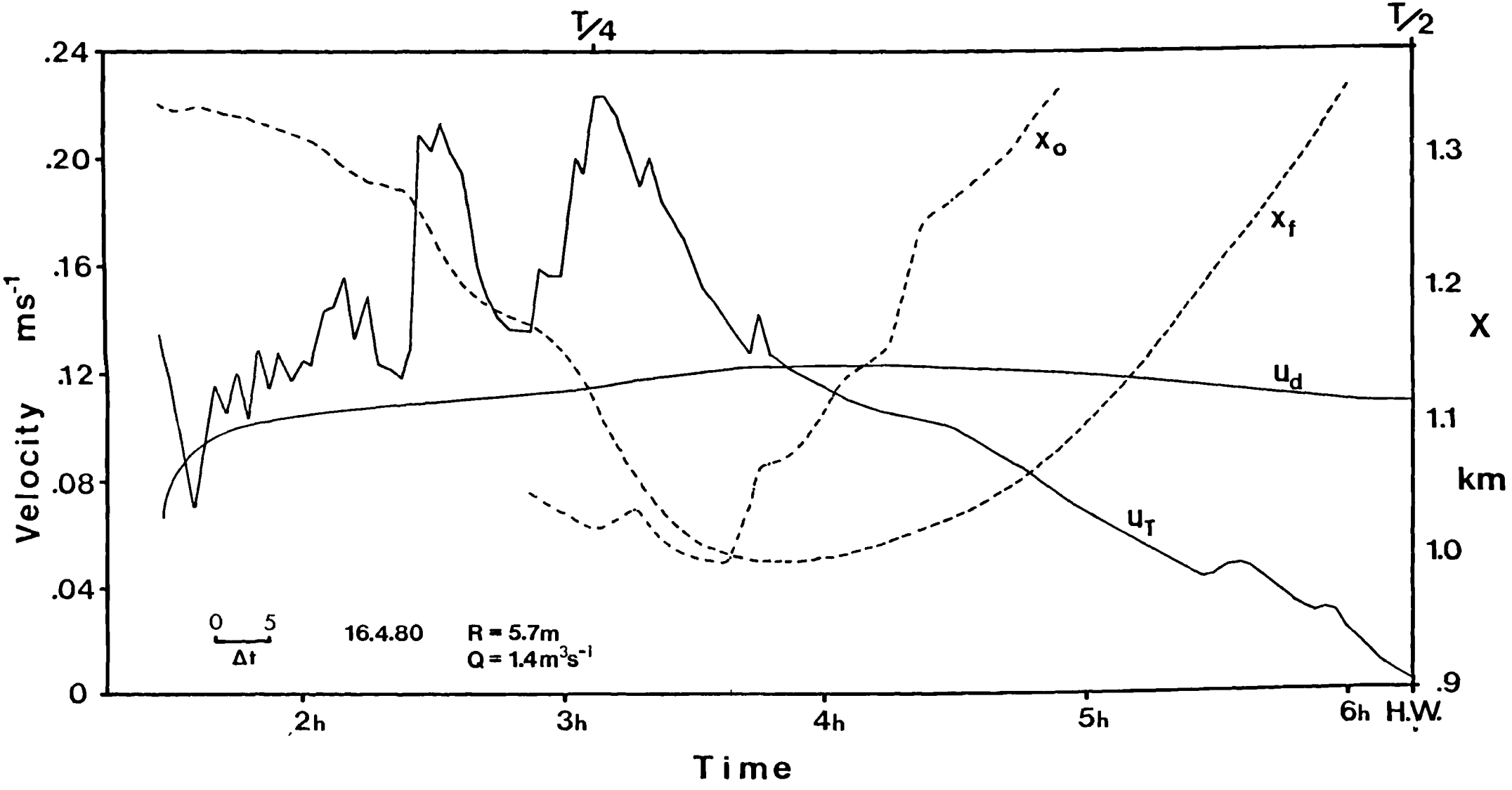
T/4
T/2
.24
.20
.16
.12
.08
.04
0
Velocity ms-1
1.3
1.2
1.1
1.0
.9
X
km
xo
xf
ud
uT
0 5
Δt
16.4.80
R = 5.7m
Q = 1.4m3s-1
2h
3h
4h
5h
6h H.W.
Time

Figure 4.26 Model predictions of: tidal velocity at the frontal position $u_T$, density current velocity (in a stationary ambient fluid) $u_d$, and frontal position, together with the observed frontal position on 14.5.80.

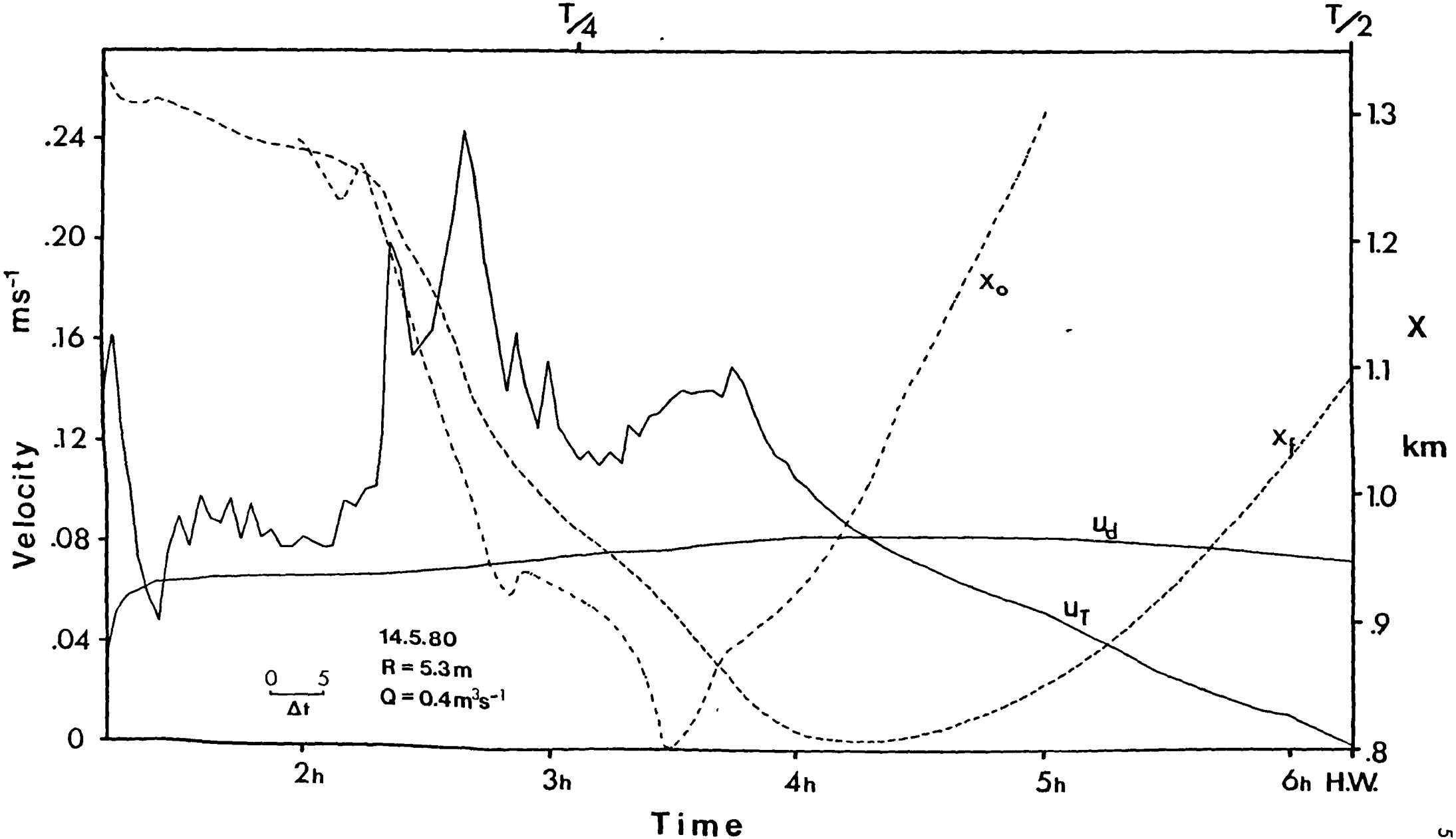
T/4
T/2
.24
.20
.16
.12
.08
.04
0
ms⁻¹
Velocity
1.3
1.2
1.1
1.0
.9
.8
X
km
$x_o$
$x_f$
$u_d$
$u_T$
14.5.80
R = 5.3m
Q = 0.4m³s⁻¹
0 5
Δt
2h
3h
4h
5h
6h H.W.
Time

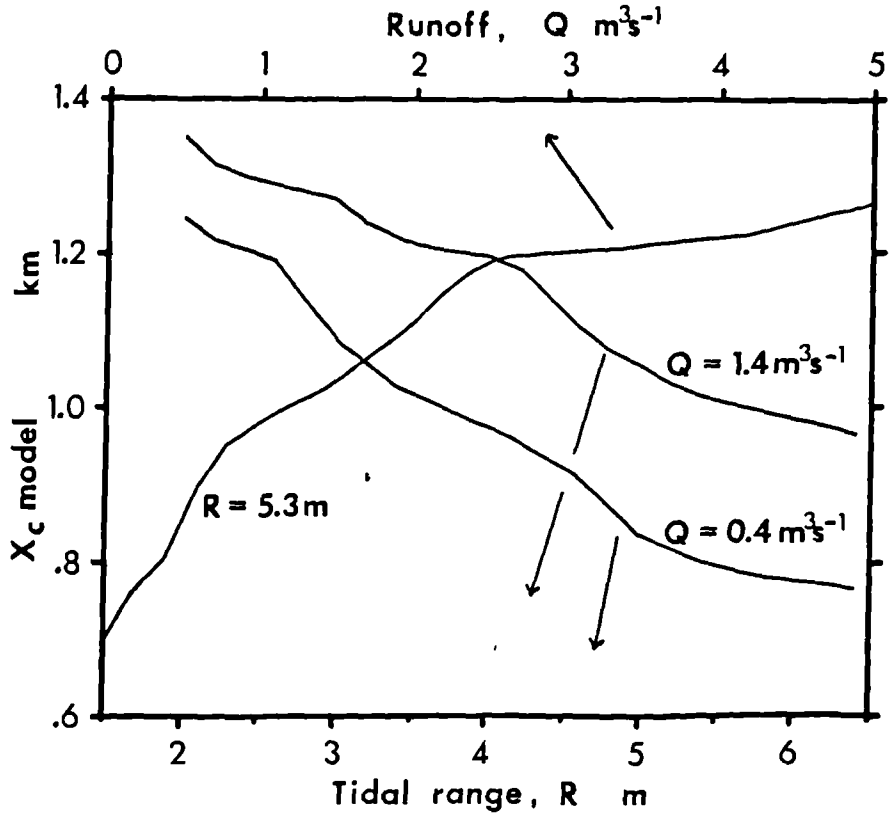


Figure 4.27 Predicted range of frontal intrusion limit as a function of tidal range for constant runoff ($Q=0.4m^3s^{-1}$ and $Q=1.4m^3s^{-1}$) and as a function of runoff for constant tidal range (R=5.3m).

Finally, figure 4.27 illustrates the model variation of x with Q and R individually. If these responses were linear, ignoring other factors, a plot of $x_c$(model) against $(Q/R^2)^{1/3}$, as in section 4.4, should give a straight line with zero standard deviation. This suggests that a part of the scatter in figure 4.20 (of section 4.4) is caused by the non-linear response of $x_c$ to changes of Q and R, which is itself purely a result of non-rectangular topography.

On the basis of reasonable agreement with prototype behaviour we may make some inferences with regard to the front in the estuary. In the model formulation we neglected real-time river runoff and allowed no fluid (or salt) exchange between the layers. We may therefore conclude that their combination in the estuary should not greatly alter these results and must therefore be of approximately equivalent magnitude. Figure 4.25 and 4.26 show that frontal movements have little effect on the value of $u_d$ which remains almost constant throughout the flood. The front thus responds principally to the tidal flow which itself depends on the location of the front in a positive feedback loop. Early frontal movement is therefore crucial in determining subsequent behaviour.

# CHAPTER 5

# LOCH CRERAN, WEST SCOTLAND

## 5.1 THE LOCH

Loch Creran is connected to the Lynn of Lorn, ~16km north of Oban on the west coast of the Scottish Highlands. The loch (figure 5.1) is 13km in length lying approximately east-west, and is divided by a shallow, narrow sill (the Crigan narrows) into upper and lower basins. The upper basin - the site of observed frontal occurrence - was the site of two investigation periods during the summer of 1980.

Figure 5.2 shows the upper basin including results from a bathymetry survey conducted by the S.M.B.A. (Scottish Marine Biological Association). The basin is fjord-like; the depth increases rapidly from a mean of ~4m at the sill to 20m in a horizontal distance of 200m. The south side has a deeper trench (maximum depth 37m) running 200m offshore although the average depth of the basin is ~20m. The river Creran joins the Loch at the north-east. It has a large, flat, flood plain at the eastern end of the Loch which is inundated by most tides and contributes significantly to the tidal demand of the upper basin. The Crigan narrows are 120m wide and 220m long with a further constriction to flow in the form of a stony bank on the northern side which tends to direct the tidal flow toward the south of the upper basin. Tidal streams through the narrows may reach speeds of $2ms^{-1}$.

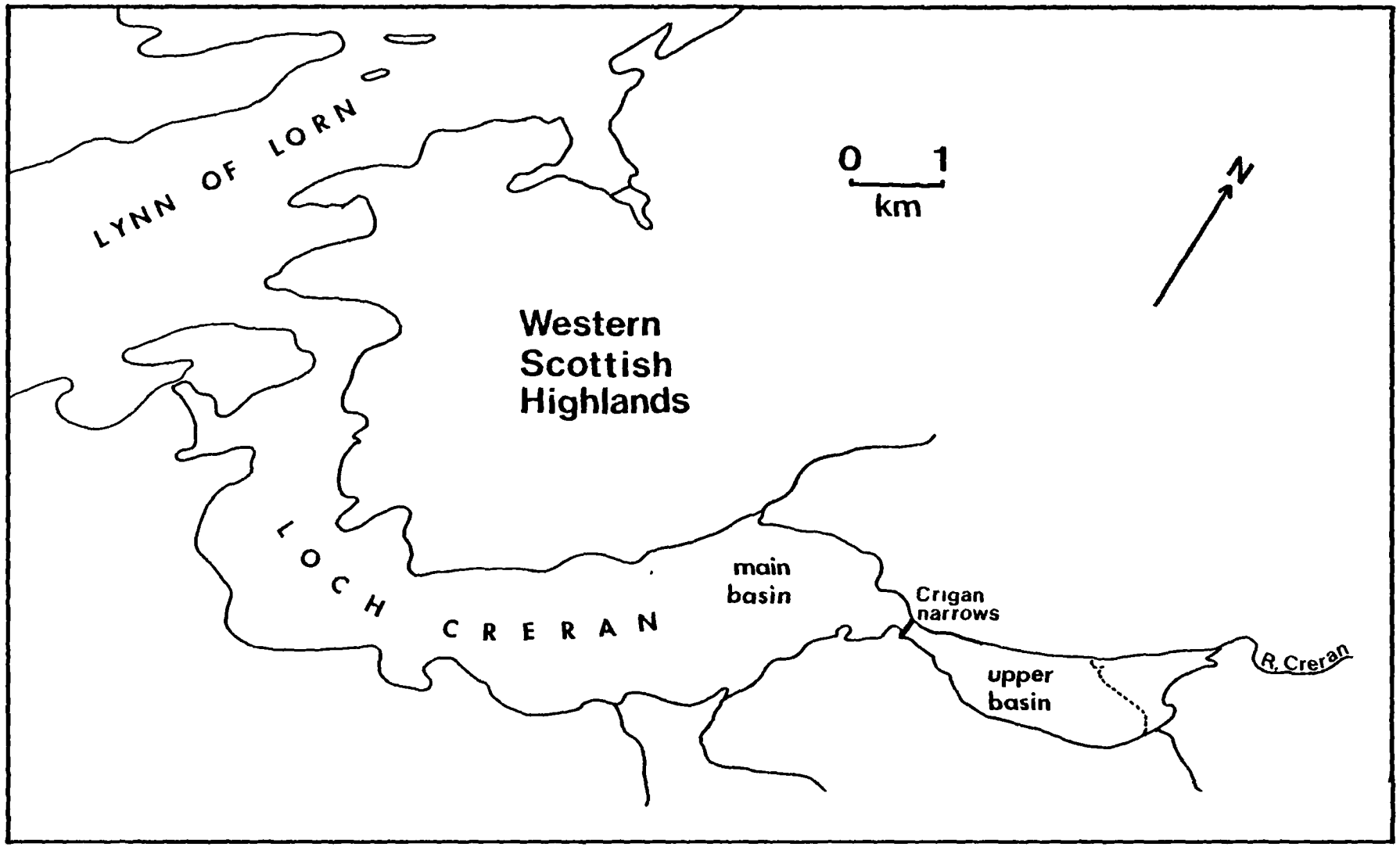


Figure 5.1 Configuration of Loch Creran upper and main basins

Figure 5.2 The upper basin of Loch Creran indicating bathymetry and typical frontal positions at early (A) and late (B) stages of the flood tide.

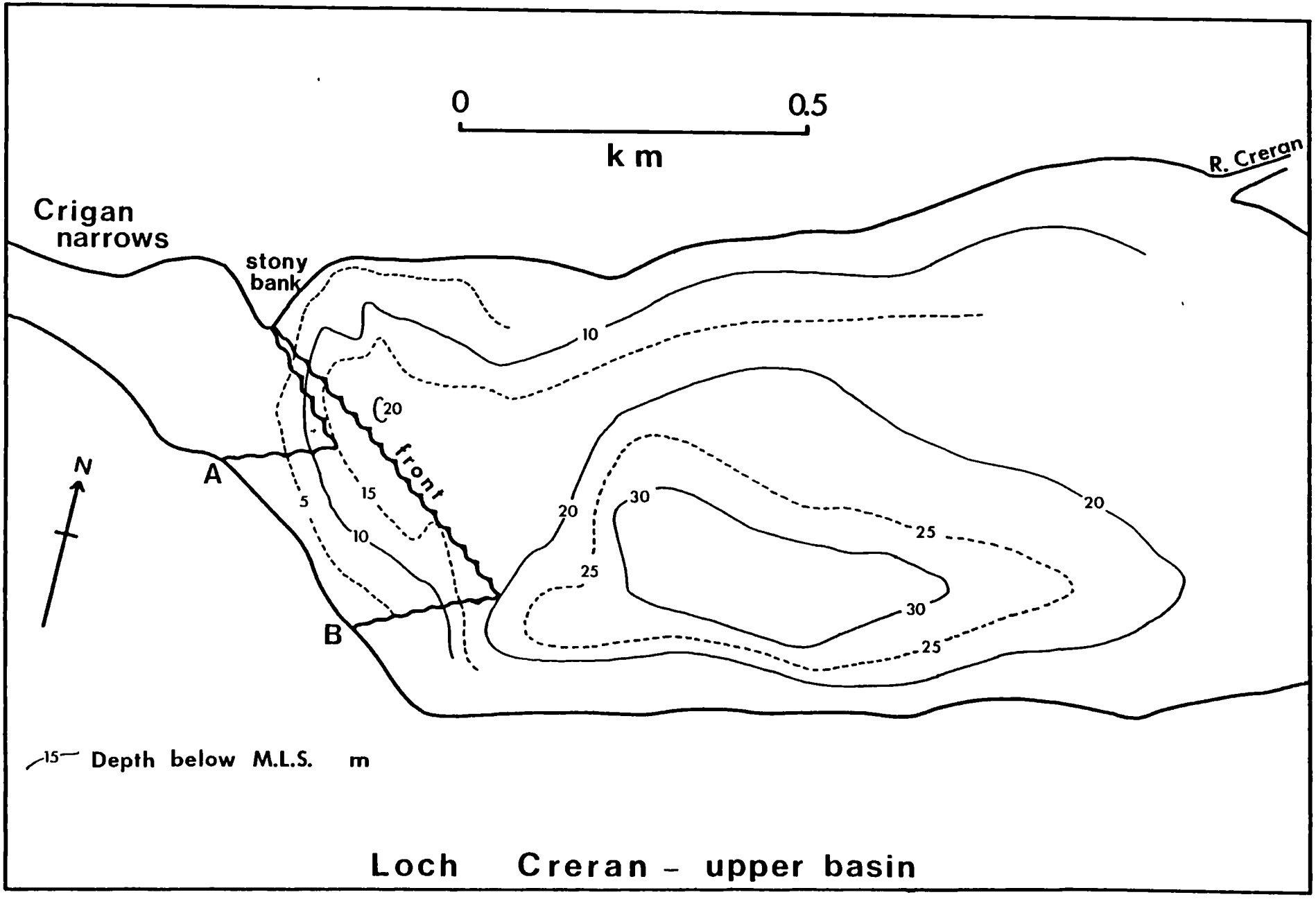


Loch Creran - upper basin

Mean springs and neaps ranges are 3.3m and 1.2m respectively for the head of the upper basin. The tidal curve is distorted by the restricted connection at the mouth of the main basin, effectively extending the ebb tidal phase by one hour during springs.

The catchment area (66km$^2$) is rugged and mountainous, and runoff responds very rapidly to changes of local weather. The Clyde River Purification Board gauge runoff from the Creran river at Taraphocain where an average of 4.9 cumecs was recorded for 1980. However, fluctuations around this figure were large with a minimum of 0.13 cumecs and a maximum of 75 cumecs. As an example of the response period, a daily mean flow of 4.4 cumecs was recorded on the day following a mean flow of 50.7 cumecs in July 1980. Figure 5.5 gives the daily mean runoff figures for the two periods of investigation in June and September.

The tidal flood through the Crigan narrows is subject to considerable contamination from the previous ebb waters. This is because of the predominantly longitudinal nature of tidal flow in both upper and lower basins. Tidal stirring over the Crigan narrows creates water of intermediate (20‰-30‰) salinity which seeks its own density level within either basin, usually at a depth of a few metres above a relatively still, high salinity water mass extending to the loch bed. Infrequently, a large spring tide provides a highly saline inflow through the narrows which, assisted by slow erosion of the bed salinity by downward entrainment, is sufficiently dense to displace the deepest water in the upper loch. These renewals of the bottom water, in the form of strong fast density currents, occur at long-separated irregular times during the year and have been the subject of study by the S.M.B.A. (Edwards and Edelsten, 1977).

## 5.2 VISUAL DEVELOPMENT

During mean tidal conditions, within an hour after low water, very strong bottom-generated turbulent stirring can be seen over the sill in the narrows. At this time a strong visible front forms, from the tip of the stone bank at the inner sill edge. The front extends the separation, initiated by the stone bank, between the mixed inflow and the stratified system of the upper basin, and is subject to considerable shear. Within a short period following its appearance, the front becomes the northern arm of a 'V'-shaped boundary that points into the loch (e.g. position A in figure 5.2: see also figures 5.3 and 5.4). The second arm, which is subject to weaker shearing flow because the tidal streams are slower on the southern side, extends from the apex to the shore in a line running approximately south-west.

Once set up, the 'V' boundary has a similar appearance to the tidal-intrusion front in the Seiont, with convergent flows apparent on both sides. It differs, however, in its pattern of movements. Throughout the progress of the flood tide the front normally advances slowly into the Loch and, in general, does not retrace its path. Only on one day during the surveys was the front seen to retreat as far as the narrows, and on this occasion it continued under the Crigan bridge before high water.

In the late stages of the flood, the apex of the 'V' may be seen well inside the loch (e.g. position B in figure 5.2); the northern arm extends considerably while the southern arm is pushed along the shore such that its length remains approximately constant. During its advance into the loch, the vigour of the front gradually lessens, and the apex and southern arm may lose their identity before high water.

During its existence, and more so in the early stages, the Creran front appears to be a particularly vigorous example of the tidal-intrusion front. Winds in the Scottish Highlands are often very strong and, compared to the Seiont, the fetch in Loch Creran is quite large. With a strong easterly wind and a fast tidal inflow, steepening waves approaching the front from the west can become very large and choppy. Whereas, on the landward side, the seaward surface currents are wind-assisted and conditions remain relatively calm. The

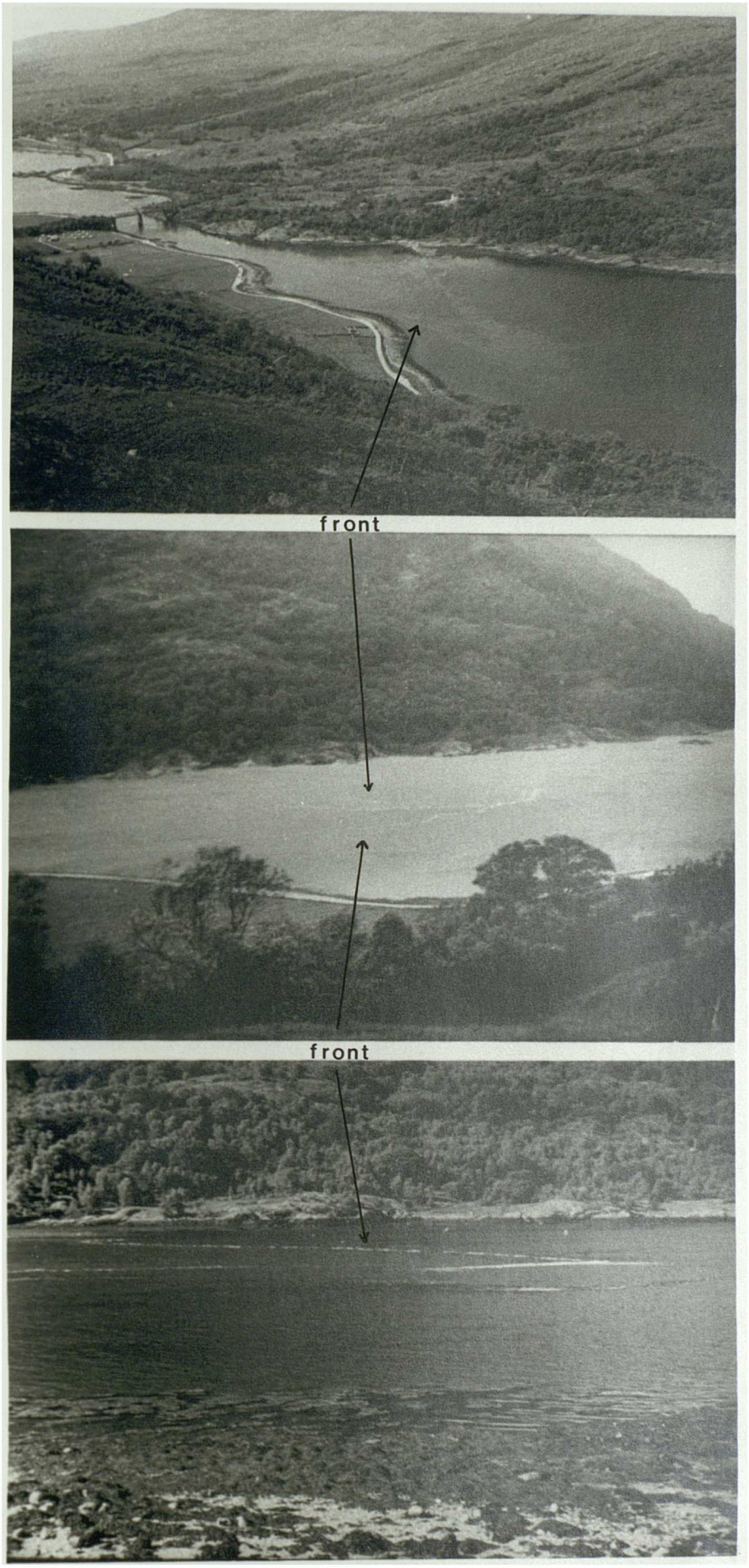


Figure 5.3 Three views of the Creran front (lowest picture provided by Dr. R. Lewis, I.C.I. Brixham).

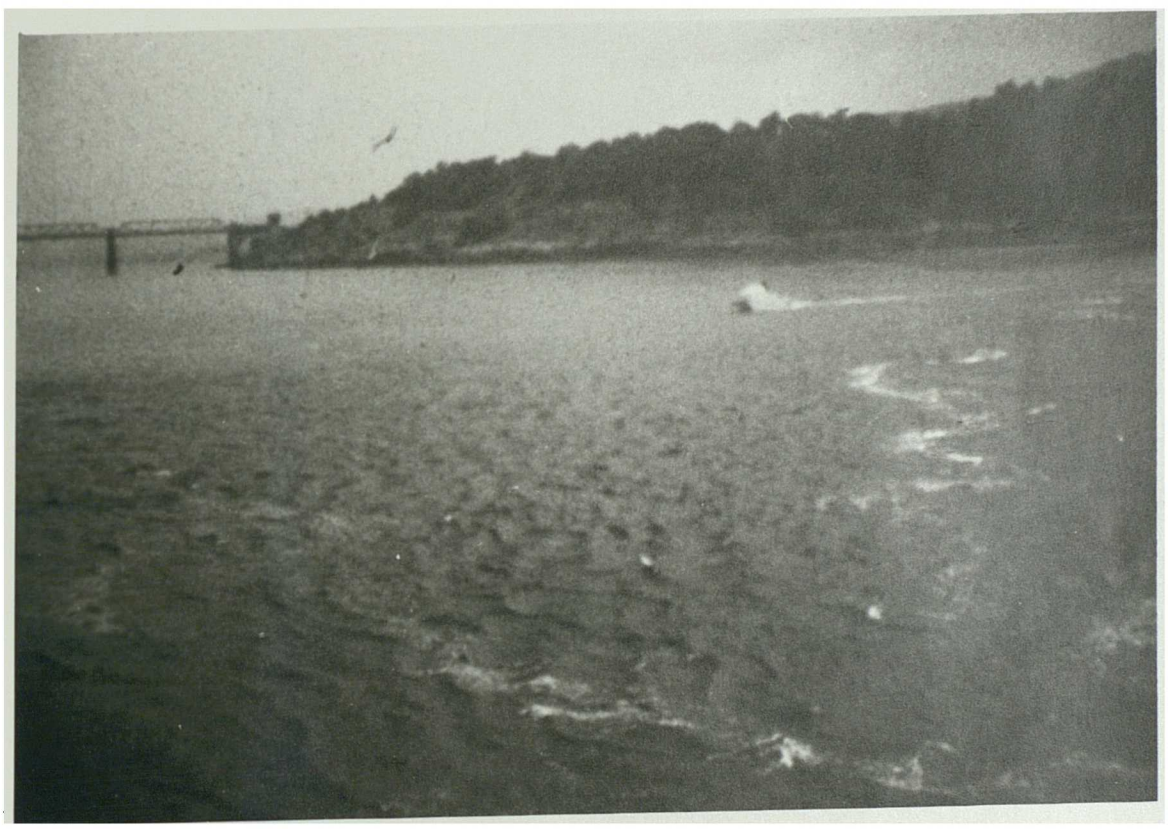

Figure 5.4 Seaward view of Loch Creran frontal 'V' including cusps along the frontal arms (enlarged cine frame).

frontal 'V' may then be a marked discontinuity of 'sea state'.

On days when the wind was particularly strong it did not appear to reduce the stability of the stratified, upper layer because the front remained sharp. However, this proposition cannot be verified at present, because strong winds usually coincided with substantial rainfall i.e. river discharge. Strong gusting, nevertheless, caused some disruption by slowing the frontal advance and, in some cases, it forced a short-lived retreat before dying down and allowing the advance to resume.

Fluorescein dye revealed the current structure to resemble that of the Seiont front. Tidal currents were landward at all depths over the sill and directed approximately parallel to the axis of the Loch. On reaching the front the tidal flow abruptly sank to a depth of 0.5m-3m and continued, laterally unperturbed, as a submerged current. On the landward side, surface downstream flow abruptly stopped at the front and was returned into the Loch as a submerged flow. Collected debris, subjected to vertical shear, moved along the frontal arms toward the apex of the 'V', but a gyre at the apex was not generally seen. During the periods of observation, wave conditions were such as to preclude the detection of the capillary bow wave ahead of the convergence lines.

The front in Loch Creran showed an additional feature not seen in the Seiont i.e. regular cusps along the length of the arms which were appreciably more distinct on the northern arm. These cusps (see figures 5.2 and 5.4), with length and width scales of ~10m, each had a sharp apex pointing into the Loch but an otherwise rounded profile.

Finally, in contrast to the Seiont, a front was almost invariably seen in the upper loch during the flood tidal phase through large ranges of tide and runoff. Nevertheless, day to day variations were still clearly evident in the duration of existence and vigour of the frontal arm discontinuities. During relatively dry periods with low runoff the arms were indistinct and lost their identity at an early stage of the flood.

In the upper basin, and in the upper regions of the main basin, no surface fronts have been seen during the ebb.

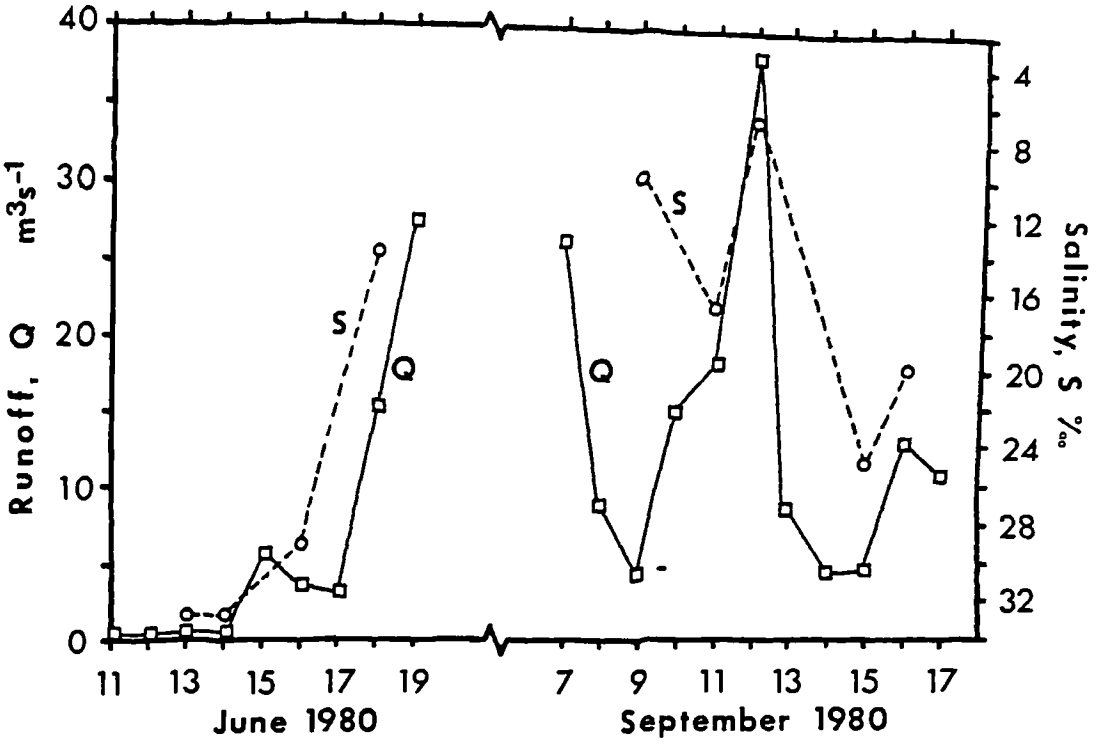


Figure 5.5 Response of the low water surface salinity to changes of mean daily runoff during the two survey periods.

## 5.3 SURVEY RESULTS

Fieldwork in Loch Creran was conducted over two periods during the summer of 1980. The first of these, 11th–19th June, followed a lengthy dry spell and river runoff was initially very low. During the second period, 8th–16th September, rainfall was generally high, and a storm on the night of the 11th swelled the runoff to the maximum recorded (~75 cumecs) in 1980. Figure 5.5 illustrates the close and rapid response shown by the low water surface salinity to changes of runoff; varying throughout the entire range of encountered salinities. Such a relationship indicates little storage of freshwater within the loch and/or strong mixing processes being operative.

Bottom water renewals within the upper basin occur at regular but infrequent intervals, and dilution of its salinity proceeds very slowly because the mid-depth and bottom currents are small. The bottom water may thus be assumed to remain constant at ~32.2‰, with the consequence that runoff determines the extent of the surface to bottom stratification within the upper basin at low water.

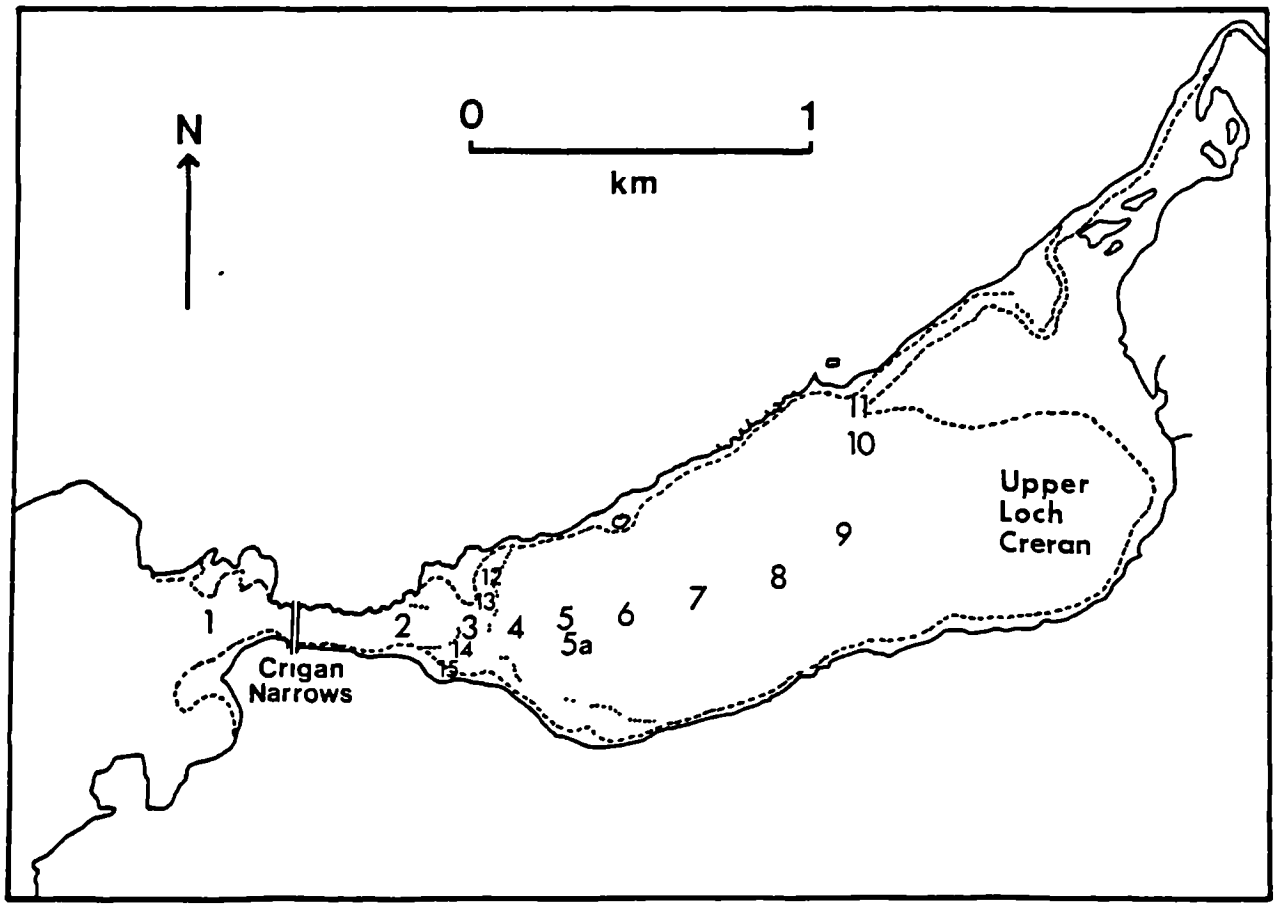


Figure 5.6 The upper basin, showing station positions for longitudinal salinity sections.

In a similar manner to the bridge-based work in the Seiont the probe/current meter arrangement (figure 3.1) was lowered by winch from a boat to produce vertical profiles. These were not truly synoptic but conditions below 10m were found to be sufficiently constant to allow the vertical column to be sampled in less than five minutes.

The Seol Mara, a research vessel of the S.M.B.A., was used for fixed position measurements at stations 5 on 13.6.80 and 5a on 18.6.80 and 11.9.80, (see figure 5.6 for station positions). On the first of these occasions stratification within the loch was minimal following a long dry spell. The records of surface and mid-depth salinities through a part of the flood tidal phase are shown in figure 5.7a. A front formed soon after low water but was very short-lived; surface salinity recorded at station 5 rose gradually through the tide.

Measurements from the Seol Mara on 18.6.80 (figure 5.7b) were accompanied by a closer investigation of the front from the Dory. Soon after low water (17:25hrs), a front formed - and was marked by a considerable accumulation of foam. At ~18:00hrs the discontinuity of salinity across its 1m width was ~8‰, while salinities in the sector between the arms and over the sill were the same. Records clearly show the passage of the front beyond the fixed station at ~19:25hrs moving into the loch, and that salinity changes were confined to the top two metres of the water column. By 20:00hrs, when the front was ~200m beyond the Seol Mara, the surface discontinuity had been reduced to ~15‰, changing gradually through a 'frontal region' of ~50m width, the entire frontal region was visible as a calm slick, marked by the suppression of the smallest waves otherwise present. Time-series records of salinity and velocity from the Seol Mara on 18.6.80 are presented in figure 5.8. These show a considerable resemblance to the spatial profile of a laboratory density current, except that early stratification was accompanied by vertically-uniform flow during the ebb part of the record.

The fixed station results of 11.9.80 are given in figure 5.7c; briefly, at ~17:10hrs, the front reached the Seol Mara, indicated by the equality of station and sill salinities. On this occasion winds were blowing constantly at force 5-6 from the east with sustained gusts of force 8-9. Periods of slow frontal advance during the flood were repeatedly halted and often reversed by the gusting winds; forcing a retreat at speeds up to $1ms^{-1}$. The record at ~17:15hrs shows one such return to stratified conditions at the fixed station.

Along a line of stations from the river outlet to the Crigan narrows many quasi-synoptic, longitudinal, salinity sections of the loch were obtained from the Dory, (figures 5.9a,b and c). Flood and ebb tide profiles are distinctive by the presence and absence respectively of a surface salinity discontinuity within the loch. Surface salinity increased gradually from the river outlet to the narrows during the ebb phase but changed abruptly at a front inside the loch during the flood phase. Slicks observed during the flood did not always have an associated salinity (or temperature) structure, but sharp salinity boundaries seen in the longitudinal profiles invariably had an associated surface visible boundary.

Figure 5.7a Surface and 5m salinities at station 5 on 13.6.80.

Figure 5.7b Surface and 1m salinities at station 5a on 18.6.80.

Figure 5.7c Surface salinity at station 5a and surface salinity over the sill on 11.9.80.

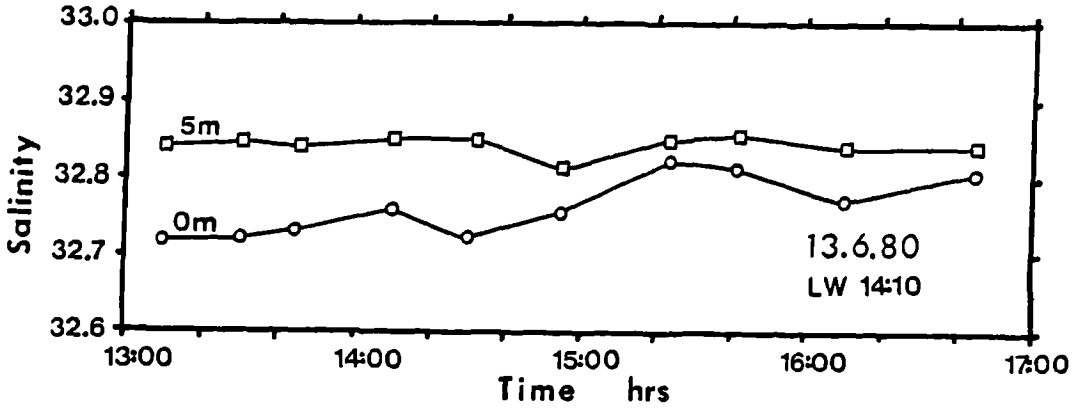
33.0
32.9
32.8
32.7
32.6
Salinity
5m
0m
13.6.80
LW 14:10
13:00
14:00
15:00
16:00
17:00
Time hrs

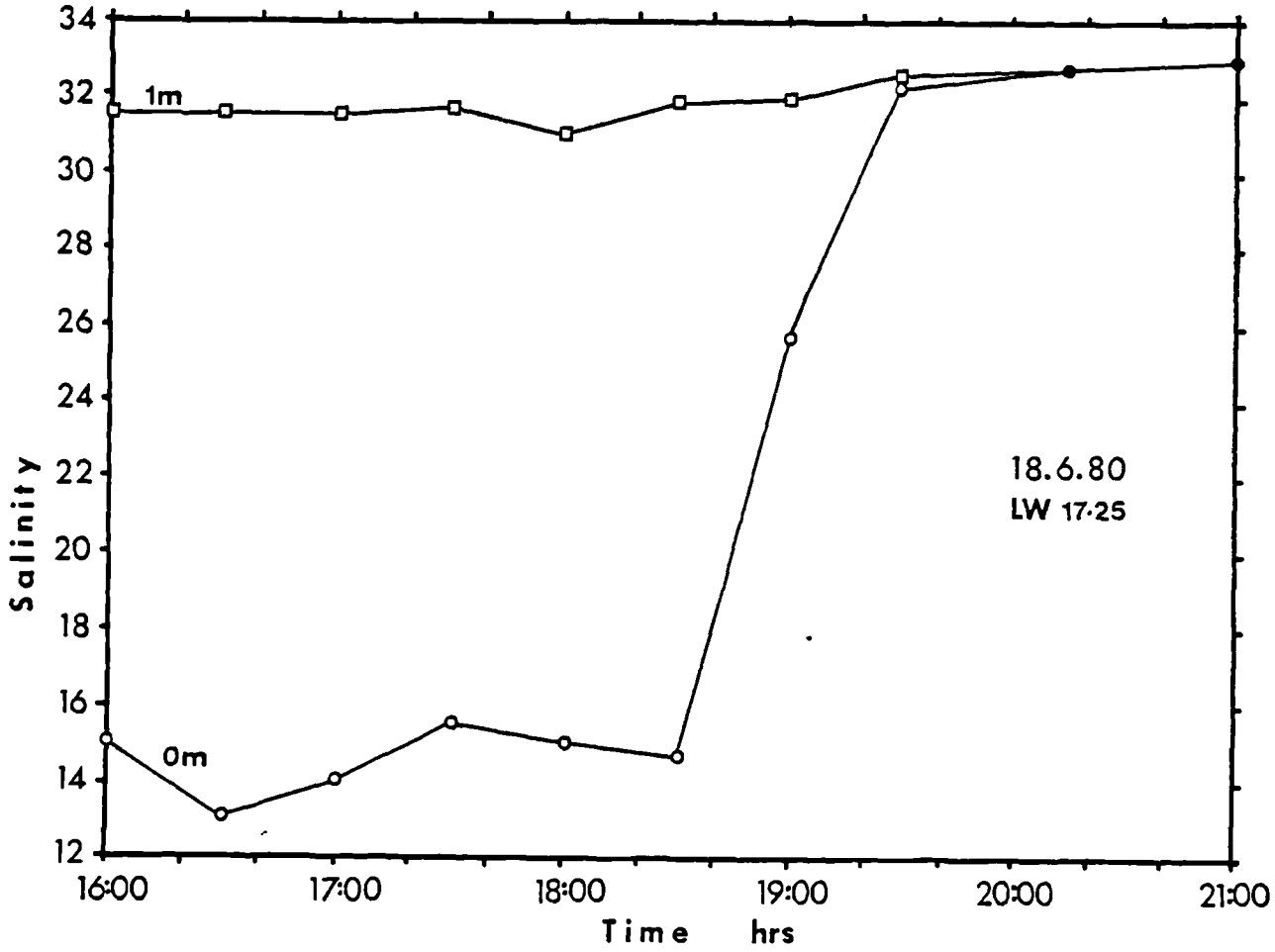
34
32
30
28
26
24
22
20
18
16
14
12
Salinity
1m
0m
18.6.80
LW 17·25
16:00
17:00
18:00
19:00
20:00
21:00
Time hrs

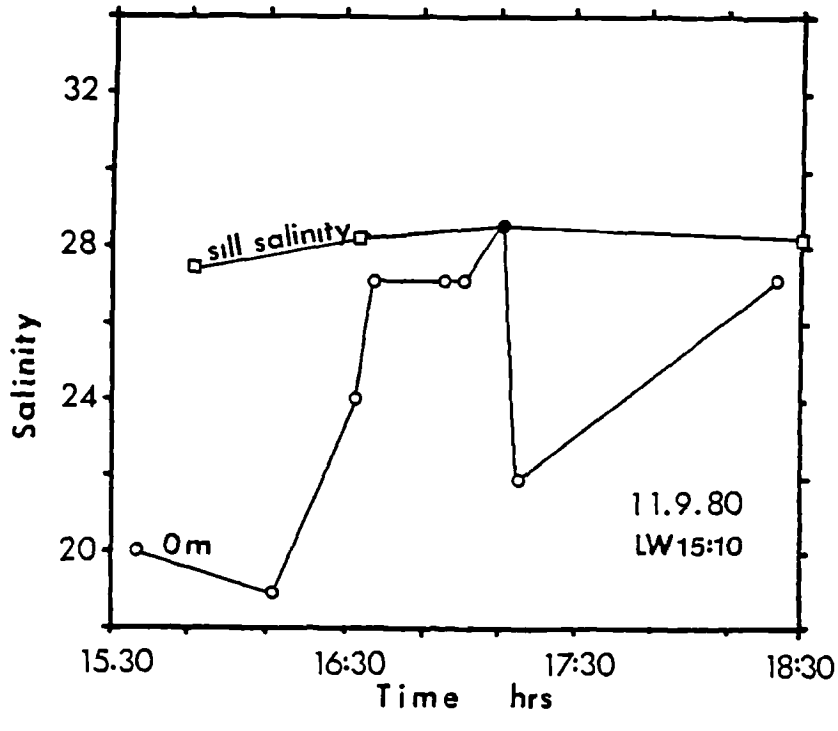
32
28
24
20
Salinity
sill salinity
0m
11.9.80
LW15:10
15.30
16:30
17:30
18:30
Time hrs

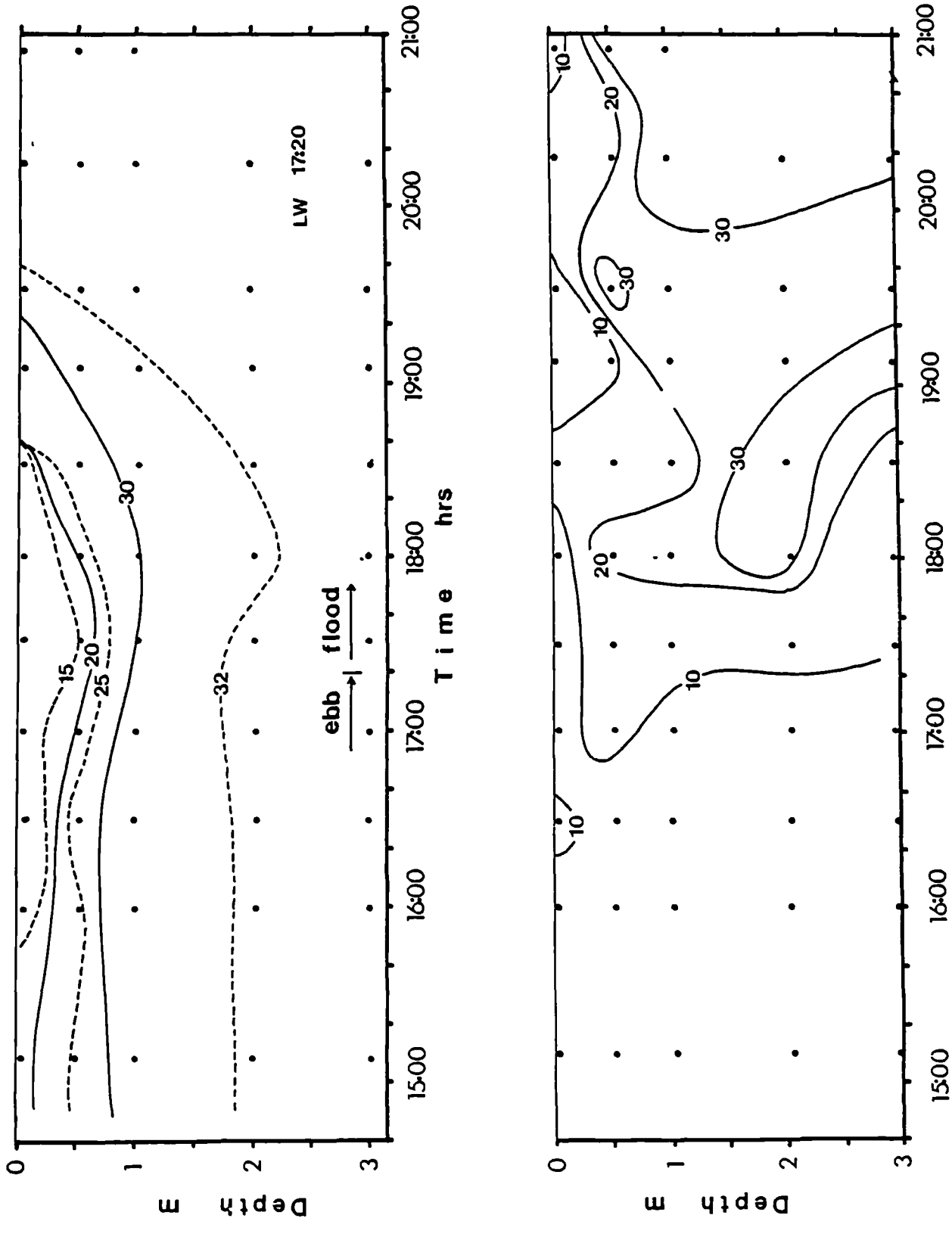


Figure 5.8 Time-series measurements of salinity and velocity at station 5a on 18.6.80.

Figure 5.9a Successive longitudinal salinity sections in Loch Creran during the flood tide of 11.9.80 (R=3.2m).

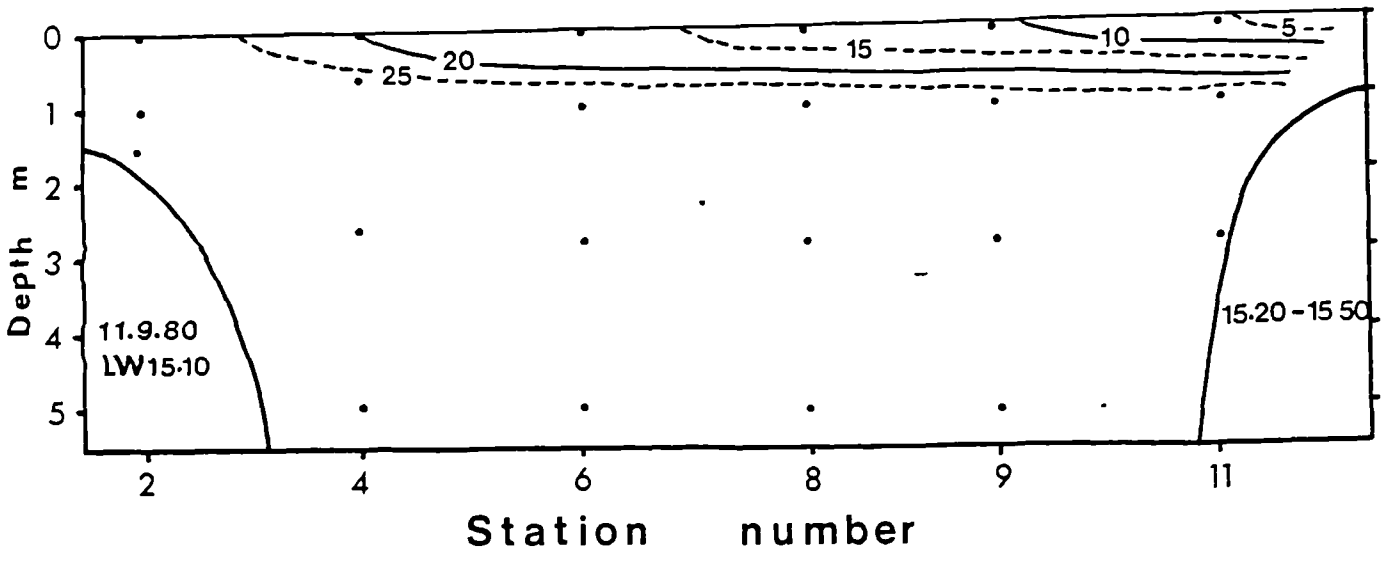
Depth m
0
1
2
3
4
5
2
4
6
8
9
11
Station number
5
10
15
20
25
11.9.80
LW15·10
15·20 - 15 50

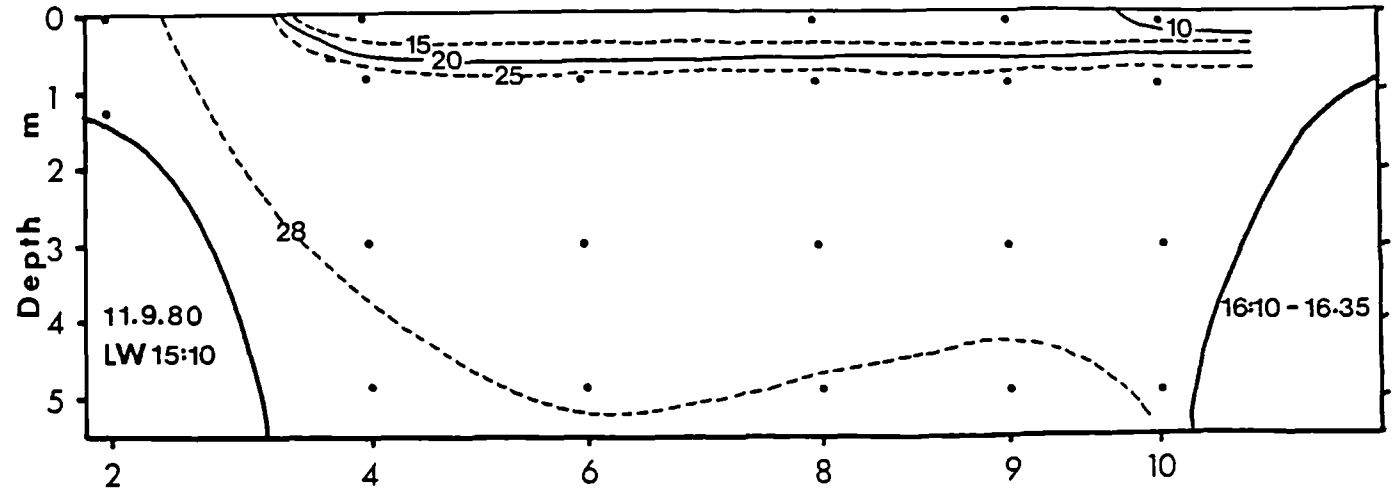
Depth m
0
1
2
3
4
5
2
4
6
8
9
10
10
15
20
25
28
11.9.80
LW 15:10
16:10 - 16.35

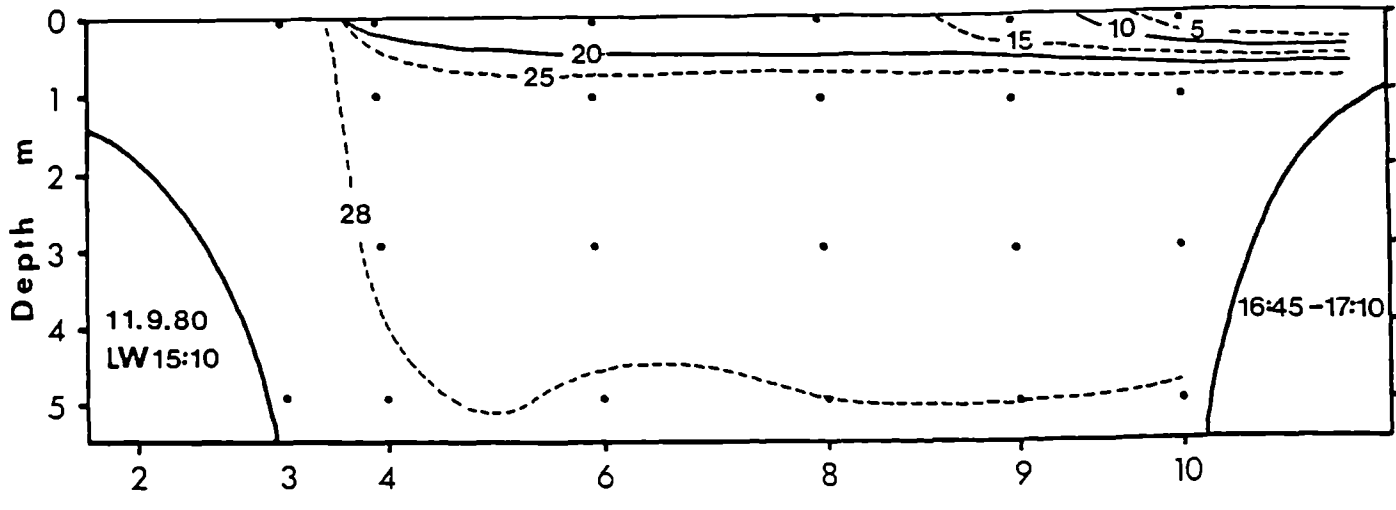
Depth m
0
1
2
3
4
5
2
3
4
6
8
9
10
5
10
15
20
25
28
11.9.80
LW15:10
16:45 - 17:10

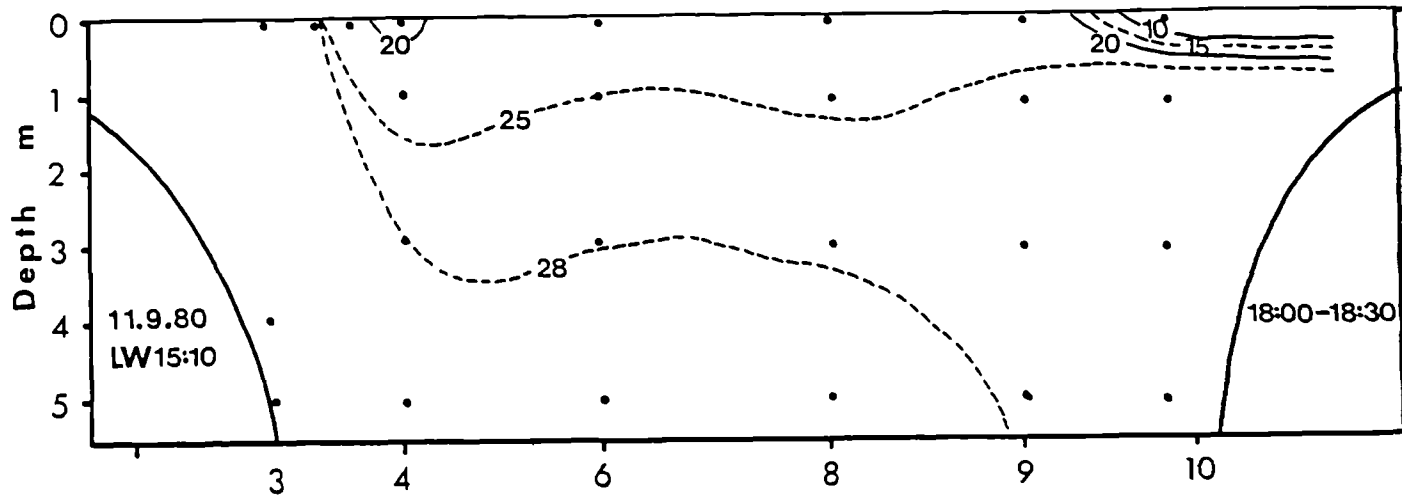
Depth m
0
1
2
3
4
5
3
4
6
8
9
10
10
15
20
20
25
28
11.9.80
LW15:10
18:00-18:30

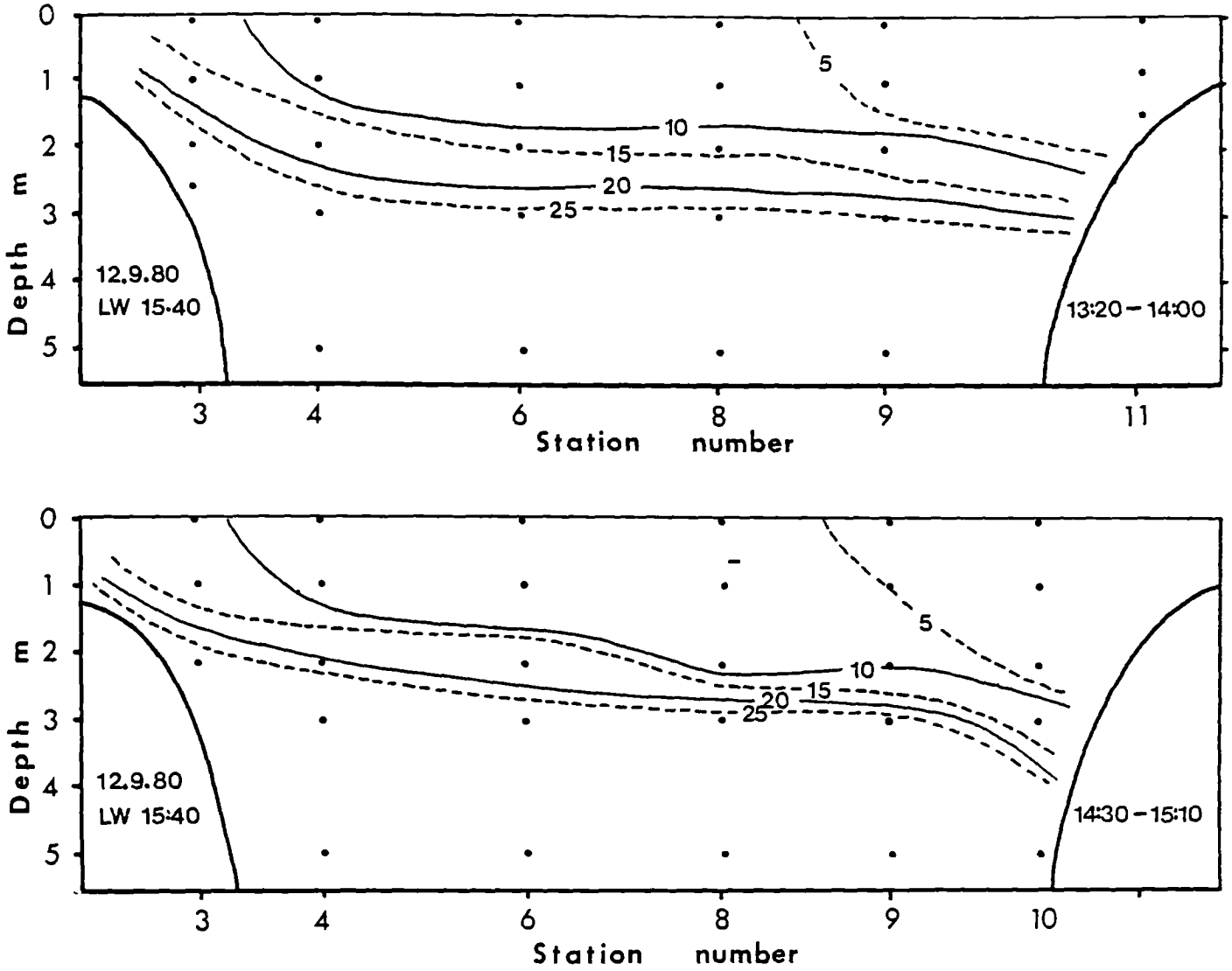





Figure 5.9b Successive longitudinal salinity sections during the ebb tide of 12.9.80 (R=3.0m).

Figure 5.9c Successive longitudinal salinity sections during the late flood and following ebb tides of 15.9.80 (R=2.1m).

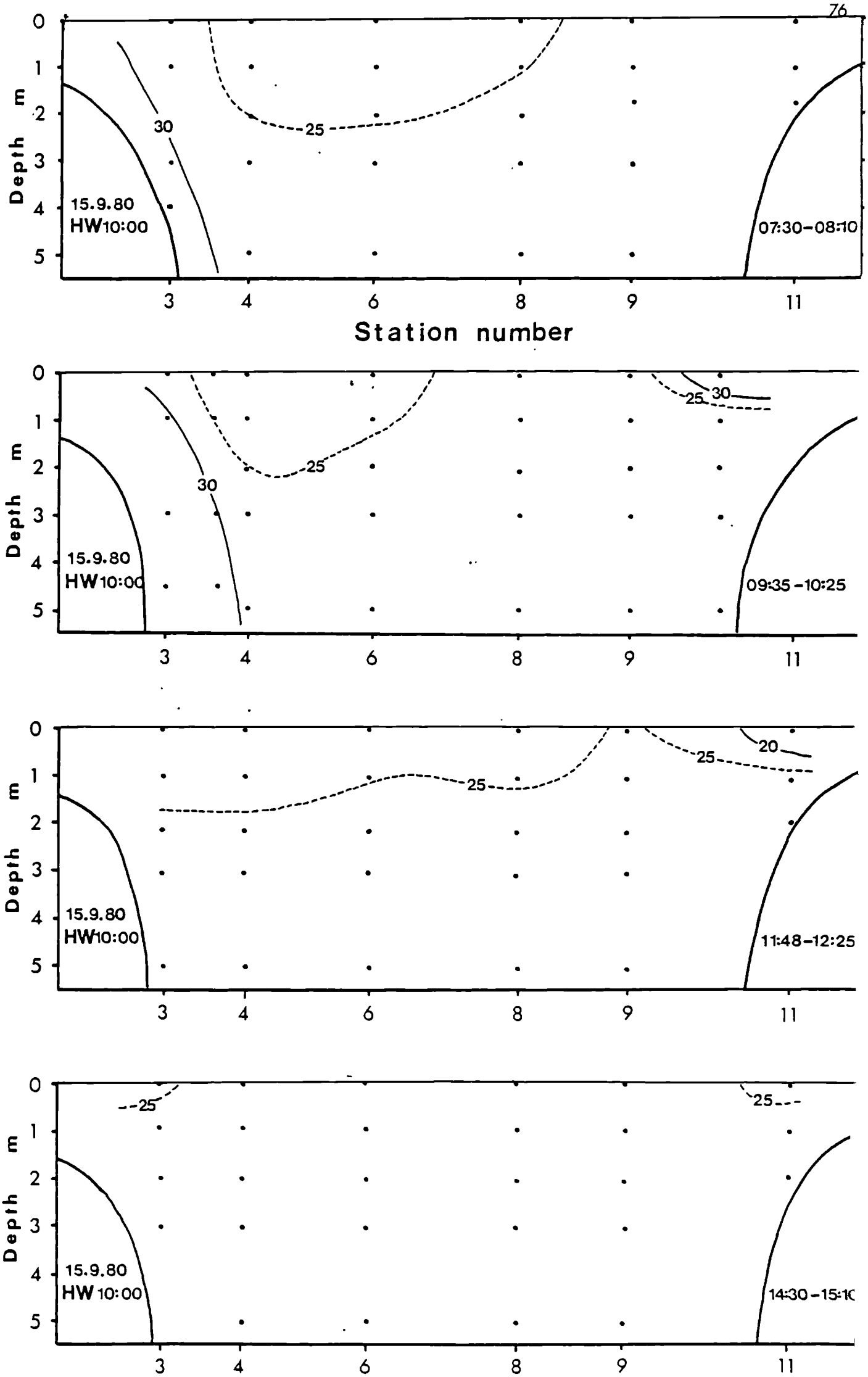
Depth m
0
1
2
3
4
5
30
25
15.9.80
HW10:00
07:30-08:10
3
4
6
8
9
11
Station number
25
30
09:35-10:25
20
11:48-12:25
14:30-15:1

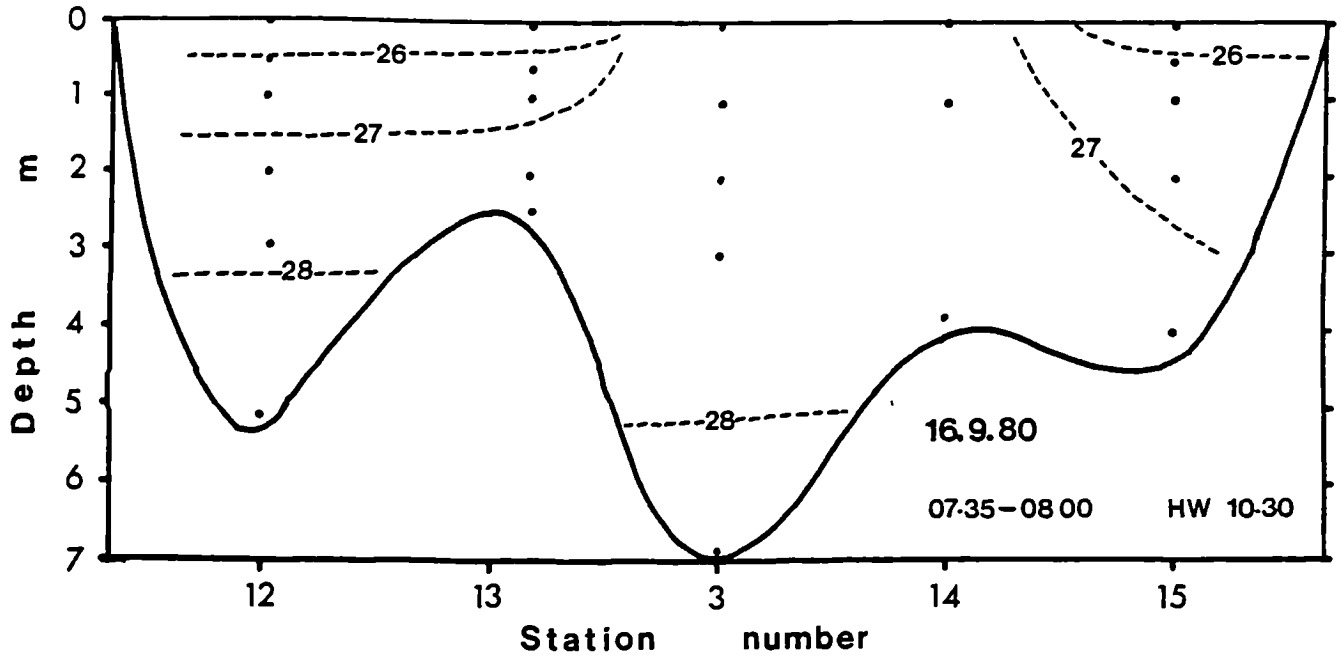


Figure 5.10 Transverse salinity section across the Loch and frontal arms.

The storm force winds and heavy rainfall created a deep, well-mixed layer of low salinity throughout the loch on 12.9.80, most of which had been mixed away by 15.9.80, after a single rainless day. Erosion of the upper layer during the flood tide is also evident in sequential longitudinal profiles.

Vertical profiles at stations transverse to the axis of the loch, across the two frontal arms, are shown in figure 5.10. The discontinuity from well-mixed to stratified regimes is again clearly evident despite the fronts being relatively weak on this occasion.

## 5.4 FRONTAL BEHAVIOUR IN LOCH CRERAN.

Obvious similarities between the frontal systems of loch Creran and the Seiont estuary extend to the limited frontal existence during only the flood tidal phase, and the three-dimensional 'V'-shaped boundary separating stratified from mixed waters. The most striking difference concerns the frontal movement within Loch Creran.

The success of the frontal model for the Seiont arises from the analogy to laboratory density currents. The front moves in order to maintain a form of critical shear condition at the head of the current and this necessitates quite substantial longitudinal adjustments in the Seiont. However, the large expansion of cross-sectional area over the sill slope in Loch Creran permits maintenance of a similar critical condition with a relatively small frontal adjustment. We can therefore envisage a cause of the initial minor and slow movements in Loch Creran and reconcile these with a similar balancing mechanism to that operating in the Seiont. However, as the flood tide progresses, the upper layer stability is continuously reduced and instead of retracing its landward path, the front continues advancing into the Loch. We must consequently identify a reason for the apparent difference in layer stabilities between the two sites. This is left until chapter 9 in which we examine the stability of the tidal-intrusion front.

# CHAPTER 6

# THE FRONTAL INTERFACE

## 6.1 VISUAL OBSERVATIONS IN THE SEIONT.

In a highly-stratified environment, where mixing events are confined to a relatively small scale, there is some scope for combining direct visual observations with instrumental measurements of subsurface phenomena. A well known example is the use of divers by Woods (1968) to observe Kelvin-Helmholtz instabilities on the layers of the Mediterranean pycnocline. These observations may be supplemented by laboratory modelling in which the governing parameters come under experimental control, but in scaled models there is inevitably a change in the relative magnitudes of the physical forces (gravity, viscosity, surface tension etc.) which may affect the character of the observed phenomena. In the comparatively sheltered waters of the Seiont estuary, observations of the frontal layer were performed relatively easily and provided useful supplementary insights to the measurements.

Observations were made during periods of high runoff when the depth of homogeneous fresh water inside the estuary is typically 30cm-50cm with a sharp interface of ~20cm thickness below. Divers held a line running from the Dory at the surface to a weight on the river bed. It was found best to use air tanks even though the

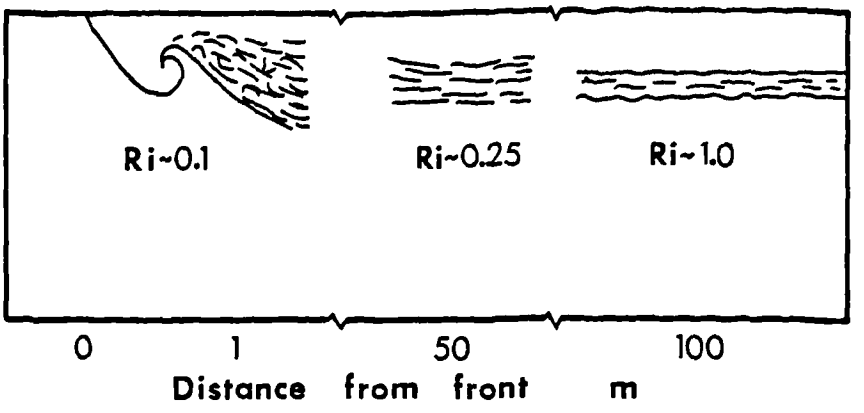


Figure 6.1 Schematic character and stability of the frontal interface related to the frontal position.

depths were small, due to the inordinate disruption caused by slight movements. Since we were interested in the effects of shearing flow on the appearance and stability of the interface, observations were made during a part of the flood tidal phase. It was hoped to relate the observations directly to the physical structure by hand-holding a temperature/salinity probe at various positions in the water column. However, the task proved difficult for a single diver involved in trying to maintain himself stationary and upright, and two divers caused unacceptable disruption. Nevertheless, some useful observations were obtained.

From the Dory, dye released just seaward of the frontal position immediately sank and rolled back towards the surface at an overturning billow (figure 6.1) with a length scale of 0.5m-1m. The shear-produced billow involves large turbulent dissipation and creates a wake of mixed water that considerably thickens the interface for some distance from the front. Observations in this highly turbulent region were difficult because any dye released was subject to such rapid dispersion that detail was immediately lost. The region extended for 50m-100m upestuary, where the interface became substantially more stable in appearance.

Away from the front, where the interface thickness reduces to ~20cm, observations were greatly facilitated by the use of fluorescein dye. This was released below the surface from a garden spray pump with a trigger held by the diver. By placing the nozzle of the spray well below the interface and releasing dye while drawing the nozzle rapidly up to the surface, a vertical column of

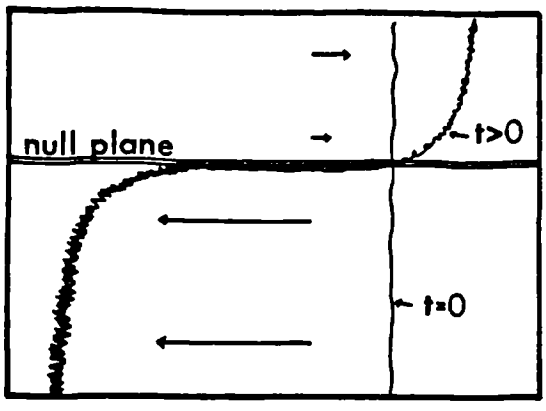


Figure 6.2 Fate of a vertical line of fluorescein dye released, at t=0, from the surface through the interface and into the lower layer.

the fluid could be marked for subsequent observation (figure 6.2). Within the surface layer there was a slow (~10cms$^{-1}$) seaward movement in which turbulent diffusion acted to spread the dye. Conversely, dye placed well below the interface moved very rapidly (~30cms$^{-1}$) landward and was plainly subject to very large turbulent diffusion before disappearing beyond the range of visibility (~2m). The dye that was released within the interface spread out longitudinally according to whether it lay above or below the point of zero velocity and, in doing so, delineated the zero velocity plane, (this will be termed the 'null plane'). Only dye placed in, or close to, the null plane remained visible for more than a few moments, the rest was quickly swept beyond visibility. The density interface itself was seen without dye by the very strong shimmering associated with changes of refractive index and it appeared to be coincident with the shear layer.

Once the interface had been located in this way, it proved instructive to release large amounts of dye only at, or near to the null point (the method being insensitive to vertical error, due to the large shear). After release and subsequent spreading, within ~30 seconds several square metres of the null plane had been dyed. Spreading along the plane occurred in both horizontal directions, with a ratio of axial to lateral spreading of ~20:1. The plane had the appearance of a large blanket with internal structures of various scales. The blanket thickness was 1cm-2cm and the smallest structures, which looked like small curls or rolls of dye intruding slightly above the blanket surface, were of the same scale uniformly covering ~50% of the plane area. The largest structures within range of visibility were internal waves on the interface; these

gently sloping, small amplitude (~20cm), long wavelength (~1m-2m) waves, tilted and curved the blanket both longitudinally and laterally.

In addition to these structures there were occasional, but relatively rare, systematic rolling billows moving slowly landward along the length of the blanket. These were ~30cm-50cm in lateral dimension and ~10cm in depth and forward length. They did not appear to become unstable.

The depth of the shear layer below the null plane appeared to be very small (figure 6.2); there was a continual visible loss of dye from the plane by removal of small downward intrusions in the fast tidal flow. The loss of dye from the blanket as a result of shear took place noticeably only on its underside and could be interpreted as slow, visible downward entrainment.

Vertical motions within the interfacial layer were evidently very small; the plane remained stable for at least as long as dye was visible within it (approximately 3-5mins). Inside each of the mixed layers, however, the turbulent diffusion of dye was testament to substantial vertical motions in these fluids. Presumably, the large density gradients of the interface were responsible for the lack of any appreciable visible exchange between the layers.

From the bridge-based vertical profiles of salinity and velocity described in section 4.3, there was little systematic trend in the Richardson number as a function of time. Regions of differing interfacial character appeared to be related to their location with respect to the front, and its large mobility confused the picture of Ri at a stationary position. Combining the profiles obtained from the bridge with indications from the visual work, a picture emerges of the spatial variation of Ri with respect to the front, included in figure 6.1. From the landward extremity of the two-layer system, where tidal velocities and hence the shear are relatively small, the Richardson number (~10) indicates considerable stability. Moving seaward, where the shear increases, the major proportion of the interfacial length has $1<Ri<0.4$, i.e. marginal stability, which reduces to the limit Ri~0.25 at 50m-100m from the front. Richardson numbers of 0.1-0.2 have been measured in the frontal region itself.

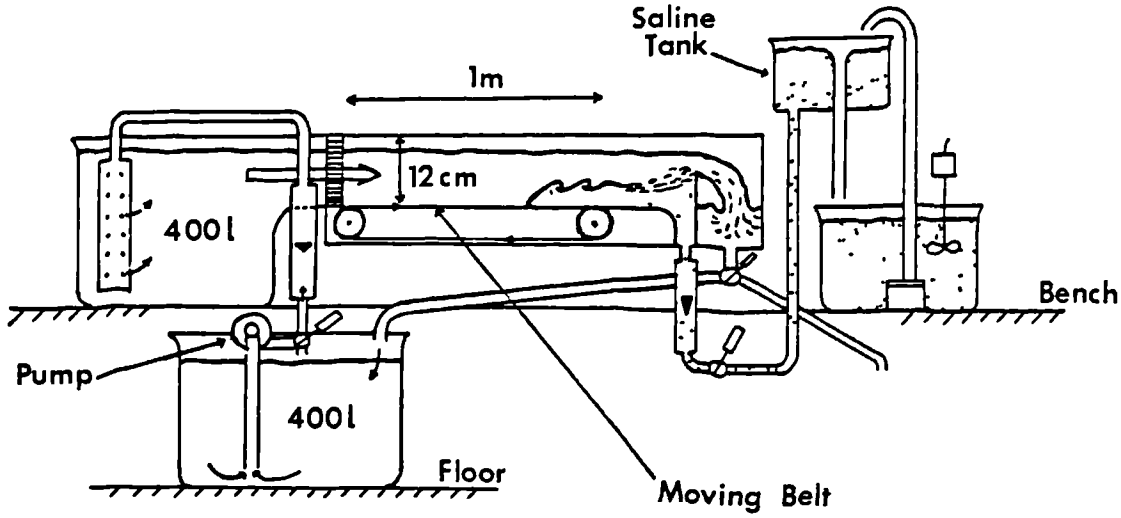


Figure 6.3 Apparatus for modelling steady-state density currents. (From Simpson, 1969)

## 6.2 THREE-DIMENSIONAL ASPECTS OF THE TIDAL-INTRUSION FRONT.

The one-dimensional movement of the T.I. front within the Seiont may be understood in terms of a dependency on the bulk parameters tidal range and river runoff, as in sections 4.4 and 4.5. Up to this point the most striking aspect of the front - its three-dimensional character - has largely escaped attention. Prompted by the success of the density current interpretation, attempts were made to produce a laboratory model of the front. The apparatus used was that designed by John E. Simpson and described in Simpson (1969) and Simpson and Britter (1979). An advantage of this particular apparatus is the incorporation of a movable floor which allows a steady-state, lower boundary density current to be subjected to a variety of boundary conditions. The apparatus is depicted in figure 6.3 and is capable of flow speeds up to $6cms^{-1}$ and Reynolds numbers of $\sim 10^4$. Figure 6.4 shows the range of boundary conditions that may be applied to a steady state density current and the resulting current profiles.

a) estuarine surface density current subject to vertically-uniform ambient flow.

b) modelled surface density current subject to non-uniform ambient flow.

c) modelled lower-boundary density current subject to non-uniform ambient flow.

d) modelled lower-boundary density current at end of fixed floor subject to vertically-uniform ambient flow.

e) modelled lower-boundary density current placed over moving floor subject to vertically-uniform ambient flow.

Relatively small surface tension allows a near-uniform vertical velocity profile

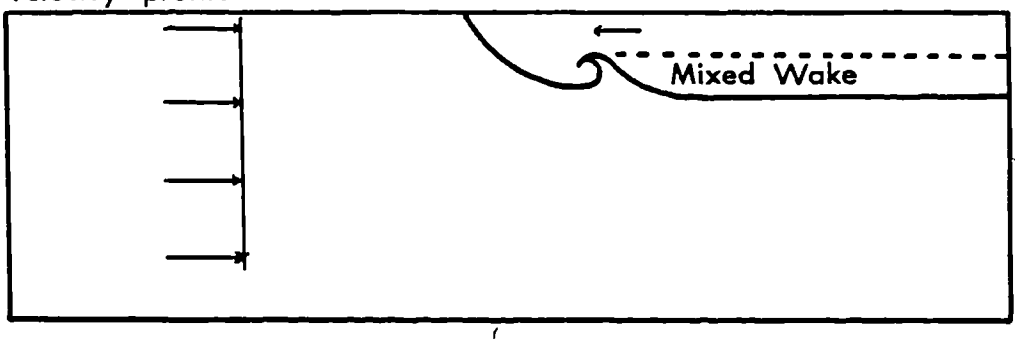


Relatively large surface tension creates a surface boundary layer

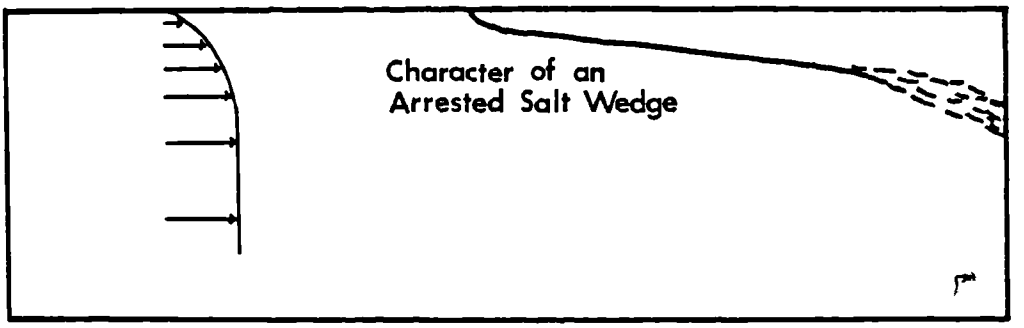


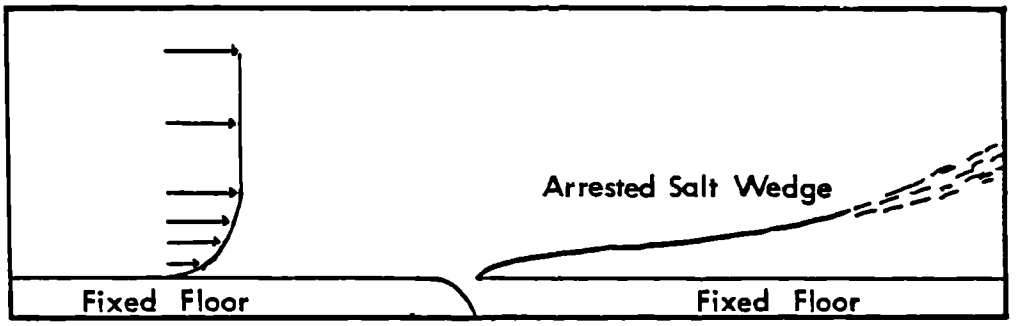


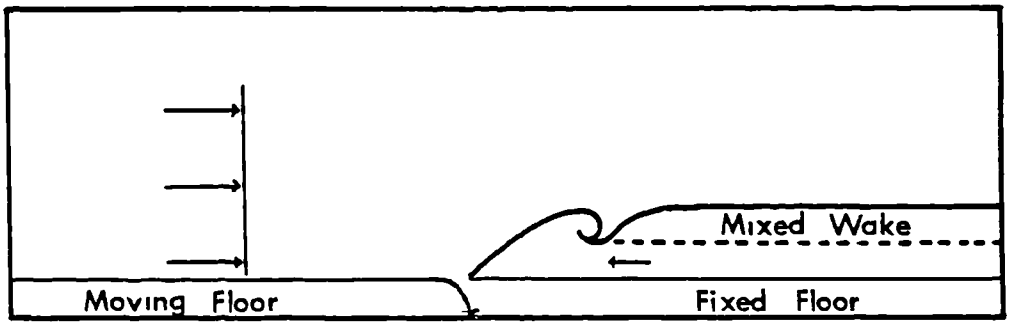


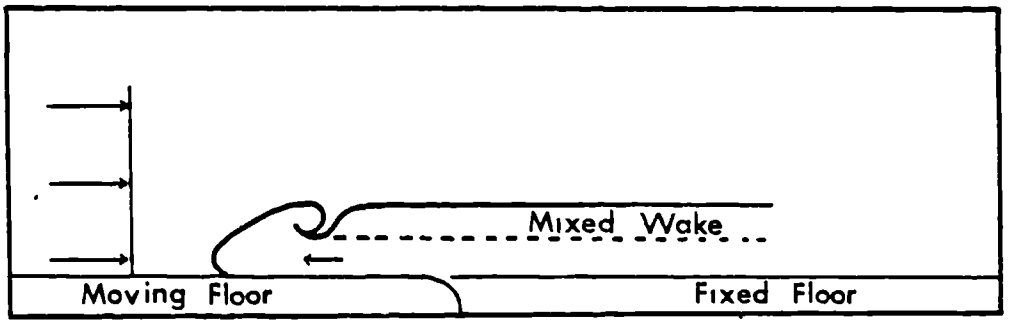


figure 6.4

On the small scale of laboratory-based models, surface tension becomes much larger in relation to other forces and effectively prevents successful modelling of surface density currents. Even with highly efficient chemical wetting agents, introduction of a surface barrier to hold the current leads to the formation of a surface boundary layer. For this reason the estuary was 'inverted' and the density current modelled on the floor. Formation of a boundary layer and thus a non-uniform vertical profile of velocity may then be overcome by moving the floor at the stream speed towards the density current. In this way, a free-slip boundary condition at the estuary surface may be modelled by holding the density current at the end of the fixed floor, where the approach flow is vertically-uniform (figure 6.4d).

The aim of the modelling was to test the hypothesis that transverse gradients of tidal velocity in the estuary are directly responsible for the three-dimensional character of the front. Thus it was proposed to create a faster central approach flow in the model and to observe its effect on the current. To this end two techniques were devised; the first, to introduce a curved gauze sheet in the approach flow and thus slow the sidewall velocities; and the second, to recreate the (inverted) estuarine topography with a submerged 'V'-section roof over the current.

Problems with the boundary condition in the first of these two methods proved insurmountable and it was soon abandoned. This was because the transverse velocity gradients set up by the gauze could not be duplicated by the moving floor.

In the second proposed method it was expected that friction at the roof would set up a small transverse gradient in the ambient flow, but its direct effects on the flow were not well understood. It was also expected that the link between density current velocity and fractional depth (equation 2.3) would produce a complex

three-dimensional head wave, tending to maintain a constant fractional depth across the tank.

Without the roof, the experimental procedure was identical to that used by Simpson and Britter (1979). At a constant rate of saline inflow a density front emerges from the settling well and advances slowly along the fixed floor inside the boundary layer (figure 6.4c), experiencing no instability at its upper surface. On reaching the end of the fixed floor its leading edge halts and further saline inflow deepens the current. At this stage it changes from the profile of figure 6.4c to that of figure 6.4d with an attendant head wave and mixed wake. Equilibrium is established when mixing losses at the head are equal to the saline supply rate, at a value determined by the speed of the ambient flow.

At this stage, a small decrease of the ambient flow velocity (and the moving floor) allows the current to advance slowly and evenly onto the moving floor. By so doing, the current profile changes from figure 6.4d to figure 6.4e which raises the 'nose' slightly above the moving floor. The head then becomes convoluted with lobes and clefts (Simpson, 1972) but its front remains approximately linear across the tank.

With the addition of the roof, a similar procedure produces a 'free-slip' density current at the end of the fixed floor that is, in all visible respects, similar to the current seen without the roof. Its front remains linear and two-dimensional (figure 6.5a).

When the current is permitted to advance onto the moving floor, however, a striking difference is immediately apparent (figure 6.5b). Progression from the fixed to the moving floor begins at the sidewalls in two leading arms of flattened, approximately conical cross-section. The two arms advance along the moving floor joining some 12-15cm behind, to form a sharp 'V' at the centre of the tank. The frontal 'V' is persistent and stable, advancing along the moving floor to its equilibrium position, appearing (dyed with milk) as in figures 6.6a,b and c.

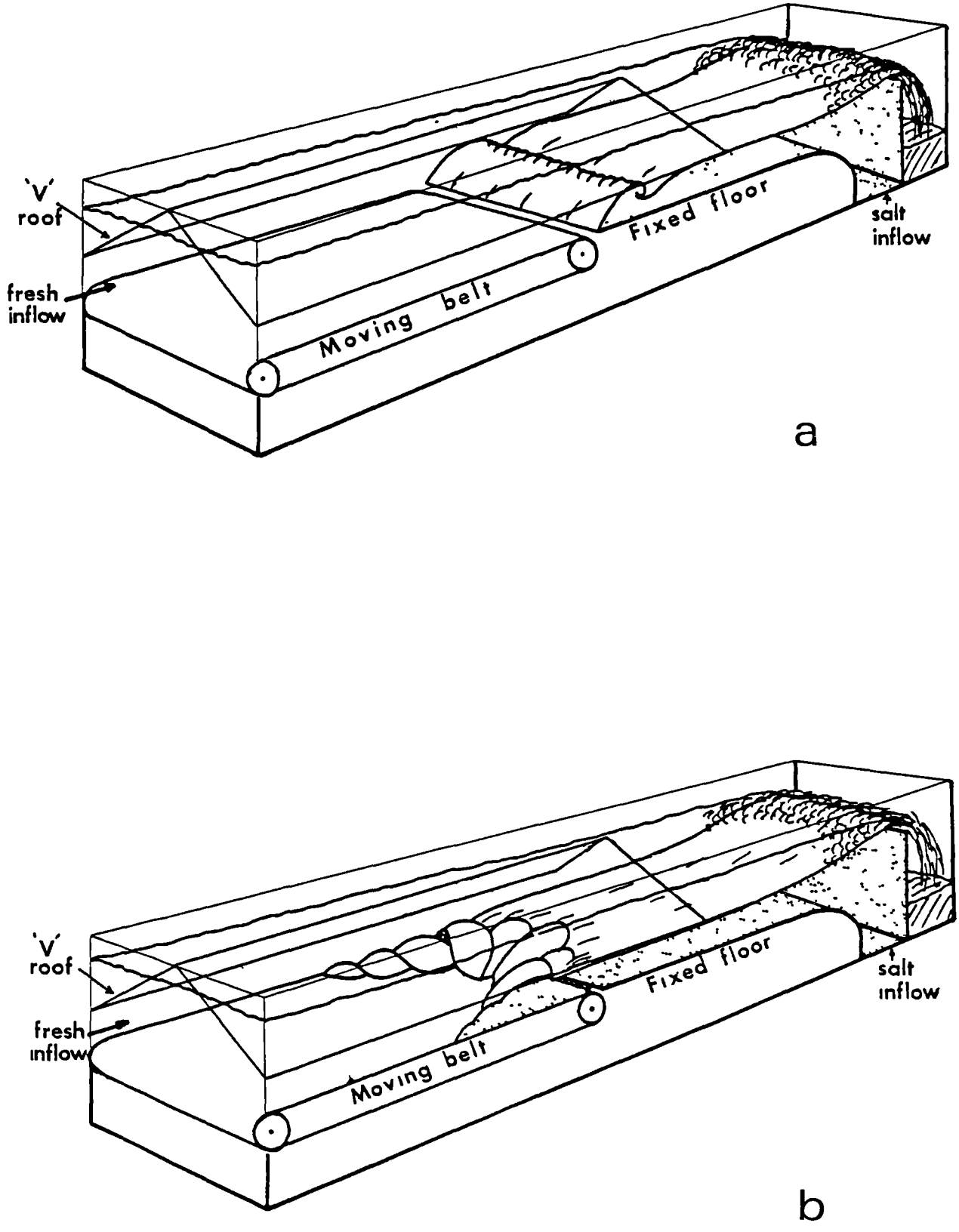


Figure 6.5 Density currents, below the 'V'-section roof and subject to a vertically-uniform ambient flow, placed at the end of the fixed floor (upper) and over the moving floor (lower).

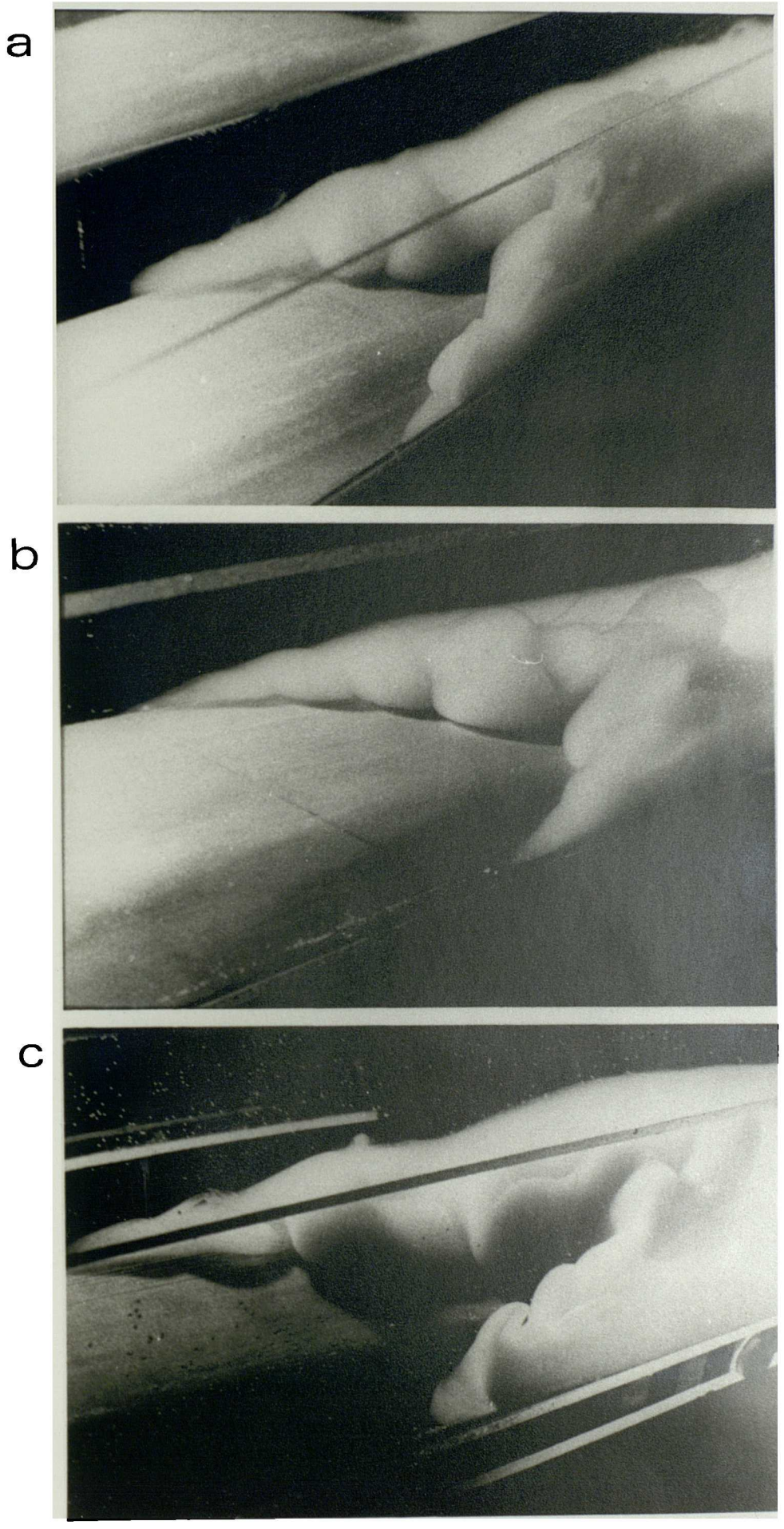


Figure 6.6 Three views of the modelled density current over the moving floor and below the 'V'-section.

Compared to the head wave seen without the roof, the 'V'-shaped head shows some remarkable features. There is a tendency to maintain a laterally-constant fractional depth in a line across the tank through the apex of the 'V'. The boundary of the current on the floor (the estuary 'surface' front) is indented at regular intervals along the arms in cusps; these are the bases of lobes in the arms of the current head. Instability and mixing, in contrast to the two-dimensional current, are concentrated predominantly in the central regions near the apex of the 'V' where a large Kelvin-Helmholtz billow may be seen. (Within one tank-width behind the apex, the current depth becomes laterally-uniform, although this may be due to its proximity to the end of the roof.)

The three-dimensional character of the system reaches a peak of complexity with the internal flow regime of the head wave. Figure 6.6b shows a near-perpendicular view of one arm, with three well defined lobes visible, decreasing in size toward the tip. The outer skin of each arm may be imagined as a solid structure rotating in such a way that fluid supplied from the density current on the bed emerges from below, revolves in the skin of the arm and returns along the upper interface. The lobes on the rotating arm thus appear to move towards the apex but the skin flow is, in fact, longitudinal. Motion inside the arms, however, is not longitudinal, but from the apex out to the tip of each arm. Dye placed inside an arm near the apex of the 'V' revolves in the same sense as the outer skin, but also makes a small advance toward the tip in the manner of a screw. The pitch of the screw is appreciably shorter than the lobe length, and the dye makes many revolutions before reaching the sidewall. Once at the side it emerges to form the outer skin of the final lobe and is then returned in a longitudinal flow along the upper interface.

One further observation should be noted. The head wave of all density current types is easily disrupted by sudden changes of flow regime, such as an increase of the approach flow velocity. Such abrupt changes inevitably occur in the establishment stages of each run and the 'V'-shaped head wave is apparently one of two stable head configurations seen in the tank. The second type is a single, linear front aligned obliquely to the ambient flow, at approximately the same angle (30°-40°) to the sidewall as the arms of the 'V'. It is deepest at its trailing end and includes lobes along its length and cusps on the lower boundary front.

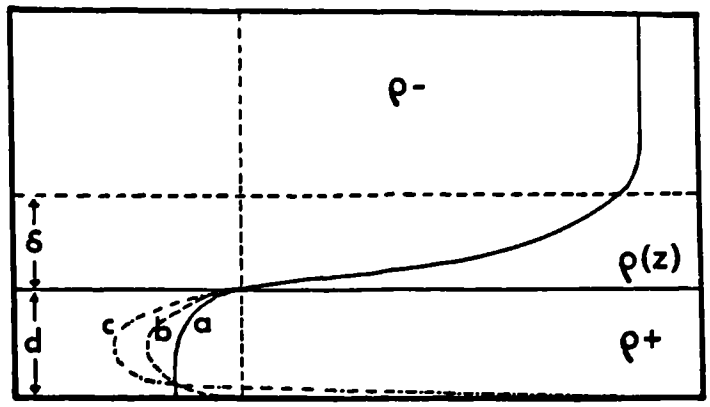


Figure 6.7 Lower boundary conditions operating in the estuary (a), the density current at the end of the fixed floor (b), and the density current over the moving floor (c).

Attempting to relate the modelled 'V' to the estuarine front reveals a discrepancy with regard to the lower boundary condition. The 'V' is produced by the arrangement of figure 6.5b with the current head placed over the moving floor (figure 6.5b). In the estuary, (after re-inverting) this arrangement would require a strong landward wind to produce the same boundary condition over the surface current and, clearly, no such wind is necessary. The 'free-slip' arrangement of figure 6.5a more closely reproduces the estuarine situation but a boundary layer is, nevertheless, present in the fluid advancing toward the stationary head. Figure 6.7 illustrates these two, and the surface estuarine boundary conditions. Although the arrangement of figure 6.5a does not produce a 'V'-shaped current head, it seems likely that any such tendency would be suppressed by the formation of a boundary layer between the 'arms', thereby assisting the re-establishment of a linear, transverse front. Furthermore, while the exact effect of the roof on the transverse gradient of the ambient velocity is not known, transverse gradients in the estuary are nevertheless substantially greater than those produced in the model.

Notwithstanding these limitations, the model experiments do demonstrate the possibility that the transverse velocity structure, associated with a variable depth section, may induce a

three-dimensional density current head with features resembling those in the Seiont. The following specific points of similarity should be noted:

i) the modelled structure displays two stable forms; a 'V' and an oblique linear front, both of which have been seen as stable configurations in the Seiont estuary and in Loch Creran.

ii) the modelled front, as a result of the lobes along the arms, is characterised by regular cusps; a feature that is very well defined and often seen in the front in Loch Creran. Cusps have only been seen, however, in the Seiont plume front and not in its T.I. form.

iii) the apex in both model and estuary is sharp.

iv) both features contain overturning billows at the fronts.

At this point, we turn to the means by which a 'V'-shaped boundary and, in particular, a sharp apex may be produced by an estuarine flow. We presume, from the model and from fieldwork, that the transverse gradient of tidal flow is the responsible agent. One further assumption is necessary to provide an explanation; that the rate of advance of a density current $u_d$ always acts perpendicular to its frontal boundary. This assumption remains untested in both our modelling efforts and the literature concerning density currents.

In figure 6.8, the frontal angle $\theta$, adjusts to a value at which the component of tidal velocity balances the density current velocity, i.e.

$$u_T \cos\theta = u_d \qquad 6.1$$

where $u_T = u_T(y)$. From which;

$$\theta(y) = \cos^{-1}(u_d/u_T) \qquad 6.2$$

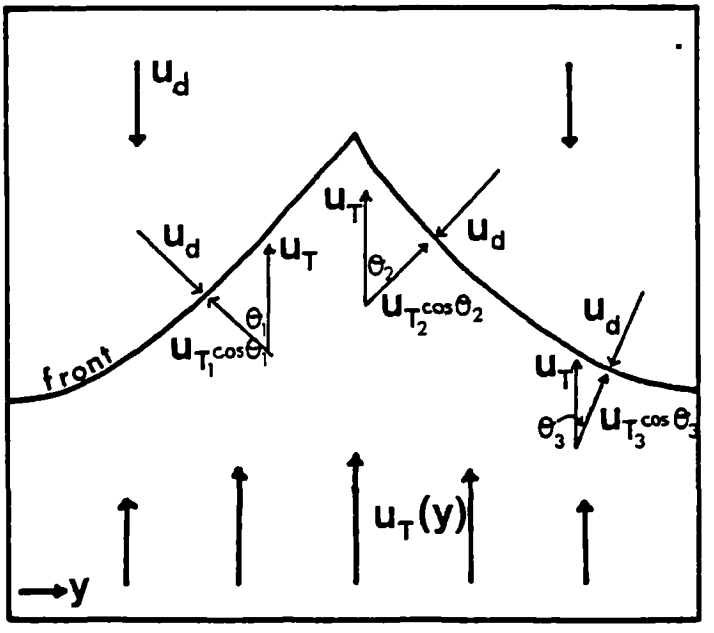


Figure 6.8 Definition sketch for calculation of frontal arm angle.

The frontal location inside the estuary responds to the lateral-mean tidal velocity, and the arm configuration reflects lateral deviations from the mean. A channel flow with the greatest velocities near the axis would thus tend to produce the largest values of $\theta$ close to the axis. Note also that there are two stable configurations arising from this argument: a 'V'-shaped front, because $\theta$ may be positive or negative, with the apex at the lateral position of the maximum tidal velocity, and a linear, oblique front in which the sign of $\theta$ remains constant across the channel. Both forms of frontal boundary were seen in the modelling experiments and in the estuary.

Hypothetically, if the upper layer and its frontal boundary were replaced by a solid, frictionless body, all tidal flow perturbations induced by the body would be vertical i.e. there would be no motion parallel to the frontal arms. Increased friction between the ambient and density current fluids leads to an increased parallel component of motion; the extent of this perturbation to longitudinal flow reflects the degree of viscous coupling between the two layers. Indications from the fate of dye in the estuary suggest very little coupling of this kind, and movements parallel to the front shown by debris appear to be the result of vertical shear acting on buoyant particles that are unable to sink below the density current layer.

## 6.3 VERTICAL EXCHANGE PROCESSES

Garvine (1974) developed a two-layer, numerical model of the dynamics of a small-scale (plume) front comprising an upper light fluid, which constituted the density current, and a lower, ambient fluid of greater density. He went on (1979a and b) to extend his model to cover fronts of all scales and, in doing so, he considered the nature of the vertical exchange processes in some detail. From the behaviour of the model he concluded that a net loss of fluid from the density current (i.e. negative entrainment) gave results most closely resembling the behaviour of the Connecticut plume reported by Garvine and Monk (1974).

Kao, Park and Pao (1977) also developed a numerical model of a surface density current by solving the full Navier-Stokes' equations. They too used a two-layer model and from the increase of surface density with time concluded that the density current experienced a net gain of fluid from below (i.e. positive entrainment).

The discrepancy between these two interpretations was due to a difference in defining the density current. Laboratory experiments clearly show a three-layered structure which includes an intermediate, finite-width pycnocline. Garvine excludes the pycnocline from his upper layer whereas, Kao, Park and Pao include it. In this thesis we have considered that only the uncontaminated fluid advancing towards the head constitutes the density current, following the line of Britter and Simpson (1978) and Simpson and Britter (1979) (BS and SB). Thus, in a two-layer model, the pycnocline is incorporated into the ambient fluid and this consequently defines the direction of fluid exchange as negative with respect to the density current.

(In the hypothetical case of an infinitessimal pycnocline, fluid loss from the density current acts to reduce the frontal velocity by reducing d in equation 2.3. However, it is a simple matter to show that positive entrainment has no effect on the frontal velocity because, while reducing $\Delta\rho$, it also increases d.)

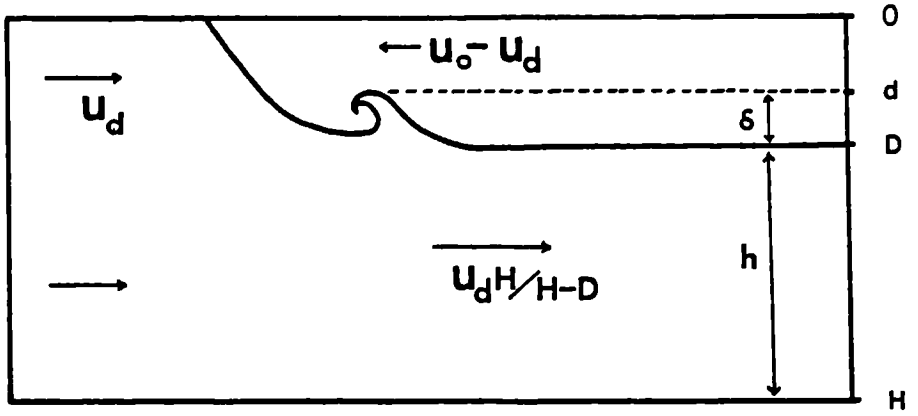


Figure 6.9 Definition sketch for extension of Stigebrandt's analysis.

Stigebrandt (1980) reported a simple analytical model of the three-layer case (outlined in chapter 2), which included a finite-width pycnocline. The model was used to determine the velocity of the current fluid with respect to the front (the 'overtaking' velocity in the terminology of BS) and the relative quantities of fresh and saltwater making up the pycnocline.

It is instructive to modify Stigebrandt's model to include the non-linear velocity and density profiles in the pycnocline measured by BS, and also the effects of an ambient layer of finite depth. With these modofications, we use the experimental result (BS) that $u_o \sim 1.16 u_d$ to determine appropriate pycnocline thicknesses and their relative constituents.

Figure 6.9 defines the quantities. We use a two-dimensional, stationary co-ordinate system in which x is a longitudinal direction and z is vertically downward. Velocity and density anomalies are defined as;

$$u(z) = \begin{cases} u_o & 0 < z < d \\ [u_o + u_d \psi][(D-z)/\delta]^m - u_d & d < z < D \\ -u_d \psi & D < z \end{cases} \qquad 6.3$$

$$\Delta\rho(z) = \begin{cases} \Delta\rho & 0 < z < d \\ [(D-z)/\delta]^n & d < z < D \\ 0 & D < z \end{cases}$$

where $\delta=D-d$, $\psi=[(H/h)-1]$ and m and n are chosen according to the experimentally-derived variation of velocity and density respectively.

By subtracting the frontal velocity $u_d$ we convert to a front-based co-ordinate system and, in the steady-state, a condition of no net buoyancy transport through the frontal zone (figure 2.3) is expressed as;

$$\int_0^D [u(z)-u_d]\,\Delta\rho(z)\,dz = 0 \qquad 6.4$$

The integration leads to;

$$u_d = u_o \frac{[(n+1)(m+n+1+S)]}{[(m+n+1)(n+1)+(n+1+mH/h)S]} \qquad 6.5$$

where $S=\delta/D$, i.e. the ratio of pycnocline to density current thicknesses. This result reduces to Stigebrandt's (equation 2.4) for $m=n=H/h=1$.

The 'overtaking' velocity $u_p$ is defined as;

$$u_p = u_o-u_d \qquad 6.6$$

which, substituted into eqation 6.5 gives;

$$S = \frac{(u_p/u_d)(m+n+1)(n+1)}{mH/h - (u_p/u_d)(n+1)} \qquad 6.7$$

Although there is no net buoyancy transport through the frontal zone, there is still a net fluid transport $Q_s$ given by;

$$Q_s = \int_0^D [u(z)-u_d]\,dz \qquad 6.8$$

After integration and non-dimensionalising with respect to the density current transport in a front-based reference frame, we obtain;

$$Q_s/u_p d = -n(m+n+2+S)/(m+1) \qquad 6.9$$

Note that this result is independent of fractional depth. (Stigebrandt non-dimensionalises in a stationary frame using $u_o d$, and obtains a result which depends upon the fractional depth of the current.)

Using the experimental results of BS and SB;

$$m \simeq n \simeq 4$$

$$u_p/u_d \simeq 0.16 \pm 0.04 \qquad 6.10$$

defines the ratio of pycnocline to density current thicknesses (S) appropriate to laboratory density currents in the physically possible range $0.65<h/H<1.0$ (from equation 6.7);

$$1.0 < S < 3.0 \qquad 6.11$$

With this range of S values in equation 6.9 leads to;

$$8.8 < Q_s/Q_f < 10.4 \qquad 6.12$$

where $Q_f = u_p d$. Stigebrandt assumed linear velocity and density profiles in the pycnocline, which gave a ratio $Q_s/Q_f$ of ~2.0. BS measured the vertical profiles and found $m \simeq n \simeq 4$, which indicates a ratio of saltwater to freshwater volumes within the pycnocline of ~10.

# SECTION II - THE AXIAL CONVERGENCE

# CHAPTER 7

# THE CONWY ESTUARY, NORTH WALES.

## 7.1 THE ESTUARY

The Conwy estuary (see Hunter and Lailey, 1980 for a multi-disciplinary literature review) discharges to the west of the Great Orme, just beyond the eastern end of the Menai Straits into the part of the Irish Sea known as Liverpool Bay (figure 4.1). It is the largest estuary in North Wales, of the coastal plain type with a very wide, but shallow cross-section. The Department of the Environment (1973) certify it as class A or pollution free, despite the 13 or so raw sewage outfalls along its length. This conclusion is supported, however, by the abundant marine life to be found in the Conwy valley including important oyster and mussel beds, salmon spawning grounds and many different species of birds.

The estuary (figure 7.1) is 22.6km in length from its mouth, at the Deganwy narrows, to the landward extremity of tidal influence, at Llanrwst. The estuary channel has two constrictions: one at the Deganwy narrows (~200m) and the second, dominating constriction (~80m) formed by the causeway (built in the 1820's) which links the town of Conwy to the Great. Orme. Both constrictions induce very rapid tidal flow which, in the case of the causeway, is responsible for the production of a deep (~18m)

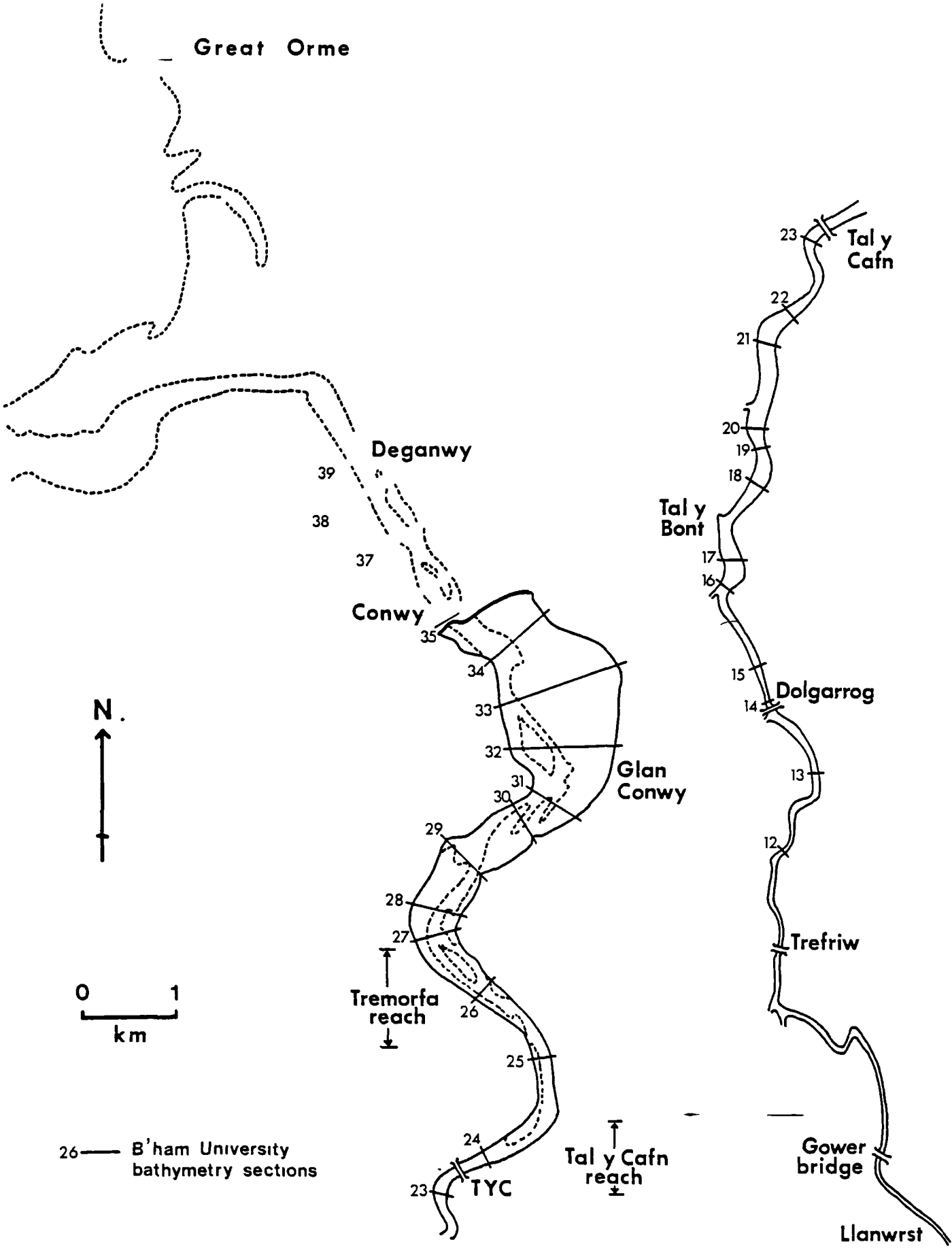


Figure 7.1 The Conwy estuary, North Wales.

scourhole below the three bridges. Landward of the causeway, the estuary widens abruptly to ~1.3km at Glan Conwy and then narrows to ~400m at the start of the Tremorfa reach (see figure 7.1). Beyond Tremorfa, the channel becomes more uniform, narrowing gradually to ~30 m at Trefriw. The bed of the estuary rises ~7 m over the entire estuary length.

Freshwater runoff is gauged at Cwm Llanerch, ~0.5km landward of Llanwrst, where the contributing catchment area amounts to 344km$^2$ of mountainous terrain. A mean runoff of 17.4 cumecs was recorded for the period 1964-1971, with summer and winter means of ~10 cumecs and ~25 cumecs respectively. An extra 316km$^2$ of catchment area supplies tributaries below the gauging station which supplement runoff to the extent of ~3 cumecs (a mean value obtained by the Catchment Losses Method). Over an eleven year period, largest and smallest recorded runoff levels were 509.4 cumecs and 0.45 cumecs.

Tides in the Conwy are predominantly semi-diurnal with very large maximum ranges. At Llandudno the mean neaps and springs ranges are 3.6m and 6.9m respectively, compared to 3.8m and 6.0m for the estuary at Conwy. Assymetry of flood and ebb durations amounts to a ratio of 0.98 for neaps and 0.52 for springs at Deganwy, whereas the change of bed datum is responsible for a ratio of 0.4 at Tal y Cafn for both neaps and springs. Channel friction, caused by the constrictions, large width and shallowness, considerably reduces the reflected component of the tidal oscillation which delays high water at Llanwrst by ~1.2hrs behind Deganwy and, similarly, low waters by ~5hrs.

Knight and West (1978) accurately surveyed water heights against time at a number of positions along the estuary producing the instantaneous surface profiles shown in figure 7.2 for the springs tide of 9.8.75. Points of interest are the rapid tidal rise in the upper reaches of the estuary associated with harmonic distortion. Inertia is responsible for the continued rise of the tide at Dolgarrog (13:00 - 14:00 hrs) when levels were falling at Deganwy.

Typically, tidal stream speeds at mid-flood attain ~50cms$^{-1}$ in the Tal y Cafn and Tremorfa reaches, but the rapid tidal rise

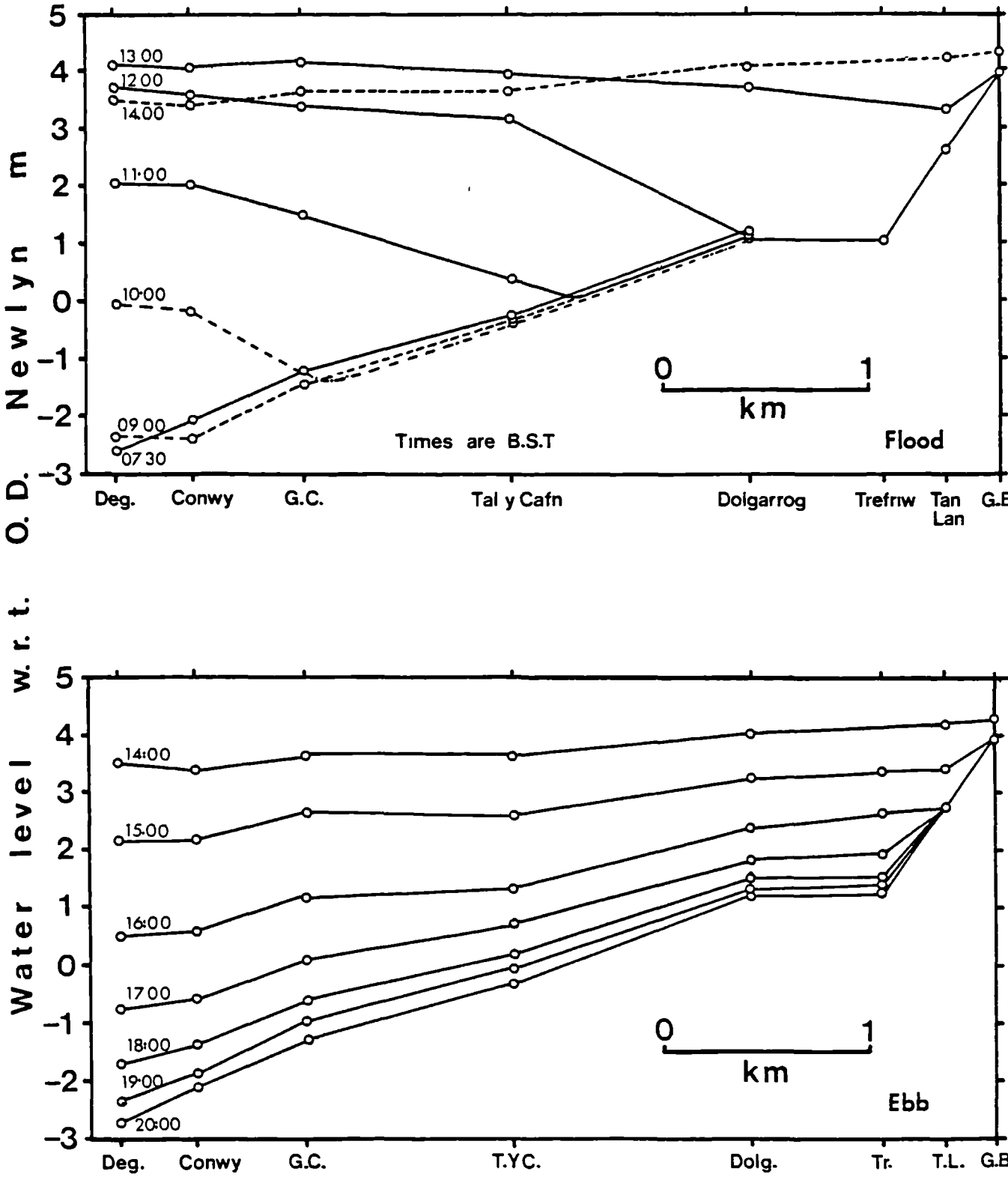


Figure 7.2 Instantaneous surface elevations at positions along the Conwy estuary during the flood and following ebb tides of 9.8.75. (From Knight and West, 1978)

from local low water, particularly during springs, may produce velocities considerably in excess of this level. Such vigorous tidal flows create a well-mixed and highly turbid water column. Stratification exists, to a greater or lesser degree, depending upon the level of runoff, the tidal range, the stage of the tide and the location in the estuary. Attempts to classify the estuary into the scheme of Hansen and Rattray (1966) broadly agree on class 2 for most of the encountered range of the above parameters (Fisher, 1970, Jones, 1974 and Jenkins, 1976). Class 2 estuaries are those for which a net seaward flow exists at the surface with a counterflow near the bed. Salt is transported by both advection (circulation) and diffusion.

Under normal conditions the tidal variation of salinity at a single point in the estuary covers only a part of the full fresh to saltwater range. The Conwy, therefore, differs from the Seiont by its retention of salt inside the estuary at low water, except during abnormally high runoff.

## 7.2 DEVELOPMENT DURING THE TIDAL CYCLE: THE OUTER ESTUARY

At low water the estuary discharge is contained in a relatively narrow, meandering stream, and most of the channel width seaward of Tal y Cafn dries out. The stream divides when it emerges from below the Conwy bridges, with the dominant flow continuing at right angles to the bridges, and a second stream turning to the east to skirt around an intervening sandbank before it re-turns seaward. Following low water, flow in the two streams reverses and strengthens while the sandbank becomes submerged. When the outer estuary is completely inundated, a well-defined frontal system may be seen (Lailey, 1980 and Pelegri, 1979) (see figure 7.3, taken from a cine frame) which bears a resemblance to the tidal-intrusion front of the Seiont, but has a less regular outline. Vertical profiles of salinity confirm that the front separates a stratified column on the upstream side from comparatively well mixed water to seaward. The mixed column is not fully saline (~20‰), however, due to considerable recycling of the previous ebb discharge, and its salinity rises in accord with a smooth longitudinal gradient and the tidal currents.

Increasing flood tide velocities, and hence interfacial shear, augment vertical exchange on the stratified side of the front. The consequent reduction of the interfacial Richardson number enhances further vertical exchange setting up a positive feedback loop which destroys stratification very rapidly. Visually, the front is broken down quite suddenly which allows the fast, surface tidal flow to extend up to, and beyond the bridges.

Following frontal destruction, two strong foam/debris lines form over the approximate paths of the low water streams in the outer estuary. The lines join in a large 'V' either below, or very near to the Conwy bridges, and supply a single continuous line that moves into the estuary meandering along its axis. The 'arms' of the 'V', however, persist as salinity fronts, with stratification on the shore side of each (figure 7.4), but stratification is usually much greater against the causeway than on the western shore.

Surface flow associated with these 'arms' has a small convergent component but is almost entirely parallel to the fronts,

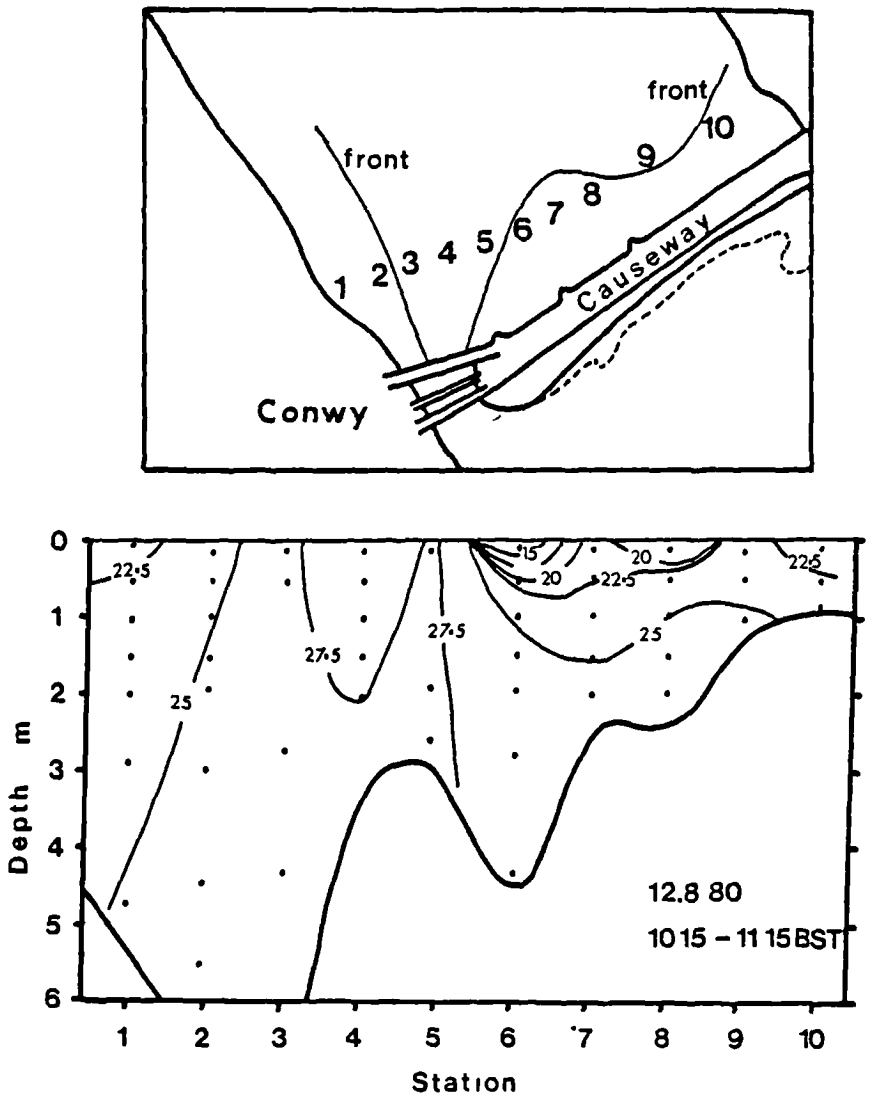


Figure 7.4 Salinity section across the two fronts in the outer estuary, after the collapse of the tidal-intrusion front.

moving landward on both stratified and mixed sides. Boats moored nearby are drawn onto the fronts and follow their course almost exactly, including all meanders (the photographich sequence of figure 7.5 attempts to show this). Stratification against the causeway is produced by a brackish surface layer trapped by the strong tidal flow, whose identity is slowly eroded as the tide continues. Should it remain identifiable until high water, time-lapse cine shows that it spreads as a surface density flow against the weaker tidal currents.

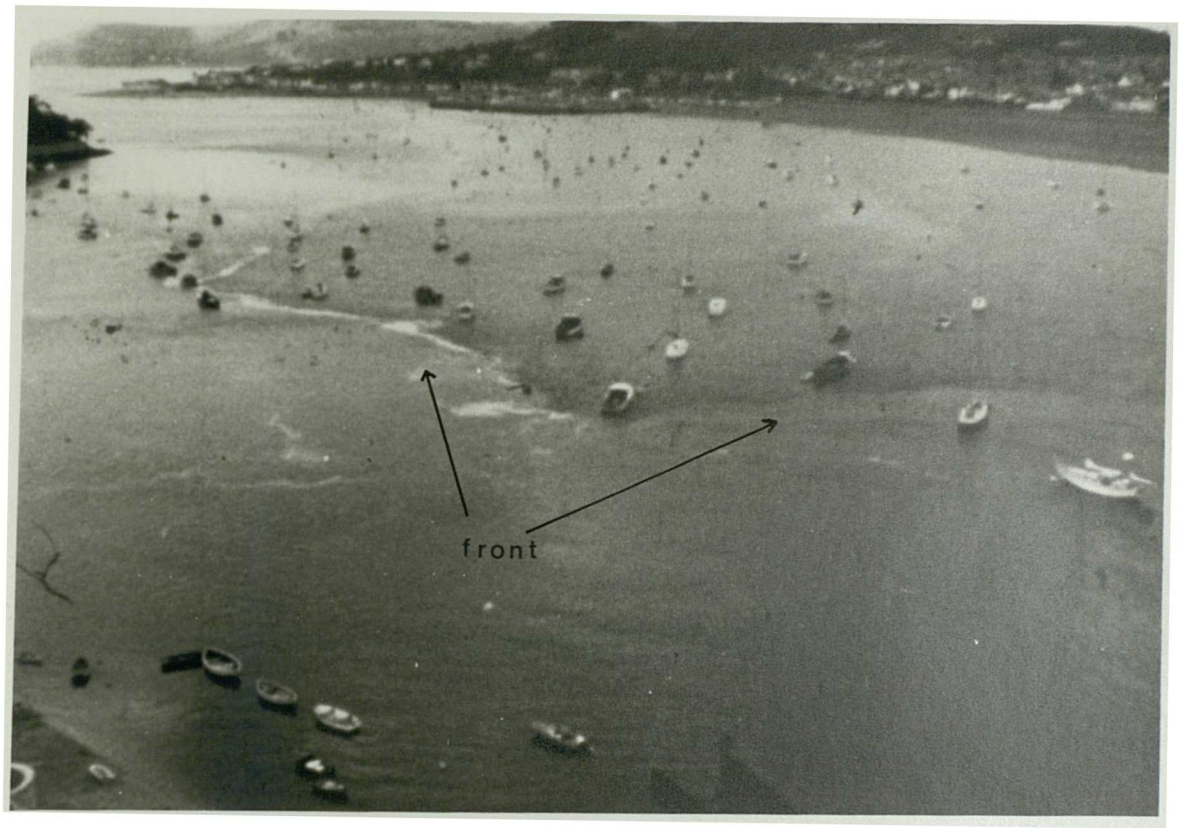


Figure 7.3 Seaward view, from Conwy castle, of the front in the outer estuary during the early stages of the flood tide.

Figure 7.5 Two sequences showing the effects of the fronts on boats moored in the outer estuary. (The main picture shows the two fronts after destruction of the tidal-intrusion front of figure 7.3.)

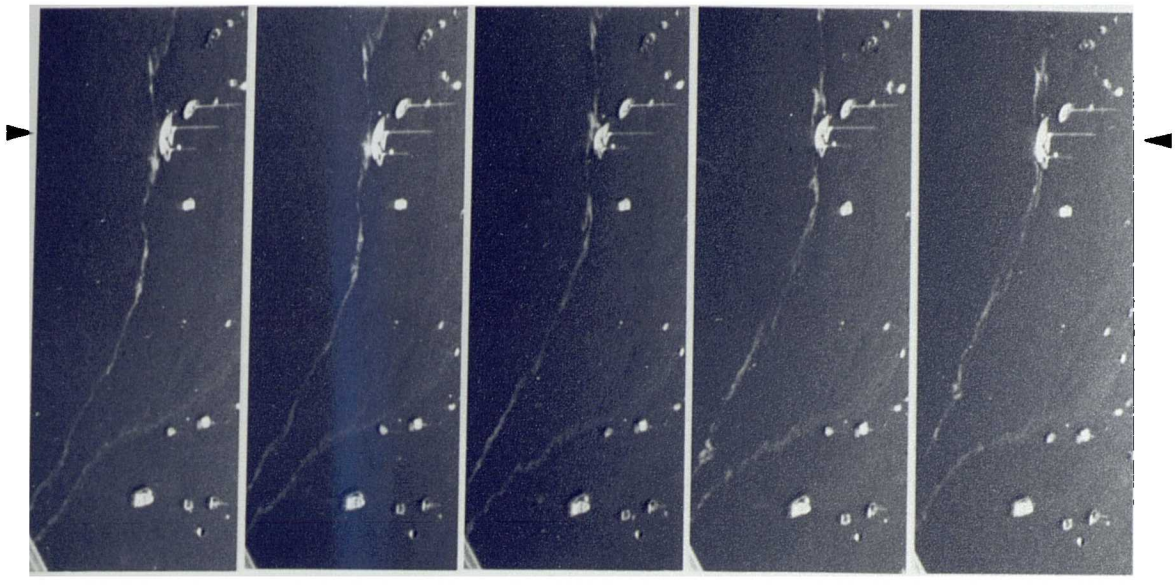

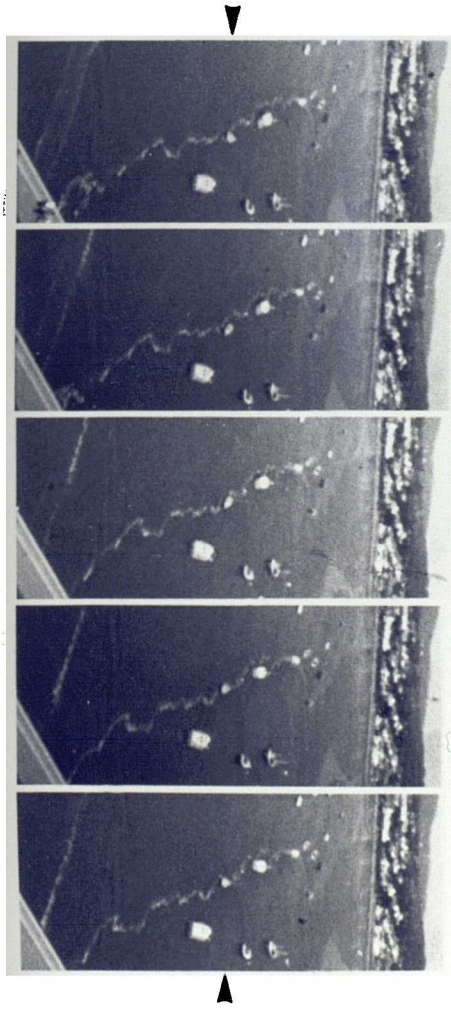

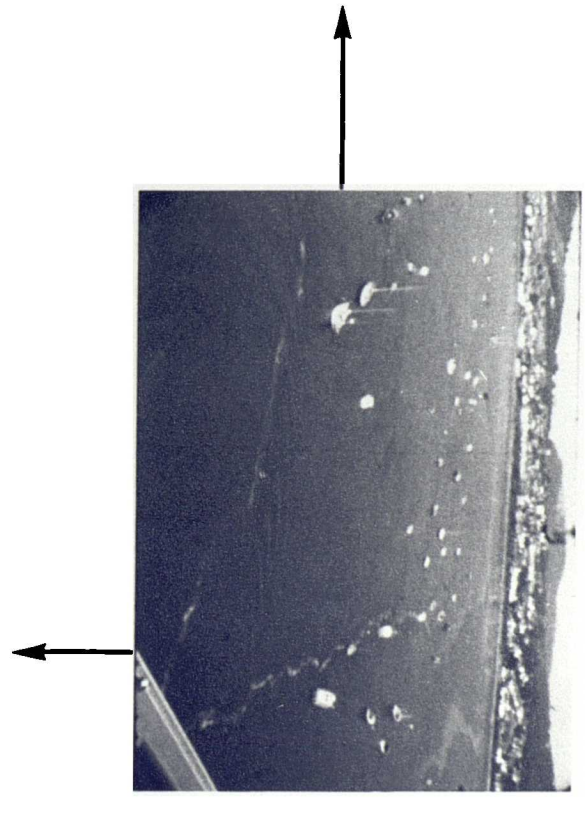

## 7.3 DEVELOPMENT DURING THE TIDAL CYCLE: THE INNER ESTUARY

Landward of the Conwy bridges, following the collapse of the tidal-intrusion front in the outer estuary, a line of debris and foam moves inland extending continuously along a considerable proportion of the estuary length (figure 7.6). The line width may vary with time and/or position from ~0.3m to ~20m either during a single flood tide or from one tide to the next, or it may remain narrow and strong for substantial periods (hours) and distances. (There is a noticeable decline in the amounts of material collected during the winter months suggesting that much of it may be of biological origin.)

In much the same way as we referred to a landward limit for the tidal-intrusion front, the axial line in the Conwy also moves inland to a limit which appears to vary with tidal range and river runoff. During a period of large tides and low runoff a very strong line was observed to move inland beyond Dolgarrog bridge whereas, its penetration during high runoff and smaller tides may be limited to the Tal y Cafn area.

In all observations, the line invariably disperses at approximately the time of local high water; a feature that is made especially clear by time-lapse photography. Following its dispersal and the change of current direction, no similar visible organisation has been observed during the ebb phase of the tide.

The persistence of the foam line in both time and position indicates continuous, active convergence along the estuary length. Superimposed upon the primary tidal flow is thus a transverse secondary circulation, at least during the flood tidal phase.

Measurements of the surface secondary flow associated with the axial convergence have been made after mid-flood when the line becomes established for some distance along the estuary. Most of these measurements were made on calm days in the central region of the Tremorfa reach (see figure 7.1) - a relatively straight, uniform channel in which the convergence is normally well-defined.

Initially, dye was used and tracked by eye to estimate

Figure 7.6 Four views of the debris collected at the Conwy axial convergence: below the Conwy bridges (upper left); from Tremorfa looking towards Glan Conwy (lower left); the Tremorfa reach (lower right) and looking seaward from Tal y Cafn bridge (upper right).

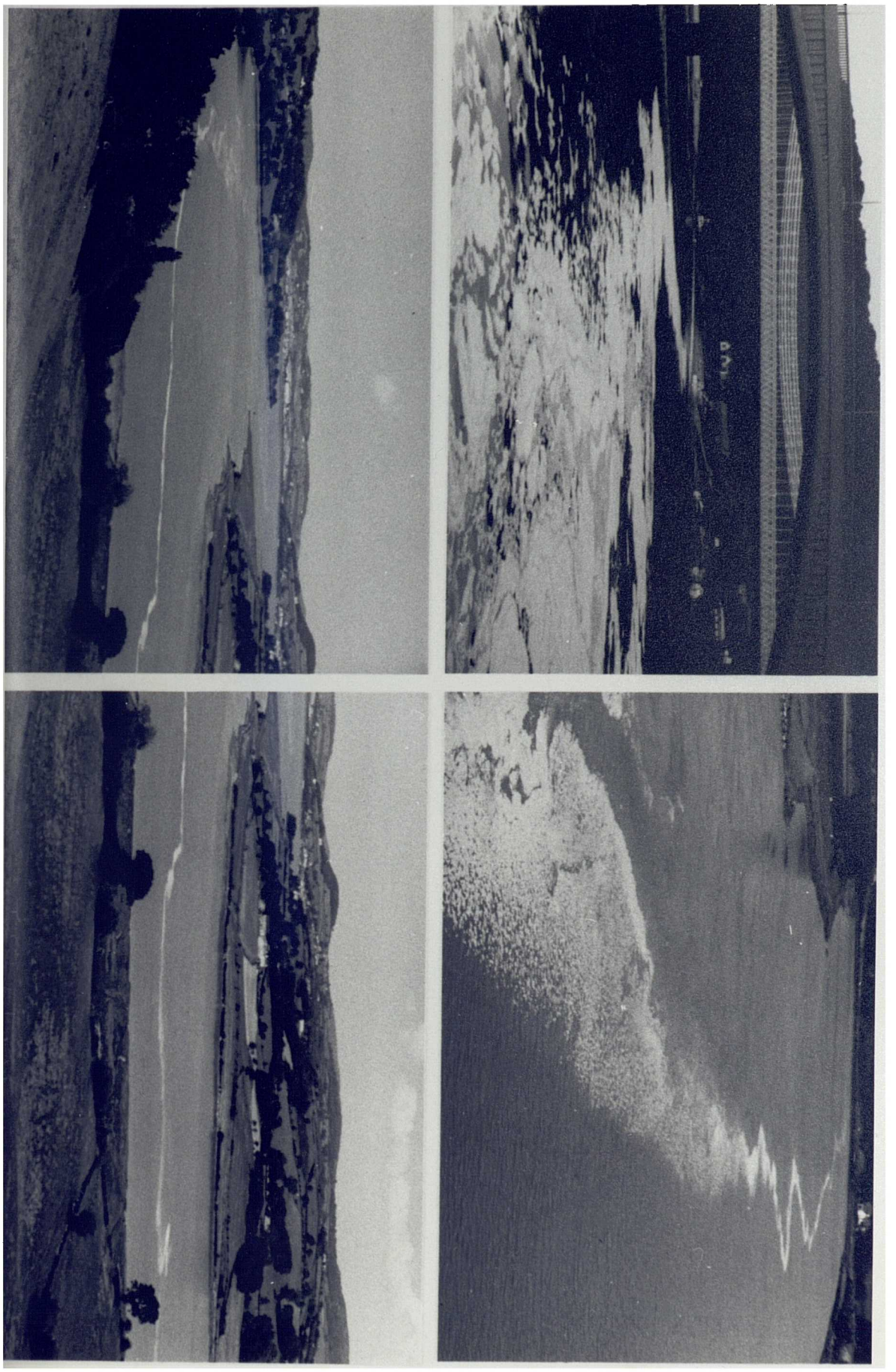

secondary velocities, but the dye was dispersed too quickly by the highly turbulent nature of the flow. Subsequent attempts were made with five-inch square marine-ply tiles coloured with a vivid luminous paint, and individually lettered. Tiles were laid rapidly in sequence at 5m intervals on a perpendicular track across the convergence and their arrivals on the line were timed. Tracks of tiles were usually limited to one side of the convergence covering most of the distance to the shore. After noting the time taken to lay the tiles and knowing their initial distance from the line, it was a simple job to time their arrival and then calculate mean secondary velocities for each one. Since the primary tidal flow is faster near the estuary axis (transverse gradient of tidal velocity) the tiles were also recovered in sequence, with those placed close to the line found at the landward head of the queue. These methods indicated secondary velocities of up to 12cms$^{-1}$ (on either side of the line) which constituted as much as 25% of the primary velocity. Surface convergence extended to a point at least half way from the line to the shore on either side but tended to end abruptly; while one tile might readily move onto the line, the next tile 5m further out would show no such tendency.

West and Cotton (1981) report on dye dispersion experiments in the Tal y Cafn reach of the Conwy during both flood and ebb tides. They found that the dye plume concentration followed the expected enlarging Gaussian curve for all seven ebb trials but only two of the seven flood tides which "....reflects the difficulties found in obtaining flood tide data. On several occasions either the plume could not be found or it could only be found intermittently." They attribute the difficulty to the "... formation of a surface scum line ....[and].....a well defined secondary flow system...during a part of the flood tide." West (personal communication) states that in a final attempt to locate the dye plume (released at the surface) during one of the flood tides, they discovered patches along the bed of the channel. Thus we might conclude that the downwelling located at the foam line extends through most of the water depth. We return to the problems of detecting the subsurface current structure in section 8.4.

There are difficulties associated with trying to determine the cross-sectional density structure in the presence of the

convergence. Surface to bottom salinity differences during the flood tide are typically of the order 1‰. Using a single T/S probe transported by the Dory, vertical profiles at positions on a transverse line are unable to give a sufficiently synoptic picture of the cross-section because the time rate of change of salinity at a single point is large enough to mask the density structure in the time required to sample the cross-section.

Nevertheless, there are good grounds for considering that the axial convergence in the Conwy is density-driven. The clearest evidence comes from the observation of secondary flows only during the flood tidal phase, and their dispersal at or about local high water. If the secondary flow were the result of a dynamical mechanism then it should be equally effective during the ebb phase. Furthermore, following a period of high runoff, fixed station profiling in the Tal y Cafn reach detected no salt in the flood waters until virtually high water. When a measurable salinity finally arrived, the head of the foam line arrived with it.

# CHAPTER 8

# THE SECONDARY FLOW IN THE CONWY.

## 8.1 POSSIBLE CAUSES

In this chapter we shall examine the various mechanisms for the production and maintenance of secondary flows in channels, and attempt to isolate and confirm a particular candidate for the Conwy.

Mechanism I: Distribution of stresses

It was more than a century ago (Darcy and Bazin, 1865) that researchers studying channel flows found that the filament of maximum velocity in a channel is situated below, rather than at the surface. Gibson (1909) proposed this to be the result of a two-celled secondary circulation (figure 8.1) distributing a layer of slower- moving fluid over the surface. He also conducted experiments in a straight, narrow stretch of the river Mersey and observed the convergence of floats toward the channel axis at a speed equivalent to ~4% of the primary velocity. Prandtl (1927) suggested that secondary currents were required to explain the measured shape of isovels (contours of equal velocity) in non-circular conduits (see figure 8.2). These secondary currents transport fluid in the direction of isovel convexity i.e. into the corners, and are induced by the distribution of Reynold's stresses (Einstein and Li, 1958). Kennedy and Fulton (1961) showed that the

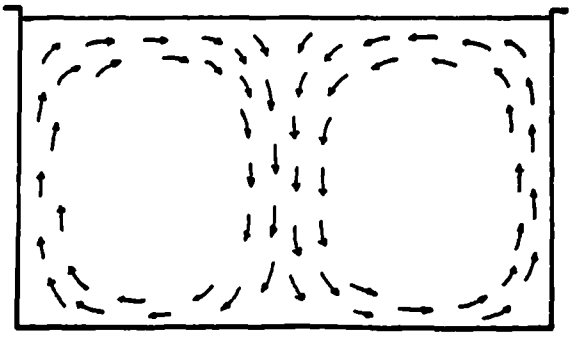

Figure 8.1 Two-celled secondary circulation including surface convergence (from Gibson, 1909).

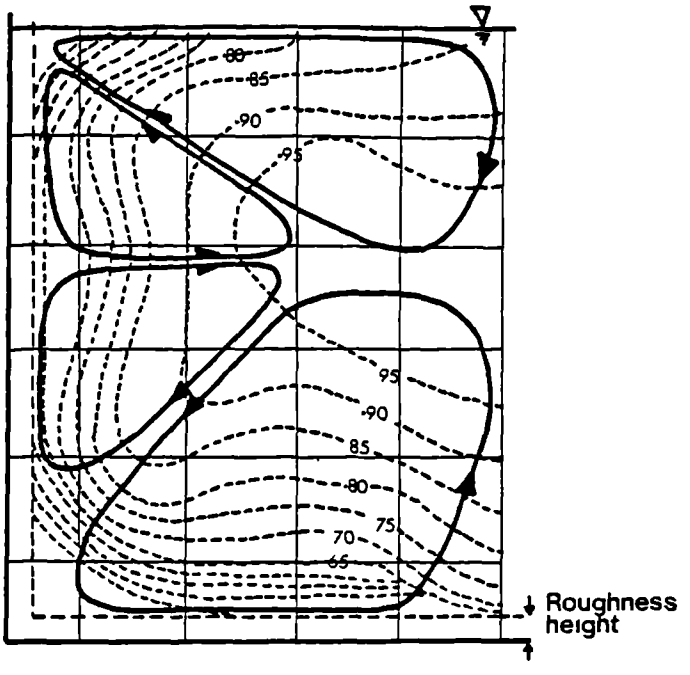


Figure 8.2 Detail of longitudinal isovels (dashed) and secondary circulations in a channel flow of a particular width/depth ratio (from Kennedy and Fulton, 1961).

pattern of secondary cells in a rectangular channel goes through abrupt re-organisations as the width/depth ratio is smoothly varied. Each change of pattern alters the transport capacity of the channel. Liggett et al (1965) calculated the field of primary velocity close to the corner of a channel flow and by comparing with the measured velocity field they deduced the secondary current system. Careful and laborious measurement of the secondary currents showed good agreement, with velocities amounting to 0.6%-2.5% of the primary flow, (for $Re \sim 4 \times 10^5$)

Mechanism II: Bend effects

An imbalance of centrifugal forces in the flow around a bend causes the faster surface flow to move outward which drives a corresponding inward flow at the bottom, (Chow, 1959). Bends have profound effects upon channel flows; alternating bends produce alternating secondary circulations with intermediate transition zones (Dyer, 1977). On the bend itself, the ciculation is normally a single-celled rotation but, in the transition zone between bends, a two-celled pattern may develop.

Mechanism III: Density effects

Prych (1970) conducted a series of experiments in a large flume to determine the transverse dispersion coefficient as a function of varying contaminant buoyancy. He introduced a vertically uniform column of dyed fluid and measured lateral concentrations at successive positions downstream. In relation to the density of the ambient flow, the buoyancy of the dyed fluid was varied from positive through neutral to negative. Prych noted considerable differences in behaviour caused by the development of secondary flows which were always in the same sense - from lower to greater density at the surface and greater to lower density at the bed (cf. density currents). Within ~10m distance down the flume, the density anomaly ($\Delta\rho/\rho$~0.015, u~30cms$^{-1}$) had been reduced to insignificance reduced by turbulent diffusion, and the secondary circulations died down. While its subsequent dispersion rate was similar in all experiments, the dye plume dimensions remained different according to the strength of the initial secondary flows.

Sumer (1976) and Sumer and Fischer (1977) report on similar dye dispersion experiments in a 350m channel without the introduced density anomaly but in stratified ambient conditions. They used a non-uniform channel cross-section produced by building regularly spaced sandbanks and troughs along one side (with a periodicity of ~3.5m; equal to the channel width). Cross-sectional salinity distributions showed signs of mixing over the non-uniform side, while stratification persisted on the uniform side. The cross-sectional density profile produced by the wavy boundary during

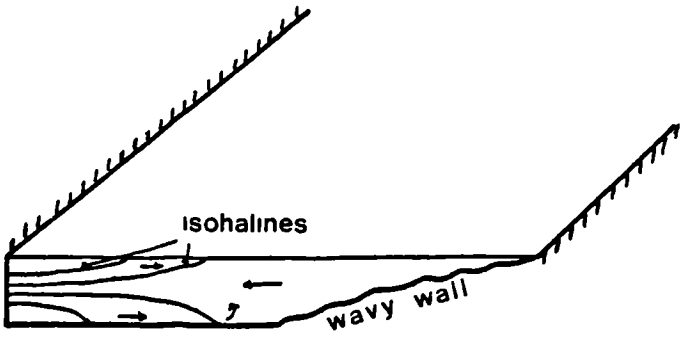


Figure 8.3 Isohaline distribution and resultant secondary currents in the experiments of Sumer, 1976 (from Fischer et al, 1979).

the flood phase resembled that shown in figure 8.3 (from Fischer et al, 1979). Lateral density gradients induced secondary circulations which were observed in the dyed fluid. The observed circulation during the flood included convergence toward the axis at the surface ($\sim 1 cms^{-1}$, i.e. ~3% of the primary flow for $\Delta\rho/\rho \sim 7x10^{-4}$), and a return flow toward the uniform side boundary at the bed. On the ebb, stratification persisted on both sides of the channel with lower salinities over the deeper, uniform side and the sense of the flood circulation was reversed.

Smith (1976), in a theoretical treatment of dispersion in estuaries, includes the effects of time-dependent, two-dimensional secondary circulations induced by lateral density gradients. He obtains an expression for the depth-dependent longitudinal velocity (relative to a reference frame moving at the mean velocity) produced by a (tidal) pressure gradient. This velocity acts upon the longitudinal density gradient to produce an advection of density relative to the moving frame. A pressure gradient acting landward (flood tide) thus produces a sidewall density deficit and corresponding elevation of density over the deepest (least resistant) parts of the section (figure 8.4). An equilibrium is achieved in which the introduction of density anomaly is balanced by transverse diffusion and the vertical advection of density by the secondary circulation, (Mangat, 1982). In this way, a reversal of the pressure gradient (on the ebb) changes the sign of the density anomaly and reverses the sense of the circulation.

In the flow of a cross-sectionally homogeneous fluid through a frictional channel, the greatest velocities are found slightly below the surface over the deepest part of the section. Provided

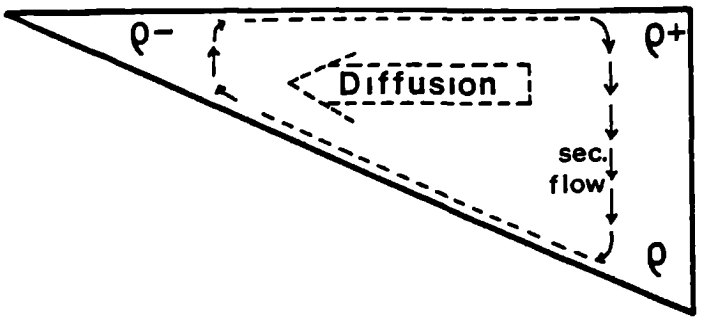


Figure 8.4 Smith's equilibrium between the input of density anomaly and the combined effects of vertical secondary circulations and lateral diffusion.

that the longitudinal density gradient is not a function of lateral or vertical dimensions, there is a resultant tendency to produce a pattern of isopycnals similar to the pattern of isovels, and thus to create a vertically unstable water column. (Currents in the opposite, ebb, sense tend to enhance stability.) Such an unstable situation promotes sinking, most markedly over the deepest regions and its circulation includes surface convergence. This may not be effective, however, if there is a limiting initial stability in the cross-section, in which case the near-bottom density flow may augment the bottom currents to maintain stability.

Outlined above are three distinct mechanisms for the production of a channel secondary circulation: the distribution of stresses in a non-circular channel flow which drives secondary flows into the channel corners; the inertia-produced circulation at a channel bend interacting in combination with those of previous bends; and the baroclinic circulations set up by a non-uniform cross-sectional density distribution. The first two of these mechanisms are properties of homogeneous flows and, as such, do not discriminate between the flood and ebb tidal phases. Observation of convergence in the estuary only during the flood tide suggests that they are unlikely to be fundamental candidates. In the next section we consider the results of an intensive investigation of cross-sectional density in the Conwy.

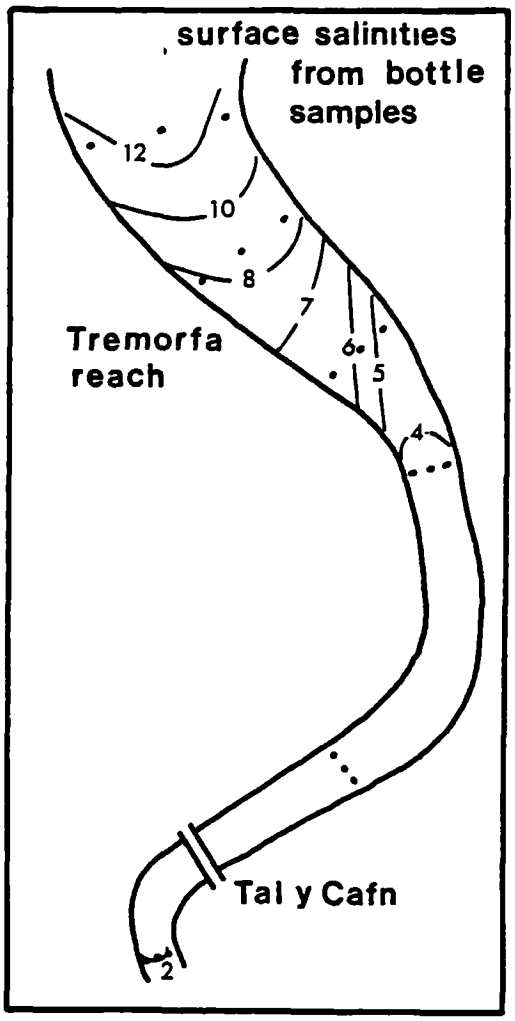


Figure 8.5 Surface salinities obtained from bottle samples during the flood tide of 10.10.80.

## 8.2 THE FIELD OF CROSS-SECTIONAL DENSITY.

It was apparent, from early attempts, that in order to obtain a synoptic picture of cross-sectional density in the estuary it would be necessary to eliminate the effects of the time derivative of salinity at a point (assuming temperature variations to be insignificant). This is because the lateral and vertical gradients in a synoptic section are small enough to be concealed relatively quickly by the temporal variations.

On 10.10.80, the Dory was used to obtain bottle samples at surface points across and along the estuary landward of Tremorfa during the flooding tide (figure 8.5). In the wider, more saline

sections near Tremorfa, highest salinities were found near the channel axis accompanied by appreciable lateral gradients. Moving landward, the highest salinity shifted over to the west bank, presumably due to inertia effects from the previous bend, and the gradients progressively diminished. The limited depth of water prevented samples being taken landward of the debris line limit, although final samples were taken within 100m of its position at the time.

To obtain the required synoptic picture of cross-sectional density, a line of five stations were set up across a transverse section of the Tal y Cafn reach (section 24, figure 8.1) to record surface and bed salinities. Close to each of the two banks a buoy was moored with a T/S probe attached to both the bottom weight and the surface float. In the channel centre, vertical profiles were taken below a moored dinghy, and two stations either side of centre were sampled rapidly at surface and bottom from the Dory. Despite calibration errors (~0.1‰) introduced by the use of six T/S probes, and a period of ~2 minutes required for the completion of one set of measurements, a consistent trend was indicated in the data obtained. A total of 17 near-synoptic profiles were recorded on 13.10.80 and 9 on 15.10.80, and in all of these the maximum salinity was found near the channel axis. To illustrate the trend of the salinity variation with transverse position, and to emphasise the speed at which these variations were concealed by the general rise of salinity with the tide, the surface salinity data from 13.10.80 and 15.10.80 have been plotted against time and position in figures 8.6 and 8.7. The data were treated statistically to find (time) mean spatial deviations from the cross-sectional mean density (as a fraction of the mean density, $\Delta\rho/\rho$) for the periods of the data records (~1hr). These are shown in figure 8.8. The indicated numbers may be read as approximate deviations in $\sigma_t$ units from a mean density of ~1005kgm$^{-3}$. Surface to bottom density differences were typically 0.3-0.55 $\sigma_t$ units (of stratification) with similar vertical gradients throughout the section. Lateral differences were 0.5-1 $\sigma_t$ units, with the greatest density consistently found at the central position.

In September 1981, a full-scale definitive survey of conditions in the Conwy estuary was organized and conducted by the Hydraulics Research Station (Wallingford) and the Civil Engineering

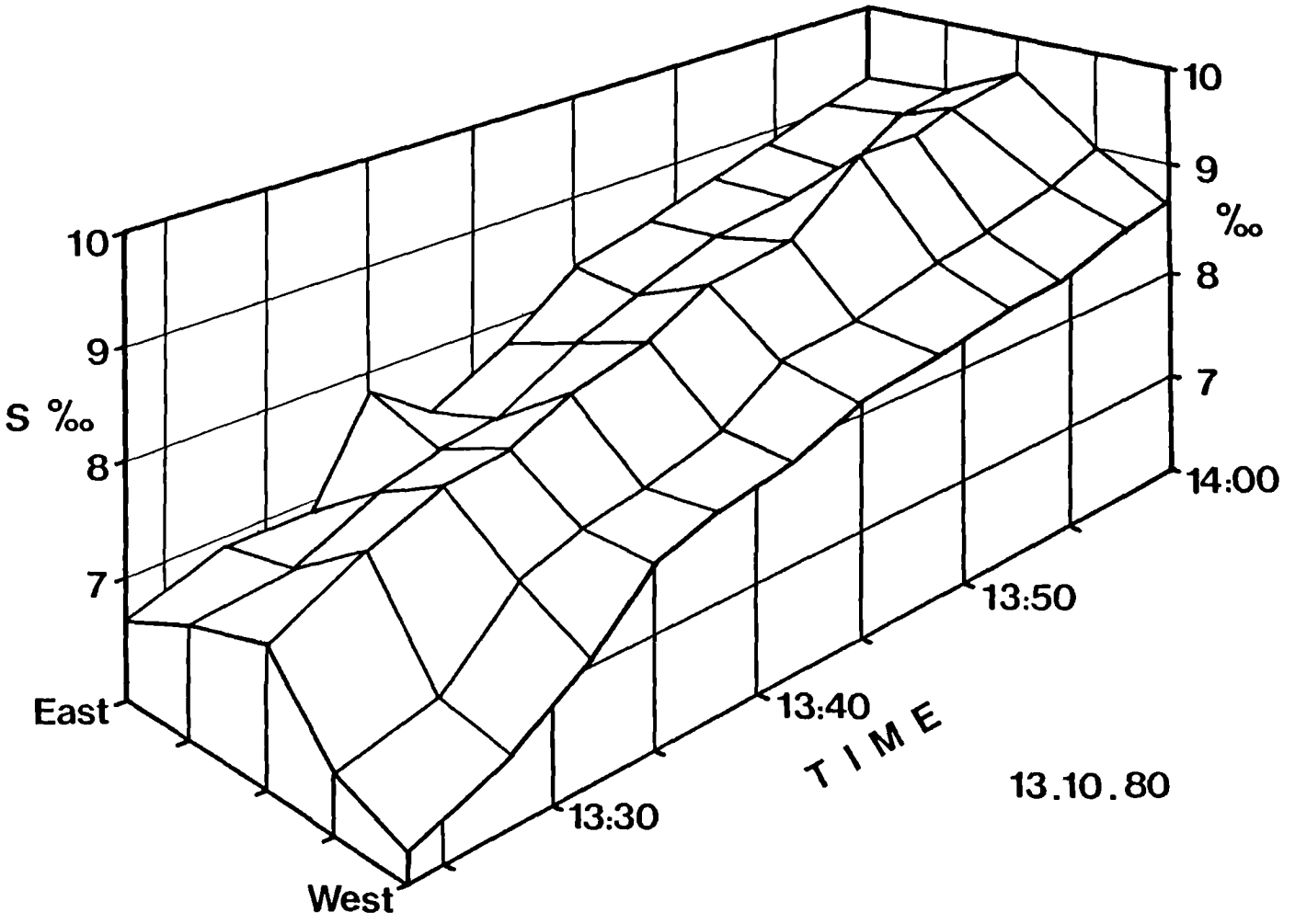


Figure 8.6 Surface salinity at five transverse positions in the Tal y Cafn reach during the last hour of the flood.

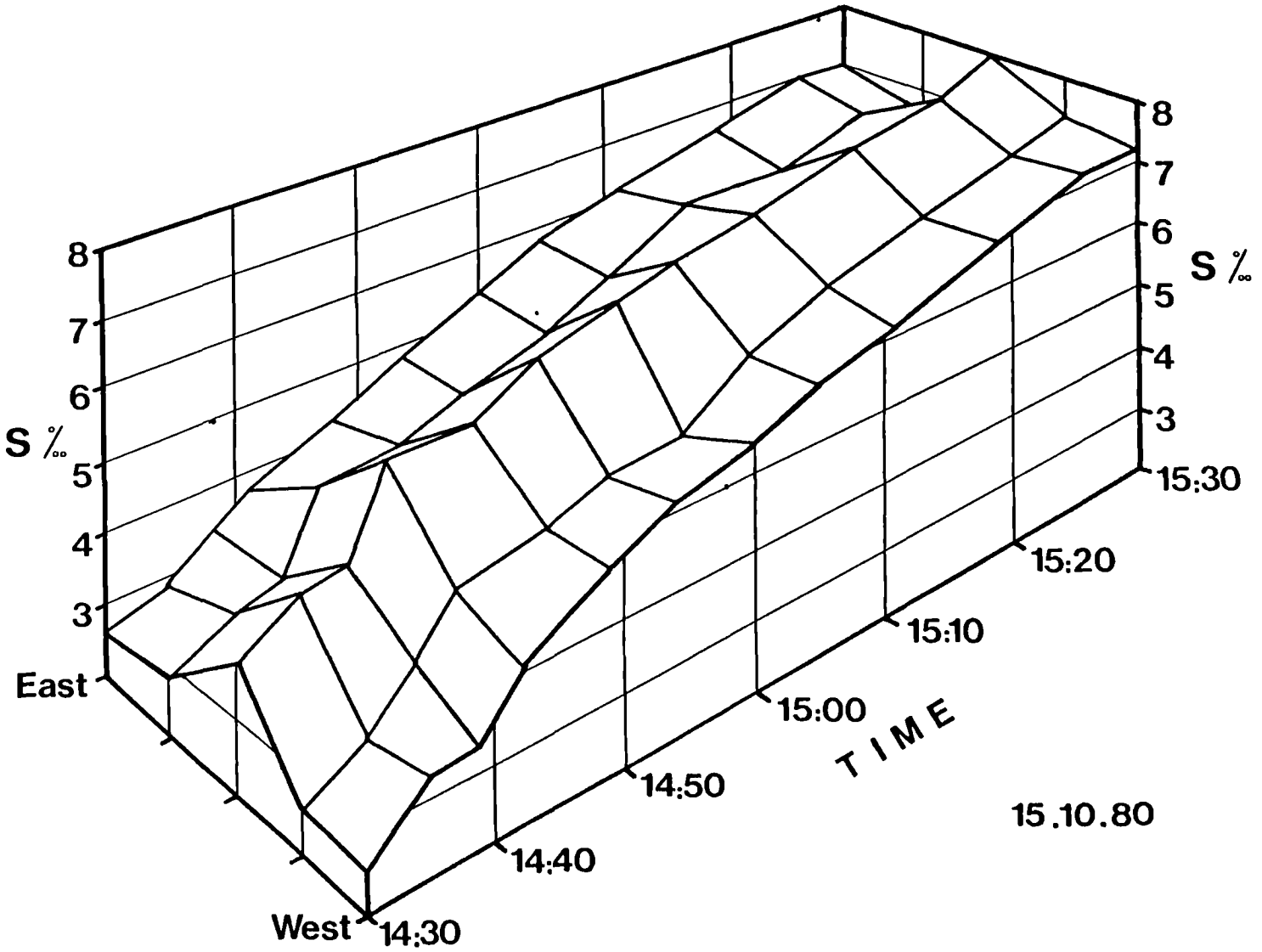


Figure 8.7 Surface salinity at five transverse positions in the Tal y Cafn reach during the last hour of the flood.

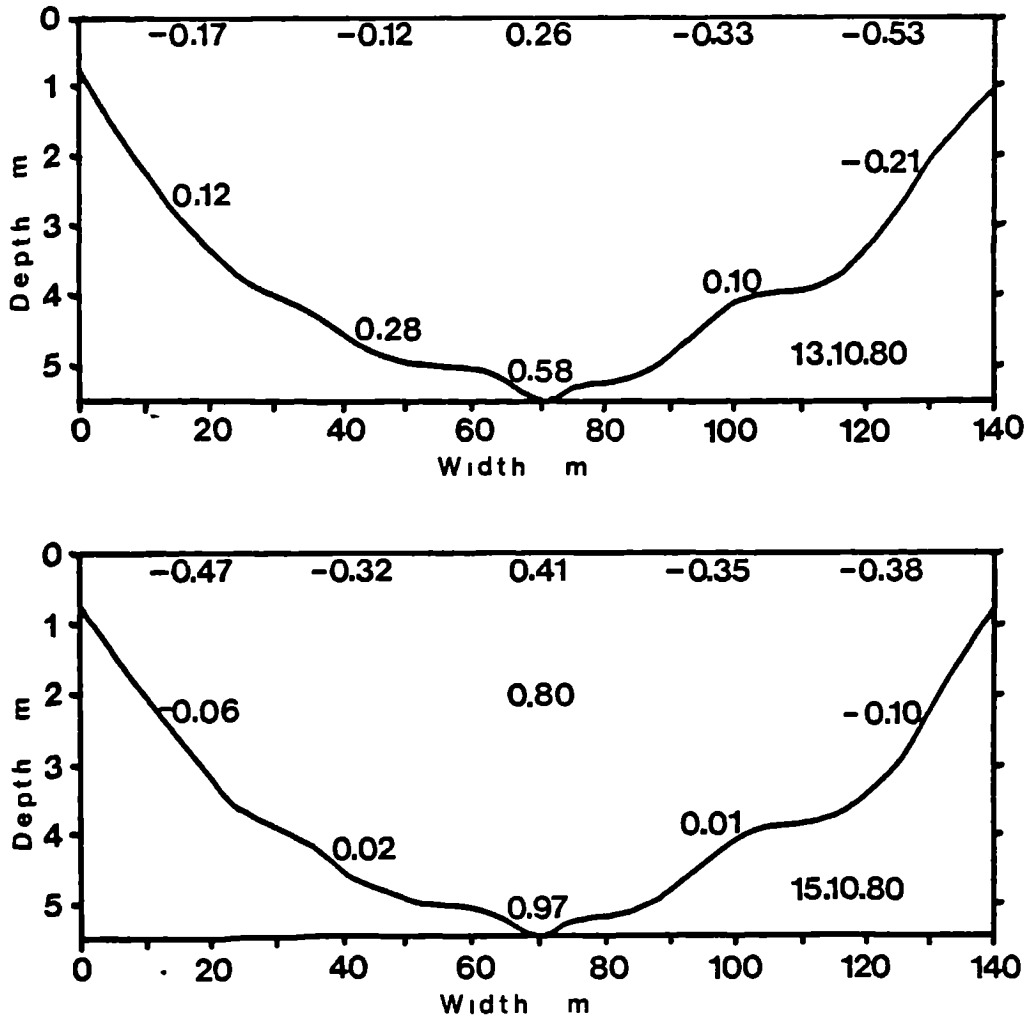


Figure 8.8 Time means (~1hr) of the fractional deviation from cross-sectional mean density in the Tal y Cafn reach, from the data of 13.10.80 (upper) and 15.10.80 (lower).

Department of Birmingham University under Dr. John West. Results were intended for use in a study of dispersion appropriate to tidal channels and will be reported by Dr. West. The survey was based in the Tremorfa reach on section 26 of figure 8.1 from boats moored at five transverse stations, each of which took simultaneous current readings and pumped water samples. On occasion during the survey, one of the boats (equipped with an inductive salinometer and pen recorder) obtained continuous traces of salinity across the channel. Some of these traces from both flood and ebb tides on 11.9.81 are shown in figure 8.9 in which the position of the axial convergence is also indicated. Compared with the characteristically smooth traces of the ebb tide, those of the flood tended to be very 'noisy', in which rapid fluctuations of 0.5-1.0‰ were quite common. These fluctuations were clearly more apparent in the shallow (0.25m)

Figure 8.9 Traces of transverse salinity at constant depth (0.25m, 1.25m and 2.25m) in the Tremorfa or Tal y Cafn reaches during the flood (upper) and ebb (lower) tides of 11.9.81.

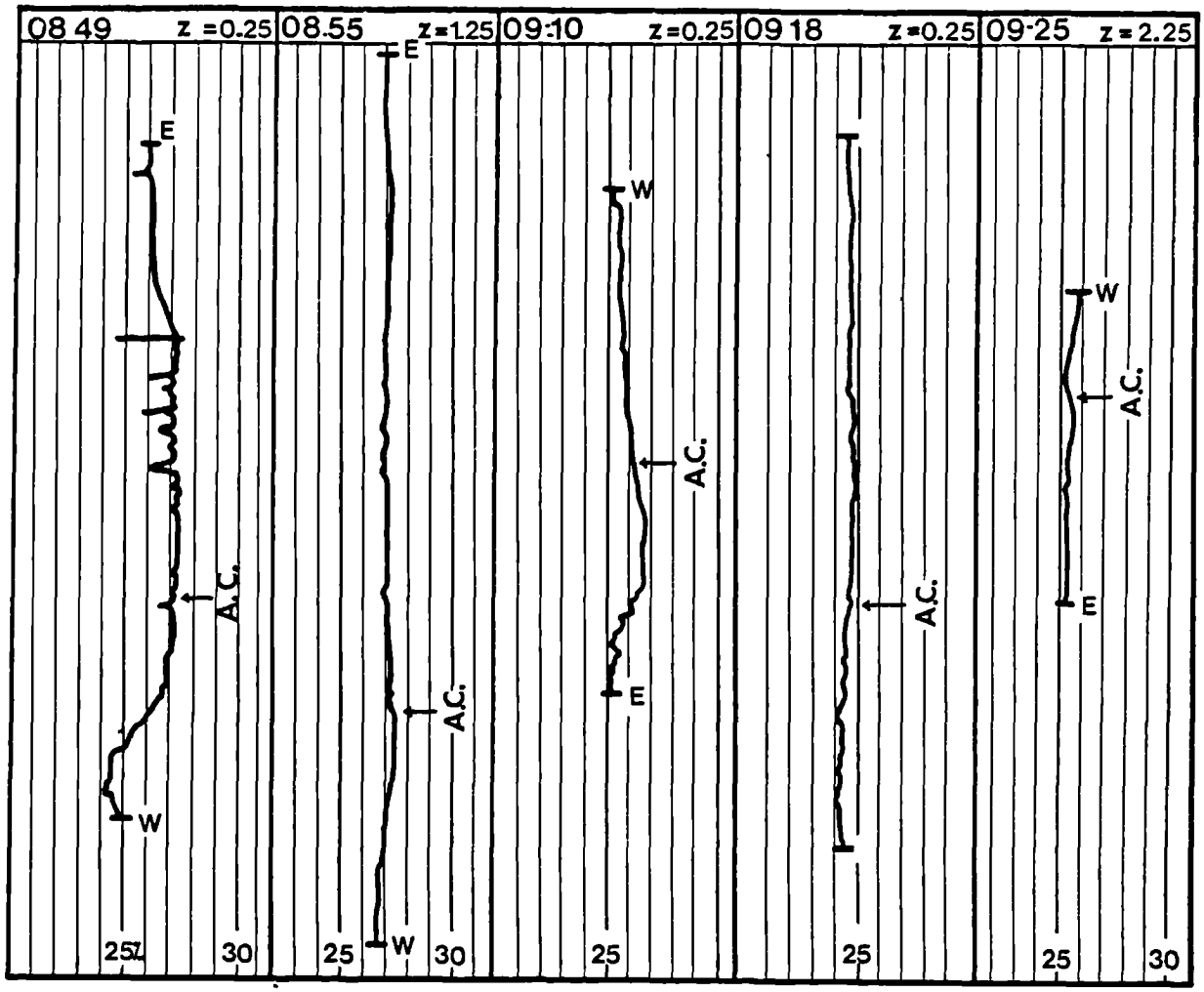
08 49
z =0.25
E
A.C.
W
25
30
08.55
z=1.25
E
A.C.
W
25
30
09:10
z=0.25
W
A.C.
E
25
09 18
z=0.25
A.C.
25
09-25
z=2.25
W
A.C.
E
25
30

EBB

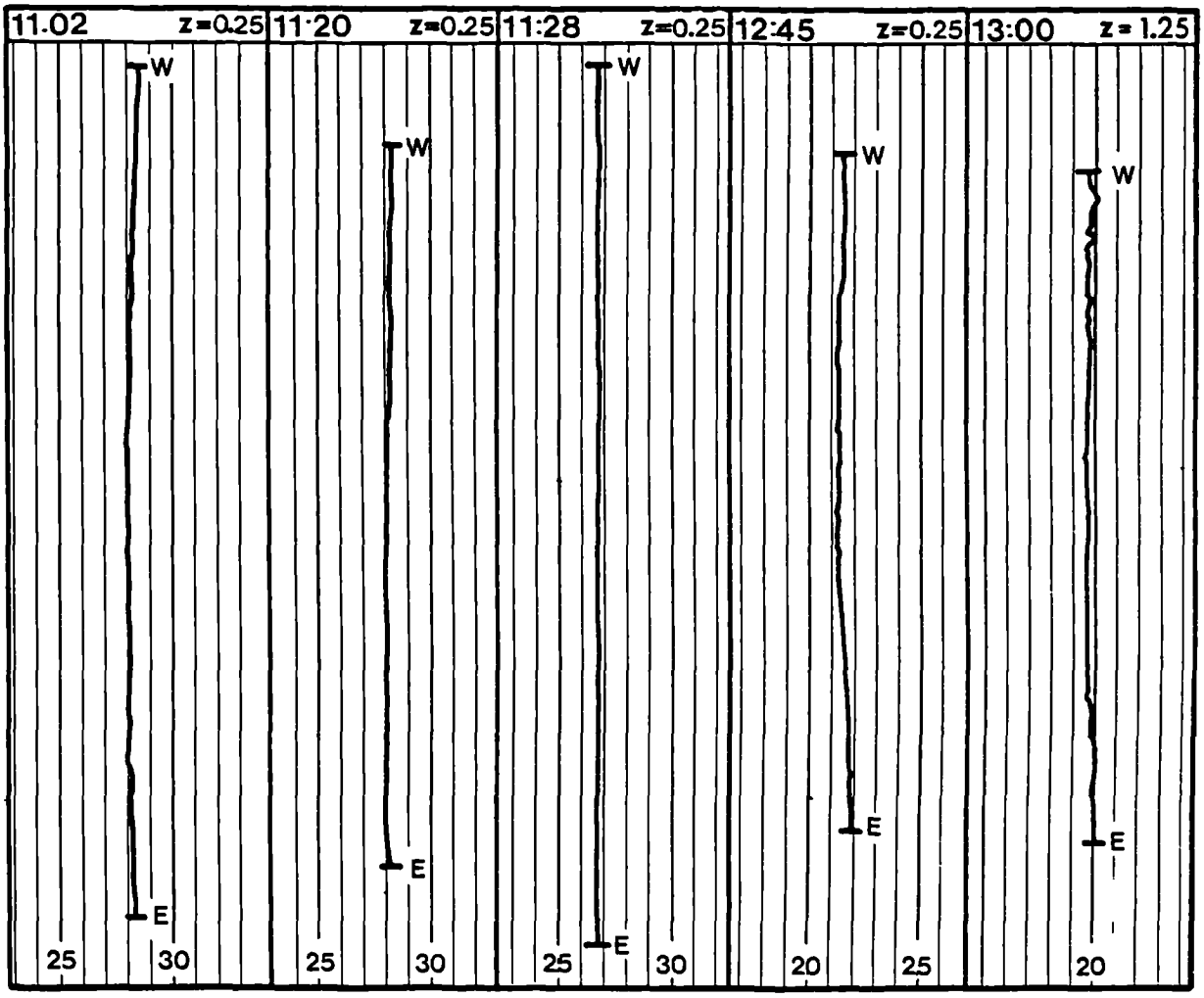
11.02
z=0.25
W
E
25
30
11·20
z=0.25
W
E
25
30
11:28
z=0.25
W
E
25
30
12:45
z=0.25
W
E
20
25
13:00
z=1.25
W
E
20

rather than deep (2.25m) traverses and since they were more often reductions from local mean salinity, they may have been small unmixed parcels of less dense water advected into the channel centre by the secondary flow. In general, there was no associated abrupt change of transverse salinity in the vicinity of the convergence, although its position occasionally coincided with an apparent salinity discontinuity. The results confirm the existence of lateral gradients which are reversed by the change of flow direction; the gradients appear to be larger at the surface than at the bed.

Finally, we look at the results of the synoptic cross-sectional salinity measured by the pumped samples of the HRS/Birmingham survey. A part of the ebb tide data are shown in figures 8.10 and 8.11 and flood data in figure 8.12. During the ebb there was a consistent trend towards lowest salinity on the east bank in all profiles up to and including the 11:48hrs (BST), as a result of greater advection velocities on the outside of the preceding, upstream bend. By ~12:48hrs the bend effect had been reduced sufficiently by the decreasing depth and currents such that the centre of the channel contained the lowest salinity water. No such bend effects were evident in the flood results (recorded at the landward end of the Tremorfa channel); these consistently showed greatest salinities over the deepest regions of the cross-section. Stratification was comparable in both flood and ebb profiles with a tendency toward a reduction of stability in the latter stages of both tidal phases. These synoptic profiles indicate central instability in the 12:48hrs ebb and 19:18hrs flood results.

Summarising the above surveys of the Conwy, we find that central densities remain greater on the flood and smaller on the ebb than sidebank densities. The presence of vertical instability, recorded in both flood and ebb profiles on 9.9.81, does not appear, from the data of 13.10.80 and 15.10.80, to be a necessary condition for the occurrence of surface convergence and downwelling.

Figure 8.10 Synoptic cross-sectional salinity in the Tremorfa reach (section 26 of figure 7.1) during the ebb tide of 9.9.81, from pumped water samples (data for this, and figures 8.11 and 8.12 supplied by Dr. J.R. West, Birmingham University).

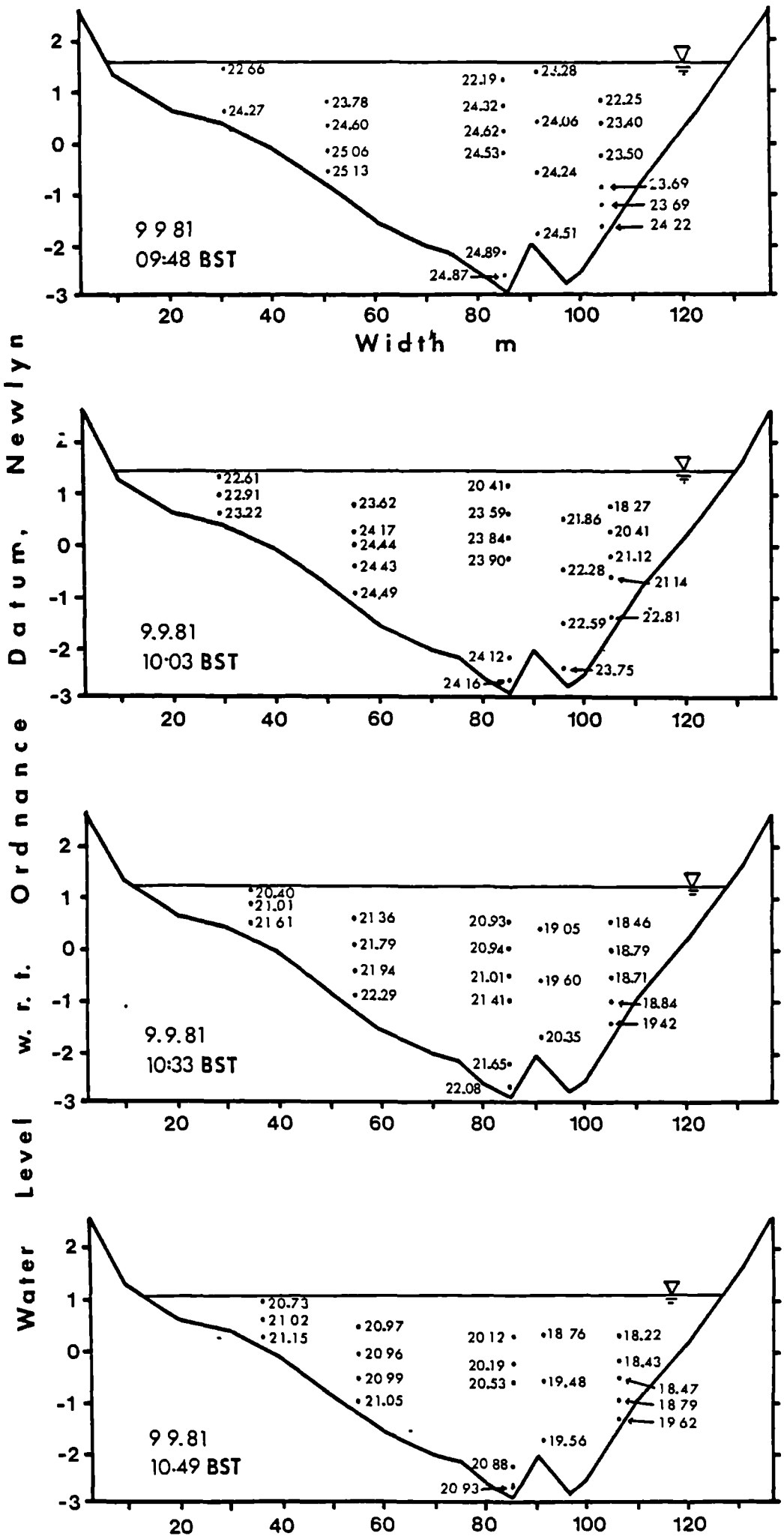
Water Level w. r. t. Ordnance Datum, Newlyn
Width m
9 9 81
09:48 BST
9.9.81
10·03 BST
9.9.81
10:33 BST
9 9.81
10.49 BST

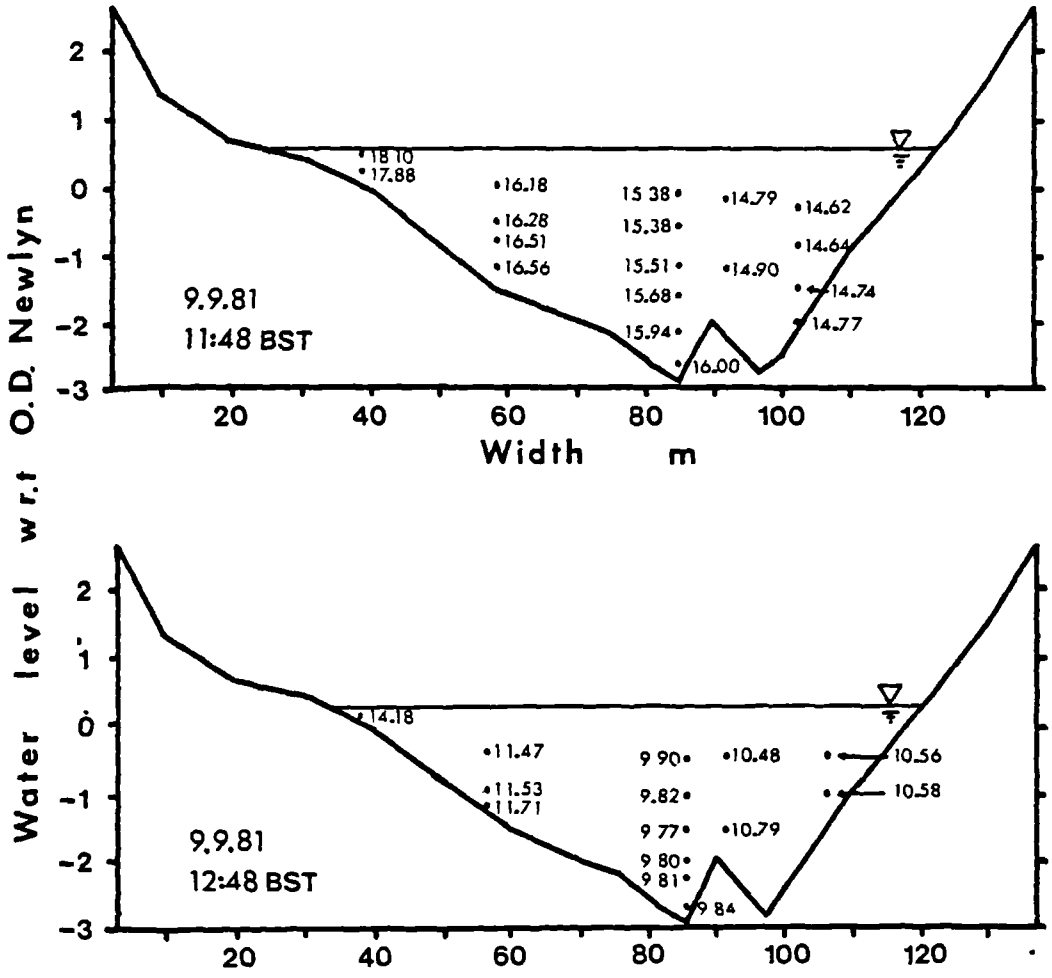


Figure 8.11 Synoptic cross-sectional salinity in the Tremorfa reach in the late stages of the ebb tide.

Figure 8.12 Synoptic cross-sectional salinity in the Tremorfa reach during the flood tide.

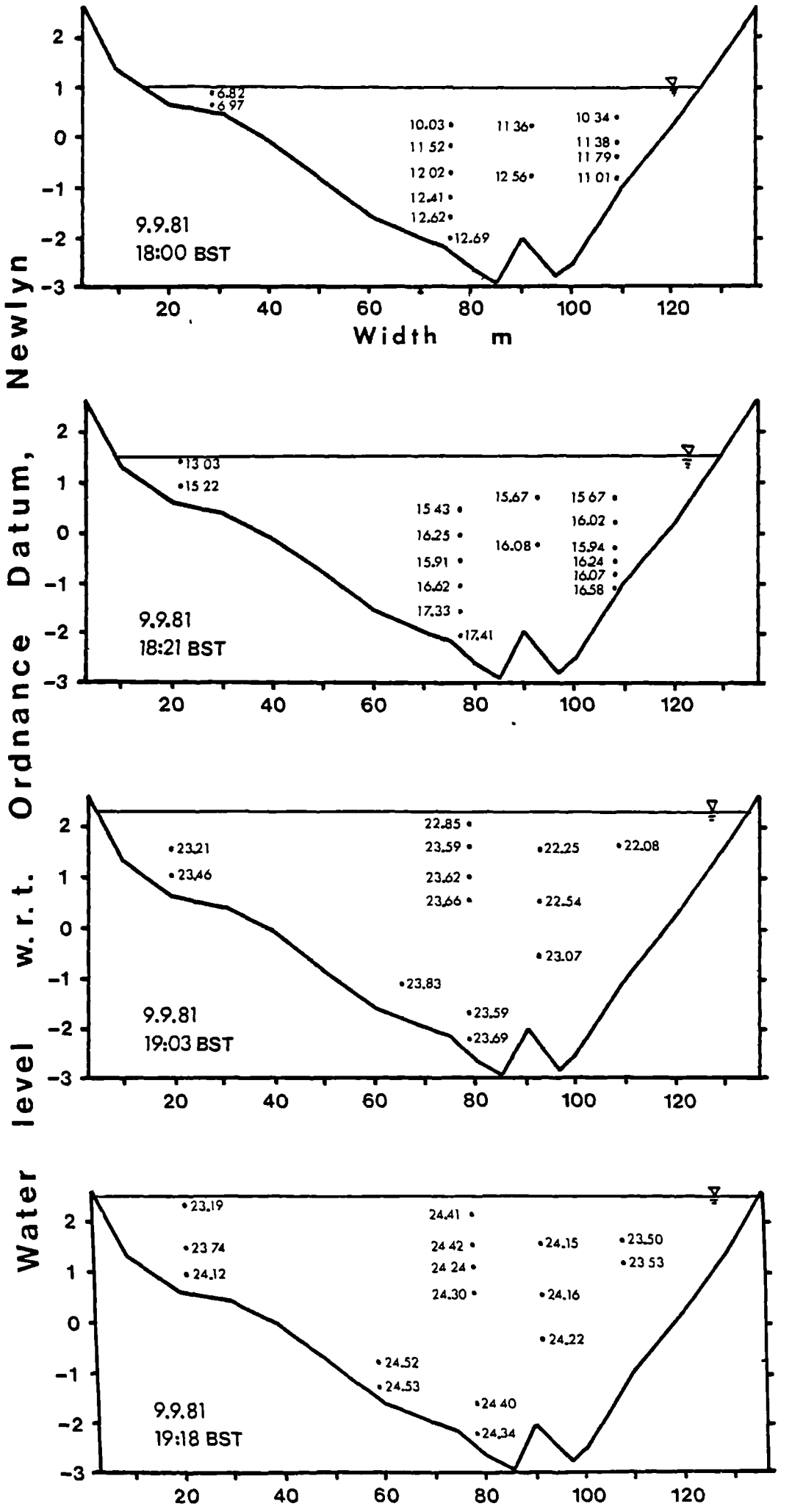
Water level w.r.t. Ordnance Datum, Newlyn
Width m
9.9.81
18:00 BST
6.82
6.97
10.03
11.52
12.02
12.41
12.62
12.69
11.36
12.56
10.34
11.38
11.79
11.01
9.9.81
18:21 BST
13.03
15.22
15.43
16.25
15.91
16.62
17.33
17.41
15.67
16.08
15.67
16.02
15.94
16.24
16.07
16.58
9.9.81
19:03 BST
23.21
23.46
22.85
23.59
23.62
23.66
23.83
23.59
23.69
22.25
22.54
23.07
22.08
9.9.81
19:18 BST
23.19
23.74
24.12
24.41
24.42
24.24
24.30
24.52
24.53
24.40
24.34
24.15
24.16
24.22
23.50
23.53

## 8.3 CONVERGENCE MODEL.

In order to investigate the effects of lateral density gradients on the primary channel flow, we turn to a theoretical treatment of the problem. Initially, the development follows the lines of Officer (1976) and was originally applied to lateral flows by Prych (1970). It is analogous to the treatment of Hansen and Rattray (1965) in describing the longitudinal density-driven circulation in an estuary. We assume that the secondary flow is driven by baroclinic forces induced by the distribution of density in the cross-section. With the analytical background, a diagnostic numerical model is subsequently described for use with the measured density distributions presented earlier.

We use a coordinate system in which x is along the estuary, y is a lateral direction and z is vertically downward. Density is assumed not to be a function of depth and the following quantities are constant in the x and y directions;

i) surface slope, $\partial\zeta/\partial y$
ii) transverse density gradient, $\partial\rho/\partial y$
iii) transverse velocity, v
iv) vertical eddy viscosity, $N_z$.

The lateral equation of motion, in the steady state, expresses a balance between the lateral pressure gradient and the viscous stress;

$$\frac{\partial p}{\partial y} = \bar{\rho} N_z \frac{\partial^2 v}{\partial z^2} \qquad 8.1$$

and the vertical equation, in a neutrally buoyant environment is given by;

$$p = \rho g(z-\zeta) \qquad 8.2$$

Differentiating with respect to y;

$$\frac{\partial p}{\partial y} = -\rho g \frac{\partial \zeta}{\partial y} + gz \frac{\partial \rho}{\partial y} \qquad 8.3$$

$$= -\rho g i + g\lambda z \qquad 8.4$$

where $i=\partial\zeta/\partial y$, the surface slope and $\lambda = \partial\rho/\partial y$ the lateral density gradient. Equating 8.4 and 8.1 gives;

$$\bar{\rho} N_z \frac{\partial^2 v}{\partial z^2} = -\bar{\rho} g i + g\lambda z \qquad 8.5$$

$$\frac{d^2 v}{dz^2} = -\frac{gi}{N_z} + \frac{g\lambda z}{\bar{\rho} N_z} \qquad 8.6$$

Equation 8.6 is now integrated twice with respect to z to solve for the lateral velocity as a function of depth;

$$v(z) = -\frac{giz^2}{2N_z} + \frac{g\lambda z^3}{6\bar{\rho} N_z} + s_1 z + s_2 \qquad 8.7$$

in which $s_1$ and $s_2$ are constants. The following boundary conditions are applied;

i) no surface stress, i.e.dv/dz=0 at z=0.
ii) bottom velocity of zero i.e. v=0 at z=H.

Condition i) eliminates the constant $s_1$ and condition ii) allows solution of $s_2$;

$$s_2 = \frac{giH^2}{2N_z} - \frac{g\lambda H^3}{6\bar{\rho} N_z} \qquad 8.8$$

which may be substituted into equation 8.7 to give;

$$v(z) = -\frac{gi}{2N_z}(z^2-H^2) + \frac{g\lambda}{6\bar{\rho} N_z}(z^3-H^3) \qquad 8.9$$

There should be no net accumulation of mass in the cross-section such that the vertical integration of 8.9 from bed to surface may be set equal to zero, leading to a solution for the lateral surface slope;

$$i = \frac{3\lambda H}{8\bar{\rho}} \qquad 8.10$$

When substituted into equation 8.9, the solution for the lateral secondary velocity as a function of depth becomes;

$$v(z) = \frac{g\lambda H}{48\rho N_z} [8(\eta^3-1) - 9(\eta^2-1)] \qquad 8.11$$

where $\eta=z/H$. The form of this solution is shown in figure 8.13 (the profile for n=0).

We shall now extend the above treatment in a diagnostic model which evaluates the circulation from an observed density structure. We thus include density as a function of both lateral and vertical dimensions and, again, consider the steady-state situation (on the assumption that secondary accelerations remain small). It is still necessary to retain a vertically-independent viscosity, $N_z$, which is the greatest weakness of the analysis. The lateral equation of motion remains unchanged;

$$\frac{\partial p}{\partial y} = \bar{\rho} N_z \frac{\partial^2 v}{\partial z^2} \qquad 8.1$$

and for the vertical equation;

$$p = g\int_{\zeta}^{z} \rho \, dz \qquad 8.12$$

which, after differentiation with respect to y, becomes;

$$\frac{\partial p}{\partial y} = -g\rho_s \frac{\partial \zeta}{\partial y} + g\int_0^z \frac{\partial \rho}{\partial y} dz \qquad 8.13$$

where $\rho_s$ is the surface density. As before we combine equations 8.1 and 8.13 to give;

$$\rho N_z \frac{\partial^2 v}{\partial z^2} = gB + g\int_0^z \frac{\partial p}{\partial y} dz \qquad 8.14$$

where $B = -\rho_s \partial\zeta/\partial y$ is the barotropic force due to the surface slope. Thus;

$$\frac{\partial^2 v}{\partial z^2} = \frac{g}{\bar{\rho} N_z} [B + \int_0^z \frac{\partial p}{\partial y} dz] \qquad 8.15$$

$$= \frac{g}{\bar{\rho} N_z} [B + I_1^z] \qquad 8.16$$

where we use the notation;

$$I_n^z = \int_0^z \ldots \int_0^z \frac{\partial \rho}{\partial y} dz_1, dz_2, \ldots dz_n$$

Integrating with respect to z, we find;

$$v(z) = \frac{g}{\bar{\rho} N_z} \left[\frac{Bz^2}{2} + I_3^z\right] + s_1 z + s_2 \qquad 8.17$$

The boundary conditions remain as before;

i) no surface stress, $\partial v/\partial z = 0$ at $z = 0$.

ii) zero velocity at the bed, $v(H) = 0$.

Condition i) eliminates $s_1$ and condition ii) permits solution of $s_2$;

$$s_2 = -\frac{g}{\bar{\rho} N_z} \left[\frac{BH^2}{2} + I_3^H\right] \qquad 8.18$$

the 'H' superscript on I means that the final (3rd) integration is taken to the limit H, which leads on substitution to;

$$v(z) = \frac{g}{\bar{\rho} N_z} \left[B(z^2 - H^2)/2 + (I_3^z - I_3^H)\right] \qquad 8.19$$

As before, the condition of no net mass accumulation is applied which gives a solution for the barotropic component;

$$B = 3(I_4^H - HI_3^H)/H^3 \qquad 8.20$$

and thus the lateral component of the secondary velocity reduces to;

$$v(z) = \frac{g}{\bar{\rho} N_z} \left[(I_3^z - I_3^H) + 3(I_4^H - HI_3^H)(z^2 - H^2)/2H^3\right] \qquad 8.21$$

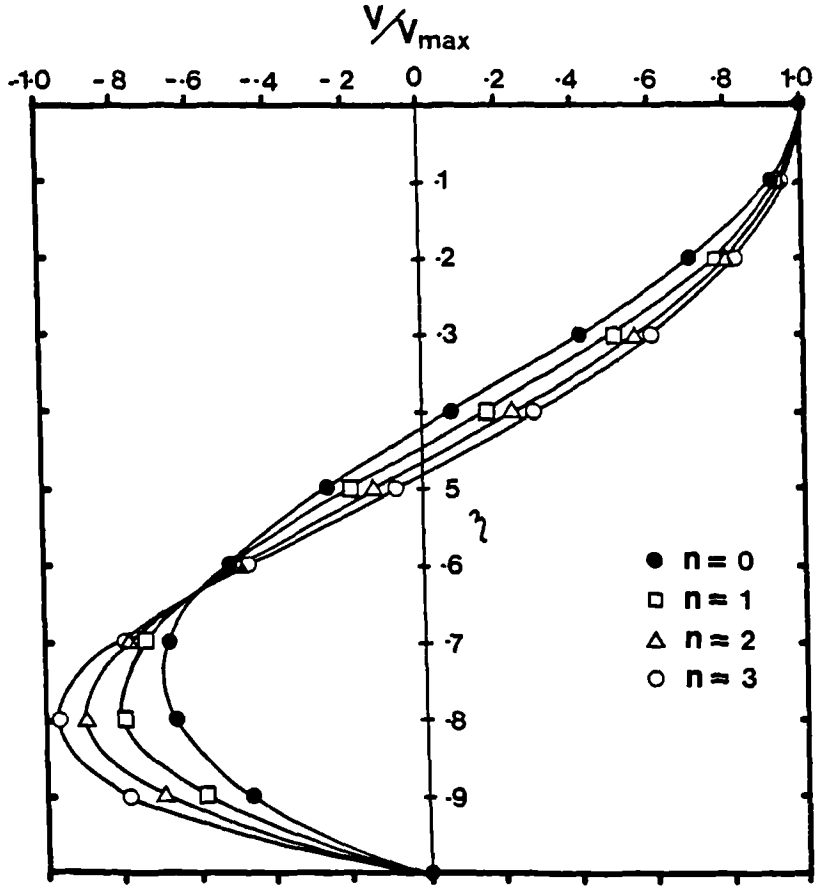


Figure 8.13 Vertical profiles of lateral secondary velocity from solution of equation 8.25, for differing forms of stratification (assuming a no-slip lower boundary condition).

The vertical component may be found by applying continuity to the cross-section;

$$\frac{\partial v}{\partial y} + \frac{\partial w}{\partial z} = 0 \qquad 8.22$$

leading to;

$$w(z) = -\frac{g}{\bar{\rho} N_z}\left[\left(\frac{\partial I^z}{\partial y} - z\frac{\partial I^H}{\partial y}\right) + (z/2H^3)\left(\frac{\partial I^H}{\partial y} - H\frac{\partial I^H}{\partial y}\right)(z^2-3H^2)\right] \qquad 8.23$$

By way of illustration, and before using equations 8.21 and 8.23 in a numerical solution, we continue the analytical approach by representing the density field as a series;

$$\rho_0 = \rho_0 + \sum_{n=0}^{\infty} \Delta\rho_n f_n(y)\eta^n = \rho_0 + \Delta\rho_0 f_0(y) + \Delta\rho_1 f_1(y)\eta \ldots + \Delta\rho_n f_n(y)\,\eta^n \qquad 8.24$$

where $\eta = z/H$, the $\Delta\rho$'s are constants, and the f's are lateral functions. After differentiation with respect to y, and the appropriate number of vertical integrations, the solutions for all

I's may be found and substituted into equation 8.21 to give;

$$v(y,z)=\frac{gH^3}{2\rho N_z}\sum_{n=0}^{\infty}\Delta\rho_n f'_n(y)\frac{n!}{(n+4)!}\,[2(n+4)(\eta^{n+3}-1)-3(n+3)(\eta^2-1)] \qquad 8.25$$

This reduces to the constant vertical density solution of equation 8.11 for n=0.

Using one individual component (i.e. a particular n) of the lateral velocity, the depth of the maximum return current is found at the turning point of the function;

$$v_{max} \quad \text{at} \quad \eta = [3/(n+4)]^{1/n+1}$$

from which we may deduce the effects of stratification. With constant vertical density (n=0) we see that $\eta(v_{max})=0.75$ (the same result is found from equations 8.11 and 8.21). In a stratified system, with a linear dependence of density on depth (n=1) the result is $(v_{max})=0.77$. Thus stratification lowers the return flow toward the bottom boundary. Figure 8.13 illustrates the form of the theoretical vertical profile of lateral velocity for different values of n (ignoring the summation sign in equation 8.25). In a complex density distribution, the factorial denominator in 8.25 ensures rapidly diminishing contributions from the higher order terms.

Turning now to a numerical approach based on equations 8.21 and 8.23;

$$v(z)=\frac{g}{\bar{\rho}N_z}\,[(I_3^z-I_3^H)+(3/2H^3)(I_4^H-HI_3^H)(z^2-H^2)] \qquad 8.21$$

$$w(z)=-\frac{g}{\bar{\rho}N_z}\,[(\frac{\partial I_4^z}{\partial y}-z\,\frac{\partial I_3^H}{\partial y})+(z/2H^3)(\frac{\partial I_4^H}{\partial y}-H\,\frac{\partial I_3^H}{\partial y})(z^2-3H^2)] \qquad 8.23$$

A relatively simple scheme was built around 8.21 which operated on densities from a given distribution on a 25x25 rectangular grid. After computing lateral gradients for all grid points, integrations were performed according to Simpson's rule on columns individually, which facilitated the use of a non-rectangular cross-section. Lateral velocities were found from equation 8.21, but it was found simpler to calculate vertical velocities by continuity directly.

The model was run with four representative density distributions: the flood tide mean distributions of 13.10.80 and 15.10.80 (figure 8.8) together with the ebb (10:33hrs on 9.9.81) and flood (18:00hrs on 9.9.81) results of the HRS/Birmingham work. (From the discrete density data points, contours were drawn with the proviso that gradients should remain as small as possible. Densities for the computational grid points were then obtained by linear interpolation between the contours.) These four distributions produce the secondary circulations shown in figures 8.14 to 8.17. (Arrow dimensions have been normalised to the greatest velocity in the cross-section.) Absolute velocities were calculated on the assumptions of a constant eddy viscosity $N_z \sim 10^{-2} m^2 s^{-1}$, density $\rho = 1005 kgm^{-3}$ and $g = 9.81 ms^{-2}$. The circulation during flood conditions includes strong surface convergence which falls of quite rapidly toward the sidebanks. Downwelling is strongest at about half the depth below the point of convergence, and the return flow, due to the assumption of zero bottom velocity, is always greatest at $\eta \approx 0.75$.. In contrast, the ebb distribution of density (which includes the effect of the upstream bend) produced a strong secondary circulation but without the convergence. Figure 8.18 illustrates the individual lateral and vertical components of the circulation shown in figure 8.15.

The variations of vertical and lateral secondary velocities as functions of depth and width changes are shown in figures 8.19 and 8.20 respectively (using the data of 15.10.80). (The lateral velocity approximates to a cubic depth dependence which indicates that the low level of stratification has not changed the character of the circulation from that of a vertically-homogeneous fluid - see figure 8.13.)

The Eulerian rate of change of density is given by;

$$\frac{D\rho}{Dt} = \frac{\partial \rho}{\partial t} + u\frac{\partial \rho}{\partial x} + v\frac{\partial \rho}{\partial y} + w\frac{\partial \rho}{\partial z} \qquad 8.26$$

If we assume that density is conserved and, for the moment, that there is no input to the cross-section from the longitudinal velocity, we obtain the time variation of density as a result of the secondary circulation;

$$\frac{\partial \rho}{\partial t} = -(v\frac{\partial \rho}{\partial y} + w\frac{\partial \rho}{\partial z}) \qquad 8.27$$

Figure 8.14 Secondary circulation generated by the density distribution of 13.10.80 (distribution shown in figures 8.8 and 8.22a).

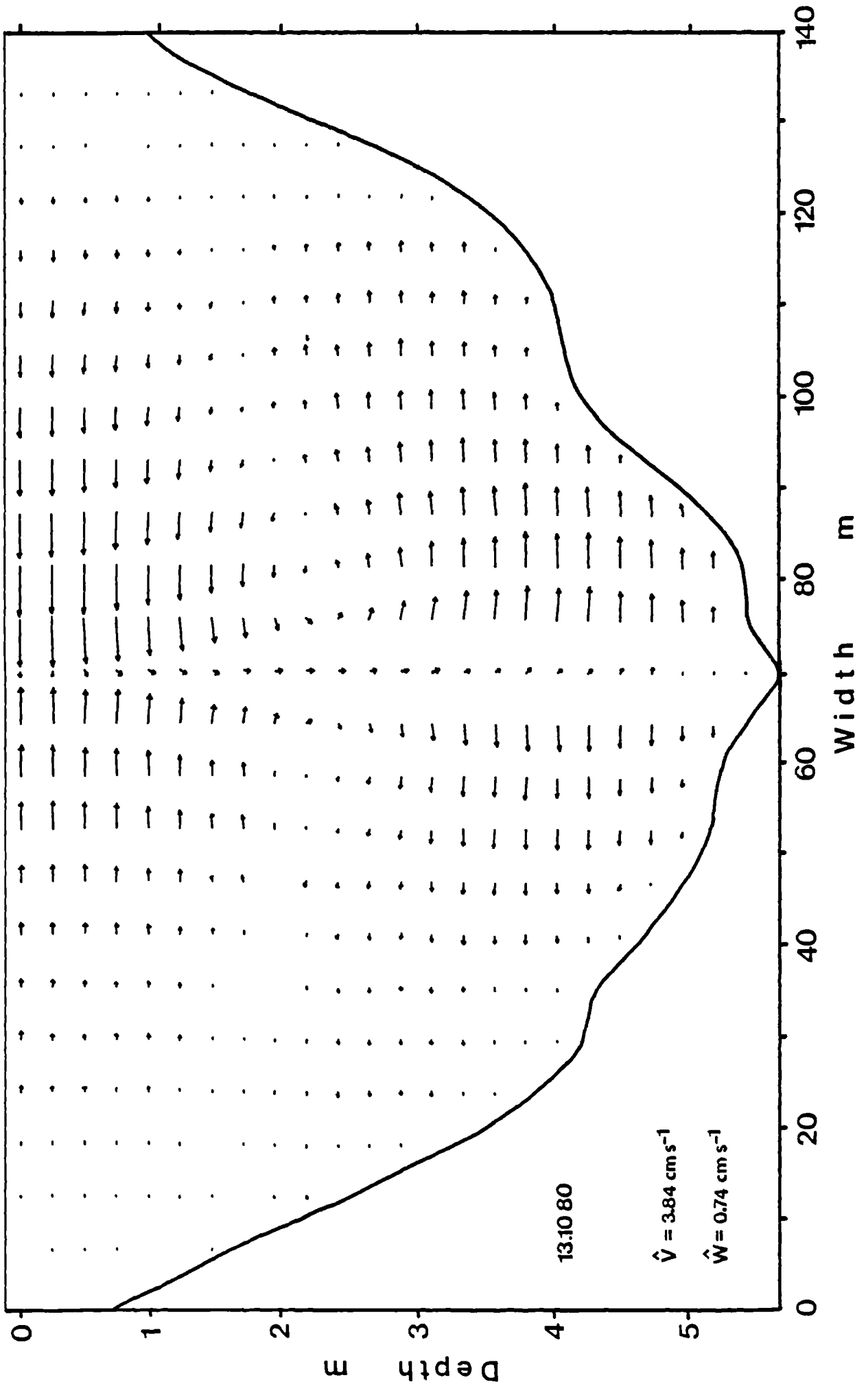
Depth m
0
1
2
3
4
5
Width m
0
20
40
60
80
100
120
140
13.10 80
$\hat{V}$ = 3.84 cm s$^{-1}$
$\hat{W}$ = 0.74 cm s$^{-1}$

Figure 8.15 Secondary circulation generated by the density distribution of 15.10.80 (distribution shown in figures 8.8 and 8.23a).

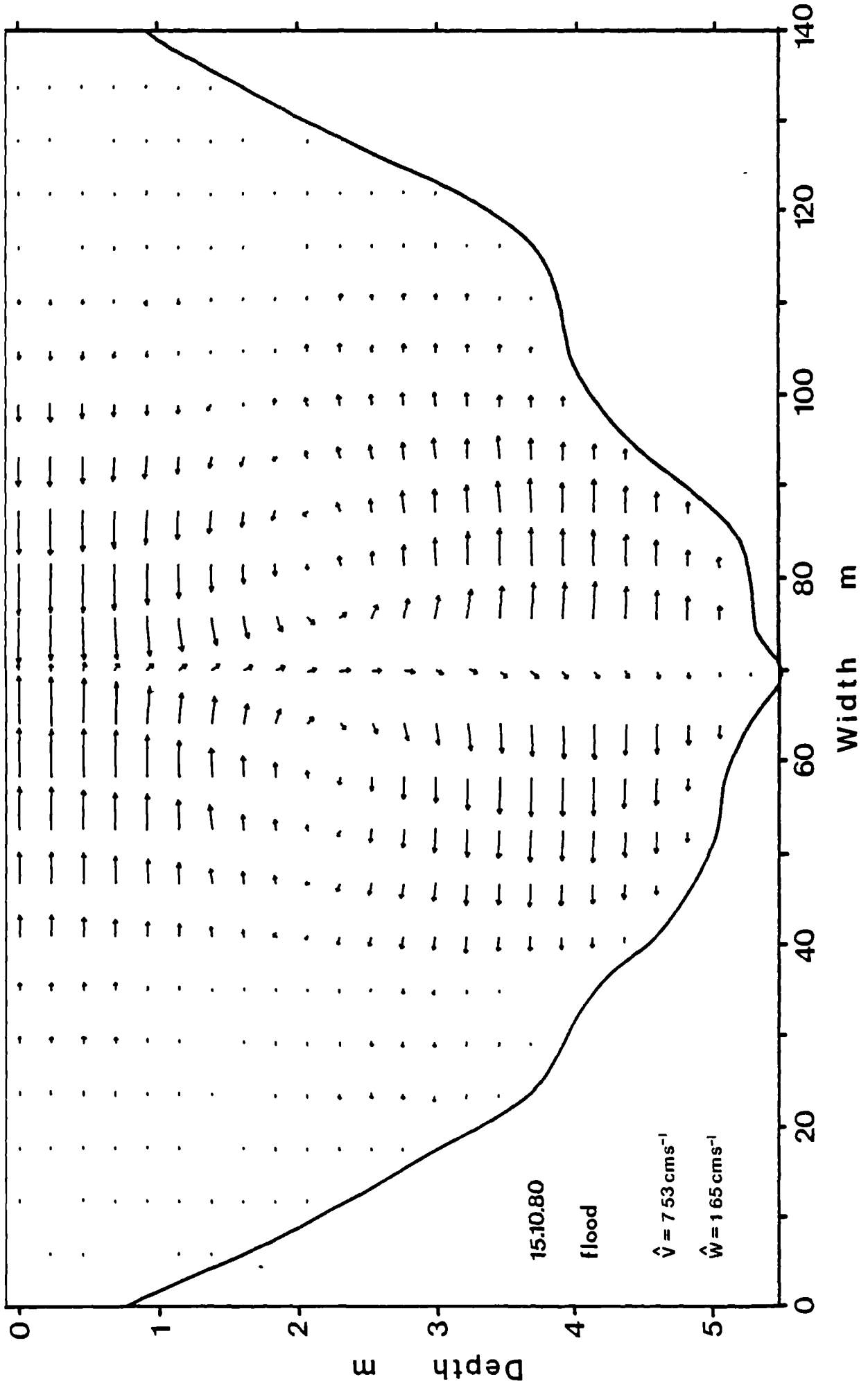
Depth m
Width m
0
1
2
3
4
5
0
20
40
60
80
100
120
140
15.10.80
flood
$\hat{V}$ = 7 53 cms$^{-1}$
$\hat{W}$ = 1 65 cms$^{-1}$

Figure 8.16 Secondary circulation generated by the density distribution of 9.9.81 at 10:33hrs (from the data shown in figure 8.10c).

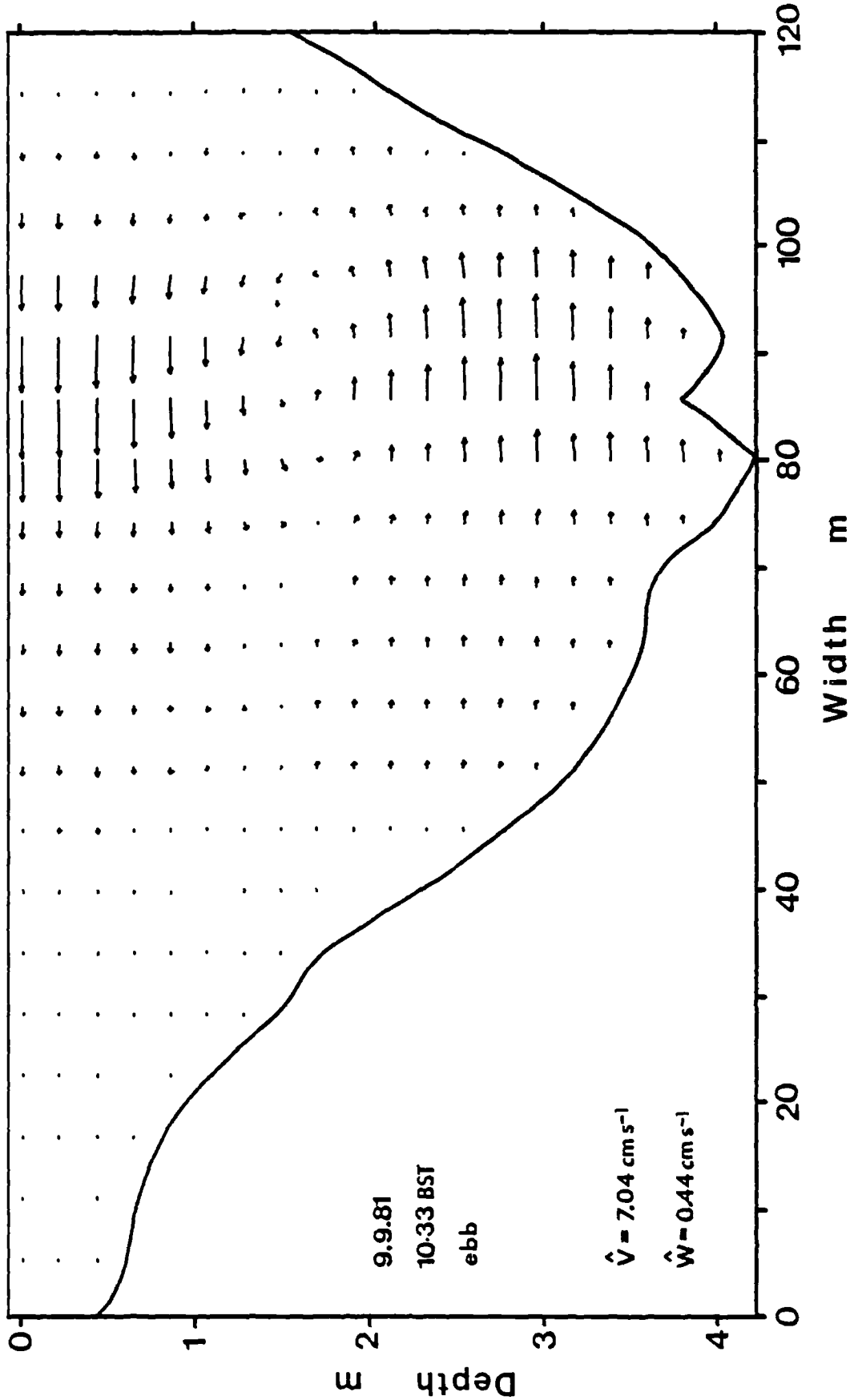
Depth m
0
1
2
3
4
Width m
0
20
40
60
80
100
120
9.9.81
10·33 BST
ebb
$\hat{V}$ = 7.04 cm s$^{-1}$
$\hat{W}$ = 0.44 cm s$^{-1}$

Figure 8.17 Secondary circulation generated by the density distribution of 9.9.81 at 18:00hrs (from the data shown in figure 8.12a).

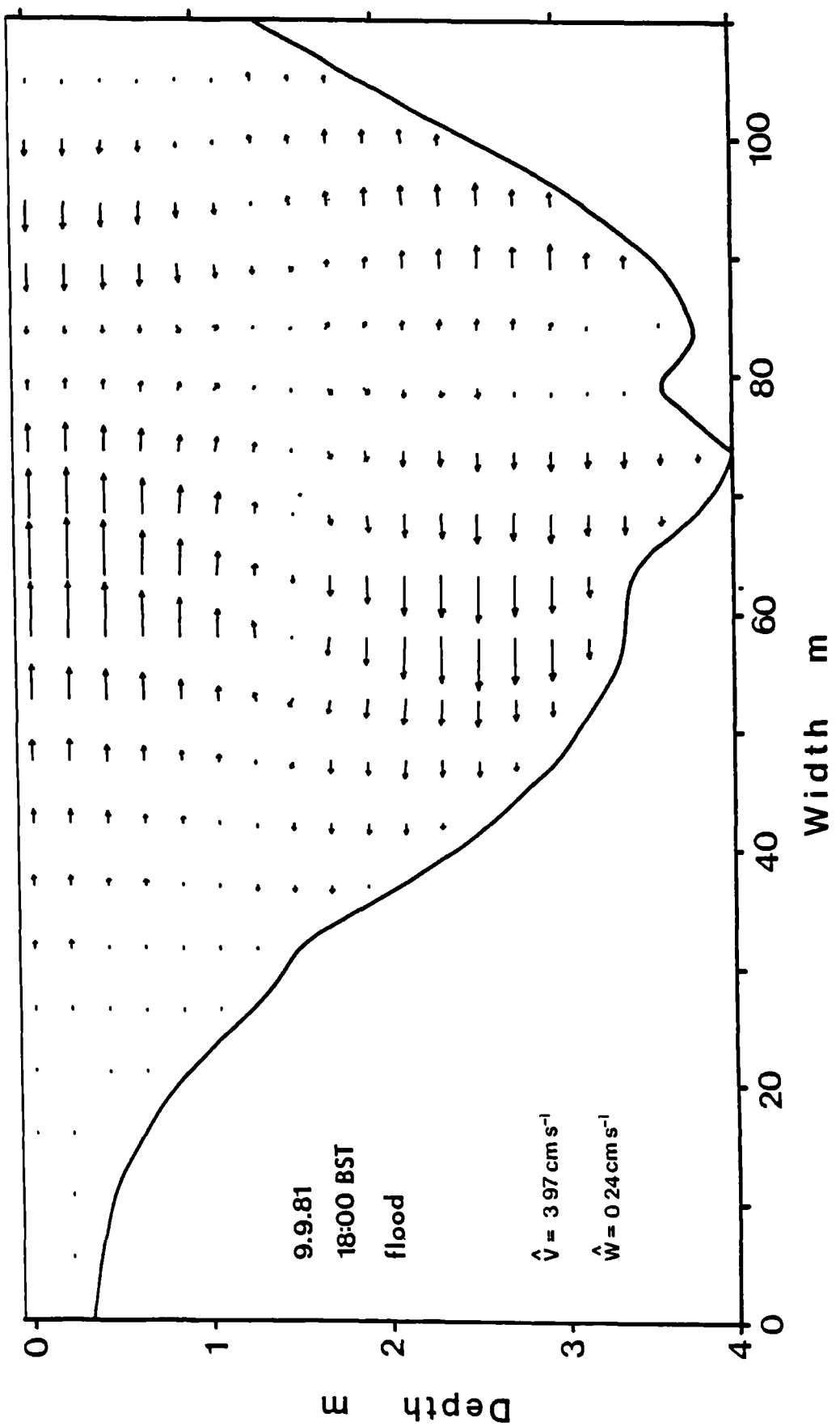
Depth m
0
1
2
3
4
0
20
40
60
80
100
Width m
9.9.81
18:00 BST
flood
$\hat{V}$ = 3 97 cm s$^{-1}$
$\hat{W}$ = 0 24 cm s$^{-1}$

Figure 8.18 Individual lateral and vertical components of the circulation shown in figure 8.14.

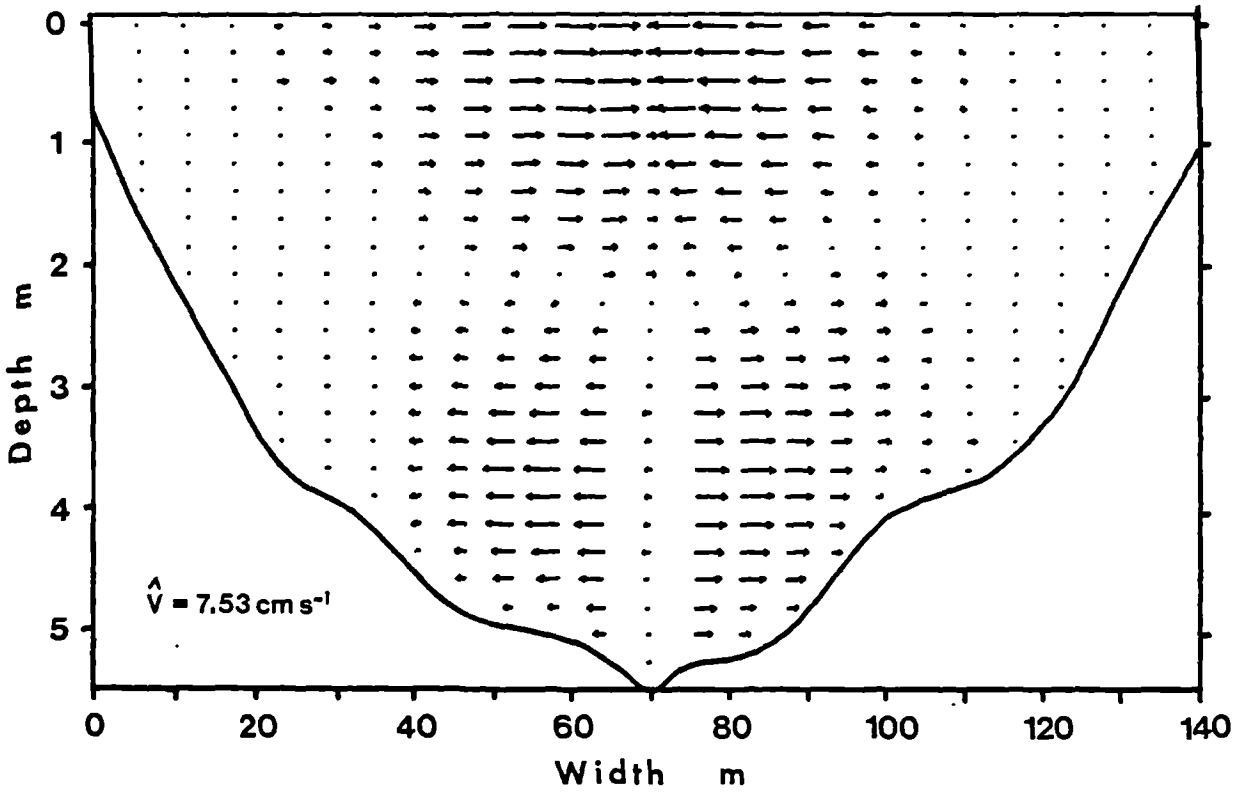
0
1
2
3
4
5
Depth m
$\hat{V}$ = 7.53 cm s$^{-1}$
0
20
40
60
80
100
120
140
Width m

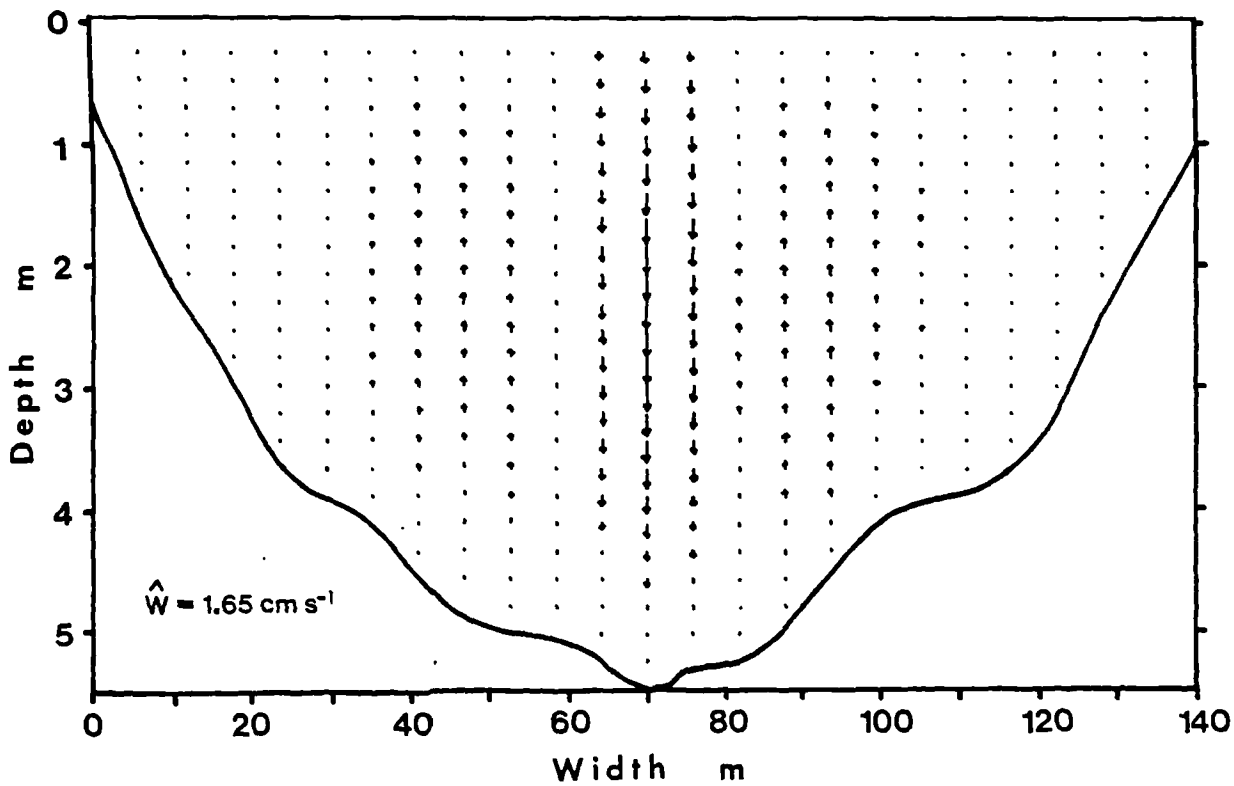
0
1
2
3
4
5
Depth m
$\hat{W}$ = 1.65 cm s$^{-1}$
0
20
40
60
80
100
120
140
Width m

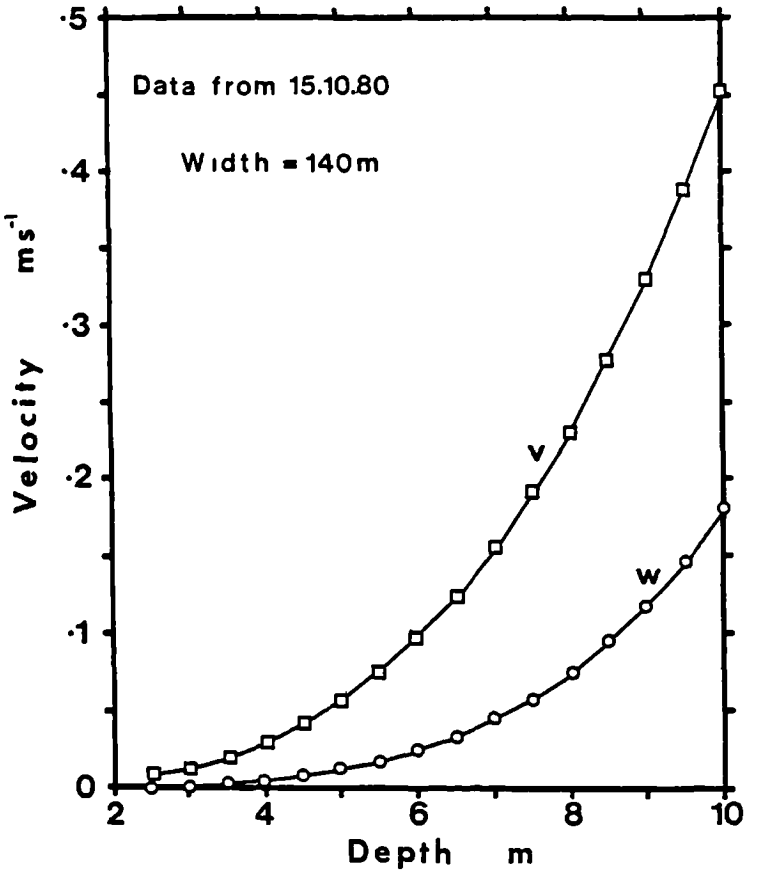


Figure 8.19 . Variation of maximum lateral and vertical secondary velocities with changing channel depth (data of 15.10.80).

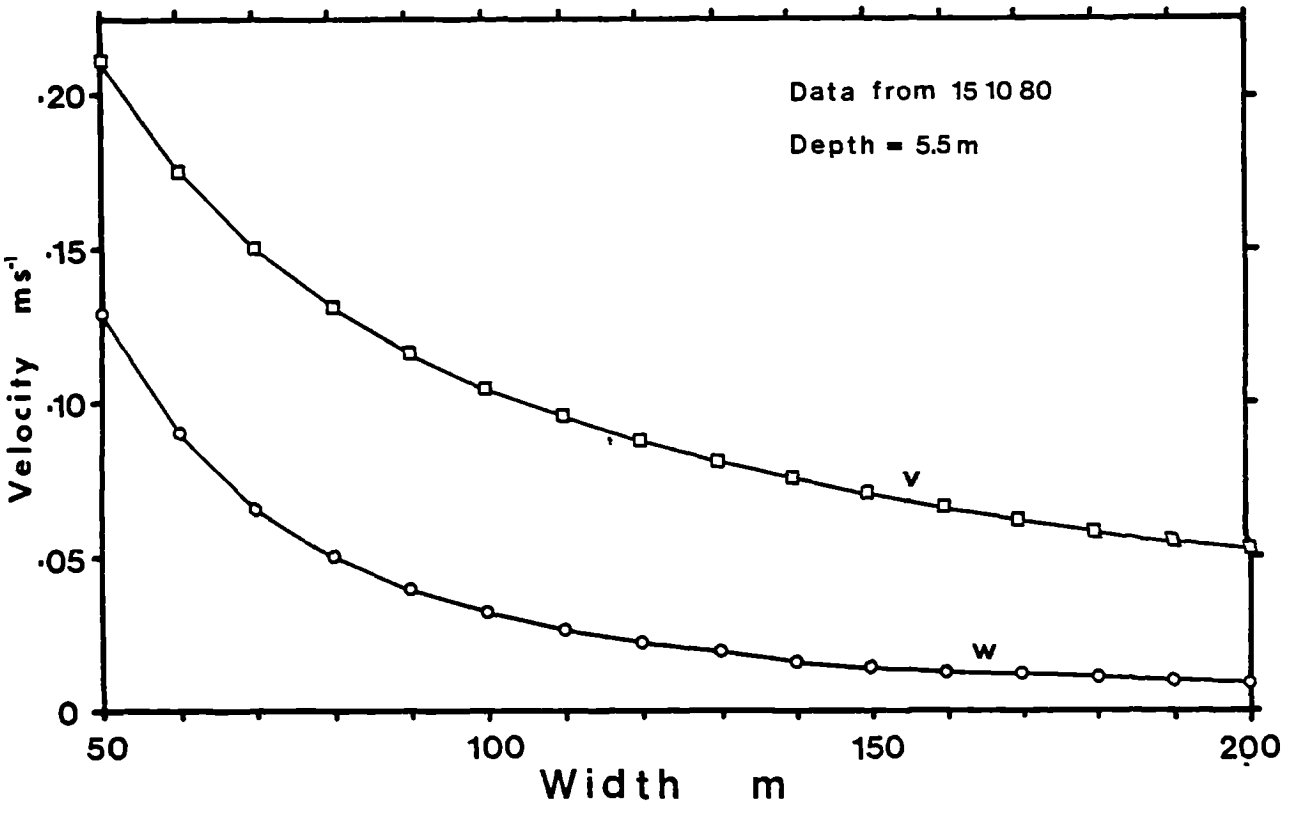


Figure 8.20 Variation of maximum lateral and vertical secondary velocities with changing channel width (data of 15.10.80).

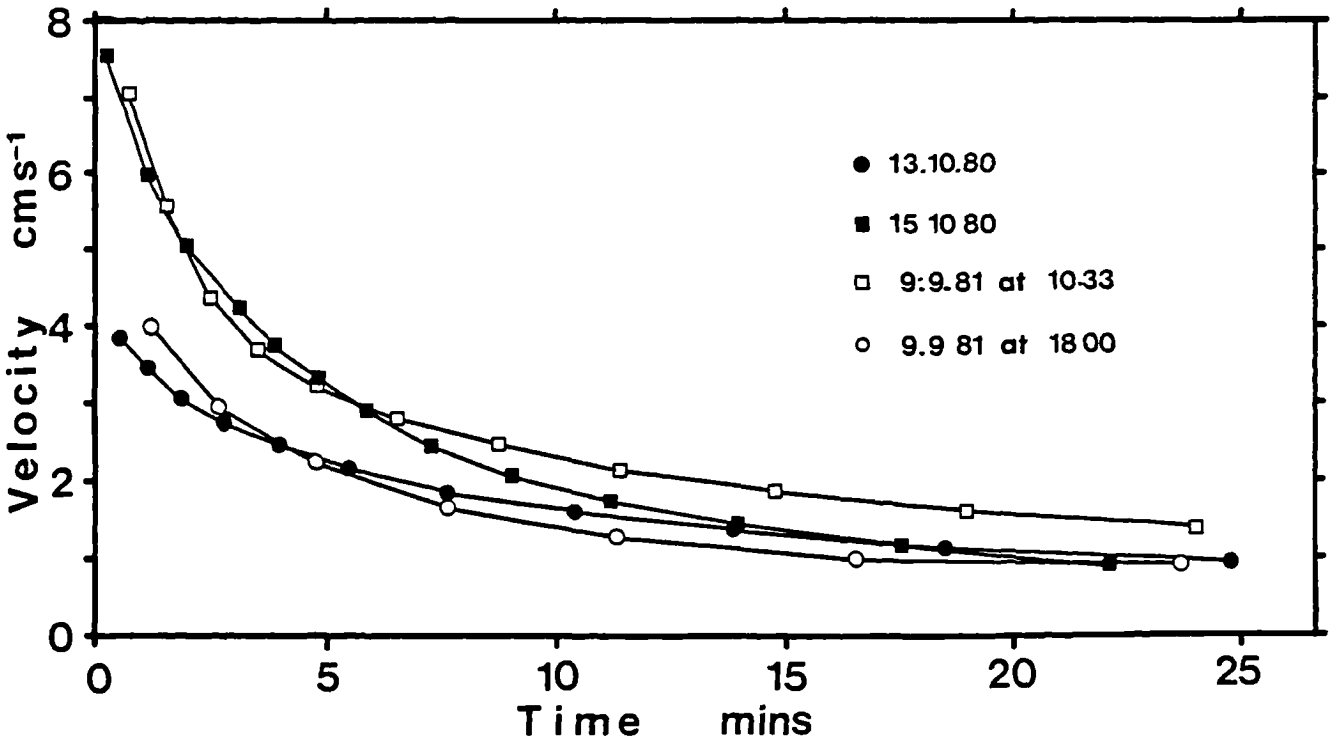


Figure 8.21 Decay of maximum lateral secondary velocity in successive distributions generated from the re-distribution of density by the secondary circulation.

When the secondary flow acts on the distribution, its advection of density reduces the gradients and thereby the secondary velocities. In subsequent computations, following establishment of the circulation, a subroutine was used to re-organise the density distribution by advection with the secondary flow, to reveal the rate of circulation decay. Diffusion was not included because its cross-sectional mixing time scale was expected to be orders of magnitude larger than the advective time scale. In the computation, a variable time step was used, being the shorter of the two times required for the maximum vertical and lateral velocities to cover their respective grid lengths. Thus, as the flow decayed, the computational time step lengthened.

Figure 8.21 gives the maximum lateral velocity as a function of time for each of the four initial density distributions, subjected to secondary flow advection. The initial decay is apparently very rapid, with a 'half-life' of the order 4-5 minutes. Thus without significant input of density anomaly by the primary flow, the secondary circulation rapidly decays to insignificance.

The distributions of 13.10.80 and 15.10.80 (figure 8.9), being mean distributions over a period of more than an hour (with small standard deviations), were relatively stable to re-organisation by the estuarine secondary flows (see figures 8.6 and 8.7). They, therefore, represent distributions in approximate equilibrium between the input of buoyancy anomalies by the primary (longitudinal) flow, and their elimination by advective (and diffusive) exchange, i.e.;

$$u\frac{\partial \rho}{\partial x} = -(v\frac{\partial \rho}{\partial y} + w\frac{\partial \rho}{\partial z}) \qquad 8.28$$

If we assume a cross-sectionally uniform longitudinal density gradient, it is a simple matter to calculate the field of primary velocity necessary to maintain constant density in the cross-section. The longitudinal gradient was assumed to be;

$$\frac{\partial \rho}{\partial x} = 0.005 \text{ kgm}^{-4} \qquad 8.29$$

equivalent to a linear variation from fresh to fully saline water over a distance of ~5km. The density distribution, after a period (~30s) of secondary advection, was compared to the original distribution and differences ($\Delta\rho_{ij}$) were restored by primary flow input (positive or negative) according to;

$$u_{ij} = \Delta\rho_{ij}/(\frac{\partial \rho}{\partial x}\Delta t) \qquad 8.30$$

(The calculated velocities represent deviations from the cross-sectional mean longitudinal velocity, because we allow no net addition of density to the cross-section.)

In figure 8.22, the top diagram shows the initial (contoured) density distribution from the data of 13.10.80. Immediately below is the computed field of longitudinal velocity (in $cms^{-}$) required to maintain the distribution unchanged (from equation 8.28, assuming $\partial\rho/\partial t=0$ and $\partial\rho/\partial x$ is cross-sectionally uniform). If instead, we allow the computed secondary circulation (figure 8.14) to re-distribute the density (from equation 8.27 and $u\partial\rho/\partial x=0$) for a short time interval (~30s), we produce a new distribution. A similar treatment on subsequent distributions produces the density field of figure 8.22c at t~18.4mins. The bottom diagram shows the

Figure 8.22 Using the initial density distribution of 13.10.80 (top), the primary velocity distribution required to maintain the distribution constant is shown immediately below. The third diagram shows the resultant distribution at t~18.4mins if the secondary circulation is permitted to re-distribute the cross-sectional density, and the final, lowermost diagram illustrates the secondary circulation appropriate to the density field immediately above.

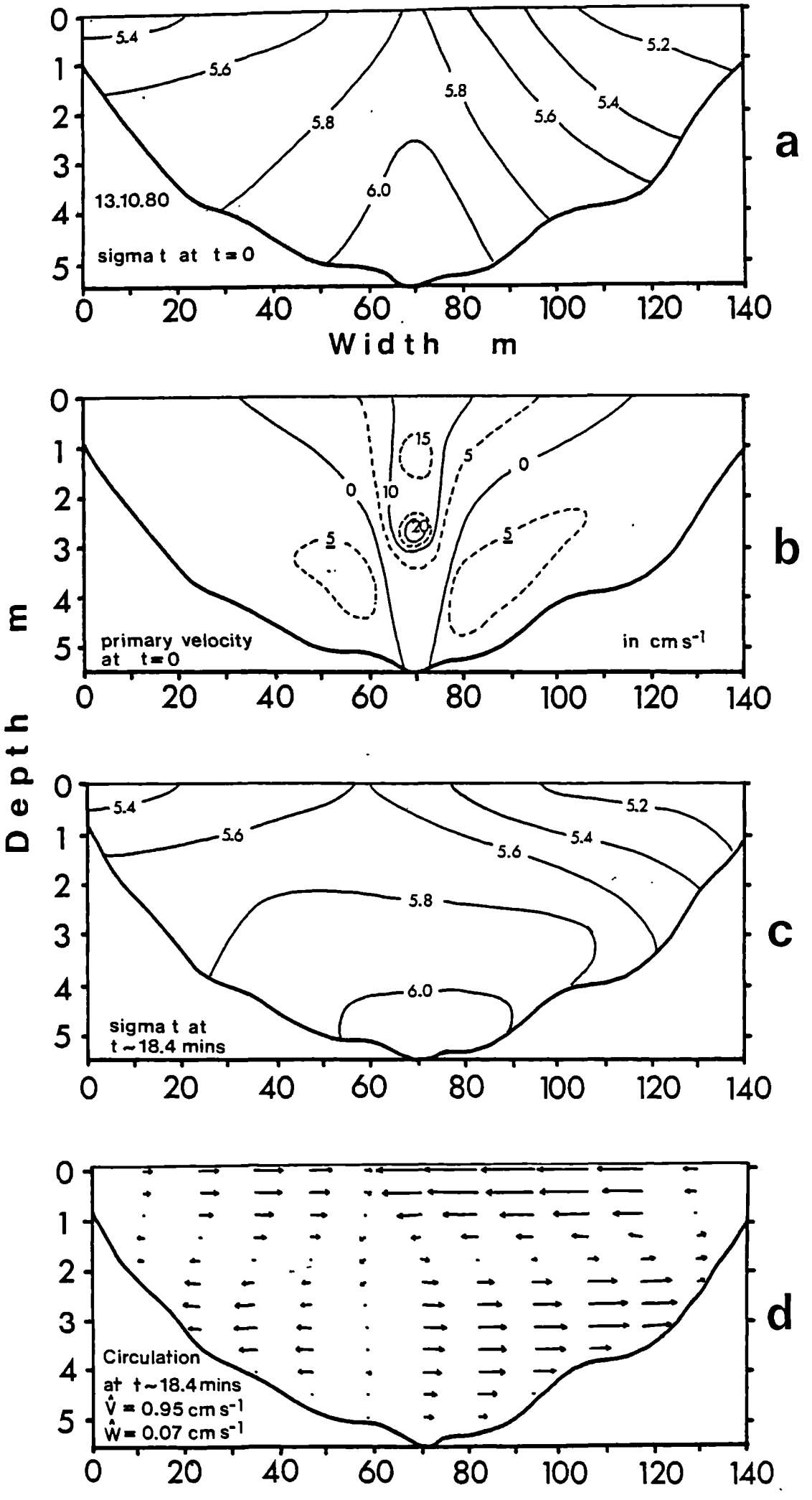
a
13.10.80
sigma t at t = 0
5.4
5.6
5.8
6.0
5.2
5.4
5.6
5.8
0 20 40 60 80 100 120 140
Width m
b
primary velocity
at t=0
in cm s⁻¹
15
10
5
0
5
5
0
Depth m
c
sigma t at
t ~ 18.4 mins
5.4
5.6
5.8
6.0
5.2
5.4
5.6
d
Circulation
at t ~ 18.4 mins
V̂ = 0.95 cm s⁻¹
Ŵ = 0.07 cm s⁻¹
0 1 2 3 4 5
0 20 40 60 80 100 120 140

Figure 8.23 Using the initial density distribution of 15.10.80 (top), the primary velocity distribution required to maintain the distribution constant is shown immediately below. The third diagram shows the resultant distribution at t~17.5mins if the secondary circulation is permitted to re-distribute the cross-sectional density, and the final, lowermost diagram illustrates the secondary circulation appropriate to the density field immediately above.

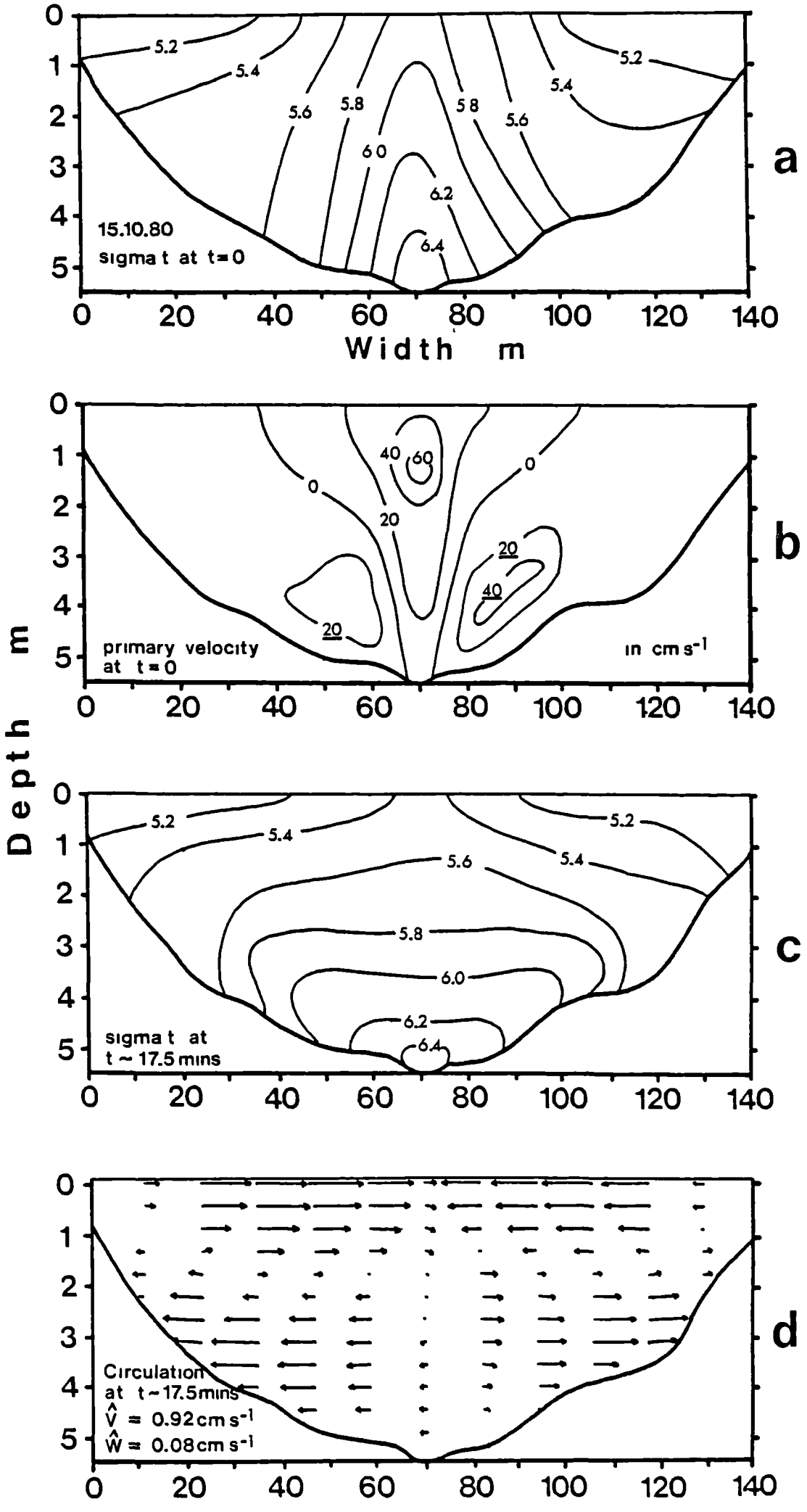
a
15.10.80
sigma t at t=0
5.2
5.4
5.6
5.8
6.0
6.2
6.4
Width m
b
primary velocity
at t=0
in cm s-1
Depth m
c
sigma t at
t ~ 17.5 mins
d
Circulation
at t ~ 17.5mins
V̂ = 0.92cm s-1
Ŵ = 0.08cm s-1

Figure 8.24 Using the initial density distribution of 9.9.81 at 18:00hrs (top), the primary velocity distribution required to maintain the distribution constant is shown immediately below. The third diagram shows the resultant distribution at t~16.5mins if the secondary circulation is permitted to re-distribute the cross-sectional density, and the final, lowermost diagram illustrates the secondary circulation appropriate to the density field immediately above.

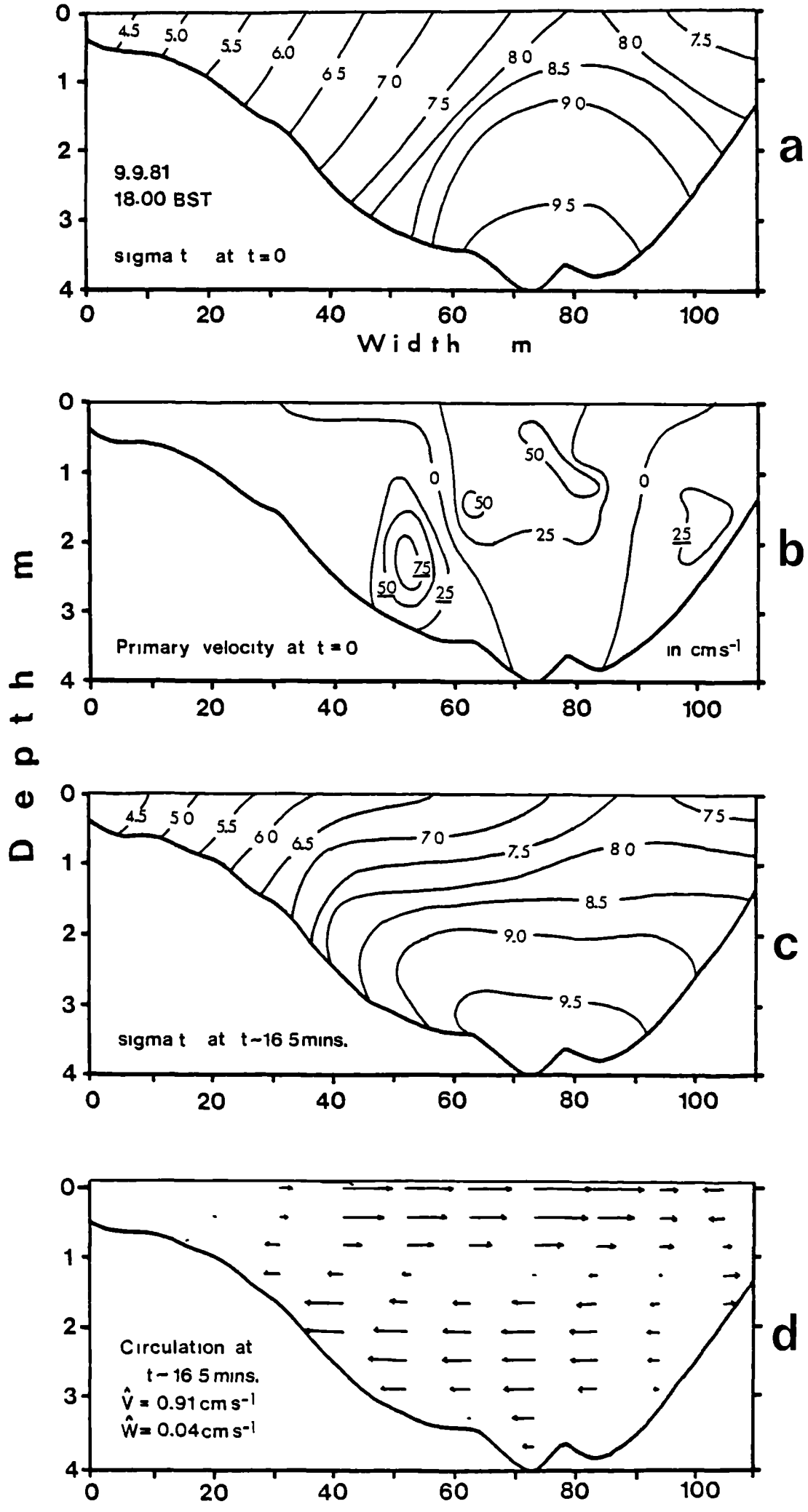
a
9.9.81
18.00 BST
sigma t at t=0
4.5
5.0
5.5
6.0
6.5
7.0
7.5
8.0
8.5
9.0
9.5
Width m
b
Primary velocity at t=0
in cms⁻¹
0
25
50
75
Depth m
c
sigma t at t=16.5mins.
d
Circulation at
t=16.5 mins.
V̂ = 0.91 cm s⁻¹
Ŵ = 0.04 cm s⁻¹

secondary circulation appropriate to the density field immediately above. In figures 8.23 and 8.24, a similar description applies to the data of 15.10.80 and the HRS/Birmingham data of 9.9.81 at 18:00 BST respectively.

Considering the three figures (8.22-8.24) together, we note that the computed primary velocity is much as we might expect for a frictional channel, except that the regions of slowest (most negative) primary flow have been raised above the bottom by the assumption of a no-slip lower boundary in the model. The subsequent distributions after advection (diagram c) are again as expected, indicating that the secondary flow behaves in such a way as to re-distribute the density into a stable system devoid of lateral gradients. The circulation pattern at the bottom of each of the figures indicates that lateral velocities tend to become more laterally-uniform, with a sharp cut-off, when compared to the circulation set up by the initial distribution.

We now take the analysis one stage further and attempt to set up an equilibrium between the input of buoyancy anomaly by an assumed distribution of primary flow, and its re-distribution by the secondary circulation. In doing this, we should note that the model is fundamentally based on a steady-state balance between the lateral pressure gradients and internal frictional dissipation. We might still study the development of the density field and its circulation under these combined influences, provided that accelerations can be assumed to remain small and the analysis can be treated as a succession of discrete quasi steady-state computations. In order to keep the accelerations small in the initial stages of its adjustment to equilibrium, we start with the density distribution of 15.10.80, rather than a uniform cross-sectional density. We again assume a cross-sectionally uniform longitudinal density gradient, given by equation 8.29, so that the primary velocity distribution (after subtraction of the mean) defines the input of density anomaly to the cross-section. As before, the computational time step is set according to the magnitude of the secondary velocities (generally ~60s).

In figure 8.25, the top diagram shows the initial density field (15.10.80) and figure 8.25b, the applied field of longitudinal

Figure 8.25 Using the initial distribution of 15.10.80 (top) and an assumed distribution of longitudinal velocity shown in the second diagram, the third diagram illustrates the density distribution at time t~26mins from the effects of the longitudinal input alone (the longitudinal density gradient is given in equation 8.29). The bottom diagram shows the density field at t~27.8mins from the combined effects of longitudinal input and secondary re-distribution.

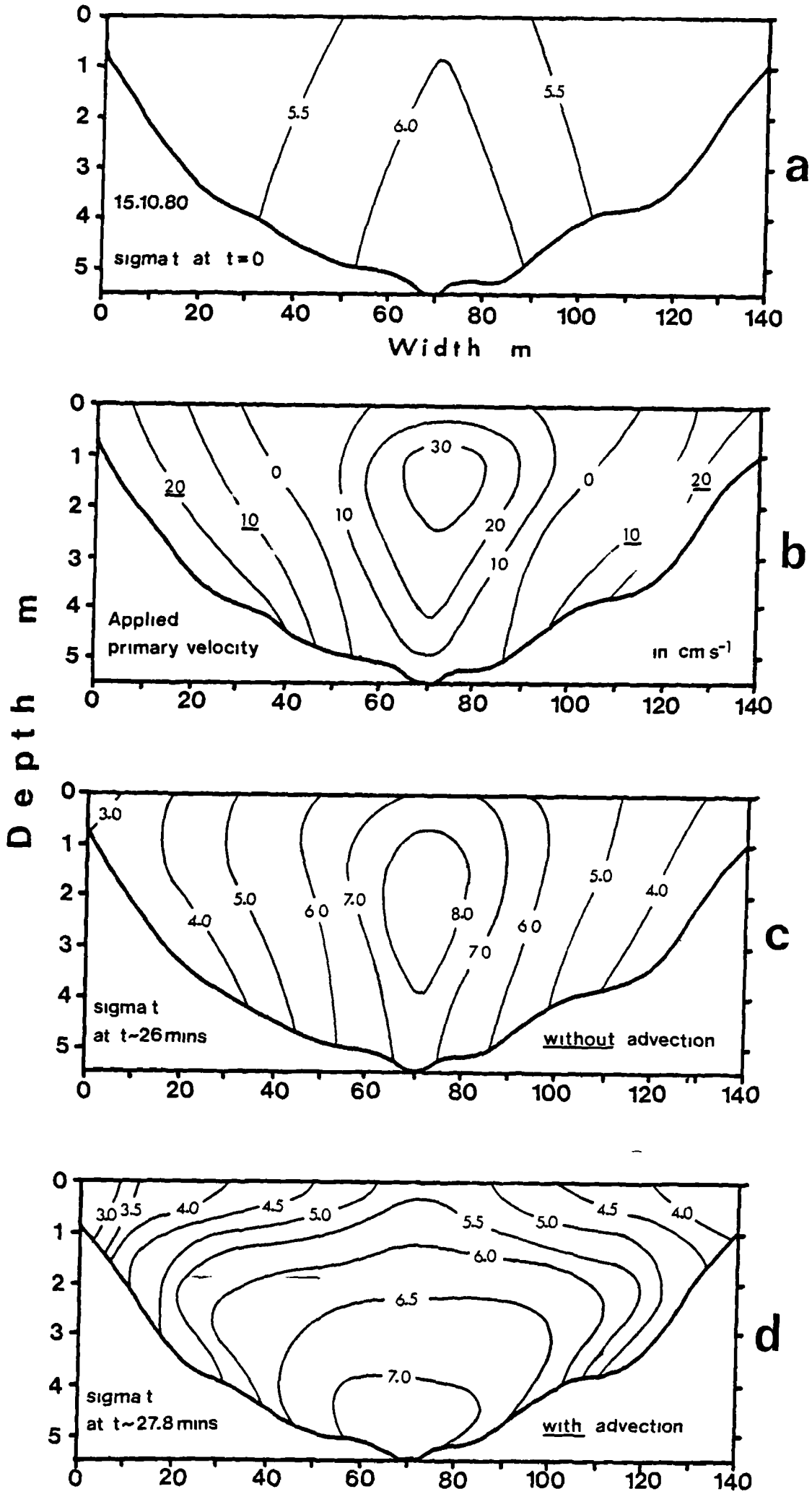
a
15.10.80
sigma t at t=0
5.5
6.0
5.5
Width m
b
Applied
primary velocity
in cm s⁻¹
30
20
10
0
20
10
10
0
20
10
c
sigma t
at t~26 mins
without advection
3.0
4.0
5.0
6.0
7.0
8.0
7.0
6.0
5.0
4.0
d
sigma t
at t~27.8 mins
with advection
3.0
3.5
4.0
4.5
5.0
5.5
6.0
6.5
7.0
5.0
4.5
4.0
Depth m
0
20
40
60
80
100
120
140
1
2
3
4
5

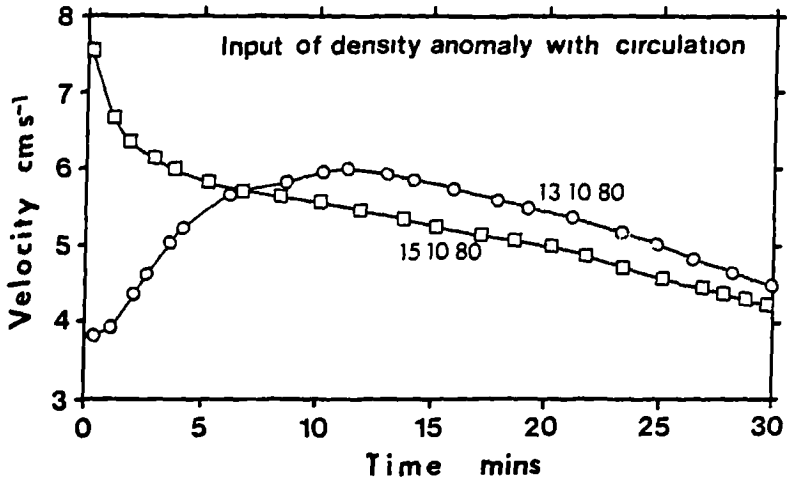


Figure 8.26 Variation of maximum lateral secondary velocity from the initial distributions of 13.10.80 and 15.10.80 under the combined effects of primary density input and secondary re-distribution.

velocity. Figure 8.25c gives the resultant density distribution at t~26mins. with the secondary circulation suppressed, showing how the primary flow tends to set up central instability. The bottom diagram shows the density field produced by the combination of longitudinal input and secondary advection. Clearly, the circulation successfully restores stability despite the de-stabilising effect of the tidal flow.

Finally, figure 8.26 illustrates the change in the maximum lateral velocity as the circulation develops from the initial conditions of 13.10.80 and 15.10.80 under the influences of primary input and secondary advection. It appears that the establishment of an equilibrium under these conditions is a very slow process, which casts doubt on the validity of our steady-state model. The difficulty is largely due to a combination of a no-slip boundary condition in the circulation model and the form of applied longitudinal velocity (figure 8.25b). The assumed velocity field introduces the greatest negative density anomalies at the bed on the basis that this is the region of slowest flow. Since all bottom secondary velocities have been set to zero, the circulation is unable to re-distribute these negative anomalies which, because the cross-section is not rectangular, also contribute to the lateral gradients. The same condition accounts for the discrepancies between the anticipated primary velocity field and that required to maintain constant conditions in figures 8.22b to 8.24b. Use of an

alternative condition, tending towards a free-slip lower boundary, should resolve the discrepancies and allow the comparatively fast establishment of equilibrium. This has not yet been attempted.

## 8.4 SUBSURFACE DIVERGENT RETURN FLOW.

The constraints of continuity dictate that to preserve a surface convergence necessarily requires a subsurface divergence. Furthermore, the inability of the surface layers to support any appreciable shear (without external forcing and provided vertical density gradients remain small) ensures that the greatest velocity gradients should be found in the lowest regions of the water column. The location of the turning point depends primarily upon the form of bottom boundary condition but if, as in the previous section, we assume a no-slip condition, then the turning point for most realistic density distributions is located in the range $0.75 \leq \eta < 0.8$, with the equality appropriate to a stratification-free system. In this section we look at the results of an attempt to detect the submerged circulation in the estuary.

One of the major difficulties with such an attempt concerns the high turbidity in the Conwy which reduces visibility to a maximum of a few centimetres. This effectively eliminates all optical possibilities such as diver observation of current direction, leaving only the remote methods e.g. dye fluorimetry. Although such a method ought to reveal the circulation of the dye concentration-maximum as it follows a helical path moving into the estuary, at best it could only offer an integral picture of the size of the circulation cell, with attendant problems caused by considerable turbulent diffusion. For these reasons it was decided that a vertical array of sensitive current direction indicators should be mounted on a framework placed into the tidal flow. With tidal velocities as large as $1 ms^{-1}$, the instruments should be capable of resolving angular differences to $\pm 1^{\circ}$, which ruled out the use of existing current meter systems.

After much trial and error feedback, the instrument shown in figure 8.27 was developed. Figure 8.28 shows an exploded view of

Figure 8.27 The assembled current-direction indicator and attached vane.

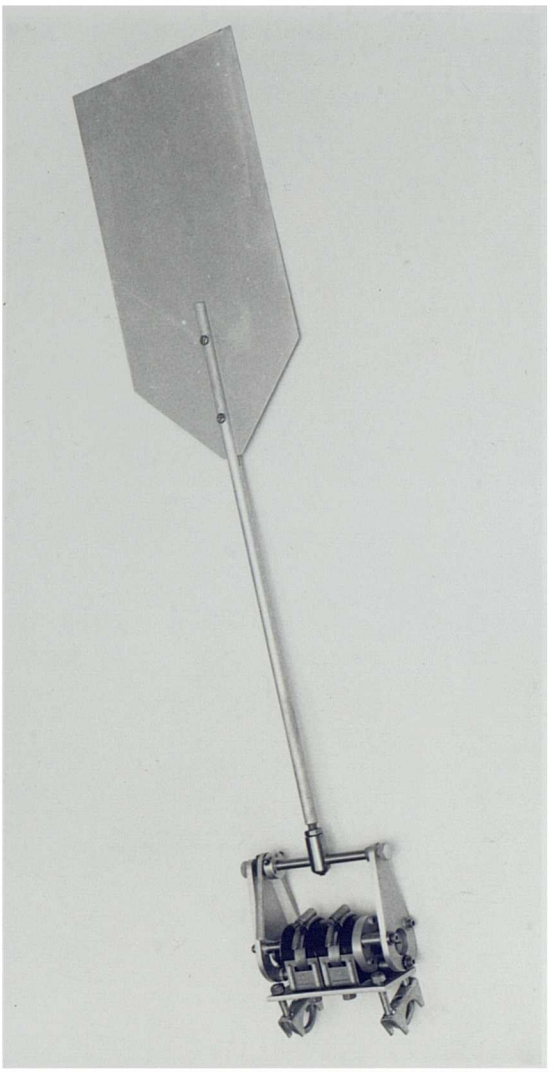

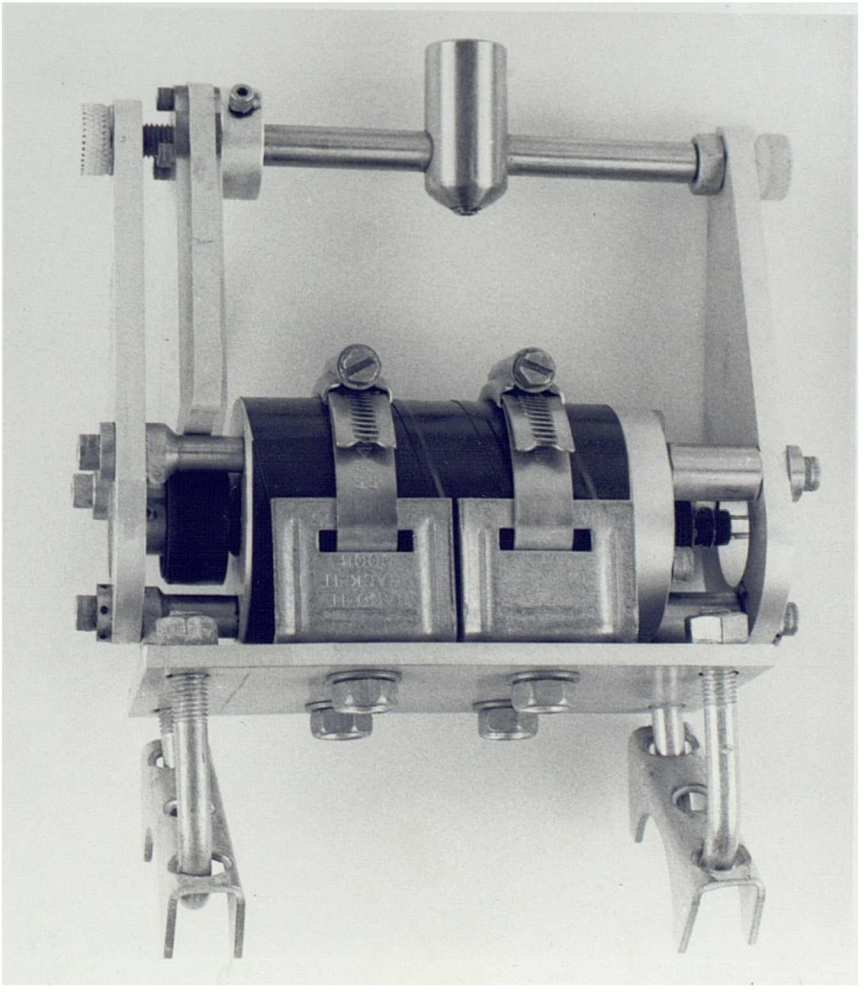

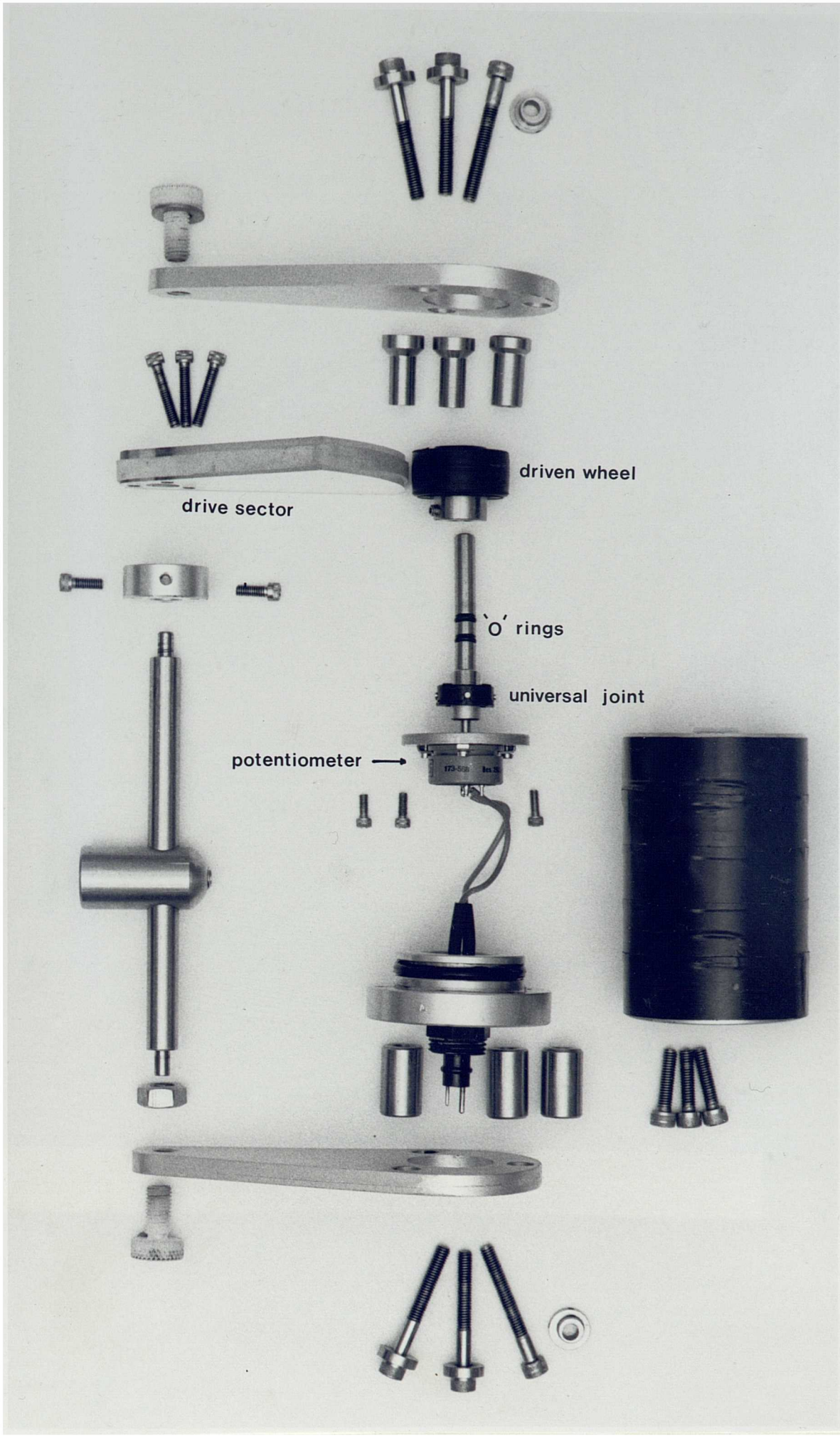


Figure 8.28 Exploded view of the components of the direction-indicating instrument.

Figure 8.29 Instrument support frame (and senior technician) in position in the Tremorfa reach of the Conwy estuary.

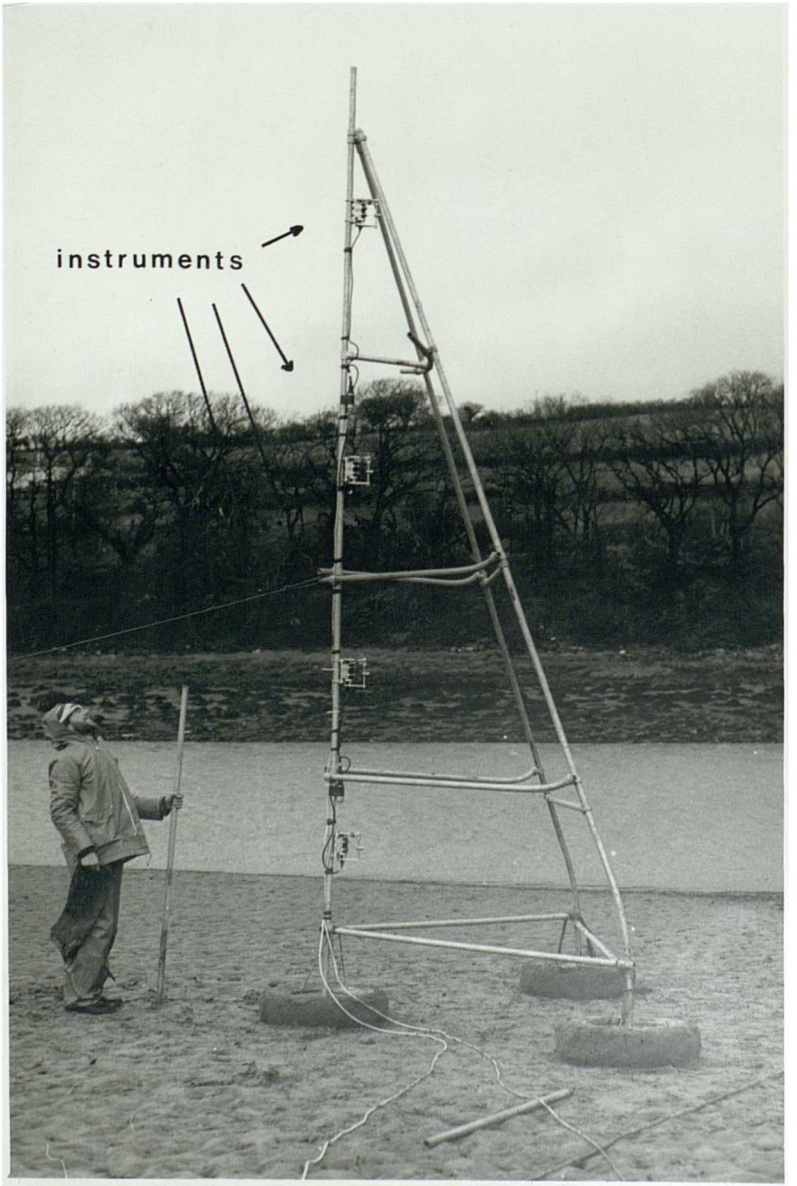
instruments

its components. It is an electronic device that measures the rotation of a vane which is coupled to a high resolution potentiometer inside a waterproof casing. The coupling, via two touching rubber surfaces, includes amplification of the vane movement (to increase resolution) achieved by an approximate 5:1 ratio of drive to driven wheel (sector) diameters. The driven wheel is connected to the potentiometer through two 'O' ring seals and a universal joint to allow for errors of concentricity. Two polythene adjustable bolts, each housing a stainless steel ball, form the top and bottom vane axle bearings.

Flume testing of the instrument revealed the need for elimination of all extraneous friction in order to reduce the angular 'dead space' around the current direction to an acceptable size. After optimum adjustment of bearings and contact pressure, the instrument static friction could be overcome in either direction by a force of 0.008N applied to the end of the 0.8m vane.

Again, after some trial and error, we arrived at the pyramid structure of figure 8.29 as a sufficiently stable and rigid platform for supporting the instruments in the strong tidal flow. For the estuarine location we chose the Tremorfa reach at the same position as the HRS/Birmingham surveys since it is a well known site in which the convergent line is normally well developed. Near its landward end the western shore dries out to more than half way across the full channel width, and remains so for some hours, presenting access to a firm sandbank which served as a bed for the frame. In this position, the flood tidal flow is relatively unperturbed by the distant bends, but due to the proximity of the landward bend, it would be unsuitable for ebb tide measurements.

The frame was constructed and materials collected on site on the day prior to taking measurements. At the Tremorfa reach, the assymetry of flood and ebb durations allows 3-4 hours for erecting the frame in its correct position and orientation, attaching the instruments and connecting these to cables run ashore. Four instruments were positioned at intervals through a total depth of ~3.5 m on the vertical support of the frame and, before raising it into position, the meter on shore was set to centre-zero for each instrument while the vanes were all pointing in the same direction.

The vanes themselves were then removed from the instruments to maintain the calibration - by preventing the wind from taking the perspex sector beyond its range of contact. Raising the frame, each leg was inserted ~0.3m into the sand through a concrete filled tyre for stability and which also served to prevent the frame from tilting into the sand bed as it became saturated.

During the tidal rise, each vane was attached when the level of water reached sufficient height to hold the vane within the drive contact range. The readout ashore indicated the voltage applied in the circuit and could be switched into four sensitivity ranges giving full scale deflection for ±4°,±8°,±16° or ±32° with a resolution of ~1% f.s.d., (although the drive contact range was restricted to ±15°). The highest instrument was positioned such that it would be submerged for only the last thirty minutes of the flood and would therefore remain close to the surface.

Measurements from this arrangement were obtained during the two morning (springs) flood tides of 29.1.82 and 30.1.82. Unfortunately, the data from the first of these two dates had to be discarded because the vane was found to be loosely connected to its perspex sector on at least one of the instruments. This was corrected and the instruments reset to zero relative to one another for the tide of 30.1.82, the results of which are presented below. As well as records of current direction, salinity at the depth of the lowest-but-one instrument was also measured, and a note was made of the approximate position of the convergent line following its appearance.

Since the absolute depth of the water column should not affect the form of lateral velocity distribution, the (variable) depth was divided into four equal intervals. Instrument readings were allocated to the appropriate interval according to their depth in relation to the total depth at the time of the reading. Figure 8.30 (a-d) shows the lateral velocity as a percentage of the primary flow (the tangent of the vane angle) for each of the four depth intervals. (Dashed connections represent those periods for which an instrument was not present within the interval.) Figure 8.30e gives salinity and the approximate position of the convergence in metres east or west of the frame. Instrument readings suggest

Figure 8.30 Results from the current-direction indicators during the flood tide of 30.1.82. From left to right the first four graphs show the deduced secondary velocity as a percentage of the primary velocity (from the deviation of the vane) in four equal fractions of the total depth from surface to bed respectively. The last graph shows coincident salinity readings at the depth of the lowest-but-one instrument, and the position of the axial convergence in relation to the instrument frame.

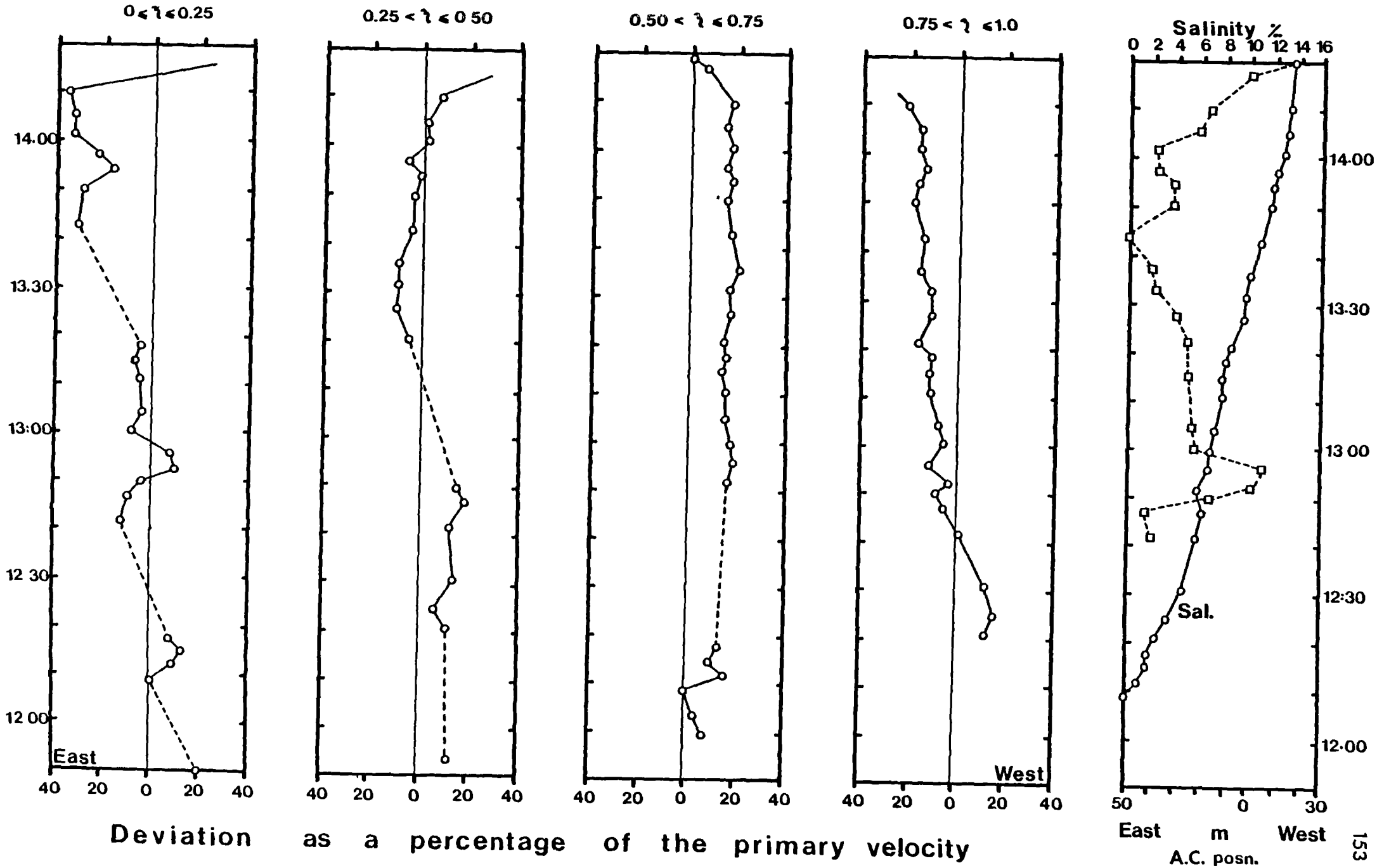
0 ≤ η ≤ 0.25
0.25 < η ≤ 0.50
0.50 < η ≤ 0.75
0.75 < η ≤ 1.0
Salinity ‰
0 2 4 6 8 10 12 14 16
14.00
13.30
13:00
12 30
12 00
East
West
Sal.
40 20 0 20 40
50 0 30
East m West
A.C. posn.
Deviation as a percentage of the primary velocity

near-unidirectional flow until the appearance of the line at ~12:42hrs (GMT). Subsequent to this, the instrument vanes diverged and followed consistent deviations from the longitudinal direction throughout the remainder of the flooding tide. The surface vane was directed towards the line at all times, including those two occasions when it crossed to the west of the frame, ~12:55hrs and 14:17hrs). Current direction in the range $0.5<\eta<0.75$ showed consistent deviation away from the line which would confirm the existence of a part of the return circulation within this depth interval. Deviations in the interval $0.25<\eta<0.5$ were intermediate between the two values above and below but the bottom depth interval showed deviations toward the line, in contrast to the expected result. This may have been caused in one of two ways. Firstly, the bottom instrument was only ~0.3m clear of the bed and may thus have indicated the direction of bottom-directed flow or, secondly, there may have been a bottom secondary velocity toward the line, and without further records from other tides the question cannot be resolved. Nevertheless, support for the form of lateral velocity profile was suggested when the entire profile switched at 14:17hrs at the time the line moved over to the west of the frame, before dispersing at about high water (14:25hrs).

# SECTION III - FRONTAL STABILITY

# CHAPTER 9

## THE STABILITY OF THE ESTUARINE TWO-LAYER REGIME.

Over the last 25 years several attempts to quantify estuarine behaviour have produced formulae, based on bulk parameters of the flow, which were intended to predict the extent of stratification in estuaries. Schultz and Simmons (1957) proposed that QT/P (in which Q is the river runoff, T is the tidal period and P the tidal prism) predicted highly stratified conditions for values much greater than unity. Many subsequent treatments have used the physically important parameters of buoyancy flux per unit width, $g'Q/b$ (where $g'$ is the reduced gravity and b is the width) and the r.m.s. tidal velocity U. Two of these formulae, $E=PU^2/gHQT$, the 'estuary number' of Harleman and Ippen (1967) and $R=g'Q/bU^3$ the 'estuarine Richardson number' of Fischer (1972) were later shown by Turner (1973) to be related according to $RE=\Delta\rho/\rho$. Implicit in these formulae is an energy argument also contained in the well known classification scheme of Hansen and Rattray (1966) which compares the potential energy input from buoyancy to the availability of kinetic energy from the tide for mixing. This same argument forms the basis of the highly successful predictive parameter $H/U^3$ for the location of shelf sea fronts (Simpson and Hunter, 1974).

The inherent variability of quantities such as Q, U, P, and H with time or position in an estuary tends to produce a very patchy

classification in the scheme of Hansen and Rattray for example. However, this patchiness does reflect a change in dominant character as we proceed landward or under varying conditions of runoff or tidal amplitude. If the Seiont tidal-intrusion front remained stationary at all times we might expect to obtain a discontinuous change in estuarine class on either side of the front (according to the formulae) reflecting the transition from two-layered to mixed regimes. In practice, the front does not remain stationary, nevertheless, we might still detect abnormally large gradients of the classification parameter suggesting an abrupt change of estuarine regime. The method would obviously require an unjustifiable research effort.

If we assume that all mixing between fresh and saltwater takes place inside an estuary, between the head and the mouth, we can treat the estuary as a box and presumably infer its qualities from the known inputs at either end. The total energy dissipation inside the estuary produced by tidal effects may be found by comparing the magnitudes of ingoing and reflected components of the tidal oscillation at the mouth. Similarly, at the head, the gauged runoff tells us the total buoyancy input to the estuary (neglecting temperature as a source of buoyancy). A comparison of the two quantities should lead to a conclusion regarding the mean level of stratification inside the estuary, of which a minimum is required to maintain conditions conducive to the occurrence of a T.I. front.

However, the dominant regime of the Conwy estuary is well mixed, which would presumably be reflected in a parameter of this kind, despite the formation of a stable T.I. front for a limited period during the flood tide. Thus, below the minumum level that defines the stable range of the two-layer regime, the parameter cannot be used in a predictive sense.

To contrast with the general approach, we shall attempt to be more specific in identifying a fundamental cause for the difference in behaviour exhibited by the Seiont and Conwy estuaries.

As a basis from which to work we would like to explain the following observations;

i) *there is almost* invariably a sharp T.I. front present in the Seiont estuary which divides one- and two-layered regimes. It is present and persistent even during conditions of minimal runoff.

ii) there is often a similar T.I. front present in the Conwy but, despite a substantial level of runoff, frontal movements in response to increasing tidal currents are very small and the interface is rapidly destroyed. The dominant regime for most of the estuary length remains well-mixed during the flood.

From this we might infer that the shear in the Conwy is substantially more effective in destabilising the interface than in the Seiont. We might then ask why the front in the Conwy does not adjust to a new position of equilibrium further upstream?

Consider a hypothetical estuary in which there is a tidal-intrusion front at the position $x=x_o$ at time $t=t_o$. The density current velocity at the front $u_d(x_o,t_o)$ is constant (ignoring runoff for the moment) and is in equilibrium with a tidal velocity that is also constant at $u_T(x_o,t_o)$. The front thus remains stationary.

Abruptly, at time $t=t_1$, the tidal velocity increases by an amount $\delta u_T$; the equilibrium is destroyed and may only be restored by a landward adjustment of the front to a new position $x=x_1$. Moving landward reduces the tidal velocity such that $u_T(x_1,t_1)=u_T(x_o,t_o)$ (if we ignore the increase of $u_d$ by compression of the freshwater layer, i.e. compression with respect to buoyancy rather than molecular forces). A finite period $\tau$ is required for restoration of equilibrium - the frontal adjustment time scale - which depends upon the separation of equilibrium positions and the frontal speed;

$$\tau \simeq 2(x_1-x_o)/\delta u_T \qquad 9.1$$

During the period of adjustment the area of interface lying between $x_o$ and $x_1$ may be considered to be unstable and subject to mixing at a rate dependent upon the value of $\delta u_T$, the 'excess shear'. If either $\tau$ or $\delta u_T$ is large we might therefore expect to see destruction of the interface between $x_o$ and $x_1$ and thus observe the front weakening and re-forming at $x_1$. (Perhaps this is the cause of observed frontal 'jumps' in the Seiont.) In response to the reduction of 'excess shear' on the approach to the new equilibrium position, there will be a tendency to produce a diffuse frontal region which will then be sharpened by the combined effects of the tidal and baroclinic flows. The parameter $\tau\delta u_T$ may thus have a critical value that when exceeded implies destruction of the interface at either a fast rate for a short interval or a slow rate over a protracted interval. If the critical value is not exceeded, the layer retains its identity during the frontal adjustment from $x_o$ to $x_1$.

The parameter $\tau\delta u_T$ is equivalent, from equation 9.1, to an alternative quantity $(x_o - x_1)$; the separation of equilibrium positions. It is significant as the distance required to reduce the tidal velocity by the increment $\delta u_T$, varying inversely with the longitudinal gradient of tidal velocity $\delta u_T/\delta x$ landward of $x_o$. In its turn, the value of $\frac{\delta u}{\delta x}T$ above $x_o$ is entirely determined by the estuarine geometry.

In a short, steep estuary, $\delta u_T/\delta x$ is large and therefore frontal adjustment distances remain small. Conversely, in a long, moderateley-sloped estuary $\delta u_T/\delta x$ is small, requiring adjustments of position which cannot be achieved before the unstable length of interface is destroyed. The process is repeated as the equilibrium position moves upstream unless $\delta u_T/\delta x$ becomes 'subcritical'.

In reality both compression of the upper layer and addition of freshwater by runoff tend to increase $u_d$ and so help to retain stability. However, if previous, downstream destruction of the interface has occurred, there are two additional factors which counteract the tendency to restore equilibrium;

i) the sections of upper layer lost by mixing cannot contribute to upper layer thickening by compression.

ii) contamination of the lower layer by mixing reduces the density contrast and undermines the stability of the upstream interface.

The quantity that emerges as an indicator of frontal stability appears to be the rate at which the flood tide velocity falls off as we move into the estuary; a quantity that will vary with both time and position. We may also conclude that the tidal-intrusion front will more often be found in a short, steep estuary (large $\delta u_T/\delta x$) with a mouth that is swept by a strong tidal crossflow (large $\rho_{lower}$) and which manages to flush itself free of salt at each low water (small $\rho_{upper}$).

It follows, that the Conwy maintains a T.I. front in its lower reaches while $\frac{\delta u}{\delta x}T$ remains large i.e. in the early stages of the flood tide. When the tidal level reaches a height at which the flood waters rapidly expand over the sandbanks near Glan Conwy, $\delta u_T$ becomes large and $\delta u_T/\delta x$ diminishes, creating large areas of substantially unstable interface. Restoration of equilibrium further upestuary is hindered because;

i) harmonic distortion of the tide causes an abrupt tidal rise in the upper reaches maintaining $\delta u_T$ very large.
ii) previous, downestuary mixing reduces $\rho_{lower}$ such that $\Delta\rho$ becomes very small.

Note, also, that the fundamental premise of the frontal model described in section 4.5 is in error. The model was designed to move the front at a velocity $u_f$, equal to the difference between the density current and tidal velocities at the frontal position. Rather, it emerges that the frontal position is determined by the equality of these two velocities and if $u_f$ is too small, a length of the upper layer will be lost.

From the above argument, frontal movement in the landward direction is always accompanied by some (excess shear) instability because adjustments are not instantaneous. Conversely, movements in the seaward direction, during the retreat phase, take place in an environment of subcritical shear as the position of equilibrium

recedes from the estuary. Thus, excess mixing during the advance phase and reduced mixing in the retreat account for faster frontal adjustments observed in the estuary than were produced by the model.

Finally, one further effect of the T.I. front remains to be discussed. The longitudinal density gradient in an estuary, in the absence of a tidal energy supply, drives a two-layer secondary circulation with the light fluid moving seaward above a slow landward-moving lower layer. By providing a tidal source of energy, we enhance the vertical density exchange thereby increasing the gravitational potential energy of the estuarine system. However, there is an alternative mechanism by which the tidal source can similarly increase the gravitational potential energy, which appears to be the option operating in the Seiont, that is to reverse the density-driven circulation by compressing the freshwater layer into the upper reaches of the estuary. Compression displaces a volume of saltwater that would otherwise occupy the upper reaches. The difference between the two mechanisms is that the latter is reversible and energy stored in the compressed state is released when the layer expands seaward. Interesting in its own right as part of the range of estuarine behaviour, the process also serves to remove the freshwater to less turbulent regions of the estuary. This ensures a much smaller contribution to tidal energy losses from mixing than is the case in estuaries that do not have persistent T.I. fronts.

# CHAPTER 10

## SUMMARY

Soon after low water in the Menai Straits near Caernarfon, a plume frontal boundary forms, that horizontally (~1m) and vertically (<0.5m) separates the fully saline (~32‰) water of the Straits from the comparatively fresh (~5‰) discharge of the Seiont estuary. During spring tide (and mean runoff) conditions, the frontal boundary is pushed into the estuary by strengthening flood tidal currents and, on reaching the mouth, it transforms from the convex outline of the plume to a landward-pointing 'V' that characterises the 'tidal-intrusion' or T.I. front. The front marks the boundary between the estuarine two-layer regime and the mixed water flowing in from the Straits. Distinguishing characteristics of the tidal-intrusion front include;

i) its mobility within the estuary

ii) the shape of the frontal boundary and the associated current structure.

Considering the first of these: the front moves into the estuary an hour or so after low water and continues moving landward until approximately mid-flood when the currents are at their strongest. As the currents weaken, the front retraces its path and

emerges from the estuary ~1-2 hours before high water. It transforms back to the plume configuration at the mouth of the estuary and continues expanding into the Menai Straits where it disperses at approximately high water.

The freshwater layer, separated by the frontal interface from the ambient waters of the flooding tide, is subject to the same forces (inertia and buoyancy-induced pressure) that govern the theoretical and laboratory-based density currents. Both theory and experiment show that a density current front advances into a stationary ambient fluid at a velocity dependent on the depth of the current, the density contrast and, to second order, the depth of the current as a fraction of the total depth. In a fixed reference frame, a front may be forced into retrograde motion by an ambient flow of sufficient magnitude, which is the case in the estuary. At the landward intrusion limit, when the front is stationary, an equilibrium exists between the (potential) velocity of the density current front and the tidal velocity at the frontal position. Assuming a sinusoidal change of tidal elevation, in an estuary that maintains a level surface at all times, together with the observation that the intrusion limit is always reached at approximately mid-flood, leads to a relationship between the landward intrusion limit $x_c$ and a parameter combining tidal range and river discharge;

$$x_c \propto (Q/R^2)^{1/3}$$

Observations in the estuary lend substantial support to this conclusion. In the Seiont estuary (total length 1.7km) a change of $(Q/R^2)^{1/3}$ from 0.25 to 0.55 $(m\ s^{-1})^{1/3}$ reduces the intrusion limit by 0.5km.

We turn now to the second of the distinguishing characteristics: that of the frontal shape and its associated currents. The surface boundary of the tidal-intrusion front is 'V'-shaped with a sharp apex that points in the landward direction. Baroclinic flows, associated with the discontinuous density field, induce surface convergent flows towards the front from both downstream and upstream sides. Material collected by the front also moves towards the apex which forms a point convergence for all

buoyant debris in the estuary. Diver observations of the subsurface interface indicate the existence of distinct regions in a front-based reference frame. Well upstream of the surface front, the interface is sharp and stable with typical Richardson numbers of ~5. Moving seaward, stability becomes marginal ($0.4<Ri<1$) and reaches a critical level ($Ri\sim0.25$) at 50m-100m from the surface front. Within the frontal region Richardson numbers of 0.1-0.2 have been measured in the wake of a Kelvin-Helmholtz billow at the front itself.

In order to understand the parameters that determine the shape of the frontal boundary, an attempt was made to reproduce the three-dimensional aspects of the T.I. front in the laboratory. The apparatus made available for these experiments was specifically designed to model steady-state bottom density currents which could be subjected to a variety of boundary conditions by the use of an incorporated moving floor. To represent the topography of the estuary in its inverted state, a 'V'-shaped roof was placed over the modelled density current. Despite difficulties in duplicating the estuarine surface boundary condition, a density current head showing three-dimensional characteristics similar to the Seiont front was observed in the experiment. The model produced two stable frontal configurations; a sharp 'V' and a linear, oblique front, both of which have been seen in the estuary.

Following the investigation of the T.I. front in the Seiont, a similar feature was studied in Loch Creran on the west coast of Scotland. A landward-pointing 'V'-shaped front forms in the upper basin soon after low water and moves upstream into the Loch during the flood tide. Although it rarely retraces its path and moves seaward, it does disperse before high water and fronts have not been seen during the ebb phase of the tide. Measurements reveal that both the frontal structure and its associated currents are similar to those of the Seiont. The surface front in the Loch is also characterised by regular cusps along its length; a feature that was observed in the laboratory model but has not been seen in the (substantially smaller) Seiont example. A balance between density current and tidal velocities may govern frontal movements in Loch Creran which, due to the large increase of cross-sectional area over the sill slope, are relatively small. However, erosion of the upper

layer by mixing, seen in successive longitudinal salinity profiles, accounts for the continued advance of the front and the absence of a retreat phase.

Reported experimental investigation of density currents indicates that surface convergence on the two-layer side of the front is enhanced by mixing losses from the current to the interface. The results of a time-dependent numerical model of frontal movement suggest that these mixing losses in the Seiont are the same order of magnitude as the rate of addition of freshwater to the upper layer by runoff. The relative quantities of salt and freshwater entrained into the interface have been estimated by a simple analytical approach to be ~10:1 respectively.

The considerable mobility of the T.I. front in the Seiont estuary represents a means by which tidal energy is re-directed from its more familiar role of driving vertical density exchange to one of reversing the natural density-driven estuarine circulation. Both processes similarly increase the gravitational potential energy of the system but the latter process is reversible. Compression of the upper layer towards the head of the estuary displaces saltwater that would otherwise occupy the upper reaches. Thus, work done on the upper layer by the tidal flow is stored and subsequently returned when the layer spreads seaward after maximum flood currents. The compression also serves to remove the freshwater to much less turbulent regions of the estuary.

The formation and persistence of the front itself relies on the stability of the upstream interface. Theoretically, the front marks the position of equilibrium between the tidal and density current velocities which is equivalent to a critical shear condition. However, the rate of frontal adjustment, following an increase of tidal velocity, may be too slow to prevent destruction of the interface between the old and new equilibrium positions, as a result of excess shear above the critical level. A new, more diffuse front will then be seen at the new equilibrium position which is sharpened by the tidal and baroclinic flows. If the frontal adjustment time scale remains too large, successive lengths of the interface will be destroyed by the tidal currents as these increase along the estuary. The criterion that distinguishes

estuaries, or different parts of the same estuary, with regard to the stability of the frontal interface, is the longitudinal gradient of estuary volume. Steep estuaries assist frontal stability by reducing the frontal adjustment distance. Following destruction of the interface the estuary occupies a position in the spectrum of estuarine classes between partially stratified and well mixed, depending on the levels of bottom-generated turbulence.

Tidal-intrusion front formation is also observed in the Conwy estuary North Wales in the early stages of the flood tide but strengthening tidal currents destroy the front and its interface at ~1-2 hours after low water. When the T.I. front is broken down, two separate density fronts remain in the outer estuary and, assisted by the dynamic convergence at the constriction below the bridges, supply foam and debris to a single line that moves into the estuary. At this stage and throughout the remainder of the flood tide, the estuary classifies as near cross-sectionally homogeneous. By the late stages of the flood tide the line extends continuously through a substantial proportion (dependent on tidal range and river runoff) of the estuary length but at high water it disperses entirely and does not re-form during the ebb phase. Its resistance to turbulent dispersion indicates the presence of active surface convergence (during the flood) in the form of lateral secondary currents. Measured by surface markers, the velocity of these secondary currents is typically ~10cms$^{-1}$.

Boundary friction, acting on the flow of a cross-sectionally homogeneous fluid with a longitudinal density gradient, tends to create both vertical and lateral density gradients in the cross-section. A flood tide pressure gradient therefore produces greatest densities at the centre of the channel with an additional tendency to induce vertical instability. Whereas, the reversed pressure gradient of the ebb phase enhances stability and reverses the lateral gradients. In the presence of the axial convergence, synoptic measurements of cross-sectional density show greatest values near the channel axis (lateral gradients of ~0.02kgm$^{-4}$) which then reverse after high water. Weak stratification (~0.1kgm$^{-4}$) exists, however, during both tidal phases. To confirm the measured gradients as the cause of the observed convergence, a diagnostic numerical model was constructed. The model was based on a

steady-state balance between the lateral (density-induced) pressure forces and internal frictional dissipation and was used to compute the circulation resulting from four measured density distributions (three flood and one ebb). Results indicated strong secondary circulations which, in the case of the flood distributions, included surface convergence.

On the assumption that lateral accelerations remain small and that a steady-state assumption is still valid, the secondary circulation was allowed to re-distribute the density in a series of discrete steady-state computations. Successive distributions indicated that the circulation tends to maximise stratification and to minimise the lateral gradients. By so doing, the circulation velocities were rapidly diminished with a 'half-life' of ~4mins. Thus, the persistence of the axial convergence in the Conwy over a period of hours suggests the existence of an equilibrium between the input of buoyancy anomalies by the longitudinal flow and their elimination by the secondary circulation (and, to a lesser extent, diffusion). At high water, when the longitudinal input ceases, the circulation rapidly decays and the line disperses.

Using an assumed form for the cross-sectional distribution of longitudinal velocity, an attempt was made to set up the equilibrium in the model. Despite difficulties with the assumption of a no-slip lower boundary condition, it demonstrated that the secondary currents can successfully maintain stability against the de-stabilising influence of the tidal flow. The model therefore remains consistent with the existence of stratification in the estuary during both tidal phases.

In the model, the circulation (during the flood) consisted of two laterally adjacent rotating cells, extending from the surface to the bed such as to produce surface convergence and strong divergence (to satisfy continuity) at a fractional depth of 0.75 (as a result of the no-slip assumption). To test this result in the estuary required the design and construction of instruments capable of resolving current direction to $\pm 1^{\circ}$, and a platform on which to mount the instruments in the estuarine flow. Initial results with the developed arrangement lend some support to the depth variation of lateral velocity indicated by the model although, to date, only a

single set of flood tide results has been obtained in the estuary. Further effort in this direction should lead to a conclusion with regard to the form of lower boundary condition operating in the estuary. The instrument platform and the model both concur with the result of direct measurements; that the surface convergent velocity constitutes ~20% of the primary velocity.

In searching for tidal convergences within estuaries reported in the literature, the most striking and likely candidate for T.I. front formation is the Fraser river in British Columbia, Canada.

Tully and Dodimead (1957), who were concerned with a physical appraisal of oceanography in the Strait of Georgia, included a description of frontal development in the Fraser estuary.

"When the tide rises, water enters the [Fraser] river from the sea (Strait of Georgia). The sea water being more dense, underruns the fresh water forming a 'salt wedge' which intrudes the river. At this time, the currents in the sea- and fresh-water layers are in opposite directions... Hence a 'tide-rip' (convergence) forms at the point where the opposing flows are equal. Upstream from this boundary in the river the deep sea water moves in the flood direction, while the surface river water moves seaward with a velocity equal to the difference of the opposing streams..."

"The boundary tide-rip forms off the river mouth as the tidal rise commences, and advances into the river as the rate of rise increases. After mid-tide the boundary retreats seaward as the rate of rise decreases, and leaves the river when the rate of rise becomes zero at high tide. During the tidal rise there is little or no outflow from the river...."

They continue; "Fjarlie (1950), studying the North Arm, showed that when the discharge of the Fraser river (metered at Hope, B.C.) exceeded 200,000 cubic feet per second, the meeting place of the tidal and river waters was outside the estuary, so that the flow

in the river was always seaward. When the discharge was between 120,000 and 75,000 cubic feet per second, the tidal currents during the large rise of the tides were greater than the river flow, sea water intruded the estuary, the river flow was reversed and there was no outflow during the flood.... Takata (1956) confirmed these conclusions in the main channel by showing that the period of sea-water intrusion varies with the tidal rise and inversely with the runoff...."

These authors make no comments regarding the surface appearance of the 'tide-rip'; furthermore, both correspondence with workers in British Columbia and a full literature report on all aspects of the Fraser estuary by Hoos and Packman (1974) produced no further evidence of frontal behaviour in the Fraser.

More recently, following initial work in the Seiont estuary, tidal-intrusion fronts were discovered in the Dulas and Ffraw estuaries in North Wales (Pelegri, 1979 and Lailey, 1980). However, a point is reached, as in the Conwy, at which frontal stability can no longer withstand the strengthening shear and the surface layer undergoes a rapid destruction by mixing. Axial convergences have been observed during the flood tide in both estuaries.

A horizontal surface variation of density, which includes a maximum turning point, appears to be the single necessary condition for the formation of a convergence similar to the axial convergence of the Conwy. Its persistence relies on a continuing supply of buoyancy anomaly to prevent the system from running down, which may be satisfied relatively easily in a tidal environment. We might therefore expect the feature to be more common than a survey of the literature on estuaries and tidal inlets would suggest. The lack of graphic evidence is likely to be due, in part, to their having been overlooked which may indicate that the Conwy is peculiar because its convergence is so plainly evident. To qualify this conclusion, we should add that the axial convergence in the Conwy is considerably less apparent during the winter months and that its collection of debris is greatly assisted by the constriction below the Conwy bridges. Without the large supply of debris and biological material a convergence is seen as a calm slick produced by the concentration of surface contaminants, and slicks are easily dismissed. As

evidence of its non-uniqueness in the coastal environment figures 10.1 and 10.2 show similar convergences with a comparable degree of organisation to that of the Conwy, although their respective causes have not been identified. The first figure shows a part of Loch Linnhe close to the east shore, just south of Fort William at ~2hrs after low water at Port Appin. The second shows the Menai Straits looking north east from the Menai bridge. With openings at both ends of the Straits, the tidal phase does not specify the sign of any density changes. The picture was taken during the ebb phase with flow towards the camera.

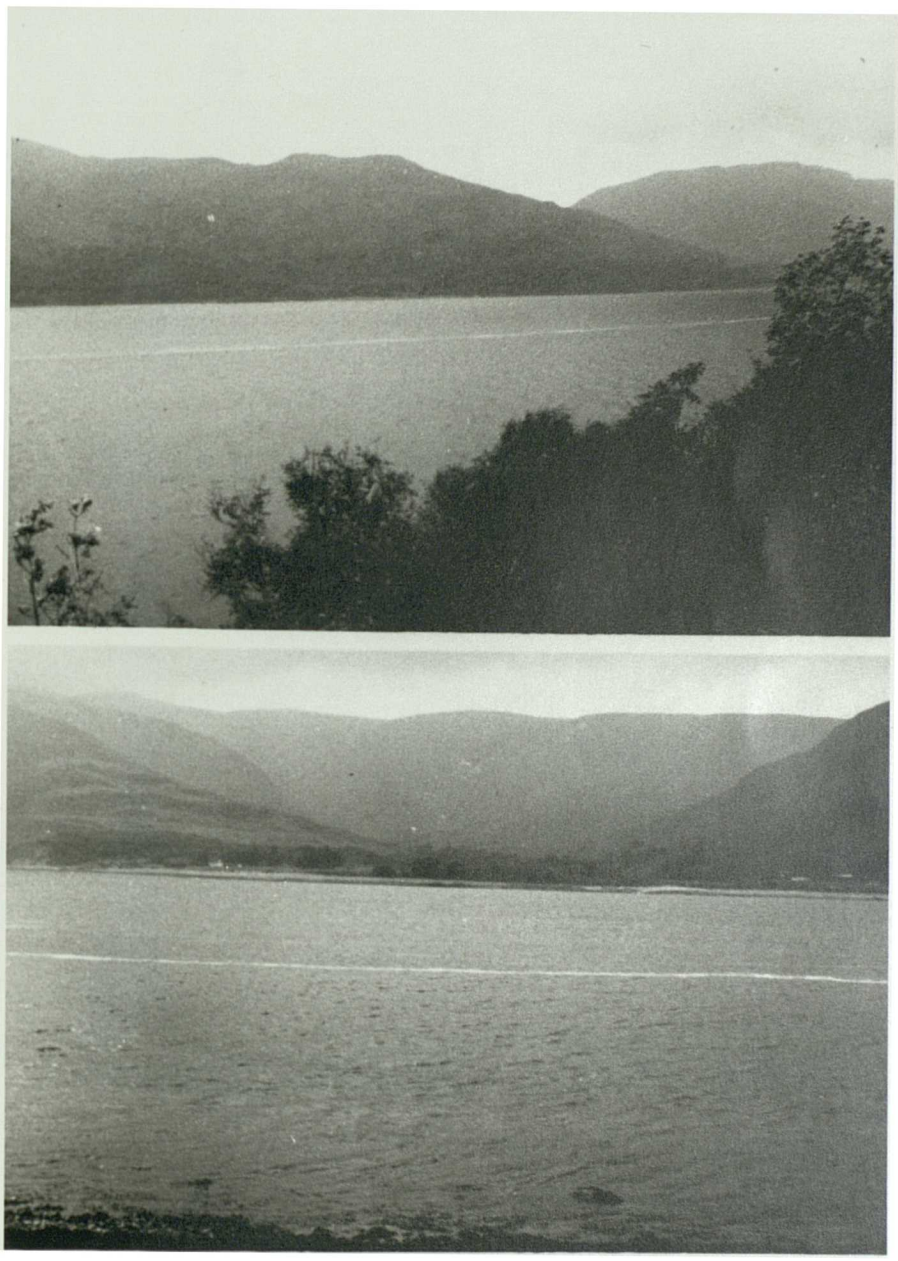

Figure 10.1 Linear collections of debris in Loch Linnhe, Scotland.

Figure 10.2 Debris colection in the Menai Straits (taken by Dr. C.P. Spencer, Marine Science Laboratories, U.C.N.W.).

# REFERENCES


Anati, D.A. Assaf, G. Thompson, R. 1977 "Laboratory models of sea straits." Journal of Fluid Mechanics 81, 341-352.

Benjamin, T.B. 1968 "Gravity currents and related phenomena." Journal of Fluid Mechanics 31(2), 209-248.

Bowman, M.J. Iverson, R.L. 1977 "Estuarine and plume fronts." Oceanic fronts in Coastal processes. Proc. Marine Science Research Center, May 25-27, State University, New York.

Bowyer, P. 1979 "Small scale aspects of the tidal-intrusive front at Caernarfon." M.Sc. thesis, U.C.N.W.

Britter, R.E. Simpson, J.E. 1978 "Experiments on the dynamics of a gravity current head." Journal of Fluid Mechanics, 88(2), 223-240.

Chow, V.T. 1959 "Open channel hydraulics." McGraw Hill Book Company, New York.

Darcy, M.H. Bazin, M.H. 1865 "Recherches hydrauliques." Imprimerie Imperiale, Paris.

Department of the Environment 1973 "Report of a survey of the discharges of foul sewage in the coastal waters of England and Wales." H.M.S.O.

Dyer, K.R. 1977 "Lateral circulation effects in estuaries." National Academy of Sciences Symposium; Estuaries Geophysics and the Environment.

Edwards, A. Edelsten, D.J. 1976 "Control of fjordic deep water renewal by runoff modification." Hydrological Sciences Bulletin, XXI (3).

Einstein, H.A. Li, H. 1958 "Secondary currents in straight channels." Transactions of the American Geophysical Union 39, 1085-1088.

Fischer, H.B. 1972 "Mass transport mechanisms in partially stratified estuaries." Journal of Fluid Mechanics 53, 671-687.

Fischer, H.B. List, E.J. Koh, R.C.Y. Imberger, J. Brooks, N.H. 1979 "Mixing in inland and coastal waters." Academic press.

Fisher, M.H. 1970 "Circulation in the Conway estuary." M.Sc. thesis, U.C.N.W.

Fjarlie, R.L.I. 1950 "Oceanographic phase of the Vancouver sewage problem." MS report, Canadian Joint Committee on Oceanography, 21pp.

Garvine, R.W. 1974 "Dynamics of small scale oceanic fronts." Journal of Physical Oceanography 4, 557-569.

Garvine, R.W. Monk, J.D. 1974 "Frontal structure of a river plume." Journal of Geophysical Research 79, 2251-2259.

Gibson, A.H. 1909 "On the depression of the filament of maximum velocity in a stream flowing through an open channel." Proceedings of the Royal Society A82, 149-158.

Godfrey, J.S. Parslow, J. 1976 "Description and preliminary theory of circulation in Port Hacking estuary." C.S.I.R.O. report 67, Division of Fisheries and Oceanography.

Hansen, D.V. Rattray, M. 1965 "Gravitational circulation in straits and estuaries." Journal of Marine Research 23, 104-122

Hansen, D.V. Rattray, M. 1966 "New dimensions in estuary classification." Limnology and Oceanography 11, 319-326.

Harleman, D.R. Ippen, A.T. 1967 "Two-dimensional aspects of salinity intrusion in estuaries." Bulletin 23, U.S. Army Corps. of Engineers, Committee on Tidal Hydraulics.

Hoos, L.M. Packman, G.A. 1974 "The Fraser river estuary: status of environmental knowledge to 1974." Report of the Estuary Working Group, Dept. of Environment, Regional Board Pacific region, special estuary series no. 1, 518pp.

Hunter, J.R. Lailey, R.S. 1980 "The investigation of the probable effects of the proposed road developments at Conwy: physical study." Report U80-2, U.C.E.S. Menai Bridge, Anglesey, North Wales.

Huppert, H.E. Simpson, J.E. 1980 "The slumping of gravity currents." Journal of Fluid Mechanics 99(4), 785-799.

Ingram, R.G. 1976 "Characteristics of a tide-induced estuarine front." Journal of Geophysical Research 81(12), 1951-1959.

Jenkins, A. 1976 "The Conway estuary." M.Sc. thesis, U.C.N.W.

Jones, G.Ll. 1973 "Investigation of the outer Conway estuary. Part 1 Circulation." B.Sc. thesis, U.C.N.W.

Kao, T.W. Park, C. Pao, H. 1977 "Buoyant surface discharge and small-scale oceanic fronts: a numerical study." Journal of Geophysical Research 82(12), 1747-1752.

Kennedy, R.J. Fulton, J.F. 1961 "The effect of secondary currents upon the capacity of a straight open channel." Transactions of the Engineering Institute, Canada 15(1), 12-18.

Keulegan, G.H. 1957 "Form characteristics of arrested saline wedges." U.S. National Bureau of Standards, report 5482.

Keulegan, G.H. 1958 "The motion of saline fronts in still water." U.S. National Bureau of Standards, report 5831.

Klemas, V. Polis, D.F. 1977 "Remote sensing of estuarine fronts and their effects on pollutants." Photogramm. Eng. and Remote sensing 43(5), 599-612.

Knight, D.W. West, J.R. 1978 "Hydrographic and hydrodynamic data for the Conway estuary." Department of Civil Engineering, Birmingham University.

Koh, R.C.Y. 1976 "Buoyancy-driven gravitational spreading." Proc. Int. Conf. Coastal Eng. 15th Honolulu, volume 4, 2956-2975.

Lailey, R.S. 1980 "Tidal convergences in the Conway estuary." M.Sc. thesis, U.C.N.W.

Lamb, H. 1932 "Hydrodynamics" Dover, New York. 738pp.

Liggett, J.A. Chiu, C. Miao, L.S. 1965 "Secondary currents in a corner." Journal Hyd Div. American Society of Civ. Eng. HY6 99-117.

Mangat, J.S. 1982 M.Sc. Thesis, Birmingham University.

McClimans, T.A. 1978 "Fronts in fjords." Geophysical and Astrophysical Fluid Dynamics 11(23)

Officer, C.B. 1976 "Physical oceanography of estuaries (and associated coastal waters)." John Wiley and Sons.

Pelegri, J.L. 1979 "Frontal systems and related topics in four estuaries." M.Sc. thesis U.C.N.W.

Prandtl, L. 1938 Explained by H. Rouse - "Fluid mechanics for hydraulic engineers." McGraw Hill Book Company, New York.

Prych, E.A. 1970 "Effects of density differences on lateral mixing in open channel flows." Report KH-R-21, California Insitute of Technology, Pasadena, California.

Schultz, E.A. Simmons, H.B. 1957 "Freshwater - saltwater density currents, a major cause of siltation in estuaries." Tech. Bull. 2, U.S. Army Corps. of Engineers, Comm. on Tidal Hydraulics.

Simpson, J.E. 1969 "A comparison between laboratory and atmospheric density currents." Quart. J. of the Royal Meteorological Society 95, 758-765.

Simpson, J.E. 1972 "Effects of the lower boundary on the head of a gravity current." Journal of Fluid Mechanics 53, 759-768.

Simpson, J.E. Britter, R.E. 1979 "The dynamics of the head of a gravity current advancing over a horizontal surface." Journal of Fluid Mechanics 94(3), 477-495.

Simpson, J.H. Hunter, J.R. 1974 "Fronts in the Irish sea." Nature 250, 404-406.

Smith, R. 1976 "Longitudinal dispersion of a buoyant contaminant in a shallow channel." Journal of Fluid Mechanics 78, 677-688.

Stigebrandt, A. 1980 "A note on the dynamics of small scale fronts." Geophysical and Astrophysical Fluid Dynamics 16, 225-238.

Sumer, S.M. 1976 "Transverse dispersion in partially stratified flow." Report WHM-20 Hyd. Eng. Lab. University of California.

Sumer, S.M. Fischer, H.B. 1977 "Transverse mixing in partially stratified flow." Journal Hyd. Div. Amer. Soc. Chem. Eng. 103, 587-600.

Tabata, S. 1956 "Sea water intrusion in Steveston Cannery Basin." Journal Fisheries Research Board Canada, Pacific Progress report 106, 3-6.

Tully, J.P. Dodimead, A.J. 1957 "Properties of water in the Strait of Georgia, British Columbia and influencing factors." Journal of the Fisheries Research Board of Canada 14, 241-319.

Turner, J.S. 1973 "Buoyancy effects in fluids." Cambridge University Press. 367pp.

West, J.R. Cotton, A.P. 1981 "The measurement of diffusion coefficients in the Conwy estuary." Estuarine, Coastal and Shelf Science 12, 323-336.

Woods, J.D. 1968 "Wave-induced shear instability in the summer thermocline." Journal of Fluid Mechanics 32, 791-800.